UNIVERSITAT POLITÈCNICA DE CATALUNYA BARCELONATECH

Mathematical modeling of advanced oxidation processes for the efficient wastewater treatment: integrated management of advanced oxidation processes and conventional bio-processes for the removal of recalcitrant components

Kourosh Nasr Esfahani

UNIVERSITAT POLITÈCNICA DE CATALUNYA
BARCELONATECH

PhD program in chemical engineering

MATHEMATICAL MODELING OF ADVANCED OXIDATION PROCESSES FOR THE EFFICIENT WASTEWATER TREATMENT

Integrated Management of Advanced Oxidation Processes and Conventional Bio-Processes for the Removal of Recalcitrant Components

Doctoral thesis by:

Kourosh Nasr Esfahani

Thesis advisor:

Prof. Dr. Moisès Graells Sobre, Prof. Dr. Montserrat Pérez Moya

Chemical engineering department

Barcelona, March 2024

"Thousands have lived without love, not one without water."
- W. H. Auden

Acknowledgements

I express my sincere gratitude to my two esteemed supervisors, Prof. Dr. Moisès Graells Sobre and Prof. Dr. Montserrat Pérez Moya, for their professional support, guidance, and invaluable insights throughout the entire research journey. Their expertise has been a cornerstone in shaping the depth and direction of this thesis.

I extend my heartfelt thanks to my dedicated advisor in Chile, Dr. Alejandro Cabrera-Reina, for providing essential perspectives and facilitating the research stages conducted in the vibrant academic environment of Chile. Additionally, my gratitude goes to my other advisor in Canada, Dr. Domenico Santoro, whose expertise and mentorship significantly enriched the scope and depth of this work.

I extend my heartfelt gratitude to Prof. Antonio, who serves as the leader of the academic group CEPIMA for the valuable professional opportunities that have unfolded under his leadership.

A special acknowledgment is extended to my fellow doctoral students and my co-authors, whose friendship, shared experiences, and intellectual discussions have added immense value to this academic pursuit. I am grateful to all members of CEPIMA for fostering a collaborative and stimulating research atmosphere.

I would like to express my appreciation to my friends and all those individuals who generously shared their time, expertise, and encouragement. Your contributions have been crucial to the success of this research endeavor.

Last but not least, my deepest gratitude goes to my family and parents for their unwavering support, love, and encouragement. Their sacrifices and belief in my potential have been my constant motivation.

This journey would not have been possible without the collective support of all those mentioned above. Thank you for being an integral part of this academic odyssey.

Kourosh Nasr Esfahani

Abstract (Summary)

The objective of this thesis is to contribute to the development of mathematical modeling of Advanced Oxidation Processes (AOPs) aimed at the competent treatment of recalcitrant organic compounds in wastewater. In particular, the Ph.D. thesis first focuses on developing mathematical models of AOPs, implementing these models in software tools, and enabling a deeper understanding of the complex nature of these processes through the detailed simulation of the evolution of chemical species along the reaction time for diverse and unexplored scenarios. Hence, these tools are next used for fitting the models to the experimental data obtained in the laboratory in the course of the thesis or reported in the literature. The fitted models are analyzed and refined through sensitivity analysis techniques, and finally, they are validated and their accuracy assessed. Models are mainly used for addressing operational issues, but also design aspects are considered in regard of the simulation of integrated processes using AOPs and conventional biotreatment processes.

The thesis specifically addresses the development of a model for AOPs, above all photo-Fenton processes, including flexible H_2O_2 supply given as a function of time. The model contributes a practical tool aimed at providing model-based simulation for solving the problem of the management of the H_2O_2 dosage profile of the photo-Fenton process.

The thesis also addresses the problem of the pH dependency of the photo-Fenton by modeling the possibility of performing the photo-Fenton process at near-neutral pH. This is studied by considering the use of iron complexing agents such as ethylenediamine disuccinic acid (EDDS). In a subsequent stage, as a step forward in improving photo-Fenton processes, a reported kinetic model of the $Fe^{3+} - EDDS$ mediated photo-Fenton process is extended to include the reactions occurring in the absence of H_2O_2, when $EDDS^{\bullet 3-}$ radical generated from the lysis of the $Fe^{3+} - EDDS$ complex is responsible for the organic matter degradation. This is achieved by adopting a novel semi-empirical approach based on lumping radical species.

Ozonation of wastewater is also studied as a different case of AOPs, focusing in the modeling of ozone decay during the treatment of secondary effluents containing

organic matter. This is addressed by proposing a new model, based again in the used of lumped or surrogate concentrations. The ozone model developed is shown to be capable of describing the complex profile of the ozone at different initial concentrations, and has proved accurate to describe the experimental data obtained in the lab, as well as data reported in the literature.

The modeling approach adopted in this thesis has also been used to explore integrated processes combining AOPs with other processes, namely conventional biotreatment processes which main acknowledged limitation is the incapacity to remove recalcitrant compounds from wastewaters. The study combined the AOP models developed with standard models such as ASM1 to map the correspondence between the variables employed in each model, and produce the simulation of different scenarios combining these two technologies.

As a final remark, the thesis has also addressed the design and development of chemical reactors, particularly prototypes for photo-Fenton processes using 3D-printing. This last study addresses the selection of materials according to different criteria for reactor prototyping and subsequent testing of the chemical suitability of the reactor for carrying out AOPs.

Resumen

El objetivo de esta tesis es contribuir al desarrollo de la modelización matemática de los Procesos Avanzados de Oxidación (AOPs) destinados al tratamiento eficiente de compuestos orgánicos recalcitrantes en aguas residuales. En particular, la tesis doctoral se centra, en primer lugar, en el desarrollo de modelos matemáticos de AOPs, la implementación de estos modelos en herramientas de software, y una comprensión más profunda de la compleja naturaleza de estos procesos a través de la simulación detallada para escenarios diversos e inexplorados de la evolución de las especies químicas a lo largo del tiempo de reacción. A continuación, estas herramientas se utilizan para ajustar los modelos a los datos experimentales, ya sean datos obtenidos en el laboratorio durante la tesis o publicados en la literatura. Los modelos ajustados se analizan y perfeccionan mediante técnicas de análisis de sensibilidad y, por último, se validan y se evalúa su capacidad para reproducir los datos experimentales. Los modelos se utilizan principalmente para abordar cuestiones operativas, pero también se consideran aspectos de diseño en relación con la simulación de procesos integrados que utilizan AOP y procesos de biotratamiento convencionales.

La tesis aborda específicamente el desarrollo de un modelo para AOPs, sobre todo procesos foto-Fenton, que incluya el suministro flexible de H_2O_2 en función del tiempo. El modelo aporta una herramienta práctica destinada a proporcionar una simulación basada en modelos para resolver el problema de la gestión del perfil de dosificación de H_2O_2 del proceso foto-Fenton.

La tesis también aborda el problema de la dependencia del pH del proceso foto-Fenton y desarrolla un modelo que contempla la posibilidad de realizar el proceso foto-Fenton a pH casi neutro. Esto se estudia considerando el uso de agentes complejantes del hierro como el ácido etilendiamino disuccínico (EDDS). En una etapa posterior, se amplía un modelo cinético del proceso foto-Fenton mediado por $Fe^{3+} - EDDS$ para incluir las reacciones que ocurren en ausencia de H_2O_2, cuando el radical $EDDS^{\bullet 3-}$ generado a partir de la lisis del complejo $Fe^{3+} - EDDS$ causa la degradación de la materia orgánica. Esto se consigue adoptando un novedoso enfoque semi-empírico basado en la agrupación de especies radicales.

La tesis también estudia la ozonización de aguas residuales como un caso diferente de AOPs y se centra en la modelización de la descomposición del ozono durante el tratamiento de efluentes secundarios que contienen materia orgánica. Para ello se propone un nuevo modelo, basado de nuevo en el uso de concentraciones agregadas. El modelo de ozonización desarrollado se muestra capaz de describir el complejo perfil de la concentración de ozono para diferentes concentraciones iniciales y ha demostrado ser preciso para describir los datos experimentales obtenidos en el laboratorio, así como los datos reportados en la literatura.

El enfoque de modelización adoptado en esta tesis también se ha utilizado para explorar procesos integrados que combinan AOPs con otros procesos, concretamente procesos de biológicos convencionales cuya principal limitación reconocida es la incapacidad para eliminar compuestos recalcitrantes de las aguas residuales. El estudio combinó los modelos AOP desarrollados en la tesis con modelos estándar como ASM1 para trazar la correspondencia entre las variables empleadas en cada modelo, y producir la simulación de diferentes escenarios combinando estas dos tecnologías.

Como comentario final, la tesis también ha abordado el diseño y desarrollo de reactores químicos, en particular prototipos para procesos foto-Fenton mediante impresión 3D. Este último estudio aborda la selección de materiales según diferentes criterios para el prototipado de reactores y la posterior comprobación de la idoneidad química del reactor para llevar a cabo AOPs.

Resum

L'objectiu d'aquesta tesi és contribuir al desenvolupament de la modelització matemàtica dels processos d'oxidació avançada (AOPs) emprats per tractar eficientment els compostos orgànics recalcitrants a les aigües residuals. En particular, la tesi de doctorat se centra primer en el desenvolupament de models matemàtics dels AOPs, la implementació d'aquests models en eines informàtiques i l'obtenció d'una comprensió més profunda de la naturalesa complexa d'aquests processos mitjançant la simulació detallada per a escenaris diversos i inexplorats de l'evolució d'espècies químiques al llarg del temps de reacció. Aquests instruments s'utilitzen després per ajustar els models a les dades experimentals, tant les obtingudes al laboratori durant el desenvolupament la tesi com les documentades a la literatura. Els models ajustats s'analitzen i depuren mitjançant tècniques d'anàlisi de sensibilitat i, finalment, es validen i se n'avalua la seva precisió. Els models s'utilitzen principalment per abordar qüestions operatives, però també s'hi consideren aspectes de disseny pel que fa a la simulació de processos integrats que combinen AOPs i processos de tractament biològic convencionals.

La tesi aborda específicament el desenvolupament d'un model per als AOPs, sobretot els processos de foto-Fenton, incloent un subministrament flexible de H_2O_2 donat com a funció del temps. El model aporta una eina pràctica destinada a proporcionar una simulació basada en models per resoldre el problema de la gestió del perfil de dosificació de H_2O_2 del procés de foto-Fenton.

La tesi també aborda el problema de la dependència del pH del procés foto-Fenton mitjançant la modelització de la possibilitat de dur a terme el procés de foto-Fenton a un pH proper a la neutralitat. Això s'estudia considerant l'ús d'agents complexants de ferro com l'àcid etilendiamin disuccínic (EDDS). En una etapa posterior, com a avanç en la millora dels processos de foto-Fenton, es revisa i s'amplia un model cinètic del procés foto-Fenton mitjançant $Fe^{3+} - EDDS$ ja reportat a la literatura per incloure les reaccions que ocorren en absència de H_2O_2, quan el radical $EDDS^{\bullet 3-}$ generat per la lisi del complex $Fe^{3+} - EDDS$ causa la degradació de la matèria orgànica. Això s'aconsegueix adoptant una nova aproximació semiempírica basada en l'agrupació d'espècies radicalàries.

També s'estudia la ozonització de les aigües residuals com un cas diferent dels AOPs, i s'aborda la modelització de la descomposició de l'ozó durant el tractament dels efluents secundaris que contenen matèria orgànica. Això es fa proposant un nou model, basat novament en l'ús de concentracions agregades. Es demostra que el model d'ozonització desenvolupat és capaç de descriure el complex perfil de la concentració d'ozó a diferents concentracions inicials i es demostra també la seva bona capacitat per descriure les dades experimentals obtingudes al laboratori, així com les dades obtigudes de la literatura.

L'aproximació de modelització adoptada en aquesta tesi també s'ha utilitzat per explorar processos integrats que combinen AOPs amb altres processos, concretament processos de tractament biològic convencionals que tenen com a principal limitació reconeguda la incapacitat per eliminar compostos recalcitrants de les aigües residuals. L'estudi combina els models AOP desenvolupats amb models estàndard com l'ASM1 per determinar la correspondència entre les variables emprades en cada model i produir simulacions de diferents escenaris que combinen aquestes dues tecnologies.

Finalment, la tesi també ha abordat el disseny i el desenvolupament de reactors químics, especialment prototips per als processos de foto-Fenton utilitzant la impressió 3D. Aquest darrer estudi aborda la selecció de materials d'acord amb diferents criteris per a la prototipació del reactor i la posterior prova de la idoneïtat química del reactor per dur a terme AOPs.

Table of Contents

List of Figures

List of Tables

List of Abbreviations

Acronyms	Definitions
ABS	Acrylonitrile Butadiene Styrene
ASM1	Activated Sludge Biodegradation Model N.1
ADE WWTP	Adelaide Wastewater Treatment Plant
AM	Additive Manufacturing
AOPs	Advanced Oxidation Processes
ASTM	American Society For Testing And Materials
NH_4^+	Ammonium Ion
$(NH_4)_2SO_4$	Ammonium Sulfate
ASBR	Anaerobic Sequencing Batch Reactor
BOD	Biochemical Oxygen Demand
μ	Biomass Growth Rate
$CaSO_4.2H_2O$	Calcium Sulfate Dihydrate
CO_2	Carbon Dioxide
CPU	Central Processing Unit
COD	Chemical Oxygen Demand
Cl_2	Chlorine
ClO_2	Chlorine Dioxide
CPCs	Compound Parabolic Collectors
CAD	Computer-Aided Design
CAM	Computer-Aided Manufacturing
CEC	Contaminants of Emerging Concern
CSTR	Continuous Stirred-Tank Reactor
Cu/Fe	Copper–Iron
K_2HPO_4	Dipotassium Phosphate
DBP	Disinfection By-Product
DOC	Dissolved Organic Carbon
DO	Dissolved Oxygen
DOM	Dissolved Organic Matter
$EDDS^{\bullet 3-}$	EDDS Radical
EfOM	Effluent Organic Matter
EDDS	Ethylenediamine-N,N′-Disuccinic Acid
EDTA	Ethylenediaminetetraacetic Acid
OMf	Fast Reacting Fraction of Organic Matter
PTFE	Filters
FEM	Finite Element Method
FPs	Flat Collector Reactors
F_2	Fluorine
FDA	Food And Drug Administration
FFF	Fused Filament Fabrication

GSA	Global Sensitivity Analysis
$g\text{-}C_3N_4$	Graphitic Carbon Nitride
HPLC	High Performance Liquid Chromatography
H_2O_2	Hydrogen Peroxide
$HO_2^{-\bullet}$	Hydroperoxyl Radicals
OH^-	Hydroxide Ion
$HO^\bullet$	Hydroxyl Radicals
HOCl	Hypochlorous Acid
IOD	Initial Ozone Demand Compounds
F	Inlet Flow Rate
IOD	Instantaneous Ozone Demand
MX_1, MX_2	Intermediates Organic Matter
$FeSO_4\_7H_2O$	Iron Sulfate Heptahydrate
$Fe(OH)_2$	Iron (II) Hydroxide (Ferrous Hydroxide)
Fe^{2+}	Iron (II) Ion
$Fe^{2+} - EDDS$	Iron (II)-EDDS Complex
$Fe(OH)_3$	Iron (III) Hydroxide
Fe^{3+}	Iron (III) Ion
$Fe_2(SO_4)_3$	Iron (III) Sulfate
$Fe^{3+} - EDDS$	Iron (III)-EDDS Complex
$Fe^{3+} - EDDS_{OX}$	Iron (III)-EDDS Complex (Oxidized)
LHS	Latin Hypercube Sampling
LED	Light Emitting Diode
LSA	Local Sensitivity Analysis
$MgSO_4$	Magnesium Sulphate
MATLAB	Matrix Laboratory
MBR	Membrane Bioreactor
MCs	Microcontaminants
MBBR	Moving Bed Biofilm Reactor
nZVI	Nanoscale Zero-Valent Iron
NOM	Natural Organic Matter
NO_3^-	Nitrate
Fe^{3+}-NTA	Nitrilotriacetic Acid Complex (Iron(Iii))
NRMSE	Normalized Root Mean Square Errors
ODEs	Ordinary Differential Equations
OM	Organic Matter
$ROO^\bullet$	Organic Peroxyl Radicals
Kla	Overall Gas-Liquid Mass Transfer Coefficient
OXF WWTP	Oxford Wastewater Treatment Plant
ICX	Oxidized Inorganic Carbon
MX	Oxidized Organic Matter
O_2	Oxygen
O_3	Ozone
PCT	Paracetamol

M	Parent Compound
PDEs	Partial Differential Equations
PRCC	Partial Rank Correlation Coefficient Index
PCP	Pentachlorophenol
MnO_4^-	Permanganate
$S_2O_8^{2-}$	Persulfate
PC	Polycarbonate
PLA	Polylactic Acid
PVA	Polyvinyl Alcohol
RPR	Raceway Pond Reactors
RFC	Radical Forming Compounds
RS	Radical Scavengers
RAM	Random-Access Memory
Xr	Recycled Biomass
RME	Recycled Mill Effluent
RMSE	Root Mean Square Error
R^2	R-Square (Determination of a linear regression)
SA	Sensitivity Analysis
SBBR	Sequencing Batch Biofilm Reactor
SWW	Slaughterhouse Wastewater
OMs	Slow Reacting Fraction of Organic Matter
Xr	Sludge Biomass
$NaHCO_3$	Sodium Bicarbonate
S	Substrate
SMX	Sulfamethoxazole
$SO_4^{-\bullet}$	Sulfate Radicals
H_2SO_4	Sulfuric Acid
$O_2^{-\bullet}$	Superoxide Radical
TC	Target Contaminant
C_i	The Concentrations
V	The Total Volume
TGA	Thermogravimetric Analysis
TiO_2	Titanium Dioxide
TIC	Total Inorganic Carbon
TN	Total Nitrogen
TOC	Total Organic Carbon
UV	Ultraviolet Radiation
UV-B	Ultraviolet Radiation with A Range Of 280-315 Nm
UV-C	Uutraviolet Radiation with A Range Of 200-280 Nm
W3	Wastewater Completely Biodegradable
W2	Wastewater Partially Biodegradable
WWTPs	Wastewater Treatment Plants
W1	Wastewater with Non-Biodegradable Contaminants
w/v	Weight by Volume

Chapter 1: Introduction, Objectives and Thesis Scope

This chapter outlines the current state and future challenges for the treatment of recalcitrant compounds (section 1.1) and integrated management of wastewater treatment plants (WWTPs) considering advanced oxidation process and biotreatment (section 1.2) with the specific focus on the mathematical modeling of WWTPs (section 1.3). The research motivation and its objectives are described in section 1.4 and section 1.5, respectively, that provide the overview of the research. Finally, section 1.6 includes an outline of the remaining chapters of the thesis.

1.1 WASTEWATER TREATMENT PROCESSES: CURRENT STATE AND FUTURE CHALLENGES FOR THE TREATMENT OF RECALCITRANT COMPOUNDS

In recent decades, the issue of water scarcity has become a prominent global concern as one of the results of climate change in the role of a major threat. Taking into account that over 80% of the wastewater generated by society flows back into the ecosystem without being treated or reused, projections indicate that approximately a 40% global water supply shortfall and over 700 million of the world's population will be displaced by intense water scarcity by the year 2030 (Lal, 2019). The National Academy of Engineering has identified the provision of access to potable water as one of the grand challenges within the field of engineering (Mihelcic et al., 2016).

This in turn has triggered a growing interest into wastewater recycling and the acceptance of recycled wastewater for consumption. However, WWTPs are designed to remove organic matter, phosphorus, and nitrogen but not other pollutants such as contaminants of emerging concern (CECs) (Fernández-López et al., 2021). CEC is the term to describe pollutants that have been detected in environmental monitoring samples, that may cause ecological or human health impacts, and typically are not regulated under current environmental laws. CECs are synthetic or natural substances, which are biorecalcitrants to conventional biological processes applied in WWTPs from point and nonpoint sources and end up in the water environment (Bacci and Campo, 2022). The abatement of CECs is increasingly considered by both the scientific community and the society as an important challenge due to issues like

toxicity and low biodegradability. In recent years, a diverse variety of CECs, also can be found as emerging microcontaminants (MCs) in low concentrations from ng.L^{-1} to µg.L^{-1}, have been detected in surface water, drinking water, subsurface water, and effluent/wastewater, including common household chemicals and industrial additives (Kumar et al., 2022). Since many municipal WWTPs are not designed to completely remove certain CECs and/or MCs, as a result, these compounds may persist in treated effluents, potentially posing environmental and public health concerns. This calls attention for an up-to-date regulation with scientific innovations and developing advanced processes to address properly the removal of CECs.

1.1.1 Advanced oxidation processes (AOPs)

One of the most promising technologies for the degradation of CECs is advanced oxidation processes (AOPs), capable of removing broad ranges of contaminants is necessary. AOPs using hydroxyl radicals ($HO^{\bullet}$) and other oxidative radical species are being extensively studied as a solution for the removal of organic compounds from various waste streams. The versatility of AOPs is also enhanced by the fact that they offer different possible processes for $HO^{\bullet}$ generation, thus allowing better compliance with the specific treatment requirements (Cheng et al., 2016). The following processes are the general AOPs as shown in Figure 1-1.

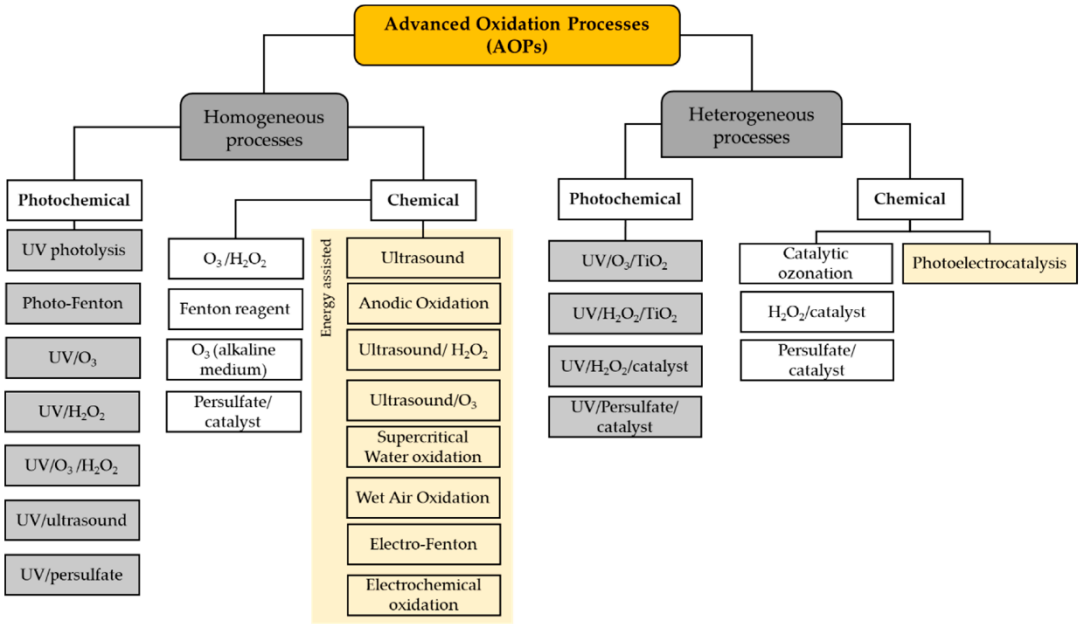

Figure 1-1 The classification of employed AOPs (Amor et al., 2019)

Table 1-1 denote that advantages and disadvantages of advanced oxidation process.

Table 1-1 Advantages and disadvantages of advanced oxidation process (Saravanan et al., 2022).

AOPs	Pros	Cons
(Photo) Fenton oxidation	• High organic removal • High performance • H_2O_2 breaks easily • Operated at room temperature and pressure	• More ferrous sludge produced • Complex pH • Risk in storage and handling reagents
Ozone oxidation	• Higher oxidation potential compared to chlorine. • Powerful oxidizer • Inhibits both bacteria and fungus • Renewable source	• High concentration dosage required • Expensive • Complex process
Electrochemical Oxidation	• Removes highly toxic compounds • No hazardous by-product • Novel contaminants treated • No additional catalyst is needed	• Energy source needed • Electrode's maintenance • Time-consuming
Photolysis and photocatalysis	• Uses natural energy source • Low catalyst used • Minimal cost • High physical stability	• Low pH needed • Difficulty in isolation of catalyst • Poor selective adsorption
Radiation	• High-power accelerator • UV radiation induces vitamin D synthesis • Used in hydroponics cultivation • Stronger disinfectan	• Heavy metals should be physically removed • Continuous power supply needed

Table 1-1 (Continued)

AOPs	Pros	Cons
Sonolysis		
	• No chemicals used • Medicals drugs removed • Short time reaction	• Machines undergoes tear and wears • Low efficiency • High cost
TiO_2 Catalytic Oxidation		
	• Nanoscale TiO_2 cannot be directly used • Higher contamination adsorption	• Insufficient purity • Better when mixed with metal oxides
UV/H_2O_2		
	• Highly intensive reaction • H_2O_2 dissolves quickly	• High turbidity • Increases nitrate concentration
UV/HOCl		
	• Kills 99% of the microbes • Chlorine-resistant microbes removed • FDA-approved method	• High power supply
Hydroxyl Radical-Based		
	• Most oxidative compounds • Treats oil waste • Reduces odor	• Acidic pH • Catalyst required
Sulfate Radical-Based		
	• Effective against organic coagulants • Degrades triclosan	• Increased salinity

Among all AOPs, the photo-Fenton process and ozonation (highlighted in Table 1-1) are two processes that play a crucial role in the removal of CECs in wastewater treatment (Salimi et al., 2017). Their importance stems from their effectiveness in addressing persistent organic pollutants and emerging contaminants that may not be adequately removed by conventional treatment methods. The photo-Fenton process, which combines hydrogen peroxide (H_2O_2) with iron catalysts activated by UV or sunlight, generates highly reactive hydroxyl radicals ($HO^{\bullet}$). These radicals exhibit exceptional oxidative power, leading to the degradation of MCs (Trovó et al., 2009). $HO^{\bullet}$ as non-selective radicals are an extremely reactive species, with the redox potential of 2.80 V that attack most of the organic molecules to destroy and even mineralize them to some extent. The Fenton-based processes often require acidic pH adjustment under reaction conditions.

In the context of wastewater treatment using AOPs, there are certain drawbacks associated with conventional Fenton processes and ozonation as listed in Table 1-1, detailed as follows:

- More Ferrous sludge produced and expensive reagents:

In traditional Fenton processes, the generation of ferrous sludge can be a concern. This sludge can be challenging to handle and dispose of, leading to environmental considerations and operational issues. The photo-Fenton process with flexible hydrogen peroxide dosage may offer a more controlled approach, potentially mitigating the formation of excess ferrous sludge and allowing for more controlled use of reagents without compromising treatment efficiency (Chapter 4).

- pH adjustment:

Conventional Fenton processes often require careful pH adjustment. This adjustment can be an additional operational step, and maintaining a specific pH range may pose challenges. Consequently, the possibility of performing the photo-Fenton process at near-neutral pH has been studied using different strategies (Chapter 5).

- Solar light activation:

Utilizing solar light to activate the photo Fenton process can significantly reduce energy costs and contribute to a more sustainable and economically viable wastewater treatment solution. The photo-Fenton reactors employing solar light indicates an exploration of environmentally friendly and sustainable options. This approach aims

to address issues related to the photo Fenton limitations while incorporating sustainable practices in wastewater treatment (Chapter 8).

The focus on the photo-Fenton process demonstrates a strategic response to the limitations associated with conventional Fenton oxidation.

On the other hand, ozone (O_3) is a powerful oxidant that readily reacts with a wide range of contaminants, breaking down their chemical structures. This makes it effective in degrading complex organic compounds (Li et al., 2019). The decision to investigate ozone decay in secondary effluent containing organic matter (Chapter 6 of the thesis) likely stems from a desire to overcome or mitigate the limitations associated with ozonation, including high concentration dosage requirements, expense, and process complexity. The research may contribute valuable insights to improve the efficiency and cost-effectiveness of ozonation as a water treatment method. The limitations of ozonation are explained as follows:

- High concentration dosage required:

Ozonation often demands the use of ozone at high concentrations to effectively treat wastewater, especially when dealing with organic pollutants. This requirement can lead to challenges in handling and controlling these high concentrations, posing safety concerns and potentially increasing operational costs.

- Expensive:

Ozone generation is an expensive process. The equipment and energy needed for ozone production contribute to high operational costs. Additionally, the cost of maintaining and ensuring the efficient operation of ozonation facilities can be significant, making it a relatively costly water treatment method.

- Complex process:

Ozonation is known for its complexity, requiring precise control of various parameters such as contact time, pH, and temperature. The complex nature of the process demands sophisticated equipment and monitoring systems. The complexity can pose challenges in terms of reliability, ease of operation, and the expertise required for successful implementation. This complexity may limit the widespread applicability of ozonation, particularly in settings with limited technical resources.

Other radicals and active oxygen species generated in AOPs are superoxide radical anions ($O_2^{-\bullet}$), hydroperoxyl radicals ($HO_2^{-\bullet}$), sulfate radicals ($SO_4^{-\bullet}$), and organic peroxyl radicals ($ROO^{\bullet}$). The standard reduction potentials of commonly used oxidants are tabulated in Table 1-2.

Table 1-2 Comparison of standard reduction potentials of commonly used oxidants (Oh et al., 2016)

Oxidant	**Oxidation Potential, E0 (V)**
Fluorine (F_2)	2.87
Hydroxyl radical ($HO^{\bullet}$)	2.80
Sulfate radical ($SO_4^{-\bullet}$)	2.60
Ozone (O_3)	2.08
Hydrogen peroxide (H_2O_2)	1.78
Persulfate ($S_2O_8{}^{2-}$)	2.12
Permanganate ($MnO_4{}^{-}$)	1.68
Chlorine dioxide (ClO_2)	1.57
Chlorine (Cl_2)	1.36

However, large-scale applications of AOPs in water and wastewater treatment are still very limited due to factors such as the radical conversion, location, delivery, operating mode and cost that require further exploitations for the scalability (Mahbub and Duke, 2023).

1.1.2 Biological treatment processes

Since biological processes are typically less expensive than chemical processes, addition of a biodegradation stage can improve the economy of the overall process, particularly for high polluted wastewater (Oller et al., 2011a).

Several biological treatment processes including activated sludge and membrane bioreactor (MBR) commonly employed for removal of the CECs in wastewater, where basically microorganisms digest and break down organic pollutants through the biological degradation process. It is effective in treating a broad range of organic pollutants, including some of the CECs, by providing an environment conducive to the growth of diverse microbial communities capable of metabolizing complex substances (Kim et al., 2018). These biological treatment processes leverage the metabolic capabilities of microorganisms to break down and transform recalcitrant compounds into less harmful or more easily treatable forms, contributing to the overall effectiveness of wastewater treatment.

However, in certain instances, traditional biological methods may not yield optimal outcomes, particularly in the treatment of industrial wastewater. This is due to

the fact that numerous organic substances generated by the chemical industry exhibit toxicity or resilience against conventional biological treatment. Therefore, the main role of the chemical pre-treatment is partial oxidation of the biologically persistent part to produce biodegradable reaction intermediates (Oller et al., 2011a).

The choice of the appropriate treatment method, either biological or chemical, depends on the specific characteristics of the wastewater and the nature of the recalcitrant compounds present.

1.2 INTEGRATED MANAGEMENT OF WASTEWATER TREATMENT PLANTS (WWTPS): ADVANCED OXIDATION PROCESS AND BIOTREATMENT

Water management is one of the most important issue from several points of view such as development of water bodies for future, protection of available water resources from pollution and over exploitation and to prevent disputes. The implementation of integrated systems in the wastewater treatment processes, which is an engineering combination of physical, chemical, and biological methods, can improve the overall efficiency of the WWTPs in terms of economic cost and environmental regulation.

As mentioned in the section 1.1, the CECs with high chemical stability and/or low biodegradability (e.g., emerging contaminants: pharmaceuticals, cosmetics, and personal care products) cannot be efficiently addressed by common WWTP. Conversely, AOPs can oxidize a broad range of non-biodegradable from wastewaters by means of highly oxidant radicals. However, such chemical oxidation for complete mineralization is much more expensive, which limits large-scale applications. Hence, combining AOPs with biological treatments has been reported as an opportunity to reduce design and operating costs (Huang et al., 2017; Oller et al., 2011a). Several configurations of hybrid AOPs as pre-treatment or post-treatment with bioremediation for wastewater treatment have been experimentally studied (Nidheesh et al., 2021). However, the design and operation of such a hybrid process require suitable models. A great deal of mathematical models for WWTP have been developed and reported (Gernaey et al., 2004), while not many works have addressed the modeling of AOPs. Models combining AOPs and bio-processes have hardly been discussed (Nasr Esfahani et al., 2021; Zimbron and Reardon, 2011). The modeling needs, and perspectives of AOPs and WWTP are different, as well as it is the nomenclature and

the lumped parameters selected to characterize the system. This may explain the divergence of the research efforts of both areas, as well as the problems that converging them to a unique hybrid model entail (Nasr Esfahani et al., 2021).

1.3 MATHEMATICAL MODELING OF AOPs

Mathematical models are increasingly being used to examine the potential impacts of processes reducing the number of practical experiments. Models can also be used to compare alternative management scenarios intended to reduce waste emissions into the environment. Models are more beneficial where measurements of variables cannot easily be obtained. In practical scenarios, the use of an experimental approach often encounters significant limitations, demanding the exploitation of mathematical models. Some illustrative instances of these constraints are provided below (Jeppsson, 2012).

- Excessive Cost: Launching rockets to the moon until achieving a successful landing and subsequently reconstructing the same type of rocket for regular use is a costly endeavor.
- Safety Concerns: Training nuclear power plant operators directly at fully operational plants is deemed unsafe and impractical.
- Time Intensiveness: Investigating all possible combinations of mixtures, temperature, and pressure in a complex chemical process to identify the optimal combination is exceedingly time-consuming. With a limited number of experiments, a model can simulate the entire experimental domain efficiently.
- Non-existent Systems: Simulating the effects of different designs on a suspension bridge, especially in adverse conditions like high winds, is essential during the design phase when the actual system is not yet in existence.

Models can be mainly categorized as first principles models (based on physical theory), data-based models (strictly based on empirical descriptions), and semi-empirical models (based on both physical theory and empirical descriptions). It is also possible to define different types of models according to the model attributes (Guergachi and Patry, 2003):

- Stochastic or deterministic (if the model contains elements of randomness);
- Continuous models: usually based on ordinary differential equations or partial differential equations in order to represent natural phenomena;
- Discrete models: usually related to decision-making processes;
- Linear or nonlinear models (depending on whether the system of equations is linear or nonlinear);
- Steady state or unsteady state models (depending on whether the process variables are constant with time or change with time);
- Lumped parameter (described by Ordinary Differential Equations ODEs) or distributed parameter (described by Partial Differential Equations PDEs) models.

Conceptually, the investigation of complex systems using models can be divided into the following steps (Figure 1-2):

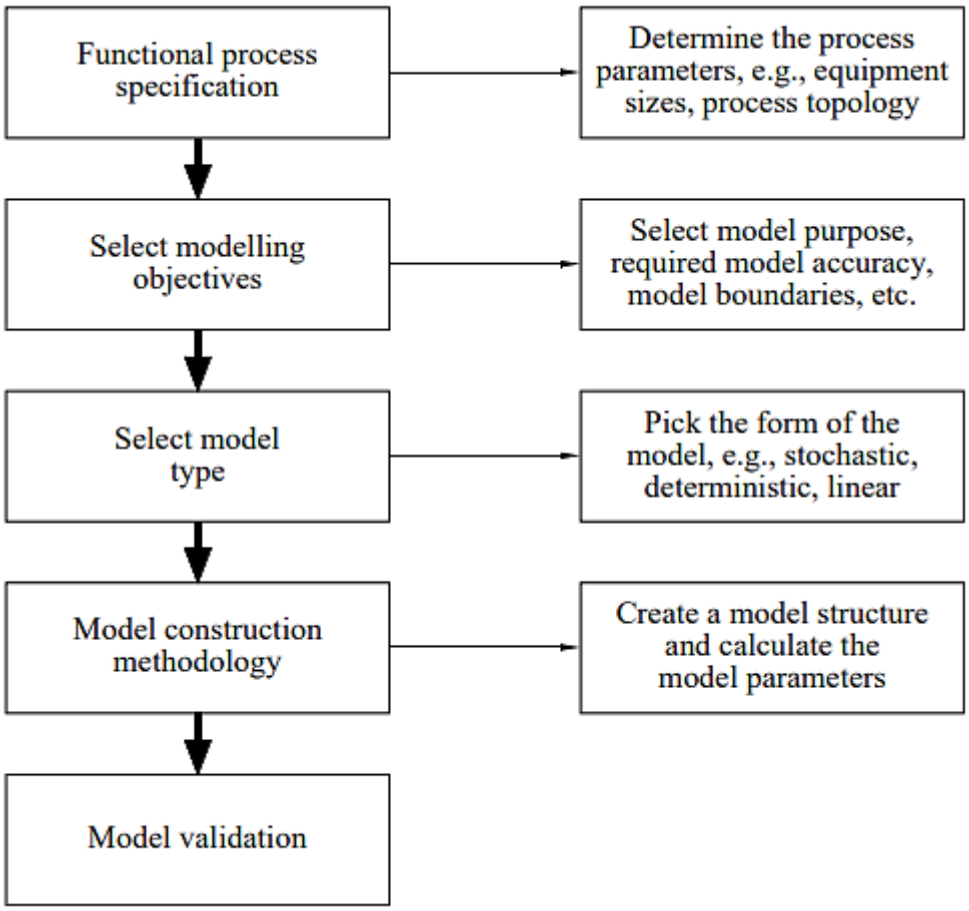

Figure 1-2 An overview of the modeling process (Jeppsson, 2012)

Within such an approach, the analytical identification provides information prior to the experimental identification procedure by means of which the parameters are estimated. It allows predicting the behavior of a system based on the variables of the system. Recent studies have emphasized improving kinetic models for AOPs to make them more accurate and useful for different types of wastewaters (Audenaert et al., 2013; Căilean et al., 2015; Kebir et al., 2023; Kusic et al., 2009; Mousset et al., 2016). The main focus is on advanced kinetics and describing the process to capture the complex interactions involved in AOPs.

1.4 MOTIVATION

The motivation of the thesis stems from the urgent challenges of wastewater treatment faces, with rapid urbanization, industrial growth, and a growing demand for water resources, which calls sustainable treatment solutions. The Ph.D. thesis focuses on the development of models for the simulation of AOPs, as well as combined models with biotreatment processes, aimed at the efficient treatment of recalcitrant organic compounds in wastewaters.

In particular, the motivation is underscored by several key considerations:

- Rising concerns over water scarcity

The escalating global concern surrounding water scarcity underscores the critical need for efficient and innovative wastewater treatment methods. As water resources become scarcer, the imperative to reclaim and reuse water through advanced technologies becomes paramount.

- Environmental impact of conventional treatment processes

Conventional wastewater treatment processes often fall short in addressing the removal of recalcitrant compounds and emerging contaminants. The motivation for this research stems from the environmental repercussions associated with incomplete removal, urging the exploration of advanced oxidation processes (AOPs) as promising alternatives.

- Advancements in AOPs and their untapped potential

The continual evolution of AOPs presents a significant motivation. Novel techniques, such as the photo-Fenton process, Fe^{3+}-EDDS mediated photo-Fenton, and ozone-based treatments, exhibit substantial potential.

- Need for sustainable and flexible treatment approaches

The motivation also arises from the recognition of the necessity for sustainable and adaptable wastewater treatment strategies. By incorporating flexible hydrogen peroxide dosages and exploring 3D printed reactors, this research aims to contribute to the development of more versatile and sustainable treatment methods.

- Application of innovative technologies for the photoreactor prototyping

The photoreactor prototyping and subsequent testing are crucial for the modeling and application of the photo-Fenton processes. Consequently, the incorporation of 3D printed reactors represents a pioneering approach, motivated by the desire to introduce innovative technologies to the field of wastewater treatment. This research is driven by the belief that such technologies hold the potential to revolutionize the efficiency and practicality of treatment systems.

In essence, the motivation behind this thesis lies in the recognition of the urgent need for advanced, sustainable, and adaptable solutions to address the complex challenges posed by contemporary wastewater treatment. By exploring the outlined objectives, this research seeks to make meaningful contributions to the field and propel the advancement of wastewater treatment practices into a more sustainable and effective future.

1.5 THESIS OBJECTIVES

The primary objective of this thesis is to advance the understanding of AOPs through mathematical modeling. The thesis specifically targets limitations associated with the dependence photo-Fenton processes on specific reagents, particularly the dosification of hydrogen peroxide; the use of iron complexing agents to enable photo-Fenton processes at circumneutral pH; and the dynamics of ozone decay as a means to provide practical monitoring of the ozonation processes of secondary effluents. A final goal is a mathematical model combining AOPs, specifically photo-Fenton, with conventional biological treatments.

The general and specific objectives of this thesis are:

1. Model flexible hydrogen peroxide dosage in photo-Fenton processes

a) Improve existing models for flexible dosage in photo-Fenton processes

b) Fit the improved model to reported experimental data on the removal of Contaminants of Emerging Concern (Paracetamol) in water solutions

c) Validate the model and quantifying its accuracy

2. Model the photo-Fenton processes with iron complexing agents

a) Develop new models including mechanisms for the complexation of iron

b) Produce experimental data for microcontaminants (Sulfamethoxazole) removal in water solutions using Ethylenediamine-N,N'-disuccinic acid (EDDS+)

c) Fit the improved model to the experimental data obtained

d) Validate the model and quantifying its accuracy

3. Model the ozonation process of water containing organic matter

a) Develop models to describe ozone decay in the treatment of secondary effluents

b) Obtaining experimental data for the ozonation of secondary effluents

c) Fit the improved model to the experimental data obtained

d) Validate the model and quantifying its accuracy

4. Model integrated processes using AOPs and standard bioprocesses

a) Develop an integration strategy mapping the variables of the two models

b) Implement and verify the consistency of the model

c) Use the integrated model to discuss alternative processing scenarios

By addressing these objectives, this research aims to contribute valuable insights, methodologies, and innovations to the field, ultimately advancing the efficiency and sustainability of wastewater treatment processes through the application of advanced oxidation techniques. Overall, these objectives collectively contribute to the advancement of wastewater treatment technologies by overcoming inherent limitations, and exploring innovative integrated approaches.

1.6 THESIS OUTLINE

The foundational section of this thesis has laid the groundwork for a comprehensive investigation into AOPs and their application in wastewater treatment. The subsequent chapters will delve into specific aspects of this research endeavor,

progressing logically from the introduction to an exploration of the state of the art, followed by a detailed account of the research design and experimental settings.

The thesis unfolds as a strategic narrative that transcends conventional wastewater treatment research. It begins by critically assessing the photo-Fenton process, identifying limitations and margins such as the need for the specific reagents (especially H_2O_2) and acidic pH adjustment as well as applying solar light in the process as Fenton-based processes can be boosted by solar light irradiation.

Chapter 4 responds innovatively by introducing a photo Fenton model with flexible hydrogen peroxide dosage, addressing some challenges for the reagent dosage and offering a pathway for enhancing the adaptability of the photo-Fenton process to varying wastewater conditions.

Expanding on the photo-Fenton theme, Chapter 5 takes a bold step by exploring the $Fe^{3+} - EDDS$ mediated photo-Fenton process at circumneutral pH, responding to another limit of the photo Fenton process. This deviation from the acidic conditions traditionally associated with Fenton-based processes represents a paradigm shift. The developed model in this chapter, incorporating a lumped radical's approach, contributes significantly to refining our understanding of reaction mechanisms and model robustness, offering insights into a more versatile and potentially less resource-intensive approach to wastewater treatment.

In Chapter 6, the focus shifts to ozone decay in secondary effluent, providing valuable insights to enhance treatment efficiency. A new kinetic model is proposed aiming at improving the ozonation process for waters containing organic contaminants, with a particular focus on the initial ozone decomposition stage often overlooked in existing literature models. Understanding this initial stage is critical due to ozone's instability and rapid decomposition.

The integration journey continues in Chapter 7, introducing the concept of combining AOPs with biological treatments. Key findings from case studies demonstrate the potential synergy between these approaches for more effective wastewater decontamination.

Chapter 8 takes an innovative leap by exploring 3D printed photo Fenton reactors, bridging theoretical insights with practical application. As Fenton-based processes can be boosted by different ways such as applying solar light, the design and

fabrication process along with experimental assessments of 3D printed photo Fenton reactors are studied to explore the potential synergies between innovative reactor design and the enhanced efficacy of the photo Fenton process under various external stimuli. This chapter not only aligns with the theoretical insights gained from previous chapters but also propels the research into the realm of practical application. The design and fabrication process, along with experimental assessments and comparisons with conventional counterparts, underscores a forward-thinking approach to advancing wastewater treatment methodologies. The summary of each chapter in detail is presented as follows:

- In chapter 2 containing the literature review upon the established context, it will provide an extensive review of existing literature, elucidating the current landscape of wastewater treatment techniques with a focused examination of AOPs. This chapter will critically evaluate the photo-Fenton process, Fe^{3+}-EDDS mediated photo-Fenton, and the ozonation process in wastewater, offering insights into recent advancements and identifying gaps in the existing knowledge.
- Chapter 3 outlines the mathematical tools utilized to convert the acquired data into information and knowledge during the subsequent stages of modeling and sensitivity analysis of AOPs. The methodology and research design in this thesis is carefully presented in each chapter.
- Chapter 4 will focus on the modeling aspects of the photo-Fenton process, with a particular emphasis on the incorporation of flexible hydrogen peroxide dosage. This section aims to develop mathematical models, validate and calibrate them against experimental data, and subsequently discuss the obtained results and their implications for wastewater treatment.
- Building on the insights gained in Chapter 4, Chapter 5 will revisit the mechanistic modeling of $Fe^{3+} - EDDS$ mediated photo-Fenton, incorporating a lumped radical's approach and conducting sensitivity analyses. This chapter seeks to refine our understanding of reaction mechanisms and assess the robustness of the developed models.
- Chapter 6 provides valuable insights into the dynamics of ozone decomposition in wastewater treatment processes by incorporating the

critical stage of ozone fast decomposition into the semi-empirical mathematical model proposed. Through mathematical modeling and experimental validation, this chapter aims to unravel the factors influencing ozone decay, providing valuable insights into enhancing treatment efficiency.

- Chapter 7 provides a concise introduction to the concept of integrating AOPs and biological treatments for wastewater decontamination. The key findings are discussed from the integration of AOPs and biological treatments considering the case studies including the combined photo-Fenton process and biotreatment (different configurations) as well as the biological treatment followed by the ozonation unit.
- Chapter 8 introduces a novel dimension to the research by exploring the manufacturing and application of 3D printed photo Fenton reactors. This chapter will detail the design and fabrication process, assess the performance of these reactors experimentally, and compare them with conventional counterparts.
- The final chapter, Chapter 9, will synthesize the findings from the preceding chapters. It will offer a summary of the study's contributions, discuss their implications for the field, acknowledge the study's limitations, and provide recommendations for future research. This conclusive chapter aims to not only recapitulate the research journey but also to chart a course for further advancements in the realm of advanced oxidation processes for wastewater treatment.

Chapter 2: State of the Art

The literature review in this chapter examines key topics related to the removal of recalcitrant compounds in wastewater, focusing on both contaminants of emerging concern (CECs) (section 2.1) and advanced oxidation processes (AOPs) (section 2.2). Additionally, it delves into the application of mathematical modeling and sensitivity analysis for wastewater treatment processes, with a specific emphasis on AOPs and biotreatment (section 2.3). Furthermore, considerations for integrated modeling in the context of combined AOPs and biological treatment processes are explored (section 2.4). Finally, Section 2.5 highlights the implications from the literature and develops the conceptual framework for the study.

2.1 RECALCITRANT COMPOUNDS IN WASTEWATER: BIOLOGICAL TREATMENT PROCESSES

Although wastewaters contain a multitude of contaminants, yet they can be broadly grouped under different classes on the basis of their chemical structure. There are currently more than 350,000 chemicals registered for production and use that might occur in wastewater. It is very important to decide which pollutants deserve more attention in wastewater in terms of concentration and toxicity as considered in the choice of priority pollutants (He et al., 2023). Enhancements in wastewater treatment are imperative to address challenges arising from the accumulation of persistent and emerging contaminants in natural water ecosystems.

Several studies dealt with the removal of the recalcitrant compounds from wastewater employing biological (Wang et al., 2022) and physio-chemical methods including zeolite or humic acid (Lin et al., 2022), Cu/Fe bimetallic system (Wu et al., 2022), nanoscale zero-valent iron (nZVI) co-modified g-C_3N_4-based photocatalyst (Liu et al., 2022), modified membrane (Zhang et al., 2023), and AOPs among others. AOPs have emerged as promising strategies, leveraging reactive oxidants to degrade persistent contaminants which is reviewed specifically in section 2.2. Above all, the integration of biological treatments has shown promise in addressing recalcitrant compounds as the selection of these techniques is contingent upon the specific attributes of the wastewater under consideration.

In case of the biological treatment of recalcitrant compounds, Wang et al. (2022) studied nitrogen removal from pharmaceutical wastewater characterized by high organic matter and nitrogen content using an anaerobic sequencing batch reactor (ASBR) combined with a modified sequencing batch biofilm reactor (SBBR). The removal efficiencies of treated effluent for chemical oxygen demand (COD), $NH_4^+ - N$, and total nitrogen (TN) were greater than 93.5, 99, and 96%, respectively (Wang et al., 2022). As another example of the biotreatment wastewater containing the recalcitrant compounds, Moloantoa et al. (2023) devised a bioremediation strategy for nitrate removal from mine wastewater with high concentration of NO_3^- . Although nitrate is mainly biodegradable, the addition of copper in the presence of iron co-factors significantly enhanced denitrification, achieving complete removal of over 500 $mg.L^{-1}$ of NO_3^- in the treated wastewater (Moloantoa et al., 2023).

While biological treatment is commonly employed for wastewater recovery, primarily driven by economic considerations, it often necessitates complementing treatment processes including coagulation, electrocoagulation, membrane processes, adsorption, and AOPs to effectively break down non-biodegradable or persistent pollutants (Santiago et al., 2023). Although these processes contribute to pollutant removal, each has its set of challenges, such as the generation of sludge, operational complexities, or limited efficacy against certain contaminants. This calls attention to develop technologies with the capacity to target a broad spectrum of contaminants, overcoming some of the drawbacks associated with conventional and supplementary methods.

2.1.1 Emerging microcontaminants (MCs) in wastewater

"Recalcitrant compounds" and "Emerging microcontaminants " are terms commonly used in the context of water and wastewater quality. While there is some overlap in their meanings, they are not entirely synonymous. Recalcitrant compounds refer to substances that are resistant to decomposition or breakdown by biological, chemical, or physical processes. These compounds are often persistent and challenging to remove using conventional water treatment methods. Emerging microcontaminants (MCs) are synthetic or natural substances, which are biorecalcitrants to conventional biological processes applied in wastewater treatment plants (WWTPs). MC term includes a large range of chemical compounds that present very different chemical natures hindering their removal. Usually, they are emitted from point and nonpoint

sources and end up in low concentrations from $ng.L^{-1}$ to $\mu g.L^{-1}$ in the water environment (Chavoshani et al., 2020).

MCs are a group of pollutants that have recently gained attention due to their potential environmental impact, even though they might not have been traditionally monitored or regulated. These contaminants are often associated with human activities and can include a wide range of substances. MCs encompass various pollutants, such as pharmaceuticals, personal care products, pesticides, and industrial chemicals, which may persist in the environment and pose potential risks to ecosystems and human health. The term emphasizes the low concentration levels rather than specific chemical properties. In summary, while MCs compounds may be a subset of recalcitrant, and both may be considered microcontaminants, the terms are not interchangeable. Each term provides a different perspective on specific characteristics or concerns related to water quality and pollution. Hence, the escalating concern about exposure to chemical mixtures that emphasizes the complexity surrounding organic micropollutants, highlighting the command and control measures continue to be the most effective approach for tackling emissions of organic MCs (Bacci and Campo, 2022).

2.2 APPLICATION OF AOPS FOR RECALCITRANT COMPOUND REMOVAL IN WWTPS

A wide range of wastewater treatment processes are available, however the continuous search for cost-effective treatment methods is necessary to comply with the legal limits of release in sewer systems and in natural waters, and AOPs present a distinct advantage in this context. AOPs, including photocatalysis, Fenton reactions, UV/hydrogen peroxide treatment, and ozonation, offer a comprehensive and versatile approach to wastewater treatment. They excel in efficiently degrading recalcitrant compounds, providing a more robust solution to persistent pollutants. Their efficacy in the removal of complex pollutants positions them as a promising and innovative choice for enhancing wastewater treatment processes (Amor et al., 2019).

AOPs, which involve the generation of highly reactive radicals such as the $HO^{\bullet}$, in sufficient quantity to influence water purification, have been productively explored for the elimination of a wide variety of recalcitrant and toxic compounds with the purpose of reducing toxicity and increasing biodegradability (Amor et al., 2019; Oh et al., 2016). The AOPs have been also applied across various scales for diverse purposes, including the degradation of the specific pollutants and MCs (Wardenier et al., 2019),

mineralization of organic matter (Yang et al., 2022), water disinfection (Chen et al., 2021), enhanced sludge dewatering and micropollutants removal (W. Lin et al., 2022), and the removal of color and deodorization (Dębowski et al., 2022).

The following section delves into a more detailed analysis of the processes employed in this study, most notably, the Fenton/photo-Fenton processes and Ozonation. Although both the Fenton/photo-Fenton processes and ozonation offer superior capabilities in the removal of persistent pollutants, making them standout choices in the realm of AOPs for wastewater treatment, the Fenton and photo-Fenton processes serves as the primary focus of the current research.

2.2.1 Fenton and photo-Fenton

Fenton process constitutes the chemical generation of the highly strong oxidant hydroxyl radicals through the Fenton reaction involving hydrogen peroxide and ferrous ion in acidic medium. This radical is able to mineralize organic compounds completely, even though they are persistent in nature. According to Eq.2-1, free hydroxyl radicals may arise concurrently without light, and the Fe^{2+} catalyst can be regenerated (Ganiyu et al., 2022):

$$Fe^{2+} + H_2O_2 \rightarrow Fe^{3+} + OH^- + HO^{\bullet} \quad (k= 63.0\text{-}76.0\ L.mol^{-1}.s^{-1}) \quad \text{Eq.2-1}$$

However, higher ferrous ion concentration, sludge generation and cost of hydrogen peroxide limited real field application of Fenton process (Masood et al., 2023). Extended Fenton processes such as electro-Fenton, sono-Fenton and photo-Fenton rectifies the drawbacks of Fenton processes significantly. The photo-Fenton process is a photocatalytic process that generates $HO^{\bullet}$ by interacting chemical reagents (Fe (II) salt and H_2O_2) between the resulting Iron (III) and UV irradiation light source, which causes a synergic effect by creating a higher rate of $HO^{\bullet}$ production. Application of UV light irradiation in Fenton process improves its efficiency by the generation of additional hydroxyl radicals via photolysis of water and H_2O_2 (Eq. 2-2 and Eq. 2-3) and enhancing ferrous ion regeneration rate (Eq. 2-4) (Ganiyu et al., 2022).

$$Fe^{3+} + H_2O + h\nu \rightarrow HO^{\bullet} + Fe^{2+} + H^+ \quad (k= 0.01\text{-}0.02\ mol^{-1}.s^{-1}) \quad \text{Eq. 2-2}$$

$$H_2O_2 + h\nu \rightarrow 2HO^{\bullet}\ (h\nu < 300nm) \quad \text{Eq. 2-3}$$

$$Fe(OH)_2 + h\nu \rightarrow Fe^{2+} + HO^{\bullet}\ (h\nu < 450\ nm) \quad (\varphi= 0.21\ mol\ Einstein^{-1}) \quad \text{Eq. 2-4}$$

The photo-Fenton reaction (Equation 2.4) is described by a quantum yield (the ratio of the number of photons emitted to the number of photons absorbed) $\varphi = 0.21$ mol. Einstein^{-1}.

Fenton and photo Fenton oxidation processes were examined to determine whether it may increase the biodegradability of a biologically treated pharmaceutical effluent. This process has been used to achieve a variety of goals in recent decades, including final polishing, reduction of high percentages of organic load in terms of chemical oxygen demand or total organic carbon, and removal of recalcitrant and toxic pollutants, allowing for further biological treatment. The effectiveness and applicability of the Fenton process have been proved with effluents from a variety of chemical and related industries and activities, including pharmaceutical (Oller and Malato, 2021), pulp and paper (Dogan et al., 2021), textile (Kumar Shivappa Masalvad and Kumar Sakare, 2021; Sarı et al., 2023), food (Sánchez Peréz et al., 2014), cork processing, and landfilling (Wang et al., 2003), pesticide (Çokay and Eker, 2022), and many others (Ribeiro and Nunes, 2021). The Fenton and photo-Fenton processes is also widespread for treating different types of MCs in wastewaters (Behrouzeh et al., 2022; Gamarra-Güere et al., 2022; Guadalupe Pinna-Hernández et al., 2023; Traid et al., 2022).

Accordingly, the Fenton-based treatment is a well-known solution for treating non-biodegradable contaminants in wastewaters that cannot be treated with conventional bio-processes (Oller et al., 2011a). It has gotten a lot of interest because of its broad range of target chemicals, robust oxidation capabilities, and rapid response pace (Lu et al., 2010).

The various factors such as pH, hydrogen peroxide dosage, initial pollutant concentration and presence of additional ions which vary accordingly have a great impact on the efficiency of the Fenton and photo Fenton processes.

The usage of catalyst in the Fenton-based process extends the range of pH. At higher pH unstable ferrous ions are stabilised as ferric ions and at alkaline pH hydrogen per oxide breaks down as oxygen and hydrogen thereby losing its oxidative nature. These changes are found to be observed because the pH influences the physicochemical properties of the catalyst used to aid the reaction. It is suggested to conduct a pre-treatment before Fenton processes (Saravanan et al., 2022).

The pH-dependency of the process due to the insolubility of the ferric aquo or hydroxy species at circumneutral pH, limits its full-scale application due to the necessity of acidic pH. Consequently, the possibility of performing the photo-Fenton process at near-neutral pH (See chapter 5) has been studied using different strategies (Carra et al., 2014; Villegas- Guzman et al., 2017).

On the other hand, the hydroxyl radical is exceedingly unstable and non-selective, so it is frequently scavenged by unwanted secondary reactions, some of them involving H_2O_2 consumption, which cut down the efficiency of the process (Gulkaya et al., 2006). Hence, it is critical to control the optimal reaction conditions for complete mineralization of the target compound, i.e., the dosage of H_2O_2. The reaction rate and process efficiency are both affected by H_2O_2, which is the most expensive reagent (Lu et al., 2011). In this regard, researchers have studied the photo-Fenton process with the dosage of Hydrogen peroxide to enhance process performance (Yu et al., 2020). More details on the dosage of Hydrogen peroxide in the photo Fenton process is presented in chapter 4.

Nevertheless, additional research and development are essential for numerous applications of the photo-Fenton processes in the treatment of various wastewaters. Several factors contribute to this need:

- Dosage sterategies: The establishment of robust and efficient dosage strategies for the oxidant in the photo-Fenton process requires further investigation. The development of dosage strategy is crucial to enhance treatment efficacy and minimize costs.
- Matrix influence: Most studies to date have focused on deionized water or ultra-pure water, which may not accurately represent the complex matrices of real wastewaters. Real-world wastewaters can contain diverse substances at varying concentrations, including carbonates, humic acids, and quinones. Understanding how these components interact with the photo-Fenton process is crucial for its reliable application in practical scenarios.
- Performance enhancement: Identifying ways to enhance the performance of the photo-Fenton process is a key area for further exploration. This involves understanding how specific substances, such as quinones, can positively influence the process, potentially leading to improved treatment outcomes.

- Application specificity: Different types of wastewaters may present unique challenges and requirements for effective treatment with the photo-Fenton process. Tailoring the application of this process to specific wastewater compositions and characteristics is essential for its broad and successful implementation.
- Improved operational conditions: Beyond dosage, further work is needed to improve various operational conditions of the photo-Fenton process in terms of efficiency and cost, such as pH, temperature, and the presence of co-existing ions. Understanding the interplay of these factors is crucial for achieving consistent and reliable results across diverse wastewater scenarios.

In summary, the need for further work arises from the complexity and variability of real-world wastewaters, the desire for an improved treatment conditions, and the goal of expanding the applicability of the photo-Fenton process to a wide range of wastewater treatment scenarios. Continuous research and development efforts are necessary to address these challenges and unlock the full potential of photo-Fenton processes in wastewater treatment applications.

2.2.2 Ozonation

Ozone primarily recognized for its presence in the stratosphere, where it safeguards living organisms by absorbing UV-B and UV-C radiation. The ozonation process is a practical AOP employed for wastewater treatment, particularly, for organic matter removal from wastewater (Zhang et al., 2023). Although ozonation is reported less cost effective than the other AOPs (Mousset et al., 2021), the use of ozonation has more industrial applications compared to all other AOPs in water treatment (Krishnan et al., 2017). Ozonation involves the controlled application of ozone, a potent oxidizing agent, used in the treatment of both drinking water and wastewater, typically as a disinfection step. However, because of its high oxidizing potential, ozone also contributes to the removal or degradation of organic matter (OM) and MPs (Yargeau et al., 2023). In recent years, ozone has been increasingly applied

for enhanced municipal wastewater treatment for ecosystem protection and for potable water reuse (Beltrán, 2004).

If ozone is added to water containing dissolved organic matter, the reaction system becomes highly complex in nature. Additionally, a significant difference exists between the ozonation of natural water and secondary effluent. This is due to differences in DOC concentration and the properties of the organic matrix. If an economical ozone dose is applied to both waters using a batch reactor, the observed ozone decomposition profile will be totally different, as shown in Figure 2-1. In both systems, a phase of rapid ozone decomposition prior to 20 (s) is observed. The amount of ozone decomposed during that phase is often called initial ozone demand (IOD) and can be attributed to compounds that have very high reaction rates with ozone. During a second phase, which does not occur in secondary effluent as all ozone is consumed during phase one, a significantly slower and first order ozone decomposition takes place (Buffle et al., 2006).

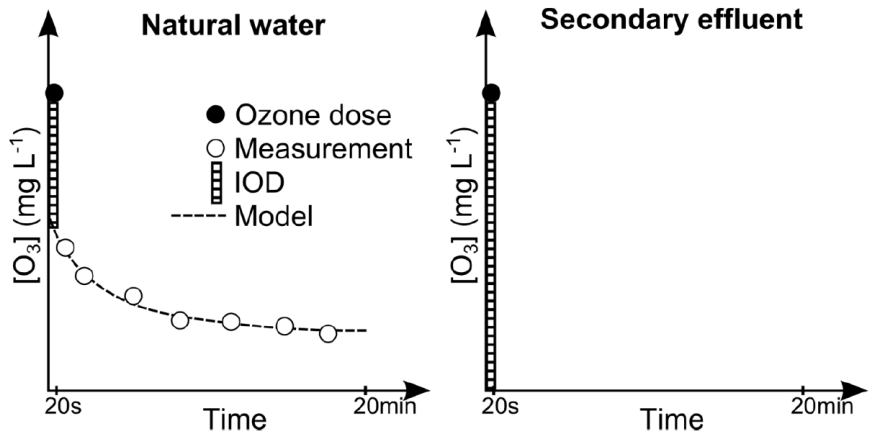

Figure 2-1 Recorded ozone degradation in a batch reactor with natural water (left) and secondary effluent (right) (Buffle et al., 2006)

As such, ozonation of secondary effluent is highly comparable to the first phase of natural water ozonation. It has to be noticed, however, that depending on the effluent composition and ozone dose applied, a second phase might be observed during ozonation of secondary effluent.

2.2.2.1 Ozonation of water and wastewater: Experimental & modeling review

$HO^{\bullet}$ production during ozonation of water that contains dissolved organic matter (DOM) is significant. For this reason, both the ozone and $HO^{\bullet}$ exposures should be known if accurate predictions of target pollutant degradations are sought. It was also

shown that ozone transformation to $HO^{\bullet}$ can be accelerated by hydrogen peroxide (H_2O_2), which opened up the possibility for ozone-based AOPs, which combine ozone and $HO^{\bullet}$ oxidation and are applicable for oxidant-resistant micropollutant abatement. The exploration of the historical development of ozonation process is crucial to provide a contextual foundation for the current study. Understanding the evolution of ozone reaction and modeling over time allows for the identification of key milestones, shifts in methodologies, and the refinement of theoretical frameworks (Figure 2-2).

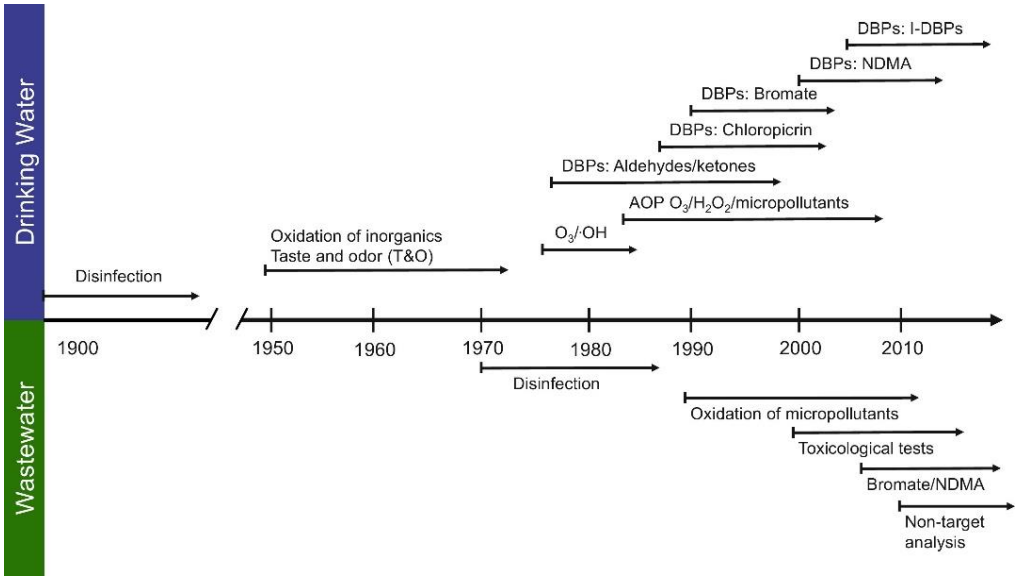

Figure 2-2 Chronology of ozone utilization in drinking water and wastewater: addressing challenges and implementing solutions (Lim et al., 2022)

Besides its major use as a drinking water disinfectant, ozone is applied for a wide variety of other applications including industrial and municipal wastewater treatment, swimming pool disinfection, cooling water treatment, groundwater remediation and water reuse (Lim et al., 2022). For over a century, ozone treatment has been utilized in water treatment, initially for disinfection and subsequently for the oxidation of both inorganic and organic pollutants. In recent times, there has been a growing use of ozone in enhancing municipal wastewater treatment for the preservation of ecosystems and facilitating potable water reuse. This expanded application has stimulated substantial research into the effectiveness of ozone in reducing organic contaminants and the subsequent formation of transformation products. Concurrently, advancements in analytical and computational chemistry have been instrumental in refining the mechanistic understanding of ozone reactions.

Ozone doses between 0.5 and 5 mg.L^{-1} can be effective for water disinfection. It is, however, likely to occur that applying these dosages does not result in a measurable aqueous ozone concentration due to the high rapid ozone demand of the effluent. For micropollutant reduction and decolorization, doses vary between 1 and 15 mg.L^{-1} and 1 and 50 mg.L^{-1}, respectively. Again, the applied dose is site dependent. In general, ozone dosages that are currently applied at full-scale plants vary between 5 and 10 mg. L^{-1} for final discharge and 10 and 15 mg.L^{-1} for reuse. Reuse requires decolorization and hence, higher dosages (Ried et al., 2009).

As a lot of literature is available on drinking water ozonation, this review section will only focus on recent developments in the application of ozone for municipal wastewater treatment and water reuse.

Similar to drinking water, ozonation has been implemented in wastewater as a disinfectant before its discharge to the receiving water bodies. However, wastewater disinfection requires quite high doses and it is expected that disinfection, including inactivation of ozone-resistant microorganisms such as protozoa, will lead to the formation of bromate above the drinking water standard of 10 µg.L^{-1} (Zimmermann et al., 2011).

Disinfection by-product formation in tertiary wastewater was reported after ozonation and advanced oxidation with O_3 and hydrogen peroxide (O_3/H_2O_2). O_3 and O_3/H_2O_2were applied at multiple dosages to investigate DBP formation during coliform disinfection and trace contaminant oxidation. Results showed O_3 provided superior disinfection of fecal and total coliforms compared to O_3/H_2O_2 (Wert et al., 2007).

Ozonation was selected as the oxidation process of choice for enhanced wastewater treatment in Switzerland and in other countries, because of the broad spectrum of MCs which can be abated during ozonation. It was shown that biologically active compounds such as estrogens, antibiotics, antivirals and pesticides lost their primary target effects during ozonation and other AOPs in laboratory in vitro studies (Lim et al., 2022). Then, the application of ozonation process has been further studied for MCs removal from the municipal wastewater effluents including pharmaceuticals (Huber et al., 2005), organic matter (Lee and von Gunten, 2016), and particularly, different sets of MCs (Lee et al., 2014, 2013; Van Gijn et al., 2022).

In the context of municipal wastewater treatment, the degradation of OM through ozonation has been investigated experimentally in several studies as an extra treatment stage for the secondary effluent, followed by sand filtration (Fallah et al., 2023).

This effort was supported by advancements in kinetic considerations, mathematical modeling, and computational chemistry, contributing to an enhanced mechanistic understanding of ozone reactions. The kinetics of ozone decomposition are often faster compared to other reactions involved in wastewater treatment. Ozone reacts rapidly with organic and inorganic substances, and understanding the kinetics of ozone decomposition provides crucial insights into the overall reaction rates and dynamic of the treatment process.

The history of modeling ozonation in water and wastewater treatment traces its roots to the mid-20th century, with early efforts focused on elucidating ozone reaction mechanisms and understanding its role in disinfection processes (Kinman and Rempel, 1975). Over time, advancements in analytical techniques and computational capabilities facilitated the development of more advanced models. In the 1980s and 1990s, researchers began incorporating kinetic models to predict ozone decomposition and elucidate complex interactions in water matrices predominantly employed pseudo-first or pseudo-second order kinetics (Eq. 2-5) to describe ozone decay in wastewater (von Gunten and Hoigne, 1994).

$$Ln\left(\frac{[C_0]}{[C]}\right) = k_{O3}\int [O_3]\,dt + k_{HO^{\cdot}}\int [HO^{\cdot}]\,dt \qquad \text{Eq. 2-5}$$

The evolving understanding of radical reactions and the formation of by-products prompted refinements in modeling approaches during the late 20th century (Mizuno et al., 2007; Wert et al., 2007). In recent years, the integration of computational tools, coupled with experimental validation, has enhanced the accuracy of models, allowing for a more comprehensive exploration of ozonation processes in diverse water and wastewater treatment scenarios. The historical trajectory reflects a continual refinement of models, driven by an increasing need for precision in ozone-based treatment strategies and a deeper understanding of the complex chemistry involved. These frameworks embraced detailed kinetics with a shift towards more complex models, incorporating initiation, propagation, and termination reactions, elucidating the complex radical pathways involved in ozone decomposition. Additionally,

contemporary models began addressing interactions with organic matter, striving to simulate the intricate reactions between ozone and diverse organic compounds present in wastewater (Audenaert et al., 2023; Chys et al., 2018).

2.3 MATHEMATICAL MODELING OF WWTPS: AOPS AND BIOTREATMENT

Despite the extensive experimental work, the mathematical modeling and sensitivity analysis of WWTPs, particularly in the context of AOPs and biological treatment (biotreatment) methods, is still under development. The description of the degradation mechanism and of the by-products involved is a very difficult task.

Current state-of-the-art research delves into developing comprehensive models that capture the intricate dynamics of wastewater treatment systems. Mathematical modeling plays a pivotal role in simulating and predicting the behavior of AOPs, such as photo Fenton reactions and ozonation, as well as biotreatment processes.

A key focus in recent literature involves refining mathematical models for AOPs to enhance their predictive accuracy and applicability to diverse wastewater compositions. Researchers have explored the incorporation of advanced kinetics and reaction mechanisms including the description of all the elementary steps of the process to better represent the complex interactions inherent in photo Fenton process (Simunovic et al., 2011). Additionally, some other approaches have resulted in promising outcome such as considering the main group of reactions (The generation and decomposition of H_2O_2 and $HO^{\bullet}$, the parent compound degradation to the partially oxidized intermediates and Fenton reactants and finally interactions between target compounds) (Cabrera Reina et al., 2012). The modeling of photo Fenton processes have been also developed across various case studies, including the degradation of the specific pollutants and MCs (Cavalheri et al., 2023; Esfahani et al., 2023; Soriano-Molina et al., 2018), mineralization of organic matter (Kebir et al., 2023), and wastewater disinfection (Sarı et al., 2023). The evolutionary efforts in this sense have resulted in some valuable didactic tools like the simulation app for the mechanistic understanding of the solar photo-Fenton process applied to the removal of microcontaminants contained in wastewater treatment plant secondary effluents (Gualda-Alonso et al., 2023).

On the other hand, the mathematical modeling of ozonation in wastewater treatment has evolved significantly, reflecting a dynamic landscape shaped by advancements in technology and a deepening understanding of the dissolved ozone dosing and decay (Audenaert et al., 2023; Mathon et al., 2021; Van der Helm et al., 2007), the photocatalytic ozonation (Beltrán et al., 2020), and biodegradability enhancement of ozonated wastewater (Otieno et al., 2019).

In the realm of biotreatment, mathematical modeling has advanced to encompass not only traditional activated sludge systems but also emerging technologies like anaerobic digestion and biofilm reactors. This tends toward the integrating mathematical models of AOPs and biotreatment processes which allows for a better understanding of their synergies and potential trade-offs in wastewater treatment efficiency.

However, challenges persist, including the need for comprehensive models that consider the influence of diverse wastewater matrices and the potential inhibitory effects of certain compounds. The state of the art in this field emphasizes the need for accurate representation of microbial activities, reaction kinetics, and mass transfer phenomena to improve the reliability of the models. Researchers are actively addressing these challenges by exploring novel modeling approaches and leveraging sensitivity analyses to unravel the intricate interdependencies within wastewater treatment systems.

2.4 CONSIDERATIONS OF THE INTEGRATED MODELING FOR THE COMBINED AOPS AND BIOLOGICAL TREATMENT PROCESSES

Although chemical oxidation for complete mineralization is usually expensive, its combination with a biological treatment is widely reported to reduce operating costs. In this context, conventional biological processes do not always provide satisfactory results, especially for industrial wastewater treatment, since many of the organic substances produced by the chemical industry are toxic or resistant to biological treatment. Therefore, the only feasible option for such biologically persistent wastewater is the use of advanced technologies based on chemical oxidation, such as the AOPs, widely recognized as highly efficient treatments for recalcitrant wastewater (Oller et al., 2011a). To design integrated processes involving AOPs and biological treatment and identify the most effective or cost-efficient operational ranges, a comprehensive kinetic model is essential. This section reviews recent

research combining AOPs (as a pre-treatment or post-treatment stage) and bioremediation technologies for the decontamination of a wide range of synthetic and real industrial wastewater. In recent years, the integrated modeling of AOPs and biological treatment processes has garnered increasing attention within the field of wastewater treatment. Research in this domain has witnessed a paradigm shift from isolated treatment methods towards a more holistic approach, recognizing the intricate interactions between AOPs and biological processes. Integrated models strive to capture the dynamic nature of these interactions, considering factors such as microbial activities, reaction kinetics, and mass transfer phenomena.

2.4.1 AOPs as a pre-treatment

It is consistently demonstrated that the biodegradability of waste undergoes alterations when exposed to prior chemical oxidation (Mantzavinos and Psillakis, 2004; Mohammed and Smith, 1992). It is aimed to create biodegradable reaction intermediates while minimizing mineralization to save on chemicals and energy, reducing operational costs. Efficient pre-treatment is crucial, considering that a significant portion of photocatalytic reactor costs (about 60%) is associated with electricity. However, a short pre-treatment duration may result in the formation of reaction intermediates resembling the original non-biodegradable or toxic components (Mecha et al., 2017).

While recent research has started to develop kinetic models for combined chemical-biological processes, the earliest publication dates back to 1996 by Scott and Ollis. In their work, they discussed steady-state biological degradation models tailored for challenging-to-degrade wastewater scenarios with chemical pretreatment. Their models incorporated common parameters like biochemical oxygen demand (BOD) or total organic carbon (TOC), widely used for assessing industrial and domestic wastewater. However, these models have limitations as the parameters lack specificity, despite their broad applicability. In recent years, research has predominantly focused on modeling only AOP remediation of wastewater, neglecting strategies that combine AOPs with biological treatments (Oller et al., 2011a).

The modeling approach has also been extended to industrial wastewater treatment including textile industry (Lafi and Al-Qodah, 2006; Ledakowicz et al., 2001), olive industry (Javier Benitez et al., 2002), and wood treating or biocide formulation operations (Zimbron and Reardon, 2011).

Nonetheless, studies to the development of kinetic models and predicting the reaction rates as a function of main parameters such as concentration of the pollutants, radical scavengers and the rates constants are very limited, indicating a critical gap in the existing literature. In this thesis, it is aimed to develop an integration strategy mapping the variables of the two models and to implement and verify the consistency of the integrated model.

2.4.2 AOPs as a post-treatment

The combination strategy is commonly in the opposite direction, first eliminating the highly biodegradable part of the wastewater and then degrading the recalcitrant contaminants (non-toxic) by a post-treatment AOP (commonly by the ozonation process). Such integrated systems are particularly favorable for effluents such as olive mill wastewater or landfill leachates, which initially contain some biodegradable fractions (i.e., sugars and proteins) which could easily be removed first and so, not compete for the chemical oxidant (Oller et al., 2011a).

Different configurations and various AOPs have been studied experimentally for the integration of biotreatment followed by post-treatment of AOP including $TiO_2/H_2O_2/UV$, $Fe^{2+}/H_2O_2/UV$, UV/H_2O_2 (Brink et al., 2018; Bustillo-Lecompte and Mehrvar, 2016; Leyva-Díaz et al., 2015).

Current literature emphasizes the significance of accurate representation of both AOPs and biological treatment within integrated models. Although mathematical modeling is crucial for efficient design and operation of wastewater treatment processes, limited kinetic models have been used for the combined system. A widely accepted kinetic modeling approaches are available for biological treatment as well as photo Fenton process, as presented in the section 2.3.

However, as a result of the complexity of the processes and implementation of different approaches and variables in the developed models, combining the models being a complicate procedure while reliable result is required. This involves addressing challenges such as the diverse composition of wastewater matrices among others. Advances in modeling techniques seek to incorporate these complexities, providing a more realistic simulation of the integrated treatment system.

The integrated modeling for combined AOPs and biological treatment processes is marked by a transformative shift towards data-driven approaches. Further research

will be oriented to improve the understanding of the potential key parameters as well as their inclusion in the model.

2.5 SUMMARY AND IMPLICATIONS

The critical analysis of the literature provides a foundation for understanding the current state of knowledge in the field. The review highlights gaps in existing research and identifies areas where further investigation is warranted. Notably, the examination of contaminants of emerging concern underscores the evolving nature of wastewater challenges, emphasizing the need for continuous research to improve treatment processes. The exploration of AOPs reveals their potential as advanced treatment methods, but also emphasizes the need for a comprehensive consideration through mathematical modeling. Several configurations of single or hybrid AOPs (as pretreatment or post-treatment with bioremediation) for wastewater treatment have been experimentally studied in the literature (Nidheesh et al., 2021).

However, the design and operation of such a hybrid process require suitable models. A great deal of mathematical models for WWTP have been developed and reported, while not many works have addressed the modeling of AOPs. Models combining AOPs and bio-processes have hardly been discussed. The modeling needs, and perspectives of AOPs are different to characterize the system. This may explain the divergence of the research efforts of both areas, as well as the problems that converging them to a unique hybrid model entail. The consideration of integrated modeling approaches recognizes the interconnected nature of AOPs and biological treatment, emphasizing the importance of holistic assessments for improved efficiency.

It is established a clear need for the current study by demonstrating the evolving challenges in wastewater treatment and the gaps in understanding, particularly to contribute in the context of AOPs and integrated processes. The review contributes to the theoretical framework by emphasizing the dynamic relationships among variables and the importance of considering various factors in wastewater treatment.

Chapter 3: Mathematical Tools: Simulation and Sensitivity Analysis

The methodology and research design sets are explicitly outlined in each chapter, providing a thorough examination of the diverse laboratory studies undertaken. Additionally, it outlines the mathematical tools utilized to convert the acquired data into information and knowledge during the subsequent stages of modeling and sensitivity analysis of AOPs.

3.1 METHODOLOGY AND RESEARCH DESIGN (FOR DIFFERENT EXPERIMENTAL SETUPS)

The methodology and research design in this thesis is meticulously presented in each chapter (separately), offering a comprehensive overview of the varied laboratory studies conducted. In Chapter 4, 5, and 6, the methodological approach unfolds through the simulation of the proposed model under diverse Advanced Oxidation Processes (AOPs) operations. This involves parameter estimation and sensitivity analysis, utilizing experimental data to validate results for practical applications. The simulations aim to validate model implementation and extract insights from a range of computational experiments. A global sensitivity analysis is undertaken to assess the impact of variations in model parameters on each measured response. Parameter estimation is pursued through minimizing the sum of squared differences between model values and training data. Validation is then executed by evaluating the fitted model's capacity to explain independent experimental datasets not used in the initial calibration (test assays). Chapter 7 introduces the novel concept of integrating AOPs with biological treatments implemented in Simulink®, addressing the need for effective wastewater decontamination strategies. Lastly, in Chapter 8, the research design takes a different trajectory, focusing on determining suitable materials that meet both chemical and mechanical requirements. This involves a multifaceted approach, employing multiple criteria in several steps to identify materials that align with the specific needs of the study. This thorough and detailed presentation of the methodology across chapters underscores the diversity and complexity of the research conducted in distinct laboratory settings.

3.2 MATHEMATICAL MODEL TOOLS

This section is dedicated to presenting various mathematical tools essential for the analysis and interpretation of data acquired in the study. The application of these mathematical tools contributes to the subsequent phases of modeling, simulation, sensitivity analysis, and parameter estimation, providing a comprehensive framework for transforming collected data into valuable information of the study.

3.2.1 Simulation, model fitting, and parameter estimation

The set of reaction rates given by ordinary differential equations (ODEs) was implemented in MATLAB/Simulink® (different versions) and solved numerically using ode15s solver with a time variable-step.

The concentration profiles of target variables were used to estimate the model parameters (model calibration) by solving a nonlinear multivariate optimization problem to minimize the sum of the squared differences between the model predicted values and the corresponding experimental data available. This problem is solved using different algorithms available in the Estimator Toolbox of MATLAB/Simulink®.

To assess the goodness of fit, the Root Mean Square Error (RMSE) as presented in Eq. 3-1, as the standard deviation of the residuals (prediction errors), was used and presented for each measured time series. The coefficient of determination R^2 (Eq. 3-2) is also presented as an informative statistical measure that is widely used.

$$RMSE_k = \sqrt{\left(\sum_{i=1}^{N_k} (\hat{y}_{ik} - y_{ik})^2 / N_k \right)} \qquad \text{Eq. 3-1}$$

$$R_k^2 = 1 - \left(\sum_{i=1}^{N} (\hat{y}_i - y_i)^2 \Big/ \sum_{i=1}^{N} (\hat{y}_i - \bar{y})^2 \right) \qquad \text{Eq. 3-2}$$

where $\hat{y}_i$ and y_i correspond to the measured and simulated values at the given time, respectively, and $\bar{y}$ is the mean of the measured data.

3.2.2 Sensitivity analysis

The study employs parameter sensitivity analysis to assess a mathematical model's robustness and identify the relative importance of various mechanisms incorporated in the model, addressing uncertainties in parameters (Latunde and Bamigbola, 2018). The exploration involves both Local Sensitivity Analysis (LSA)

and Global Sensitivity Analysis (GSA). LSA, though computationally efficient, has limitations, such as exploring only a small portion of the solution space (Castillo et al., 2004). The study opts for GSA, particularly using Monte Carlo techniques, to overcome LSA's limitations and assess multiple correlated outputs simultaneously. Various GSA techniques, including Morris method, Sobol's method, Fourier Amplitude Sensitivity Test, and Latin hypercube sampling with partial rank correlation coefficient index (LHS-PRCC), are discussed. The study selects the LHS-PRCC method, leveraging Latin hypercube sampling for an optimized input trial structure and efficient stratification Monte Carlo sampling for extracting significant uncertainty and sensitivity information with a relatively small sample size (Marino et al., 2008a). This method is applied to analyze correlations between model parameters and output, considering general monotonic relationships while removing the effects of other parameters. In PRCC, also referred to as Spearman analysis and ranked transformation, a model with P number of model parameters and a model output y can be written as a function of all the model parameters values x_k $(k = 1, 2, \dots, P)$ so that $y = f(x_1, x_2, \dots, x_P)$. Hence, N samples $(i = 1, 2, \dots, N)$ for each model parameter will produce a set of P sample vectors X_k $(1 \times N)$ and an associated vector Y $(1 \times N)$ of output values. Then, the partial rank correlation coefficients for each parameter (R_{X_kY}) are calculated as follows (Eq. 3-3) (Marino et al., 2008b):

$$R_{X_kY} = \frac{cov(X_k, Y)}{\sqrt{Var\,(X_k) Var(Y)}} = \frac{\sum_{i=1}^{N}(x_{ik} - \bar{x})(y_i - \bar{y})}{\sqrt{\sum_{i=1}^{N}(x_{ik} - \bar{x})^2 (y_i - \bar{y})^2}} \qquad \text{Eq. 3-3}$$

The R values, ranging from -1 to 1, indicate the influence of parameters in a model, with magnitude signifying importance and the sign indicating the direction of the influence (increase or decrease) (Helton et al., 2006a). The combined Latin hypercube sampling and partial rank correlation coefficient (LHS-PRCC) procedure, as detailed elsewhere (Marino et al., 2008a), involves sampling the parameter space, obtaining model outputs for each set of sampled parameters, ranking parameter and output values, replacing them with their ranks, and calculating R values for each input parameter. Regarding model output, the study opts for summation of square errors, treating them independently for the three experimentally monitored process variables.

Chapter 4: Modeling of the Photo-Fenton Process with Flexible Hydrogen Peroxide Dosage

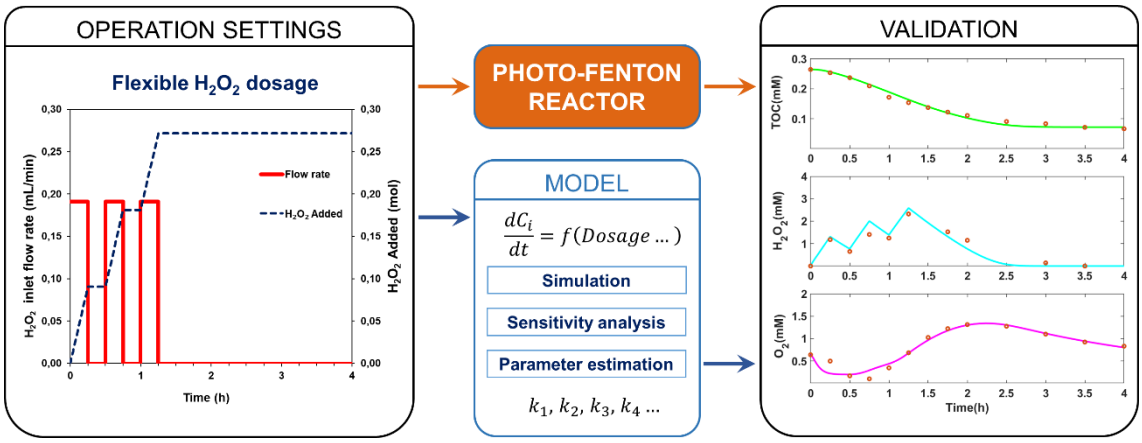

Redrafted from: (Nasr Esfahani et al., 2022a)

Nasr Esfahani, K., Pérez-Moya, M., & Graells, M. (2022b). Modeling of the photo-Fenton process with flexible hydrogen peroxide dosage: Sensitivity analysis and experimental validation. Science of The Total Environment, 839, 155941. https://doi.org/https://doi.org/10.1016/j.scitotenv.2022.155941

The supply of hydrogen peroxide (H_2O_2) controlling the amount of highly oxidant hydroxyl radicals is the most critical operational issue for the photo-Fenton process. Accordingly, this study (Chapter 4) addresses the development of a model for photo-Fenton processes including a flexible H_2O_2 supply given as a function of time. The model is aimed at its future exploitation in treatment optimization and the determination of the optimal profile for H_2O_2 supply. The work adopted a photo Fenton model previously reported that includes the inlet flow (fed-batch) and describes the system dynamics under a flexible dosage. Thus, model global sensitivity analysis (GSA) and parameter estimation were performed using Simulink® to examine the behavior of the model under flexible H_2O_2 dosage. GSA was carried out using partial rank correlation methods and the Latin hypercube sampling to assess to which extent variations of the model parameters affect each measured response (H_2O_2, total organic carbon, TOC, and dissolved oxygen, O_2 –the experimentally available information). Hence, the model is discussed in regard of its hypothesis and chances for reducing its complexity. This resulted in the rejection of two reactions of the initial model. Next, a set of 12 kinetic, stoichiometric and operative parameters was estimated through the fitting of H_2O_2, TOC, and O_2 profiles. Discussion on model fitting includes computational issues, the role of initial values for the estimation process, the goodness of fit criteria, and the sampling method. The model was fit to experimental data with assorted H_2O_2 supply profiles and validated, and Root Mean Square Error (RMSE) below 0.009, 0.42, and 0.127 mM were obtained for TOC, H_2O_2 and O_2, respectively. Therefore, this work contributes a practical model aimed at providing model-based optimization for the H_2O_2 dosage profile of the photo-Fenton process.

4.1 INTRODUCTION

The presence of many non-biodegradable organic pollutants in wastewaters or surface waters (including industrial compounds, pharmaceuticals, personal-care products, biocides, and plant protection substances) may result in important environmental issues even in very low concentrations. Ineffective treatment of the organic pollutants in wastewaters, as well as the direct release of them into the environment, may lead to the infiltration of profoundly poisonous and low biodegradable species into the natural aquatic ecosystems.

Several treatment techniques including both physicochemical and biological methods could be applied to contaminated wastewaters. In any case, few strategies are adequately broad-based and helpful for real-time applications (Lu et al., 2011; Oller et al., 2011a)

Advanced oxidation processes (AOPs) have been broadly acknowledged as promising strategies either individually or in combination for the remediation of contaminated wastewaters containing non-biodegradable organic pollutants (Tufail et al., 2020)

Among these processes, the photo Fenton treatment is a well-known solution for treating non-biodegradable contaminants in wastewaters that cannot be treated with conventional bio-processes (Oller et al., 2011a). It has gotten a lot of interest because of its broad range of target chemicals, robust oxidation capabilities, and rapid response pace (Lu et al., 2010).

The photo-Fenton process is a photocatalytic process that generates highly oxidizing hydroxyl radicals ($HO^{\bullet}$) by interacting chemical reagents (Fe (II) salt and H_2O_2) with a UV irradiation light source, which causes a synergic effect by creating a higher rate of $HO^{\bullet}$ production.

However, the major limitations of this method are the need for H_2O_2, Fe^{+2} salts and pH adjustment (mostly acidic) (Lu et al., 2010; Pignatello et al., 2006) Furthermore, the hydroxyl radical is exceedingly unstable and non-selective, so it is frequently scavenged by unwanted secondary reactions, some of them involving H_2O_2 consumption, which cut down the efficiency of the process (Gulkaya et al., 2006).

Hence, it is critical to control the reaction conditions through the dosage of H_2O_2 for achieving the complete mineralization of the target compound. The reaction rate and process efficiency are both affected by H_2O_2, which is the most expensive reagent (Lu et al., 2011). This represents a compromise between decontamination efficiency of the process due to H_2O_2 deficiency and excess concentration of H_2O_2 that forces extra cost. In this regard, researchers have studied the photo-Fenton process with the dosage of Hydrogen peroxide to enhance process performance (Santos-Juanes et al., 2011).

As a straightforward approach for the supply of hydrogen peroxide, constant concentration ratios of H_2O_2 to contaminant and iron were studied to minimize the scavenging effect (Gulkaya et al., 2006; Mahmoudi et al., 2021; Sinnaraprasat and

Fongsatitkul, 2011). While such ratios may suit steady operation, time-varying batch operations may require constantly adapted H_2O_2 supply to optimize the operation performance (Yu et al., 2020). As a result, the key research issue is the optimization of a time-dependent H_2O_2 dose profile to maximize process performance by reducing the scavenging effects through the supply of the required amount of hydrogen peroxide supply at all times.

Towards this end, Ortega-Gómez et al. (2012) investigated a control strategy for the automatic addition of hydrogen peroxide and the linking behavior of dissolved oxygen to hydrogen peroxide consumption. It was demonstrated that, through the application of this control strategy, the hydrogen peroxide consumed can be reduced by 50% compared to the more traditional addition strategies employed in the photo-Fenton process (Ortega-Gómez et al., 2012). More recently, Yu et al. (2020) presented a conceptual basis and an experimental approach to address the problem of hydrogen peroxide dosage for Fenton and photo-Fenton processes. The mineralization was further improved in a specific H_2O_2 dosage (by 4.75%) rather than the same amount of hydrogen peroxide without dosage (Yu et al., 2020). Whereas most of the previous experimental works verified an increase in the photo Fenton process efficiency using flexible dosage strategies (Hamad et al., 2016; Yamal-Turbay et al., 2014; Yu et al., 2020), they are useful in particular situations and cannot provide the optimal solution.

On the other hand, despite some attempts proposing different models for hydrogen peroxide dosage in the Fenton based processes (Audino et al., 2019; Bacardit et al., 2007), solutions reported in the literature are still incomplete and fall short of offering a dynamic model of batch and fed-batch operations of the photo Fenton process using systematic approaches.

Furthermore, the computational costs associated with developing a comprehensive model can be a limiting factor in terms of model parameter estimation and sensitivity analysis. Several studies with sensitivity analysis have been performed for the Fenton-based processes and it has been confirmed the usefulness of the different kinetic reactions, especially the scavenging reactions to be considered (Căilean et al., 2015; Mousset et al., 2016). Still, based on the different range of parameter values found in the literature (Shinozawa et al., 2020), it is necessary to study kinetic parameter estimations and sensitivity analysis for each specific model in order to better fit the experimental results.

In other words, the lack of suitable dynamic models for Fenton and photo-Fenton processes makes model-based optimization challenging, and determining the optimum hydrogen peroxide supply profile has been hardly addressed (Audino et al., 2019) In fact, scarce attention has been paid to the development of systematic procedures and optimization strategies to efficiently operate the photo Fenton process including flexible dosage.

The rigorous model-based optimization of the dosage profile is beyond the scope of the present work. The target is determining a continuous function for the dosage level to be applied at each differential time step so that any given cost function (economic, environmental, etc.) is minimized at the end of the dosage. However, in order to address such a dynamic optimization problem, a dynamic model is first required allowing the estimation of the evolution of the outcome of the process (i.e., TOC) from a time-controlled input (i.e., the H_2O_2 dosage profile). The objective and scope of this work are shedding new light on the dosage problem and the development and fitting to experimental data of a practical photo-Fenton model including flexible H_2O_2 dosage. This work is a necessary step towards solving the model-based optimization problem, which is not immediate and would require further research.

The work follows and extends the approach by Cabrera-Reina et al. (2012) and Audino et al. (2019) to model a time-dependent supply of hydrogen peroxide to a batch reactor, and uses the experimental data obtained by Yu et al. (2020) using different dosage schemes for the mineralization of paracetamol solutions at a pilot plant scale.

Thus, sensitivity analysis is the first step allowing balancing the complexity and the accuracy of the model. Next, the model is fit to different sets of experimental data and validated using new data (cross-validation). Finally, the precision and accuracy of the model are discussed in regard to its potential for addressing the optimization of a continuous time-dependent H_2O_2 dosage profile that would in turn support informed decision-making on the H_2O_2 supply problem in photo-Fenton treatments.

4.2 METHODOLOGY

The proposed methodology consists of the simulation of the model for a variable operation of the reactor with different H_2O_2 supply, sensitivity analysis, parameter estimation using experimental data, and final validation with the evaluation of the results

for the practical applications. The flow diagram of the methodological framework followed is illustrated in Figure 4-1.

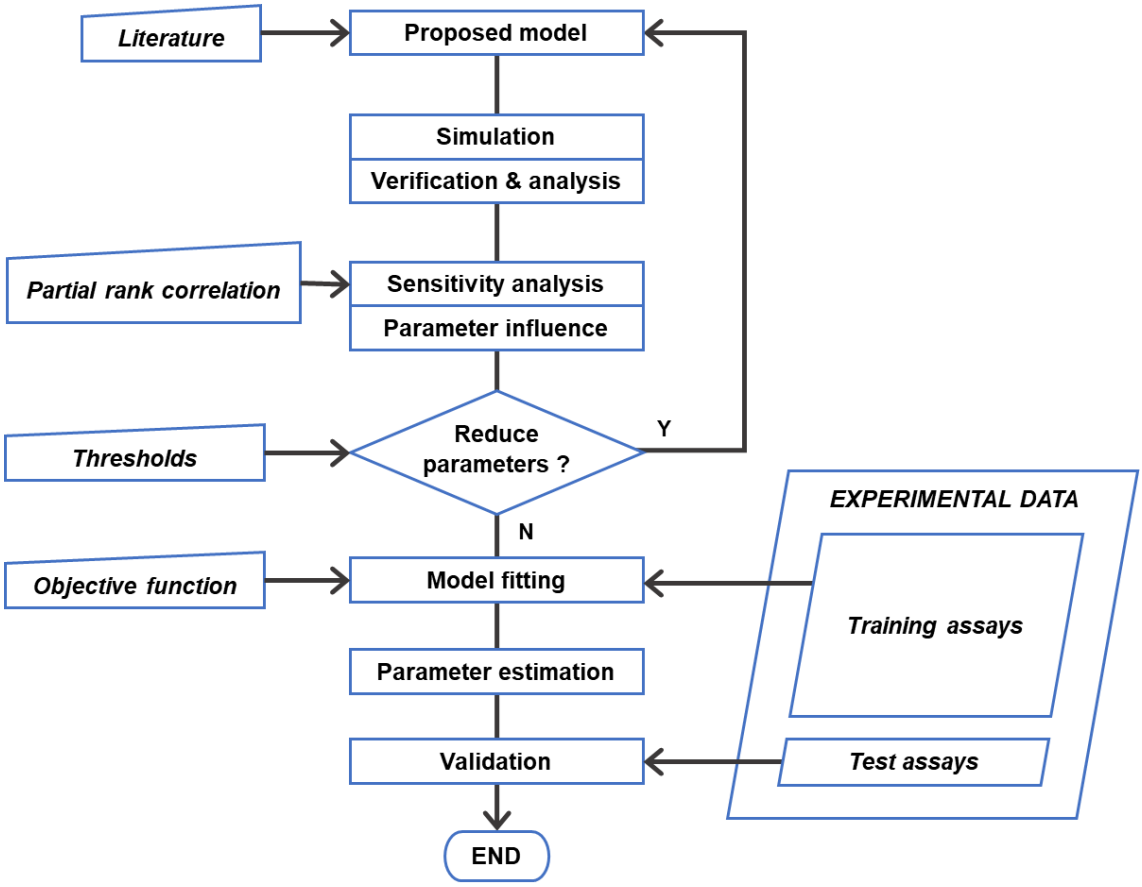

Figure 4-1 Methodological framework

Accordingly, this section describes and discusses the model adopted and its implementation in Simulink® (Sub-section 4.2.1); the data used to calibrate and validate the model (Sub-section 4.2.2) the methods employed for the quantitative assessment of the fidelity of the model, and the sensitivity of its output to model parameters (Sub-section 4.2.3); and the procedure to use this information to assess and discuss its consistency and complexity through sensitivity analysis (Sub-section 4.2.4). Finally, Section 4.3 presents and discusses the results obtained.

Simulations and analysis of the model are proposed with the ultimate goal of verifying the model implementation and learning from the different computational experiments that can be produced. Next, global sensitivity analysis is intended for assessing to which extent variations of the model parameters affect each measured response (TOC, H_2O_2, and O_2) with a quantified correlation coefficient for each parameter. Thresholds are established and discussed. Results reveal non-significant

parameters that are eliminated as their absolute correlation coefficients below 0.10 for TOC, H_2O_2, and O_2 (the experimentally available information).

Parameter estimation is proposed through the minimization of the sum of the squared differences between the model values and the training data (88% of the experimental assays). Finally, validation is proposed by assessing the capacity of the fitted model to explain independent experimental data sets not used in the calibration of the model (test assays).

4.2.1 Mathematical Modeling and simulation

The photo-Fenton process model adopted is based on that by Cabrera-Reina et al. (2012) and later extended by Audino et al. (2019) to include flexible dosage via fed-batch operation. The reaction scheme is given in Figure 4-2.

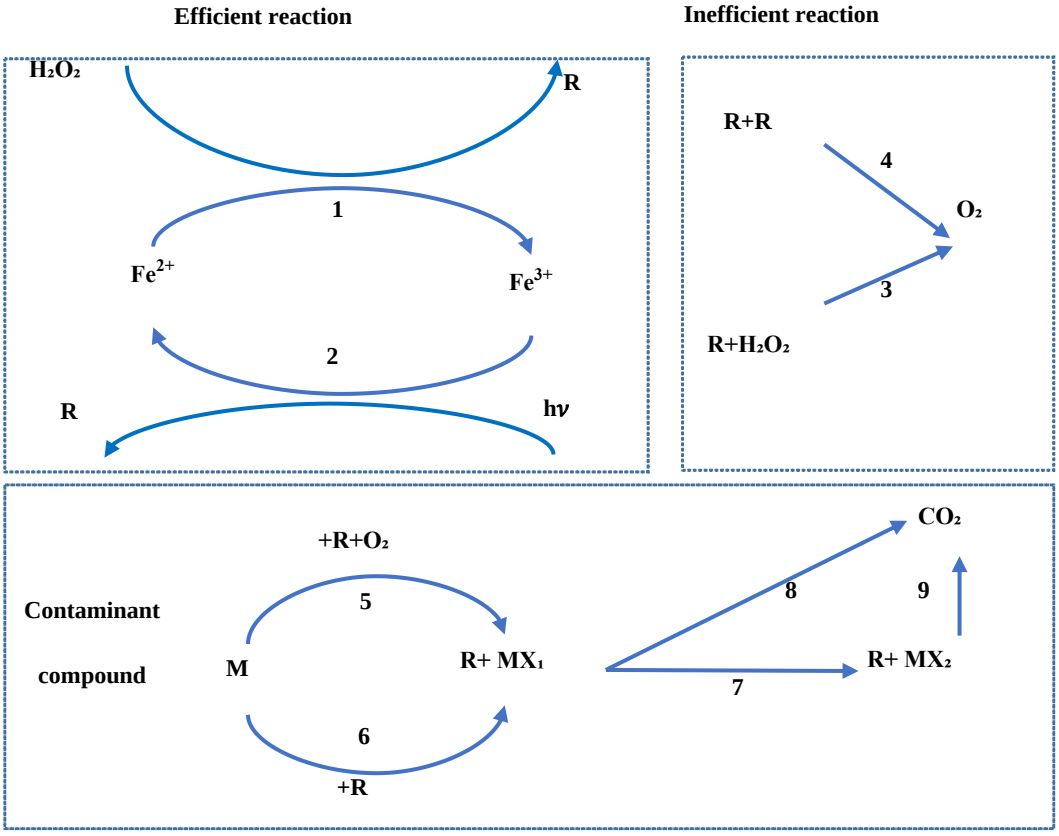

Figure 4-2 The reaction scheme of the photo Fenton model according to Cabrera Reina et al. (2012)

The formation of hydroxyl radicals is described through efficient reactions (Eq. 4-1, Eq. 4-2) between Iron (II) and hydrogen peroxide (H_2O_2), as well as efficient reactions between the resulting Iron (III) and UV irradiation. The low pH requirement (between 3 and 6) is assumed, as usual, as an important condition for iron-induced reduction of hydrogen peroxide. In the same way, a convenient light source with a proper constant wavelength (nm) is assumed and not included in the model; thus, the model is limited to the specific wavelength used. Contrariwise, the model does contemplate light intensity [I] and it can be fitted to the experimental data, but again the model will be limited, this time because all the experimental data used are obtained under constant irradiation.

$$r_1 = k_1.[Fe^{2+}][H_2O_2] \quad \text{Eq. 4-1}$$

$$r_2 = k_2.[Fe^{3+}][I] \quad \text{Eq. 4-2}$$

Radicals R decompose H_2O_2 (Eq. 4-3) and combine (Eq. 4-4) producing oxygen in both cases. Thus, an excess of H_2O_2 and radicals can go through these inefficient paths instead of being used in the oxidation of the organic matter M.

The existence and propagation of any of these reactions highly depend on the amount of H_2O_2 as well as the rate constant. It's also worth noting that increasing the hydrogen peroxide concentration lowers the process efficiency because it raises the concentration of radicals [R].

$$r_3 = k_3.[R][H_2O_2] \quad \text{Eq. 4-3}$$

$$r_4 = k_4.[R][R] \quad \text{Eq. 4-4}$$

The model also assumes the consumption of radicals R in a series of oxidations leading the parent compound M to the partially oxidized intermediates MX_1 and MX_2, and finally to CO_2 (Eq. 4-5 to Eq. 4-9). The concentrations of three species determine the measurement of Total Organic Carbon ($TOC = M + MX_1 + MX_2$) and allow modeling the delayed response of such a lumped parameter.

Reactions 5 and 6 are associated with the degradation of the main organic matter to produce MX_1 and then MX_2 by means of reaction 7. Finally, the degradation of the intermediates is modeled through reactions 7 to 9.

$$r_5 = k_5.[M][R][O_2] \quad \text{Eq. 4-5}$$

$$r_6 = k_6.[M][R] \quad \text{Eq. 4-6}$$

$$r_7 = k_7.[MX_1][R] \quad \text{Eq. 4-7}$$

$$r_8 = k_8.[MX_1][R] \quad \text{Eq. 4-8}$$

$$r_9 = k_9.[MX_2][R] \quad \text{Eq. 4-9}$$

The mass balance equations, including the overall gas-liquid mass transfer coefficient for O_2 ($K_L a$) and the stoichiometric coefficients related to the oxygen balance (c_1, g_1, and g_2), are shown below (Eq. 10-18):

$$\frac{d[H_2O_2]}{dt} = \left(\frac{F}{V}\right) \cdot ([H_2O_2]_{in} - [H_2O_2]) - r_1 - r_3 \quad \text{Eq.4-10}$$

$$\frac{d[M]}{dt} = \left(\frac{F}{V}\right) \cdot ([M]_{in} - [M]) - r_5 - r_6 \quad \text{Eq.4-11}$$

$$\frac{d[MX_1]}{dt} = \left(\frac{F}{V}\right) \cdot ([MX_1]_{in} - [MX_1]) + r_5 + r_6 - r_7 - r_8 \quad \text{Eq.4-12}$$

$$\frac{d[MX_2]}{dt} = \left(\frac{F}{V}\right) \cdot ([MX_2]_{in} - [MX_2]) + r_7 - r_9 \quad \text{Eq.4-13}$$

$$\frac{d[TOC]}{dt} = \frac{d[M]}{dt} + \frac{d[MX_1]}{dt} + \frac{d[MX_2]}{dt} \quad \text{Eq.4-14}$$

$$\frac{\mathrm{d}[O_2]}{\mathrm{dt}} = \left(\frac{F}{V}\right) \cdot ([O_2]_{in} - [O_2]) + g_1 r_3 + g_2 r_4 - c_1 r_5 + (K_L a([O_2]^* - [O_2])) \quad \text{Eq.4-15}$$

$$\frac{d[Fe^{2+}]}{dt} = \left(\frac{F}{V}\right) \cdot ([Fe^{2+}]_{in} - [Fe^{2+}]) - r_1 + r_2 \quad \text{Eq.4-16}$$

$$\frac{d[Fe^{3+}]}{dt} = \left(\frac{F}{V}\right) \cdot ([Fe^{3+}]_{in} - [Fe^{3+}]) + r_1 - r_2 \quad \text{Eq.4-17}$$

$$\frac{d[R]}{dt} = \left(\frac{F}{V}\right) \cdot ([R]_{in} - [R]) + r_1 + r_2 - r_3 - 2r_4 - r_5 - r_6 - r_7 - r_8 - r_9 \quad \text{Eq.4-18}$$

where F, represents the inlet flow rate ($\mathrm{L.\,h^{-1}}$); V (L), the total volume of the reactor and $[C_i]_{in}$ as well as $[C_i]$ refer to the concentrations ($\mathrm{mmol.\,L^{-1}}$) for each component in the inlet flow rate and inside the reactor, respectively. In this particular study, all inlet concentrations are considered null except $[H_2O_2]_{in}$.

Hence, the model parameters of the photo Fenton process model to be considered are k_1 to k_9, $K_L a$, and the stoichiometric coefficients c_1, g_1, and g_2.

The model is based on the main following assumptions (Audino et al., 2019):

The different radical species that may exist are represented by their aggregated concentration [R] and common behavior.

The reaction between Fe^{3+} and H_2O_2 is neglected so that the model is only applicable to the photo Fenton process (UV light is necessary);

H_2O_2 hydrolysis is neglected;

An intermediate partially oxidized compound is assumed to be present before any CO_2 is released from the process.

The main features of the model include the focus on parameters easy to monitor such as dissolved oxygen, hydrogen peroxide, and TOC; the use of unspecified intermediates (MX_1, MX_2, as artificial, dummy variables) to model the delay in the response of this practical lumped measurement; and the easy modeling of the scavenging of H_2O_2 by means the non-linear consumption of radicals (Eq. 4-3, Eq. 4-4).

The model given by the set of Ordinary Differential Equations (Eq.4-10 to Eq.4-18) is implemented in MATLAB/Simulink® version R2021b and solved numerically using ode15s solver as a variable order solver based on the numerical differentiation formulas with a time variable-step.

Figure 4-3 illustrates the capability of describing the evolution of the concentration of all the components included in the simulation of the kinetic model. The normalized values are calculated according to unity-based normalization as shown in Eq.4-19.

$$Normalized\ C_i = \frac{C_i - C_{min}}{C_{max} - C_{min}} \qquad \text{Eq.4-19}$$

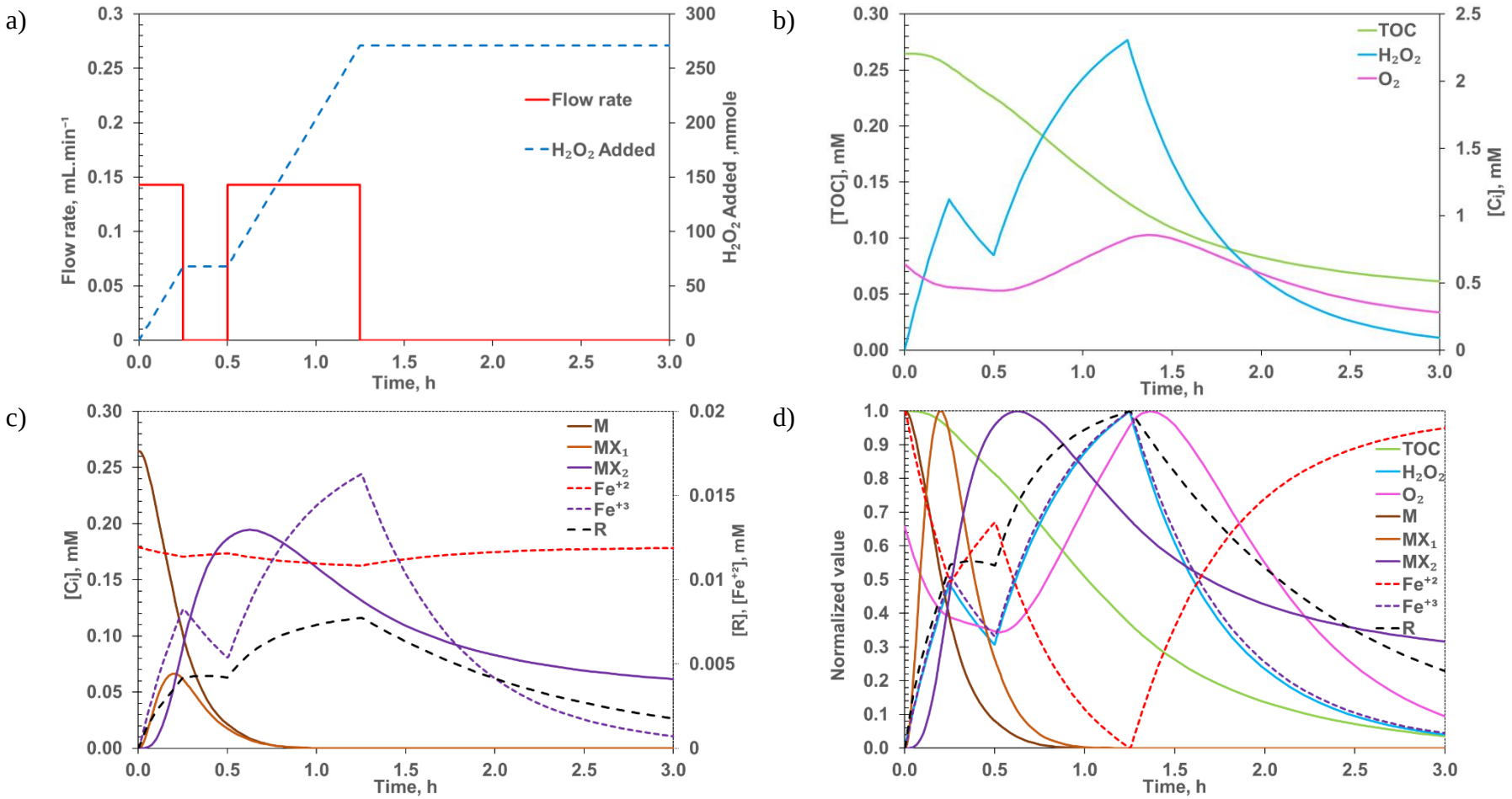

Figure 4-3 Simulation of concentration profiles: (a) Variable H_2O_2 input profile: a constant flow rate ($0.14318\ mL \cdot min^{-1}$) is kept from 0 to 15 min and from 30 to 75 min; totaling (8.5909 mL, 271.29 mmol) at the end of the 3h reaction time simulated; (b) Concentration profiles of the measured output: TOC, H_2O_2, O_2 ; (c) Concentration profiles (absolute values) for organic species (M, MX_1, MX_2), radicals (R), and iron species (Fe^{2+}, Fe^{3+}); (d) Concentration profiles for all species (normalized values)

Table 4-1 provides the data given by Cabrera Reina et al. (2012) used for the simulations shown in Figure 4-3 (as mentioned, only $[H_2O_2]_{in}$ is different from zero, while the rest of inlet concentrations are null).

Table 4-1 Model parameters and initial concentrations (Cabrera Reina et al., 2012)

Kinetic constants	**Value**	**Initial concentrations**	**Value**
$K_La(h^{-1})$	2.7	$[H_2O_2]_0$ (mM)	0
c_1	0.1	$[TOC]_0$ (mM)	0.26
g_1	0.75	$[O_2]_0$ (mM)	0.64
g_2	0.47	$[Fe^{2+}]_0$ (mM)	0.179
$k_1(mM^{-1}.h^{-1})$	8.81	$[Fe^{3+}]_0$ (mM)	0
$k_2\ ((W.m^{-2})^{-1}.h^{-1})$	5.63	$[M]_0$ (mM)	0.26
$k_3(mM^{-1}.h^{-1})$	75.8	$[MX_1]_0$ (mM)	0
$k_4(mM^{-1}.h^{-1})$	42798	$[MX_2]_0$ (mM)	0
$k_5(mM^{-2}.h^{-1})$	2643	$[R]_0$ (mM)	0
$k_6(mM^{-1}.h^{-1})$	257	$[O_2]^*$ (mM)	0.21
$k_7(mM^{-1}.h^{-1})$	2865	I $(W.m^{-2})$	36
$k_8(mM^{-1}.h^{-1})$	271	$F(ml.min^{-1})$	0.143
$k_9(mM^{-1}.h^{-1})$	107	Total volume, V (L)	15

The simulation example corresponds to a variable of H_2O_2 dosage profile stemming from a flow rate of 0.143 $(mL \cdot min^{-1})$ that is switched on from 0 to 15 min and from 30 to 75 min (Figure 4-3 (a)). These operational settings will produce an experimentally monitored response (TOC, H_2O_2 and O_2) displayed in Figure 4-3 (b). Furthermore, simulation provides deeper insight into the process by revealing the concentration of intermediates and other unobservable species: the profiles of M, MX_1, MX_2 show the successive transformation of M to $MX_1$and to MX_2, with both intermediates peaking at early reaction times and gradually declining as the mineralization progresses (Figure 4-3(c)). As a result, TOC remains unaltered for a short time and then asymptotically decreases, exhibiting a delayed response. The simulated profile of dissolved oxygen concentration shows a correspondence with the levels of both H_2O_2 and R and also supports the idea that dissolved oxygen may indicate an unproductive decomposition of hydrogen peroxide that should be avoided. Finally, Figure 4-3 (d) presents the concentrations of all species using normalized values for comparative purposes. Figure 4-3 (d) clearly shows the parallel evolution of hydrogen peroxide and iron and the delayed response of the radical species R respect to the concentration of H_2O_2.

4.2.2 Experimental data

The experimental data used to calibrate the model is also obtained from the literature (Yu et al., 2020). The work by Yu et al. (2020) addresses the formulation of the

optimization of a fully flexible H_2O_2 dosage profile in photo-Fenton processes and reports data series according to this idea. The work is limited because of the unaffordable experimental burden but stresses the need for a reliable process model and provides suitable data for calibrating such a model. The work by Yu et al. (2020) specifically studied the photo-Fenton remediation of a Paracetamol (PCT) and the experimental results include the evolution of the concentration of TOC, H_2O_2, and O_2. The data reported corresponds to a set of systematically designed dosage profiles covering a complete domain of alternatives (Table 4-2). The reaction time (2h) was divided into eight-time slots of 15 minutes (S1 to S8) and for each one dosage was set active or not (1,0) so that the same amount of H_2O_2 was fractioned and distributed along such time span. For all profiles, the first slot (S1) is obviously always on (1), while for the last three (S6, S7, and S8) dosage was decided to be off (0). Thus, there are four degrees of freedom (S2, S3, S4, and S5, shadowed in Table 4-2) and 16 cases leading to the codification used in Table 4-2. The label "No dosage" refers to the assay for which the same total amount of H_2O_2 was supplied all at once at the beginning, and for which this codification does not apply (N/A).

Table 4-2 Design of experiments (Yu et al., 2020)

ID (Code)	**ID (bin)**	**S1**	**S2**	**S3**	**S4**	**S5**	**S6**	**S7**	**S8**	**Fraction per slot**
No dosage	N/A	N/A	N/A	N/A	N/A	N/A	N/A	N/A	N/A	N/A
0	**0000**	1	**0**	**0**	**0**	**0**	0	0	0	1
1	**0001**	1	**0**	**0**	**0**	**1**	0	0	0	1/2
2	**0010**	1	**0**	**0**	**1**	**0**	0	0	0	1/2
3	**0011**	1	**0**	**0**	**1**	**1**	0	0	0	1/3
4	**0100**	1	**0**	**1**	**0**	**0**	0	0	0	1/2
5	**0101**	1	**0**	**1**	**0**	**1**	0	0	0	1/3
6	**0110**	1	**0**	**1**	**1**	**0**	0	0	0	1/3
7	**0111**	1	**0**	**1**	**1**	**1**	0	0	0	1/4
8	**1000**	1	**1**	**0**	**0**	**0**	0	0	0	1/2
9	**1001**	1	**1**	**0**	**0**	**1**	0	0	0	1/3
10	**1010**	1	**1**	**0**	**1**	**0**	0	0	0	1/3
11	**1011**	1	**1**	**0**	**1**	**1**	0	0	0	1/4
12	**1100**	1	**1**	**1**	**0**	**0**	0	0	0	1/3
13	**1101**	1	**1**	**1**	**0**	**1**	0	0	0	1/4
14	**1110**	1	**1**	**1**	**1**	**0**	0	0	0	1/4
15	**1111**	1	**1**	**1**	**1**	**1**	0	0	0	1/5

In order to illustrate the design of experiments, three cases (Code 02, Code 05, and Code 07) are represented in Figure 4-4, showing each dosage profile set and the corresponding response obtained (TOC, H_2O_2, and O_2). All experiments were repeated twice, and the average values are represented and used as reported by Yu et al. (2020).

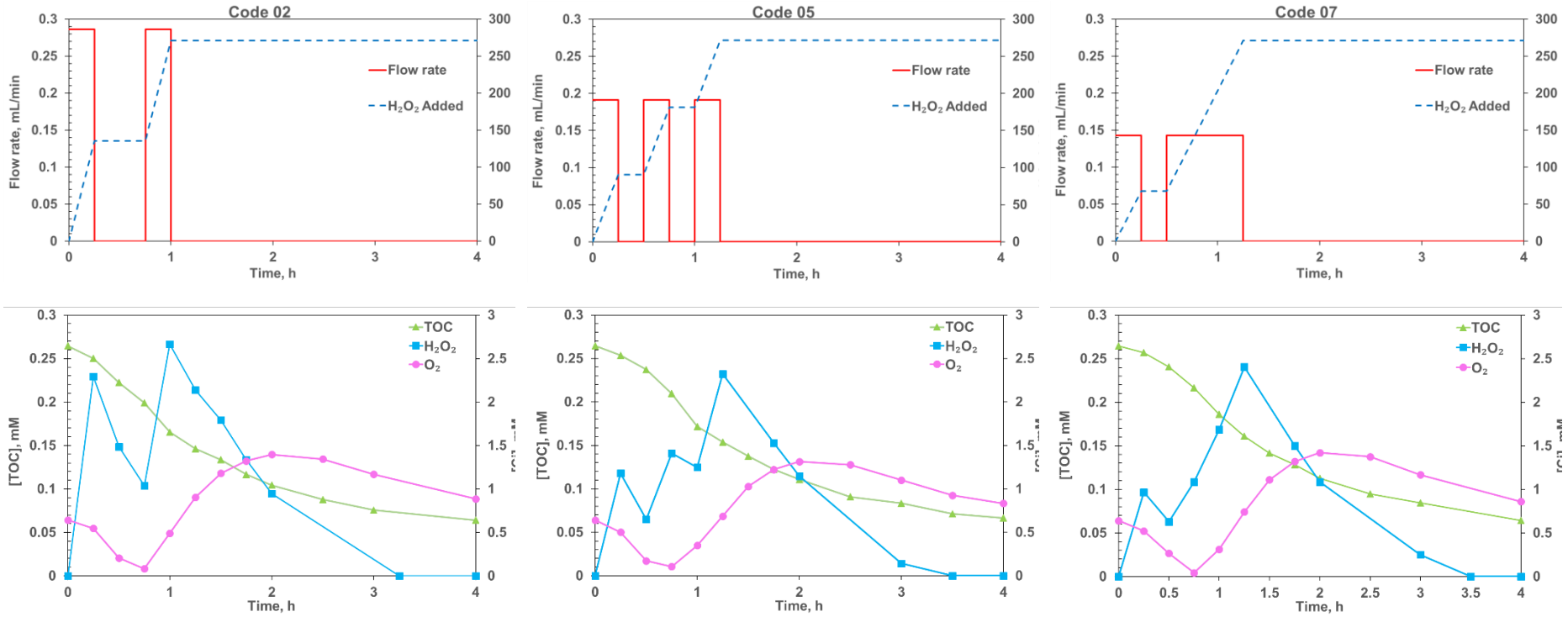

Figure 4-4 Experimental data for 3 particular hydrogen peroxide dosage profiles (codes 2, 5, and 7; 4 hours reaction time). Above: flow rate and amount of H_2O_2 added. Below: TOC, H_2O_2 evolution

4.2.3 Model fitting and parameter estimation

The model is calibrated by estimating the best parameter values. This is done by solving a nonlinear multivariate optimization problem to minimize the sum of the squared differences between the model values and the corresponding experimental data available. In this case, this includes the easily monitored TOC, H_2O_2, and O_2 concentrations, while excluding dummy variables such as the concentrations of intermediates (MX_1, MX_2, etc.). This is summarized by Eq.4-20.

$$min\, Z = \sum_i \left([\widehat{TOC}]_i - [TOC]_i\right)^2 + \sum_j \left([\widehat{H_2O_2}]_j - [H_2O_2]_j\right)^2 + \sum_k \left([\widehat{O_2}]_k - [O_2]_k\right)^2 \quad \text{Eq.4-21}$$

where the circumflex denotes experimental data.

This problem is solved using the Non-linear least-squares method with the Levenberg-Marquardt algorithm available in the Estimator Toolbox of MATLAB/Simulink® version R2021b.

To assess the goodness of fit, the Root Mean Square Error (RMSE), as the standard deviation of the residuals (prediction errors), will be used and presented for each measured time series k (TOC, H_2O_2, and O_2). The coefficient of determination R^2 (Eq.4-22) is also presented as an informative statistical measure that is widely used. Caution is required in the use and interpretation of R^2 in nonlinear models since the total sum-of-squares is not equal to the regression sum-of-squares plus the residual sum-of-squares, as in the case of linear regression (Spiess and Neumeyer, 2010). It is used along with RMSE for illustrative purposes.

$$RMSE_k = \sqrt{\left(\sum_{i=1}^{N_k} (\hat{y}_{ik} - y_{ik})^2 \Big/ N_k\right)} \quad \text{Eq.4-23}$$

$${R_k}^2 = 1 - \left(\sum_{i=1}^{N} (\hat{y}_i - y_i)^2 \Big/ \sum_{i=1}^{N} (\hat{y}_i - \bar{y})^2\right) \quad \text{Eq.4-24}$$

where $\hat{y}_i$ and y_i correspond to the measured and simulated values at the given time, respectively, and $\bar{y}$ is the mean of the measured data.

4.2.4 Global sensitivity analysis

Parameter sensitivity analysis is used to examine a mathematical model to reveal the relative importance of the various mechanisms included in the model and the robustness of its output with respect to parameter uncertainty (Latunde and Bamigbola, 2018).

One approach to sensitivity analysis is Local Sensitivity Analysis (LSA), which is computationally inexpensive. They are based on derivatives (numerical or analytical) and analyze the effect of one parameter at a time, while the other parameters are kept constant. However, these methods are limited to the exploration of only a small portion of the solution space (Castillo et al., 2004). Another approach is global sensitivity analysis (GSA), often implemented using Monte Carlo techniques to overcome the limits of LSA (linearity and normality assumptions and local variations). GSA uses a globally representative set of samples to explore the solution space. Furthermore, several input factors can be simultaneously varied to evaluate not only the effect of one factor at a time but also the effect of interactions between inputs, since the sensitivity to an input may depend on other inputs (Saltelli et al., 1999). In this study, GSA is adopted as it has been implemented frequently for models having multiple correlated outputs.

There are several GSA techniques, mostly statistical and analytical methods. New analytical and statistical methods are reported such as global screening methods (e.g., Morris method) (Campolongo et al., 2007), variance-based methods (e.g. Sobol's method and Fourier Amplitude Sensitivity Test) (Saltelli et al., 1999), sampling-based methods (e.g. Latin hypercube sampling with partial rank correlation coefficient index, LHS-PRCC) (Helton et al., 2006a) and others. These techniques have been developed specifically for complex models of policy and allocation problems.

One of the statistical methods for GSA using the sampling techniques is the application of partial rank correlation coefficients (PRCC) as a measure of sensitivity for a large, complex computerized model. The best of the sampling schemes, Latin hypercube sampling (LHS), is a procedure that structures input trials in an optimum and comprehensive model-testing design. The LHS method is selected along with an efficient stratification Monte Carlo sampling method allowing the extraction of a large amount of uncertainty and sensitivity information with a relatively small sample size (Marino et al., 2008a). The combined LHS-PRCC method is used to analyze how the model parameters and the output are correlated, removing the effects of the remaining parameters and

considering general monotonic relationships between inputs and outputs. In PRCC, also referred to as Spearman analysis and ranked transformation, a model with P number of model parameters and a model output y can be written as a function of all the model parameters values x_k $(k = 1, 2, \dots, P)$ so that $y = f(x_1, x_2, \dots, x_P)$. Hence, N samples $(i = 1, 2, \dots, N)$ for each model parameter will produce a set of P sample vectors X_k $(1 \times N)$ and an associated vector Y $(1 \times N)$ of output values. Then, the partial rank correlation coefficients for each parameter (R_{X_kY}) are calculated as follows (Marino et al., 2008a):

$$R_{X_kY} = \frac{cov(X_k, Y)}{\sqrt{Var\,(X_k) Var(Y)}} = \frac{\sum_{i=1}^{N}(x_{ik} - \bar{x})(y_i - \bar{y})}{\sqrt{\sum_{i=1}^{N}(x_{ik} - \bar{x})^2 (y_i - \bar{y})^2}} \qquad \text{Eq.4-25}$$

The R_{XY} values range from -1 to 1, their magnitude indicates the parameter influence, and the sign indicates whether an increase in the parameter value corresponds to an increase or decrease in the output (Helton et al., 2006a). Generally, it is assumed, also in this work, that a R_{XY} values between -0.1 and 0.1 ($-0.1 < R_{XY} < 0.1$) reflect a poor level of importance of a parameter.

The combined LHS-PRCC procedure is fully described elsewhere (Marino et al., 2008a), but generally involves (i) sampling of the parameter space, (ii) obtaining model output for each set of sampled parameters, (iii) ranking parameter and output values and replacing their original values with their ranks, and (iv) calculating the R_{XY} for each input parameter.

In regard to the model output, different options are possible, and a decision is required. The model produces many different calculated values that need to be pondered and/or aggregated to produce a reduced and comprehensive set of output values Y. The option in this work is the summation of the square errors, which be considered independently for the three process variables that are experimentally monitored (TOC, H_2O_2, and O_2):

$$Y1 = \sum_i \left([\widehat{TOC}]_i - [TOC]_i \right)^2 \qquad \text{Eq. 4-26}$$

$$Y2 = \sum_j \left([\widehat{H_2O_2}]_j - [H_2O_2]_j \right)^2 \qquad \text{Eq.4-27}$$

$$Y3 = \sum_{k} \left([\widehat{O_2}]_k - [O_2]_k \right)^2 \quad \text{Eq.4-28}$$

This choice favors the fidelity of the model to the available experimental data but would be open to discussion in other situations (e.g., an economic output in case of further using the model for optimization).

GSA is implemented in Simulink Design Optimization software using 150 samples obtained by LHS and all experimental data sets provided by Yu et al., 2020. Finally, the results ($R_{X_{kr}Y_r}$) for each parameter are averaged accordingly. Hence the model is discussed in regard to the chances for reducing complexity.

4.3 RESULTS AND DISCUSSION

4.3.1 Model simulation, verification, and analysis

A first step aimed at verifying the procedure and providing comparative results is fitting the model to the ideal data without experimental error from the simulation of the model using the same parameter values by Cabrera Reina et al. (2012).

Figure 4-5 shows the simulations before and after parameter estimation for two cases: one with no dosage using the data provided in Table 4-1 and one with an additional H_2O_2 dosage profile defined by an inlet flow active from 0 to 15 min and from 45 to 60 min (Code 02).

Results show excellent agreement between the ideal data and predicted data. In the case of no dosage, the RMSE resulted in 0.0008, 0.017, 0.005 mM for TOC, H_2O_2, and O_2, respectively. In the case of dosage case, the lowest values of RMSE of 0.005, 0.029, 0. 013 mM for TOC, H_2O_2, and O_2, respectively. This is summarized in Table 4-3.

a) Without dosage. Initial simulation.

b) Without dosage. After model fitting.

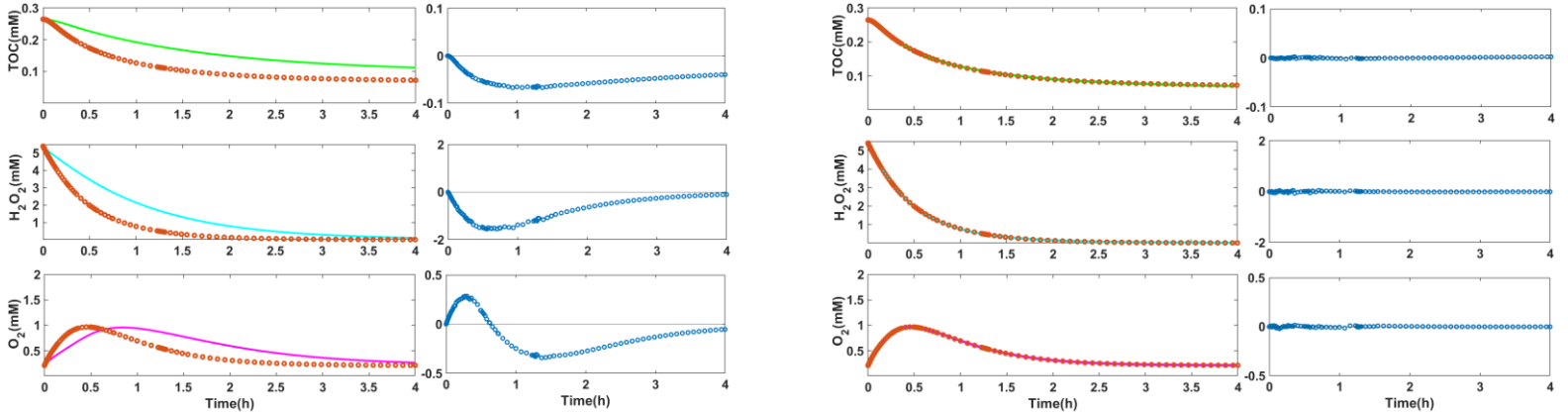

a) With dosage (Code 02,0010). Initial simulation.

b) With dosage (Code 02,0010). After model fitting.

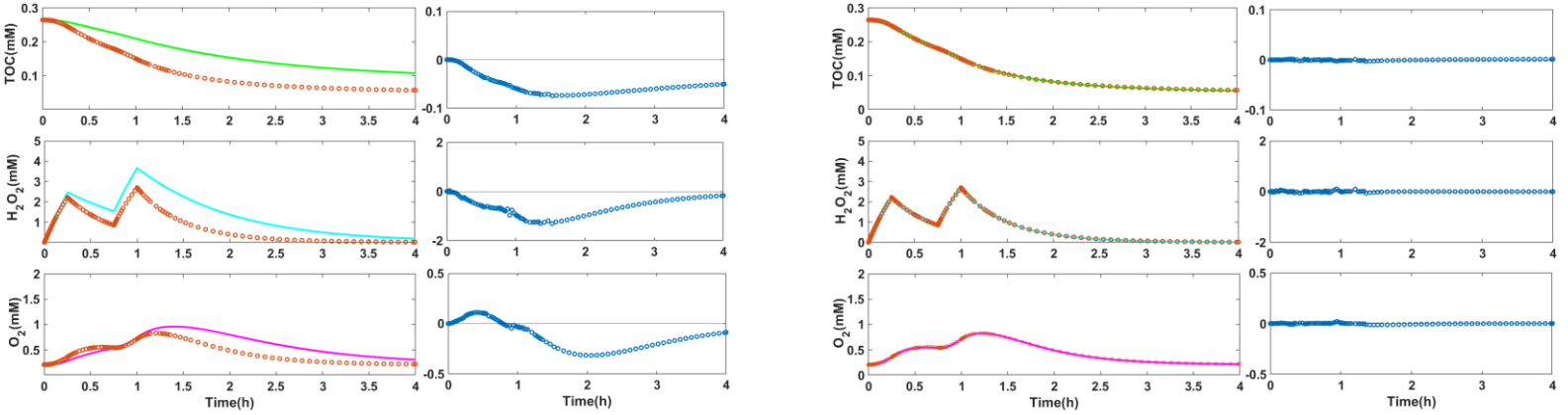

Figure 4-5 Parameter estimation and residual values for two illustrative cases with and without dosage (simulated data)

Table 4-3 The goodness of fit for the model adjusted to simulated data

Goodness of fit	**RMSE (mM)**		R^2	
Case study	**Dosage**	**No dosage**	**Dosage**	**No dosage**
TOC	0.005	0.0008	0.998	0.999
H_2O_2	0.029	0.017	0.999	0.999
O_2	0.013	0.005	0.997	0.999

Thus, the quantitative results in Table 4-3 confirm a good tuning of the fitting method, efficient performance, and the capability to attain accurate fitting of the model to the data. Residual values and RMSE (mM) obtained with simulated data attained are much lower than the usual experimental error associated with the measurements of TOC, H_2O_2, and O_2

4.3.2 Global sensitivity analysis

The robustness and complexity of the model are next analyzed via GSA, assuming independent model parameters and adopting 150 samples for each parameter using LHS-PRCC. The output is the sum of square errors between simulated and experimental data through all samples and for each measured variable (TOC, H_2O_2, and O_2).

Figure 4-6 shows the corresponding averaged correlation coefficients obtained for each parameter of the photo Fenton model, sorted by its influence on the signal matching of the simulated data (obtained by LHS) to the all data sets of the experimental data for TOC, H_2O_2, and O_2 as well as the average of all those in the role of the sensitivity function. Particularly, Figure 4-6 reveals that correlation coefficients for k_5, k_6, and k_8 are below the threshold $|R_{XY}| \geq 0.10$ for all three outputs TOC, H_2O_2 and O_2, which indicates their scarce relevance to the capability of the model to fit the experimental data.

The negligible effect of k_6 and k_5 suggests that two different reactions with hydroxyl radicals (reaction 4-5 with O_2 and reaction 4-6 without O_2) equally compete for producing the same output. Consequently, reactions 4-5 and 4-6 are coupled, assuming that reaction 4-5 is the only reaction converting M to MX_1. Certainly, this analysis and this assumption are acceptable only in the presence of light.

On the other hand, the negligible effect of k_8 suggests that the reaction of MX_1 and R generating CO_2 (and intermediate compound MX_2) is not necessary for the model to accurately describe the delay in the conversion of M to CO_2.

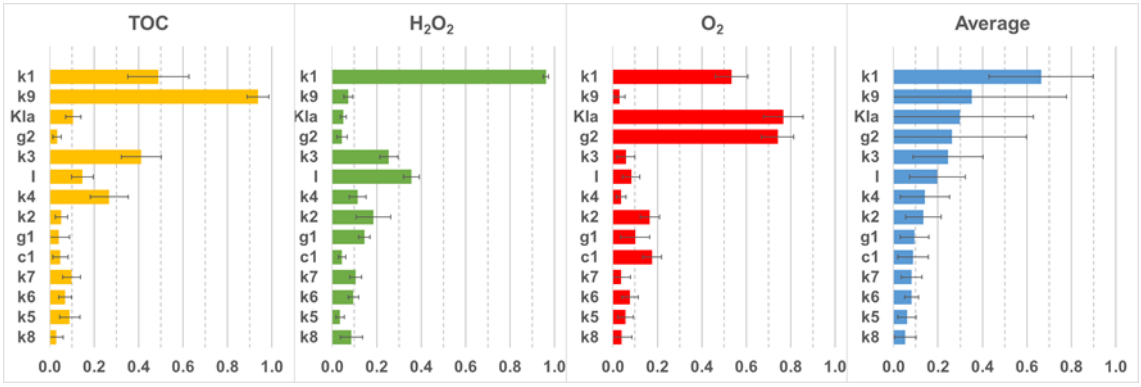

Figure 4-6 Sensitivity analysis and correlation coefficients R_{XY} for all model parameters (absolute value)

These parameters with scarce influence on the model output can be omitted to reduce its complexity. Hence, they were removed, and GSA was run again without k_6 or k_8 to assess the importance of the rest of the parameters. Results are shown in Figure 4-7.

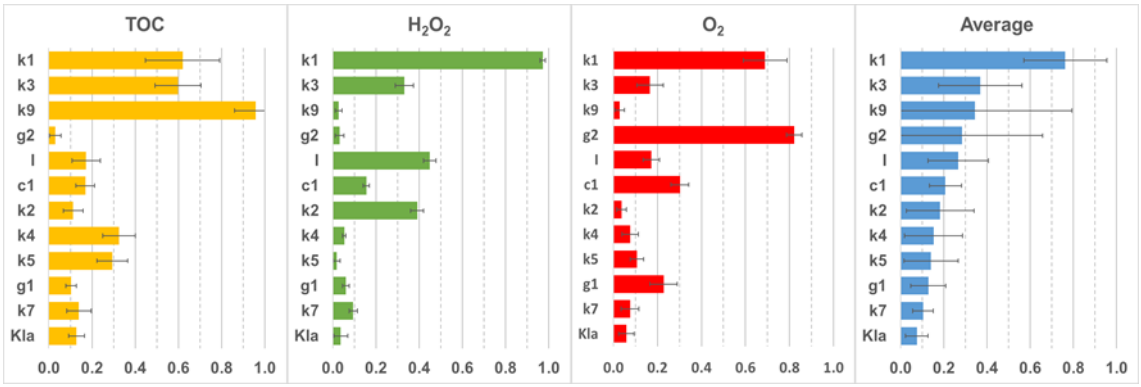

Figure 4-7 Sensitivity analysis and correlation coefficients R_{XY} for all parameters of the model without k_6 and k_8 (absolute value)

Considering the same criterion ($|R_{XY}| \geq 0.10$), all the remaining parameters were revealed necessary as their corresponding $|R_{XY}|$ values were obtained greater than this threshold for at least one measured variable (TOC, H_2O_2, or O_2). Therefore, the kinetic constants (k_1, k_2, k_3 ,k_4 ,k_5 ,k_7 ,k_9, K_La), stoichiometric coefficients c_1, g_1, and g_2, in addition to operational parameter I, are finally the 12 parameters to be estimated.

It is worth discussing the change in the relative significance of certain parameters after reducing the model. The most relevant variation is found for K_La, which becomes the least influential parameter. Surprisingly, K_La is revealed as the less influential parameter for explaining the behavior of dissolved oxygen. On the one hand, the rate change of $[O_2]$ depends on (Eq.4-15):

- the oxygen input via dosage $[O_2]_{in}$, which is considered zero,
- the internal generation of O_2 via reactions 3 and 4 (parameters g_1 and g_2),

- the internal consumption of O_2 via reaction 5 (parameter c_1),
- and the diffusion of O_2 from/to the environment (parameter $K_L a$)

On the other hand, $[O_2]$ values are close to saturation, $[O_2]^*$; the gradient $[O_2] - [O_2]^*$ is almost null, and the product is hardly affected by the value of $K_L a$. This point is relative to the values attained by $g_1 r_3 + g_2 r_4 - c_1 r_5$, and certainly, the same sensitivity analysis shows that g_1, g_2, and c_1 have the most significant effect on the model output after k_1. The values of g_1, g_2, and c_1 can freely combine, and effectively they do, to adjust the model response to the experimental data.

This interesting result shows that different model fittings could be able to explain the same experimental data. This is clearly connected to the prior discussion on the multiple local optima that can be encountered by the optimization algorithm and reveals that while a model can be correctly adjusted for practical purposes, further mathematical research beyond the scope of this work is required to determine the best number of model parameters and their optimal value.

4.3.3 Model fitting and parameter estimation

The issue when attempting the fitting of a nonlinear model to experimental data is the initial guess of the iterative optimization procedure. Fitting methods may find different sets of parameter values or may converge to local solutions, if at all (Dattner, 2015). Convergence problems and the existence of multiple optima have been detected in this work depending on the selection of the set of initial parameters values. While these problems are reported, a general solution approach is out of the scope of this work and it is not attempted. Hence, an ad-hoc heuristic is employed and presented based on using a multi-start algorithm that fits the model to individual data sets and finds a set of parameter values that applies to all the dosage profiles.

The proposed approach is summarized to execute a preliminary step with a set of initial values in the parameter space and generate a first-round fit for all assays. Then, following the strategy, the average of estimated parameter values for all the data sets are evaluated in terms of capability to predict different dosage profiles as well as acceptable goodness of fit. In the case of unacceptable fit, the new fitting round is performed starting with the best fitting results out of all data sets as the initials for the parameter search. In other words,

1. Use the reported values for the parameters (Cabrera-Reina et al., 2012) as the initial values
2. Use the best fitting results out of all trials in the first round as initial values for the second tuning round

The parameter values reported by Cabrera Reina et.al (2012) were used as initial guesses. Next, the best fitting results (lowest RMSE) were chosen as the initial values to be used for the second round of parameter estimation.

Table 4-4 provides the estimation results of the kinetic parameters for Code 02 as the best fit among all reflected assays with RMSE values below 0.20 mM for TOC, H_2O_2, or O_2 using the reported values for the parameters as initials.

Table 4-4 Estimation results of the kinetic parameters for Code 02 as the best fit through the first round

Kinetic constants	**Initial value**	**Fitted values**
I $(W.m^{-2})$	32	29.75
$K_La(h^{-1})$	2.7	0.49
c_1	0.1	5.9
g_1	0.75	0.32
g_2	0.47	0.63
$k_1(mM^{-1}.h^{-1})$	8.81	8.07
k_2 $((W.m^{-2})^{-1}.h^{-1})$	5.63	28.46
$k_3(mM^{-1}.h^{-1})$	75.8	0.97
$k_4(mM^{-1}.h^{-1})$	42,798	43,962
$k_5(mM^{-2}.h^{-1})$	2,643	1,113
$k_7(mM^{-1}.h^{-1})$	2,865	42,133
$k_9(mM^{-1}.h^{-1})$	107	93.27
Goodness of fit	**RMSE (mM)**	R^2
TOC	0.010	0.99
H_2O_2	0. 200	0.96
O_2	0. 111	0.94

Table 4-5 displays the parameter values produced by the fitting of the model to each of the experimental data sets obtained from each dosage profile using the results obtained in the first round (See Table 4-4) as initial values. While the quality of the fitting is similar for all the cases, the set of values obtained for each parameter presents different distribution patterns with a very large variance in some. Parameters, k_9, c_1, k_4, k_5, g_2, k_1 present low variance (in increasing order) and, k_9 is revealed as the most certain value. Parameters, k_2, K_La , k_7, g_1, I and k_3 (in increasing order) present large variance and some disparate values. k_3 is the most fluctuating parameter.

To address this disparity, values beyond 3σ are highlighted in Table 4-5 (bold shadowed). These values may indicate outliers, but also suggest that fittings for No dosage, 3 and 8 may be following another pattern (which suggests in turn the determination of a different local optimum).

On the one hand, this indicates that further work may be required in regard to global optimization and attaining the same fitting in all the cases. On the other hand, identifying outliers requires a lot of caution and has no definitive criteria. From a practical point of view, the point is investigating to which extent this produces a good enough model for predicting the evolution of the process as a function of the dosage.

Hence, values beyond three standard deviations (3σ, 1 out of 370 measurements) are discarded as unlikely to have a set of 15 measurements (2.98σ was used for k_3). This allows producing more sensible data sets and average values for the next step.

Table 4-5 Estimated kinetic parameters (k_i ($\mathrm{mM}^{-1}.h^{-1}$), k_2 ($(\mathrm{W}.m^{-2})^{-1}.h^{-1}$), k_5 ($\mathrm{mM}^{-2}.h^{-1}$), I ($W.m^{-2}$) and $K_L a$ (h^{-1})

Code	I	$K_L a$	c_1	g_1	g_2	k_1	k_2	k_3	k_4	k_5	k_7	k_9
No dosage	**221.550**	0.653	5.325	0.247	**1.007**	7.954	36.317	**68.719**	42125	1008.7	31853	96.878
0	14.859	0.426	7.157	0.248	0.694	11.638	38.077	**43.987**	35152	1045.0	85686	88.710
1	25.332	0.534	5.493	0.151	0.644	7.408	34.344	0.033	44273	1064.3	10343	84.674
2	29.751	0.493	5.902	0.319	0.633	8.073	28.458	0.971	43962	1113.0	42133	93.265
3	25.471	0.388	6.172	0.418	0.701	8.807	29.139	1.593	50899	**1694.1**	**163780**	90.318
4	28.004	0.491	5.905	0.466	0.639	8.555	22.501	0.048	44969	1118.7	51767	92.468
5	42.079	0.532	5.960	0.335	0.597	9.305	38.622	0.114	44871	1117.3	41309	90.406
7	29.595	0.511	5.897	0.321	0.621	9.650	28.423	0.155	50391	1118.5	40982	94.287
8	23.972	**1.625**	6.566	1.294	0.579	7.153	**93.918**	1.091	40703	1128.6	47280	87.024
9	57.256	0.517	5.837	0.893	0.607	8.620	52.795	9.306	48131	1080.5	53672	90.116
10	30.901	0.522	5.964	0.327	0.630	8.700	35.568	0.168	46679	1096.0	55000	89.894
11	7.159	0.440	6.428	0.904	0.606	12.423	39.853	3.440	51131	1266.6	51990	95.191
12	32.721	0.509	5.871	0.491	0.636	8.619	19.920	2.949	47142	1071.0	40721	94.046
13	69.654	0.497	5.793	0.348	0.610	9.908	19.693	9.612	47334	1119.8	41749	90.309
14	30.097	0.474	5.903	0.325	0.640	8.514	27.604	0.881	46018	1047.6	44529	89.449
Mean	44.560	0.574	6.011	0.472	0.656	9.022	36.349	9.538	45585	1139.3	53520	91.136
Median	29.751	0.509	5.903	0.335	0.633	8.620	34.344	1.091	46018	1113.0	44529	90.318
Std. Dev.	51.280	0.297	0.440	0.313	0.102	1.433	18.131	19.816	4186	164.0	34217	3.229
Confidence	28.398	0.164	0.244	0.173	0.057	0.794	10.041	10.974	2318	90.8	18949	1.788
Int.(α=0.05)	(± 64 %)	(± 29 %)	(± 4 %)	(± 37 %)	(± 9 %)	(± 9 %)	(± 28 %)	(±115%)	(± 5 %)	(± 8 %)	(± 35 %)	(± 2 %)
After discarding values beyond 3σ												
Mean	31.918	0.499	6.011	0.472	0.631	9.022	32.237	2.335	45585	1099.7	45644	91.136
Median	29.673	0.503	5.903	0.335	0.632	8.620	31.742	0.971	46018	1104.5	43331	90.318
Std. Dev.	15.816	0.061	0.440	0.313	0.034	1.433	8.993	3.343	4186	60.0	16090	3.229
Confidence	8.758	0.034	0.244	0.173	0.019	0.794	4.980	1.852	2318	33.2	8910	1.788
Int.(α=0.05)	(± 27 %)	(± 7 %)	(± 4 %)	(± 37 %)	(± 3 %)	(± 9 %)	(± 15 %)	(± 79 %)	(± 5 %)	(± 3 %)	(± 20 %)	(± 2 %)

Despite their variability, the average values estimated for the model parameters allow producing practical model responses matching the experimental results (Figure 4-8). Figure 4-8, compares the experimental data and the simulated TOC, H_2O_2, or O_2 profiles for all dosage schemes used in model fitting, and shows a qualitative image of the overall capability of the model to reproduce the measured behavior of the process, remarkably the changing trend of the H_2O_2, or O_2 profiles.

Table 4-6 presents the quantification of the goodness of fit for each assay. TOC values for all simulated examples were accurately predicted, and the RMSE values were lower than 0.015 mM and R^2 values were close to unity. Also, the simulation for H_2O_2 and O_2 resulted in good agreement with the experimental data, but to a lesser extent. The concentration values estimated for the monotonic evolution of TOC are accurate, within the limits of the experimental error and the precision of the measurements. Conversely, the trends estimated for the fluctuating H_2O_2 and O_2 concentration profiles (the derivatives, which may be useful for the process monitoring) follow the evolution of the experimental data, but the residual values are larger. However, these differences cause a minor influence on the practical application of the model to describe the performance of the process, which is expressed in terms of the evolution of TOC.

The average CPU time required by the multi-level method to reach convergence for one single run of parameter estimation or GSA is 20 to 30 mins in a PC i7-Intel(R) Xeon(R) Silver 4114 CPU @2.20GHs 128Gb RAM. However, using Parallel Computing Toolbox™ software speeds up parameter estimation/GSA of Simulink models by distributing the simulations, and significantly reduces the total estimation run-time by 5 to 7 times.

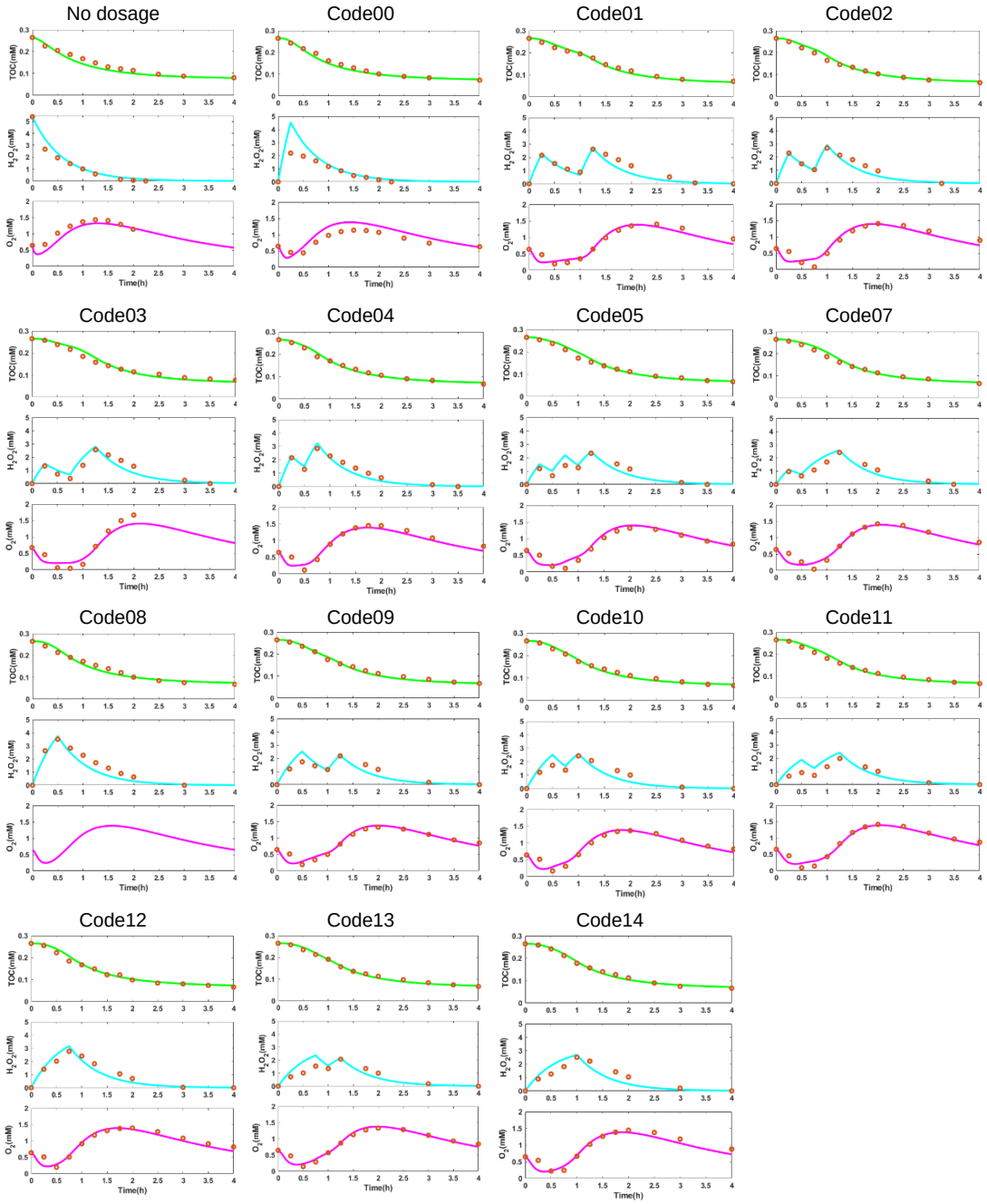

Figure 4-8 Experimental data and predicted profiles in different dosage modes with final average values for the parameter

Table 4-6 Root mean square error (RMSE) and coefficient of determination (R-Squared) for all the sets of experimental data, including those not used for model fitting (validation cases Code 06 and Code 15, which appear shadowed)

ID	ID	RMSE			R^2 Ordinary		
(Code)	(bin)	TOC (mM)	H_2O_2 (mM)	O_2 (mM)	TOC	H_2O_2	O_2
No dosage	N/A	0.0151	0.3854	0.1513	0.97	0.97	0.87
0	0000	0.0101	0.8595	0.2097	0.99	0.91	0.95
1	0001	0.0084	0.2761	0.0835	0.99	0.93	0.96
2	0010	0.0096	0.2630	0.1204	0.99	0.93	0.92
3	0011	0.0118	0.3282	0.1780	0.98	0.86	0.96
4	0100	0.0072	0.2475	0.0959	0.99	0.95	0.95
5	0101	0.0097	0.3670	0.1126	0.99	0.82	0.94
6	0110	0.0082	0.3931	0.1067	0.99	0.85	0.95
7	0111	0.0097	0.3050	0.1067	0.99	0.90	0.95
8	1000	0.0117	0.3728	-	0.97	0.95	-
9	1001	0.0078	0.3741	0.0908	0.99	0.83	0.95
10	1010	0.0077	0.4006	0.0913	0.99	0.83	0.95
11	1011	0.0091	0.4841	0.0893	0.99	0.79	0.96
12	1100	0.0087	0.3045	0.0812	0.99	0.93	0.96
13	1101	0.0064	0.4609	0.0793	0.99	0.77	0.96
14	1110	0.0065	0.4114	0.0991	0.99	0.82	0.95
15	1111	0.0089	0.2109	0.1294	0.99	0.94	0.95

4.3.4 Validation

Model validation is an important part of the study that was carried out to confirm that the model actually achieves the purpose of explaining the process dynamics under dosage schemes not included in the model fitting. Thus, the experimental data sets Code 06 and Code 15 that were not used in the calibration of model parameters were compared to the simulations obtained by setting the same dosage profiles to the model fit to the rest of the data sets. These two dosage profiles follow two different H_2O_2 supply strategies: dosing H_2O_2 continuously from 0 to 15 min and from 30 to 60 min for Code 06; and dosing H_2O_2 continuously from 0 to 75 min for Code 15 15. Figure 4-9 displays the simulations and the experimental data along with their residuals for these two cases.

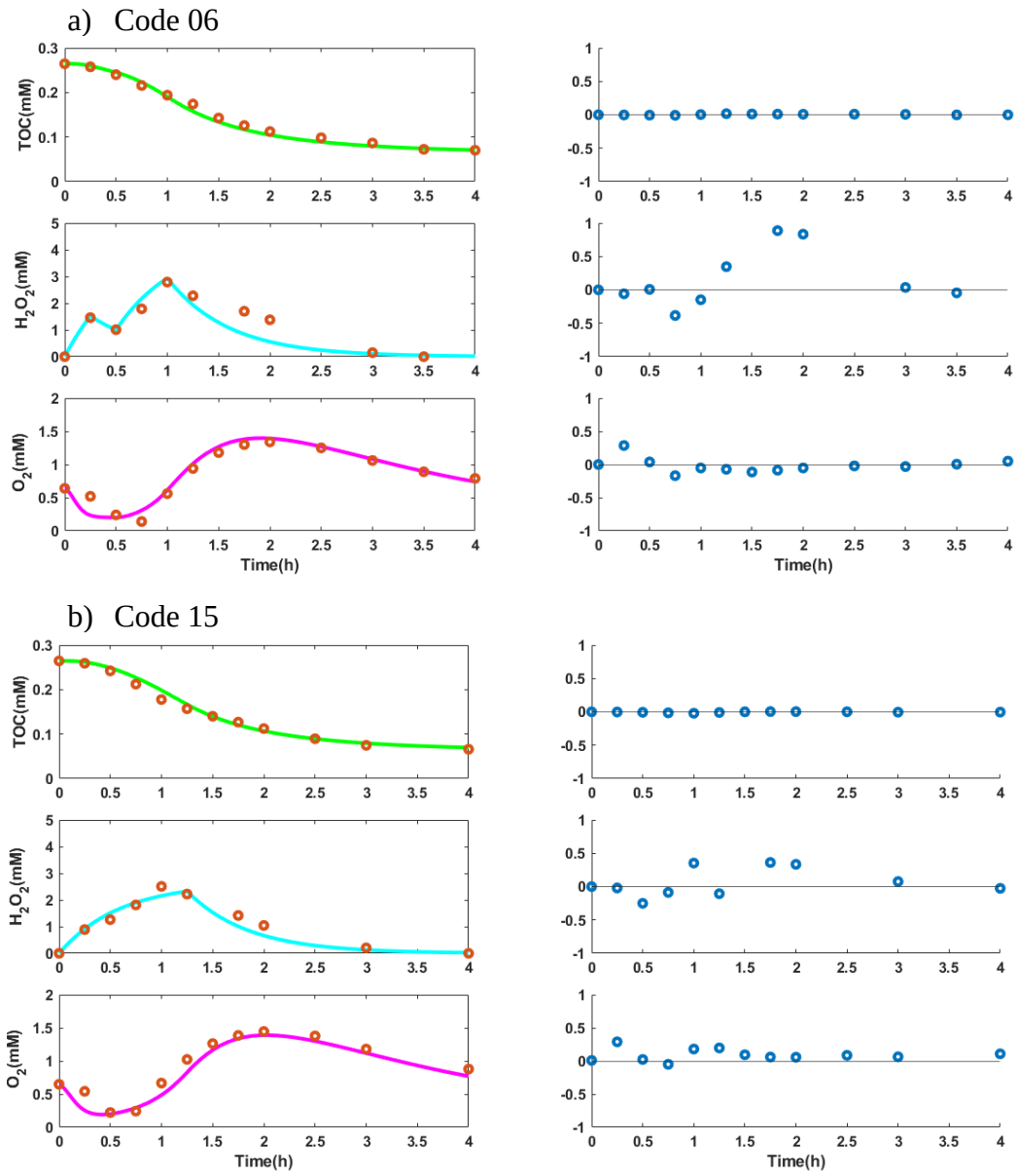

Figure 4-9 Validation: experimental data (codes 06 & 15) and predicted profiles

In both cases, the model very accurately explains the monotonic decay of the TOC concentration (RMSE<0.009 mM) as well as the convex behavior of the derivative due to the initial delay that the presence of intermediates causes in TOC response. The model also describes very well the fluctuating concentrations of hydrogen peroxide and dissolved oxygen along the 4h reaction time. However, the residuals values for H_2O_2 and O_2 are greater than those obtained for TOC.

The quantification of the goodness of fit is also presented in Table 4-6. The prediction is given in the validation cases with an RMSE<0.009 mM for TOC, close to the detection error of the measurement, which is 0.02 mM. The R-squared value of 0.99 shows the good fit of the model in the case of TOC. The model is capable of

describing the evolution of H_2O_2 under variable dosage with an RMSE value lower than 0.42 mM, which corresponds to 8% of the maximum H_2O_2 concentration (5.397 mM) in the reactor. Likewise, O_2 evolution was predicted properly by an RMSE < 0.127 mM close to 9% the maximum O_2 concentration (1.406 mM) in the reactor.

The model validation process indicated the adequacy of the model representation of the system under study. The model and the procedure to adjust it is shown to be capable of reproducing the evolution of the reaction under diverse and variable dosage schemes and predicting future situations under new operating conditions. Hence, the tools and the methodological approach, the main contribution of this work, are ready for easily testing and assessing new dosage strategies that could be designed. On one hand, the use of a fitted model to test any given continuous time-dependent H_2O_2dosage profile would clearly provide a deeper understanding of the photo-Fenton treatment and support informed decision-making on the H_2O_2supply problem. On the other hand, the possibility of developing and fitting such a model enables the future use of model-based optimization techniques so that the systematic exploration of alternatives could subsequently lead to determining the optimal dosage strategy for each situation.

4.4 CONCLUSIONS

This work contributes a novel step towards solving the optimal dosage scheme required by photo-Fenton processes. Experimental approaches are essential to providing the necessary insight into the mechanisms involved in the efficient use of hydrogen peroxide, but the exploration and assessment of all possible dosage profiles cannot be attempted experimentally. Hence, this work has presented and discussed the development, fitting, and validation of a dynamic photo-Fenton model including a flexible hydrogen peroxide supply aimed at being further exploited in determining the optimal dosage profile for a given photo-Fenton treatment. The work relies on the previous works by Cabrera-Reina et al (2012) and Audino et al. (2019) to propose the model and uses the experimental results provided by Yu et al. (2020) to fit the model to the comprehensive set of hydrogen peroxide supply schemes.

After verifying the model with the adjustment to simulated data, a sensitivity analysis of the model fitting was performed. This analysis provided valuable insight

into the nature of the model, as well as on the mathematical challenges still pending in regard to determining globally optimal fittings. Two of the reactions proposed were found to have a scarce influence on the fitting of the model, for which they were excluded. Hence, the model has been adjusted to a series of experimental data with different dosage profiles, and has been next validated using independent experimental data sets that were not used in the calibration of the model.

The validation using different dosage profiles confirmed the capacity of the model to accurately explain alternative dosage schemes, showing average errors such as RMSE<0.009 mM for TOC, RMSE<0.42 mM for H_2O_2, and RMSE < 0.127 mM for O_2. Such a fidelity of the model in describing the experimental measurements can be acceptable at this point, but it will require further analysis when addressing the optimization of the dosage profile and considering the capacity of the model to accurately describe the objective function (e.g., a process economic output). Therefore, the model development is ready to address further attempts the model-based optimization of the dosage profile in subsequent investigations.

Chapter 5: Mechanistic Modeling of Fe^{3+} – EDDS Mediated Photo-Fenton Revisited: Lumped Radicals and Sensitivity Analysis

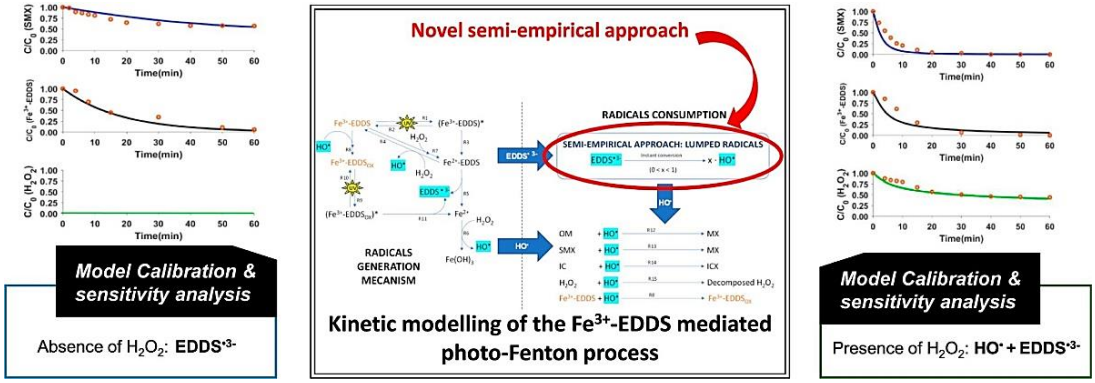

Redrafted from: (Nasr Esfahani et al., 2023)

Nasr Esfahani, K., Pérez-Moya, M., Graells, M., Miralles-Cuevas, S., & Cabrera-Reina, A. (2023). Mechanistic modeling of Fe^{3+}-EDDS mediated photo-Fenton revisited: lumped radicals and sensitivity analysis. Chemical Engineering Journal, 142559.

This study (Chapter 5) proposes a new kinetic model of the $Fe^{3+} - EDDS$ mediated photo-Fenton process at circumneutral pH when applied to microcontaminants (MCs) removal. The model is also able to work in the absence of H_2O_2, when $EDDS^{\bullet 3-}$ radicals generated from the lysis of the $Fe^{3+} - EDDS$ complex are responsible for MCs degradation, representing a new advance in this research field. A novel semi-empirical approach based on lumping radical species is adopted. This is done by including a factor in the model to describe the lower oxidation capacity of $EDDS^{\bullet 3-}$ radicals in front of hydroxyl radicals. Model calibration demonstrated the effectiveness of the semi-empirical strategy to successfully predict the system behaviour in terms of sulfamethoxazole (SMX, model MC), $Fe^{3+} - EDDS$ and H_2O_2 (when needed) concentration evolution during the process. Then, a global sensitivity analysis (GSA) was carried out to reduce the computation cost of the model, indicating that once the initial $Fe^{3+} - EDDS$ complex is oxidized to $Fe^{3+} - EDDS_{OX}$, its photo-activation to $(Fe^{3+} - EDDS_{OX})^*$ is not actually reversible despite possible. Finally, the model was validated, showing that experimental data could be predicted properly, with NRMSE (Normalized Root Mean Square Errors) <0.08 for SMX and <0.15 for $Fe^{3+} - EDDS$ (normalized data). The oxidation capacity of the $EDDS^{\bullet 3-}$ radicals was estimated to be approximately 11% that of the hydroxyl radicals.

5.1 INTRODUCTION

Emerging microcontaminants (MCs) are synthetic or natural substances, which are biorecalcitrants to conventional biological processes applied in wastewater treatment plants (WWTPs). MC term includes a large range of chemical compounds that present very different chemical natures hindering their removal (Bacci and Campo, 2022). Usually, they are emitted from point and nonpoint sources and end up in low concentrations from $ng \cdot L^{-1}$ to $\mu g \cdot L^{-1}$ in the water environment (Chavoshani et al., 2020). Pharmaceuticals, as an example of MCs, have obtained growing attention due to the increasing hazard posed by the presence of these chemicals and/or their transformation products in the natural environment that, even in very low concentrations, threatens human health (Ortega-Moreno et al., 2022). Among them, Sulfamethoxazole (SMX) is a common antibiotic prescribed to treat infectious and respiration diseases, which is frequently detected in surface water ecosystems (Patrolecco et al., 2018). Since SMX contains a sulfonamide group that is present in many drugs, it is a representative drug for a broad range of antibiotics (Thiebault,

2020). This antibiotic has been classified as an emerging contaminant, and has been found in water resources at concentration levels from $ng \cdot L^{-1}$ to $\mu g \cdot L^{-1}$ (Al Aukidy et al., 2012; Bueno et al., 2012). Thus, considering that SMX is an archetypal and extended pharmaceutical that presents frequent occurrence in different water bodies, it has been selected as a model pollutant to study the removal of MCs in WWTP secondary effluents by different processes such as membrane technologies (Echevarría et al., 2020), heterogeneous photocatalysis (Matos Rodrigues et al., 2019) or even the combination of different treatments (Echevarría et al., 2019), among many others.

One of the most promising technologies for the degradation of MCs is advanced oxidation processes (AOPs), and among all AOPs, the photo-Fenton process has shown a high oxidation efficiency (Ayoub et al., 2019; Rizzo et al., 2020). Several studies have demonstrated that the photo-Fenton process efficiently degrades a wide range of MCs in different water matrices at lab-scale (Kowalska et al., 2021), pilot-scale (Cabrera-Reina et al., 2021) and even large-scale (Gualda-Alonso et al., 2022a).

However, the photo-Fenton process is pH-dependent due to the insolubility of the ferric aquo or hydroxy species at circumneutral pH, which limits its full-scale application due to the necessity of acidic pH. Consequently, the possibility of performing the photo-Fenton process at near-neutral pH has been studied using different strategies (Carra et al., 2014; Gomis et al., 2015; Villegas- Guzman et al., 2017; F.-X. Wang et al., 2022). In this regard, polycarboxylic compounds that form a complex with iron, such as citrate, oxalate, maleate, and ethylenediamine disuccinic acid (EDDS) have been investigated to operate the photo-Fenton process at near-neutral pH (Dong et al., 2019; Li and Gan, 2022; Manenti et al., 2015; Ting et al., 2022). Probably, the most studied chelating agent is EDDS, which is a biodegradable structural isomer of Ethylenediaminetetraacetic acid (EDTA) with efficient performance in the pH range 3-9 (Huang et al., 2013; Maniakova et al., 2022; Soriano-Molina et al., 2018; Zhang et al., 2016). The reduction of $Fe^{3+} - EDDS$ to $Fe^{2+} - EDDS$ is a crucial step that governs the formation of hydroxyl radicals, mainly responsible for the degradation of the contaminants (Huang et al., 2013) but, additionally, the use of EDDS under UV radiation causes the production of organic radicals that directly or indirectly contribute to MCs removal.

From an analytical and computational point of view, the development of robust mathematical models governing the dynamics and transport phenomena is a crucial step to improving the deep knowledge of the system and the process efficiency of almost any existing process. The availability of kinetic models allows for eliminating the dependency on the time and energy needed for intensive experimentations, which can be substituted by process simulation (Hosseini and Denayer, 2022). The kinetic modeling of the photo-Fenton process presents an important difficulty due to its complex reaction mechanism that has resulted in a lack of non-empirical models. Despite this, important efforts have been made in this field, especially by the research groups of Alfano from Consejo Nacional de Investigaciones Científicas y Técnicas (Argentina) (Farias et al., 2009; Venier et al., 2021), G. Li Puma from Loughborough University (UK) (Cabrera Reina et al., 2015; Peralta Muniz Moreira et al., 2021) or J.A. Sánchez-Pérez from the University of Almería (Spain) (Cabrera Reina et al., 2014; Soriano-Molina et al., 2018). In this context, while the kinetic modeling of the photo-Fenton process when operated at acidic pH has been typically investigated (Audino et al., 2017; Cabrera Reina et al., 2012; Kusic et al., 2009; Nasr Esfahani et al., 2022b), the literature reveals low records on kinetic modeling at circumneutral pH. Within this frame of reference, only the mechanistic modeling of $Fe^{3+}-$ EDDS and Fe^{3+}-NTA mediated photo-Fenton has been assessed. Soriano-Molina et al. (2018) studied the modeling of the photo-Fenton process with $Fe^{3+}-$EDDS, reporting higher photon absorption of iron complexed with EDDS compared to iron aquo complexes (Soriano-Molina et al., 2018). The model performance against different perturbations was also evaluated by analyzing its prediction capability when the treatment was applied to remove micropollutants from five different Spanish MWWTP secondary effluents (Soriano-Molina et al., 2019). Recently, Gualda-Alonso et al. (2022b) studied the mechanistic modeling of solar photo-Fenton mediated by Fe^{3+}-NTA when applied to the removal of microcontaminants. Despite both models presenting excellent results, none of them implicitly included the effect of the organic radicals generated from the lysis of the iron chelate on process performance, limiting the model application only to the addition/presence of the oxidant agent (hydrogen peroxide) (Gualda-Alonso et al., 2022b).

This work faces up the mechanistic modeling of the $Fe^{3+}-$EDDS mediated photo-Fenton process, including the stand-alone option of oxidant agent absence

(UVA/$Fe^{3+}-$EDDS process). With this purpose in mind, SMX removal in synthetic MWWTP secondary effluent by UVA/$Fe^{3+}-$EDDS process under different UVA radiation levels was initially evaluated. Afterwards, the same procedure was done but applying the $Fe^{3+}-$EDDS mediated photo-Fenton. A new semi-empirical mechanistic model was then proposed, and the experimental data was used for parameter estimation and model prediction capability evaluation. Finally, the impacts of fluctuations of the dynamic model parameters on the fitting performance were assessed through a sensitivity analysis reviewing the model structure.

5.2 MATERIALS AND METHODS

5.2.1 Reagents and Chemicals

SMX (>99%), selected as a model pollutant, was provided by Sigma Aldrich. Ferrous source $Fe_2(SO_4)_3.H_2O$ and hydrogen peroxide (H_2O_2, 33% w/v) used for the photo-Fenton process were supplied by Panreac. EDDS was provided by Sigma-Aldrich. HPLC grade acetonitrile, methanol, glacial acetic acid (> 99%, w/v), ortho-phenanthroline (99%, w/w) and sulfuric acid (96%, w/v) were also obtained from Panreac. All solutions were prepared in ultrapure water, produced with a Milli-Q® water purification system (PURELAB Option Q-7) with a specific resistance of 18.2 MΩcm and less than 5 $\mu g \cdot L^{-1}$ of DOC.

5.2.2 Water matrix

All the experiments were done in synthetic WWTP secondary effluent, which included: $CaSO_4.2H_2O$ (60 $mg \cdot L^{-1}$), $MgSO_4$ (60 $mg \cdot L^{-1}$), KCl (500 $mg \cdot L^{-1}$), $(NH_4)_2SO_4$ (23.6 $mg \cdot L^{-1}$), K_2HPO_4 (7.0 $mg \cdot L^{-1}$), $NaHCO_3$ (76.2 $mg \cdot L^{-1}$), beef extract (1.8 $mg \cdot L^{-1}$), peptone (2.7 $mg \cdot L^{-1}$), humic salts (4.2 $mg \cdot L^{-1}$), sodium lignin sulfonate (2.4 $mg \cdot L^{-1}$), sodium lauryl sulfate (0.9 $mg \cdot L^{-1}$), acacia gum powder (4.7 $mg \cdot L^{-1}$), and Arabic acid (5.0 $mg \cdot L^{-1}$). The total organic carbon (TOC) concentration of this recipe is ≈10 $mg \cdot L^{-1}$, and the total inorganic carbon (TIC) concentration is ≈15 $mg \cdot L^{-1}$, high enough to buffer the pH during the treatment so that it is possible to work at natural pH.

5.2.3 Experimental work plan

The first experimental series was focused on the removal of SMX by the $Fe^{3+}-$EDDS/UVA process, i.e., in the absence of H_2O_2. With this purpose in mind, several

assays were done changing the power of the LED lights from 25% up to 100%. All the experiments, Table 5-1, were done at natural pH using 0.1 mM $Fe^{3+}-EDDS$ at 1:1 Fe^{3+}:EDDS molar ratio. In this way, the contribution of the $EDDS^{\bullet 3-}$ radicals generated due to the breakage of Fe^{3+}-EDDS could be determined. Then, the same experimental series was carried out but this time, adding the oxidant agent, i.e., using Fe^{3+}-EDDS mediated photo-Fenton process. Once again, the experiments were done at natural pH using 0.1mM $Fe^{3+}-EDDS$ at 1:1 Fe^{3+}:EDDS molar ratio and 1.5 mM of H_2O_2. Thus, the contribution of the $Fe^{3+}-EDDS$/UVA process on the $Fe^{3+}-EDDS$ mediated photo-Fenton process could be studied and modeled.

Table 5-1 Experimental series

Assay ID	**SMX ($mg \cdot L^{-1}$) ±0.05**	**Fe^{3+}EDDS (mM) ±0.02**	**H_2O_2 (mM) ±0.01**	**UV ($W \cdot m^{-2}$)**	
A1	1.00	0.12	0	14	Fitting
A2	1.00	0.12	0	42	Fitting
A3	1.00	0.12	0	56	Fitting
B1	1.00	0.12	1.50	14	Fitting
B2	1.00	0.12	1.50	42	Fitting
V1	1.00	0.12	0	28	Validation
V2	1.00	0.12	1.50	28	Validation

5.2.4 Experimental setup and experimental procedure

The experimental series was done in a UVA-LED photoreactor (Figure 5-1) consisting of two Pyrex glass tubes (5cm internal diameter) connected to a recirculation tank. The system included 1200 LEDs (365nm) equally distributed in 8 stripes and symmetrically placed around the tubes (4 stripes/tube). The stripes were connected to a computer through a datalogger so that the power of the LEDs in each stripe could be independently selected. The working volume was 8L, and water flow ($20\ L \cdot min^{-1}$) was obtained by a centrifugal pump (Pan World NH-40PX).

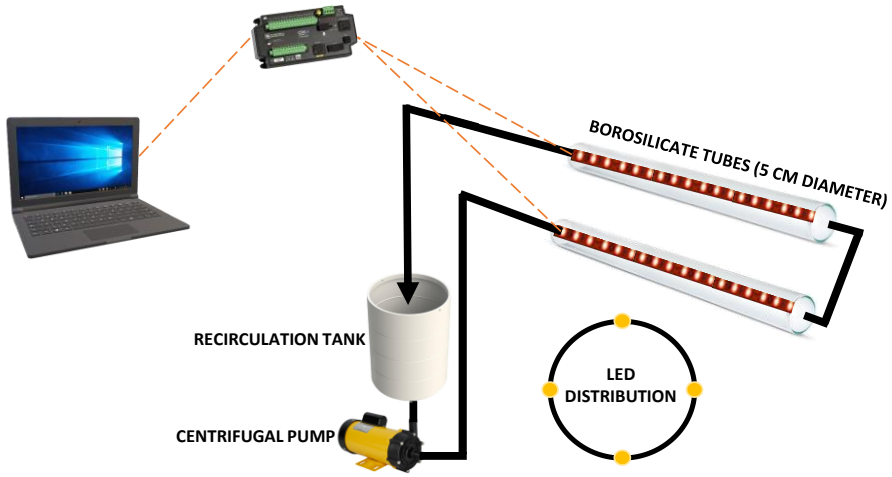

Figure 5-1 Experimental setup

Initially, the pilot plant was loaded with 8L of the synthetic MWWTP secondary effluent, and SMX (1 $mg \cdot L^{-1}$) was added. After 10 min of recirculation, 0.1 mM $Fe^{3+}-$EDDS was added, and after another 5 min of homogenization, the oxidant agent (when required) was added (1.5 mM). Immediately after, LED lights were switched on. Samples were taken every 2 min during the first 10 min, then every 5 min until 20 min and, from that moment, every 10 min until the end of the experiments (60 min).

5.2.5 Analytical determinations

All samples related to the quantification of SMX and $Fe^{3+}-$EDDS were quenched and filtered through 0.22 µm PTFE filters (Millipore) before injection in a JASCO Extrema HPLC equipped with a Supelco LICHROSPHER RP18-5 column and coupled to a JASCO DAD detector (model MD-4015). For SMX determination, an isocratic method was used in which the mobile phase A was 95% methanol and the mobile phase B was 5% formic acid (0.1%). SMX retention time was 4.7 min, and the resulting area was quantified at 267 nm. For $Fe^{3+}-$EDDS determination, an isocratic method was used in which the mobile phase A was 5% methanol, and the mobile phase B was 95% buffer solution (15 mM sodium formate, 2 mM tetrabutylammonium hydrogen sulphate adjusted to pH 4 with acetic acid). The $Fe^{3+}-$EDDS retention time was 6.8 min and the resulting area was quantified at 240 nm.

H_2O_2 was measured following DIN38402H15 based on titanium (IV) oxysulfate, while dissolved iron concentration was determined following ISO 6332 based on 1,10-phenantroline. Dissolved Organic Carbon (DOC) and total inorganic

carbon (TIC) concentrations were measured in a Shimadzu TOC-VCN analyzer. Samples were filtered through 0.45 μm Nylon filters (Milipore).

5.2.6 Kinetic model

The kinetic model proposed in this work revisits the reaction scheme published by Soriano-Molina et al. (2018) with the main objective of expanding its applicability by considering the contribution of the organic radicals yielded by the breakage of $Fe^{3+}-EDDS$. However, the direct inclusion of the $EDDS^{\bullet 3-}$ radical into the mechanistic model inexorably involves the differentiation between the microcontaminant degradation reactions by hydroxyl radicals ($HO^{\bullet}$) and by EDDS radicals ($EDDS^{\bullet 3-}$). This is almost unaffordable from a computational point of view for real applications. Actual MWWTP secondary effluents contain hundreds of microcontaminants; therefore, each new radical considered in the model would be translated into hundreds of new reactions and, consequently, into hundreds of additional model parameters. To overcome this critical problem, this work proposes a new semi-empirical approach consisting of lumping the concentrations of oxidizing radicals into the concentration of a single species, the hydroxyl radical. Hence, $EDDS^{\bullet 3-}$ radicals are assumed to be instantly converted into $HO^{\bullet}$ radicals (Figure 5-2). At the same time, however, its concentration is also assumed to be reduced by a factor (named "x" in the model) that represents the lesser oxidation capacity of the $EDDS^{\bullet 3-}$ radical in front of the $HO^{\bullet}$ radical, a factor that will be later calibrated when fitting the model to the experimental data. In this way, despite the complexity of the real mechanism, the $EDDS^{\bullet 3-}$ radical can be easily introduced in the system using a single additional parameter (the reduction factor, $0<x<1$).

Regarding the model structure (Figure 5-2), very briefly, it can be divided into the reaction mechanism related to radicals' generation and the reactions related to radicals' consumption. In the former (R1-R11), the initial $Fe^{3+}-EDDS$ evolves into $Fe(OH)_3$ and radicals (both $HO^{\bullet}$ and $EDDS^{\bullet 3-}$) due to its interaction with H_2O_2, UVA radiation and the own radicals. In the latter, radicals can (efficiently) react with the model microcontaminant (R13) or can be (inefficiently) consumed by organic matter (OM) (R12), inorganic carbon (IC) (R14) or H_2O_2 (R15), giving rise to oxidized organic matter (MX), oxidized inorganic carbon (ICX) and decomposed H_2O_2, respectively. OM includes the amount of total organic carbon provided by the chelating agent. Notice that R8, which is part of the radicals generation mechanism,

also comprises the consumption of radicals. As explained above, the model considers the instant conversion of $EDDS^{\bullet 3-}$ into $HO^{\bullet}$ by applying the reduction factor (semi-empirical approach).

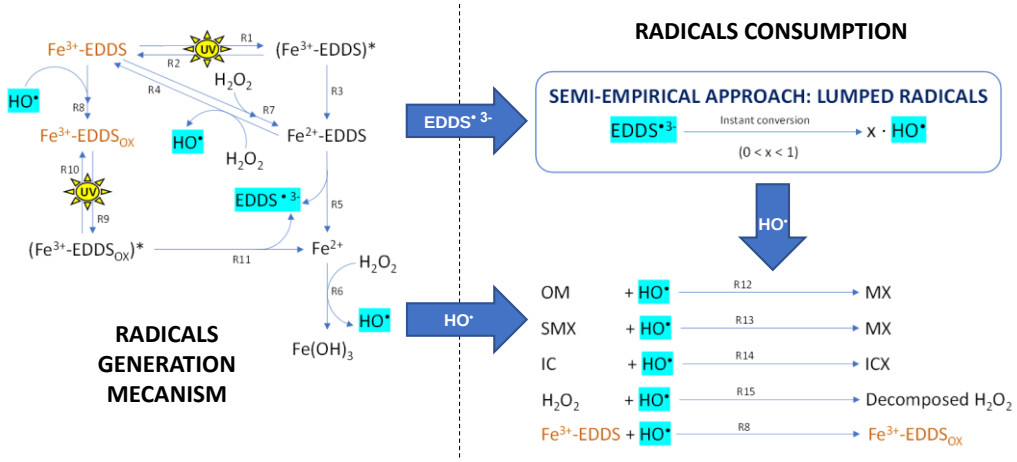

Figure 5-2 Model scheme and semi-empirical approach

On the other hand, the dynamic model is based on reaction rates (Table 5-2) and mass balances to the most relevant components of the model. Reaction rates are calculated following conventional equations in which a kinetic constant is multiplied by the concentration of the corresponding reagents participating in the reaction. In the reaction rates where UVA is involved, a saturation expression for irradiance was included according to the experimental results (see Section 5.3.1). A similar strategy was proposed by Rivas et al. (2015) (Rivas et al., 2015). These equations should be ideally substituted in the future by more accurate expressions based on the volumetric rate of photon absorption; nevertheless, this deserves a whole scientific publication due to its high complexity. The concentration of OM and IC in the reaction rates is represented by DOC concentration and TIC concentration, respectively. The mass balances for each component can then be easily determined considering the generation and consumption rates of the reactions where they participate. Special attention requires the $HO^{\bullet}$ mass balance. Since the conversion of $EDDS^{\bullet 3-}$ into $HO^{\bullet}$ is instantaneous, the $HO^{\bullet}$ mass balance also includes the $EDDS^{\bullet 3-}$ generation rates (R5 and R11) that are multiplied by the reduction factor (x).

$$R_1 = k_1.[Fe^{3+} - EDDS]\left(\frac{I}{I+1}\right)$$ Eq.5-1

$$R_2 = k_2.[(Fe^{3+} - EDDS)^*]$$ Eq.5-2

$$R_3 = k_3.[(Fe^{3+} - EDDS)^*]$$ Eq.5-3

$$R_4 = k_4.[Fe^{3+} - EDDS][H_2O_2]$$ Eq.5-4

$$R_5 = k_5.[Fe^{2+} - EDDS]$$ Eq.5-5

$$R_6 = k_6.[Fe^{2+}][H_2O_2]$$ Eq.5-6

$$R_7 = k_7.[Fe^{3+} - EDDS][H_2O_2]$$ Eq.5-7

$$R_8 = k_8.[Fe^{3+} - EDDS][HO^{\bullet}]$$ Eq.5-8

$$R_9 = k_9.[Fe^{3+} - EDDS_{OX}]\left(\frac{I}{I+1}\right)$$ Eq.5-9

$$R_{10} = k_{10}.[(Fe^{3+} - EDDS_{OX})^*]$$ Eq.5-10

$$R_{11} = k_{11}.[(Fe^{3+} - EDDS_{OX})^*]$$ Eq.5-11

$$R_{12} = k_{12}.[O.M][HO^{\bullet}]$$ Eq.5-12

$$R_{13} = k_{13}.[SMX][HO^{\bullet}]$$ Eq.5-13

$$R_{14} = k_{14}.[IC][HO^{\bullet}]$$ Eq.5-14

$$R_{15} = k_{15}.[H_2O_2][HO^{\bullet}]$$ Eq.5-15

Accordingly, the mass balance equations are shown below (Eq.5-16 to Eq.5-26):

$$\frac{d[Fe^{3+}-EDDS]}{dt} = -R_1 + R_2 + R_4 - R_7 - R_8$$ Eq.5-16

$$\frac{d[(Fe^{3+} - EDDS)^*]}{dt} = R_1 - R_2 - R_3$$ Eq.5-17

$$\frac{d[Fe^{2+}]}{dt} = R_5 - R_6 + R_{11}$$ Eq.5-18

$$\frac{d[Fe^{2+}-EDDS]}{dt} = R_3 - R_4 - R_5 + R_7$$ Eq.5-19

$$\frac{d[Fe^{3+}-EDDS_{OX}]}{dt} = R_8 - R_9 + R_{10}$$ Eq.5-20

$$\frac{d[(Fe^{3+} - EDDS_{OX})^*]}{dt} = R_9 - R_{10} - R_{11}$$ Eq.5-21

$$\frac{d[H_2O_2]}{dt} = -R_4 - R_6 - R_7 - R_{15}$$ Eq.5-22

$$\frac{d[HO^{\bullet}]}{dt} = R_4 + R_6 - R_8 - R_{12} - R_{13} - R_{14} - R_{15} + x \cdot (R_5 + R_{11})$$
$$(0 < x < 1)$$ Eq.5-23

$$\frac{d[OM]}{dt} = -R_{12}$$ Eq.5-24

$$\frac{d[SMX]}{dt} = -R_{13} \quad \text{Eq.5-25}$$

$$\frac{d[IC]}{dt} = -R_{14} \quad \text{Eq.5-26}$$

5.2.7 Model parameter estimation

The set of reaction rates given by Eq.5-1 to Eq.5-15 and the set of ordinary differential equations given by Eq.5-16 to Eq.5-26 was implemented in MATLAB/Simulink® (version R2022a) and solved numerically using ode15s solver with a time variable-step.

The concentration profiles of SMX, $Fe^{3+} - EDDS$ and H_2O_2 were used to estimate the model parameters (model calibration) that include 15 kinetic constants and the reduction factor. This was done by solving a nonlinear multivariate optimization problem to minimize the sum of the squared differences between the model predicted values and the corresponding experimental data available (Eq.5-27).

$$\min Z = \sum_{j=1}^{m}\left(\sum_{i=1}^{n}\left(\frac{[\widehat{SMX}]_{(i,j)}-[SMX]_{(i,j)}}{[\widehat{SMX}]_{(1,j)}}\right)^2 + \left(\frac{[\widehat{H_2O_2}]_{(i,j)}-[H_2O_2]_{(i,j)}}{[\widehat{H_2O_2}]_{(1,j)}}\right)^2 + \left(\frac{[\widehat{Fe^{3+}-EDDS}]_{(i,j)}-[Fe^{3+}-EDDS]_{(i,j)}}{[\widehat{Fe^{3+}-EDDS}]_{(1,j)}}\right)^2\right) \quad \text{Eq.5-27}$$

Where the circumflex stands for the experimental data, the subscript i for each sample at specific reaction times and the subscript j represents the different experiments.

This problem was solved using the nonlinear least-squares method with the Levenberg-Marquardt algorithm available in the Estimator Toolbox of MATLAB/Simulink®. The Root Mean Square Error (RMSE), as the standard deviation of the residuals (prediction errors), was calculated by Eq.5-28 in order to test the model reliability and the goodness of fit. The coefficient of determination R^2 (Eq.5-29) is also presented for illustrative purposes because it has been widely used, though R^2 in nonlinear models is not equal to the regression sum-of-squares plus the residual sum-of-squares, as in the case of linear regression (Spiess and Neumeyer, 2010).

$$RMSE_k = \sqrt{\left(\sum_{i=1}^{N_k} \left(\frac{\hat{y}_{ik} - y_{ik}}{\hat{y}_{1k}} \right)^2 \Big/ N_k \right)} \quad \text{Eq.5-28}$$

$$R_k{}^2 = 1 - \left(\sum_{i=1}^{N} (\hat{y}_i - y_i)^2 \Big/ \sum_{i=1}^{N} (\hat{y}_i - \bar{y})^2 \right) \quad \text{Eq.5-29}$$

Where $\hat{y}_i$ and y_i correspond to the measured and simulated values at the given time, respectively, and $\bar{y}$ is the mean of the measured data.

5.2.8 Sensitivity analysis

Parameter sensitivity analysis (SA) allows for examining a mathematical model and assessing the robustness of its output with respect to parameter uncertainty (Latunde and Bamigbola, 2018). For a kinetic model, SA reveals the relative importance of the different steps included in the model.

The selection of a SA approach among the various reported studies in the literature was discussed in a previous paper (Nasr Esfahani et al., 2022b). Hence, Global sensitivity analysis (GSA) is adopted since it is widely used for models with multiple correlated outputs. GSA assigns the outputs uncertainty to the uncertainty in each input factor over their entire range of interest. In many complex and nonlinear spatial phenomena, input factors usually show interactions and assessing the impact of a model input on a given output, being other factors constant, results inappropriate. Thus, SA is considered global when all the input factors are varied simultaneously, and the sensitivity is evaluated over the entire range of each input factor. Hence, SA quantifies the importance of model inputs and their interactions with respect to model output (Zhou et al., 2008).

Among the assortment of GSA techniques, mostly statistical and analytical, the combined Latin Hypercube Sampling-Partial Rank Correlation Coefficient (LHS-PRCC) method (Helton et al., 2006a) is used, following the analysis of previous work (Nasr Esfahani et al., 2022b) to analyze the correlation between the model parameters and the output.

A model with P parameters and a model output y can be written as a function of all the model parameter values so that $y = f(x_1, x_2, \dots, x_P)$.

A distribution of N samples ($i = 1, 2, \dots, N$) for each model parameter x_k ($k = 1, 2, \dots, P$), will produce a set of P sample vectors X_k ($1 \times N$) and an associated vector Y ($1 \times N$) of model output values. Hence, the partial rank correlation coefficient for the k-the parameter (R_{X_kY}) is given by (Marino et al., 2008a):

$$R_{X_kY} = \frac{cov(X_k, Y)}{\sqrt{Var\ (X_k) Var(Y)}} = \frac{\sum_{i=1}^{N}(x_{ik} - \bar{x})(y_i - \bar{y})}{\sqrt{\sum_{i=1}^{N}(x_{ik} - \bar{x})^2 (y_i - \bar{y})^2}} \quad \text{Eq.5-30}$$

The value of the partial rank correlation coefficient, ranging from -1 to 1, rates the extent to which an increase in the parameter value produces an increase (or decrease) in the model output (Helton et al., 2006a). Thus, it is commonly assumed that obtaining values in the range -0.05< R_{XY} < 0.05 reveal a negligible significance of a parameter in the model output.

A model producing multiple outputs may be managed by focusing on a reduced set of aggregated output values Y providing the most insight into the model analysis. In this case, the conformity of the model to the available experimental data is the criterion for selecting as the output values of interest the sum of the square errors produced for all the measured variables (SMX, $Fe^{3+} - EDDS$ and H_2O_2)). Thus, the output values for the sensitivity analysis and the calculation of the partial rank correlation coefficients are the following:

$$Y1 = \sum_i \left([\widehat{SMX}]_i - [SMX]_i\right)^2 \quad \text{Eq.5-31}$$

$$Y2 = \sum_j \left([\widehat{Fe^{3+} - EDDS}]_j - [Fe^{3+} - EDDS]_j\right)^2 \quad \text{Eq.5-32}$$

$$Y3 = \sum_k \left([\widehat{H_2O_2}]_k - [H_2O_2]_k\right)^2 \quad \text{Eq.5-33}$$

5.3 RESULTS AND DISCUSSION

5.3.1 SMX removal by UVA/$Fe^{3+} - EDDS$ process and photo-Fenton mediated by $Fe^{3+} - EDDS$

SMX degradation by the UVA/$Fe^{3+} - EDDS$ process was initially studied. In this experimental series, the radiation level was varied from 14 $W \cdot m^{-2}$ (25%) to 56 $W \cdot m^{-2}$ (100%) to understand how this variable affects process performance (Figure

5-3) and, afterwards, translate this behaviour into the model. Photo-saturation effect was observed. The SMX removal efficiency improved with irradiance level only up to a certain level, from which process performance remained almost constant. This is directly related to the $Fe^{3+}-$EDDS evolution during the process. Since the oxidant species responsible for SMX degradation are generated from the $Fe^{3+}-$EDDS breakage and equivalent $Fe^{3+}-$EDDS concentration profiles were observed from 28 $W \cdot m^{-2}$ (50%), this also resulted in equivalent SMX removal curves.

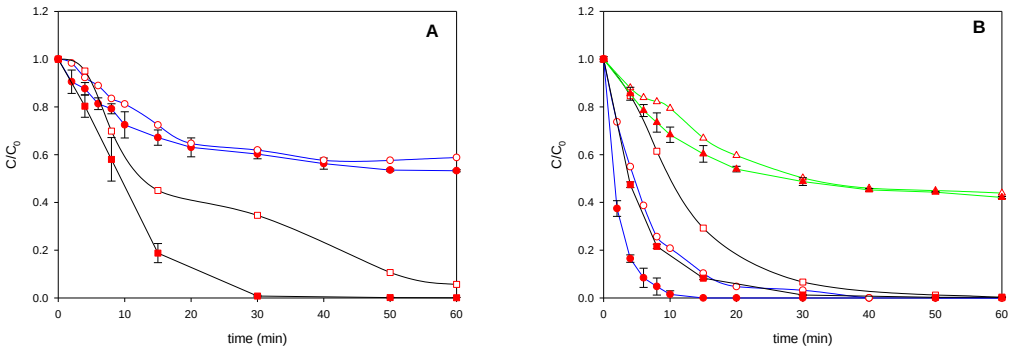

Figure 5-3 Experimental data (-●- SMX, -■- $Fe^{3+}-$EDDS, -▲- H_2O_2) for the I=14 $W \cdot m^{-2}$ experiment (empty symbols) and average experimental data for the I=28 $W \cdot m^{-2}$, I=42 $W \cdot m^{-2}$ and I=56 $W \cdot m^{-2}$ experiments (closed symbols). Experimental conditions: [SMX] = 1.00±0.05 $mg \cdot L^{-1}$; [$Fe^{3+}-$EDDS]=0.12±0.02; (A) $Fe^{3+}-$EDDS /UVA assay [H_2O_2]=0 mM and (B) photo-Fenton assay [H_2O_2]=1.5±0.01 mM

A similar trend was observed during the photo-Fenton treatment. Both $Fe^{3+}-$EDDS concentration and H_2O_2 consumption profiles showed once again almost equivalent behaviours from 28 $W \cdot m^{-2}$, which resulted in extremely similar SMX removals from this irradiance level.

5.3.2 Model fitting and parameter estimation

Model fitting is a non-convex optimization problem for which multiple optima may exist. Thus, different sets of parameter values (local optima) may be found depending on the starting point used by the search algorithm. Indeed, this may also lead to further discussion on global optimization, but this is beyond the scope of this work since the solution attained will finally be validated on experimental tests. In this work, the parameter values reported by Soriano-Molina et al. (2018) were used as initial guesses (Table 5-2). Regarding parameter x (Eq.5-23) since it is bounded between 0 and 1, the initial value was set to 0.5.

The model was fit to each of the experimental data sets using the MATLAB/Simulink® R2022a Optimization Toolbox™ (lsqnonlin).

The adjustment of the model to all experimental data sets (Table 5-1) always resulted in fitting with NRMSE greater than 0.16 for all the cases. Model fitting to each experimental data set produced a set of parameter values that were averaged; these values and the corresponding standard deviation are given in Table 5-2.

Table 5-2 Estimation of the kinetic parameter values for the proposed model

Kinetic constants	**Initial value**	**Fitted value (average)**	**SD**
k_1 (min^{-1})	$5.80 \cdot 10^{-2}$	$5.30 \cdot 10^{-2}$	$1.50 \cdot 10^{-2}$
k_2 (min^{-1})	$2.50 \cdot 10^{-1}$	3.11	$1.20 \cdot 10^{-2}$
k_3 (min^{-1})	$1.71 \cdot 10^{+1}$	$8.97 \cdot 10^{+2}$	$2.44 \cdot 10^{+2}$
k_4 $(mM^{-1}.min^{-1})$	$1.90 \cdot 10^{+3}$	$1.10 \cdot 10^{+4}$	$2.70 \cdot 10^{+3}$
k_5 (min^{-1})	$3.57 \cdot 10^{+1}$	3.45	2.06
k_6 $(mM^{-1}.min^{-1})$	4.56	$2.98 \cdot 10^{+2}$	$3.37 \cdot 10^{+1}$
k_7 $(mM^{-1}.min^{-1})$	$4.00 \cdot 10^{-1}$	$1.44 \cdot 10^{-1}$	$4.10 \cdot 10^{-2}$
k_8 $(mM^{-1}.min^{-1})$	$5.60 \cdot 10^{+7}$	$4.10 \cdot 10^{+9}$	$8.21 \cdot 10^{+8}$
k_9 (min^{-1})	$2.11 \cdot 10^{+1}$	1.17	$4.36 \cdot 10^{-1}$
k_{10} (min^{-1})	$1.05 \cdot 10^{+1}$	$5.61 \cdot 10^{-1}$	$1.78 \cdot 10^{-3}$
k_{11} (min^{-1})	3.31	$3.40 \cdot 10^{+2}$	3.59
k_{12} $(mM^{-1}.min^{-1})$	$1.76 \cdot 10^{+4}$	$8.41 \cdot 10^{+4}$	$2.30 \cdot 10^{+2}$
k_{13} $(mM^{-1}.min^{-1})$	$4.80 \cdot 10^{+4}$	$8.80 \cdot 10^{+9}$	$1.99 \cdot 10^{+9}$
k_{14} $(mM^{-1}.min^{-1})$	$5.10 \cdot 10^{+5}$	$5.16 \cdot 10^{+5}$	$1.42 \cdot 10^{+4}$
k_{15} $(mM^{-1}.min^{-1})$	$1.60 \cdot 10^{+6}$	$4.40 \cdot 10^{+8}$	$5.38 \cdot 10^{+7}$
x	$5.00 \cdot 10^{-1}$	$1.15 \cdot 10^{-1}$	$5.40 \cdot 10^{-2}$

In the reactions related to radicals generation, the differences found between the initial guesses and the fitted values of the model parameters were lower than one order of magnitude. Probably, these differences are related to the UV radiation source (solar light vs LED light) and how the catalyst-UV radiation interaction is mathematically considered in the model. On the other hand, the differences were higher in the reactions related to radicals consumption, which is indeed coherent because (i) the selected model MC was not the same in both works (acetamiprid vs SMX, being the former extremely recalcitrant) and (ii) the model proposed by Soriano-Molina does not consider the contribution of $EDDS^{\bullet 3-}$ radical to MCs degradation. In this sense, model fitting suggests that one $EDDS^{\bullet 3-}$ radical could be considered as ≈0.1 $HO^{\bullet}$ radical. The SD values were found, in general, high but in the range of the ones obtained in similar modeling works (Cabrera Reina et al., 2014). Given the set of averaged model parameter values fit to the experimental data, simulations were performed to check and

illustrate the fitting. Figure 5-4 shows the experimental data and predicted profiles for the same experimental conditions, with and without the addition of hydrogen peroxide (assays A1, B1):

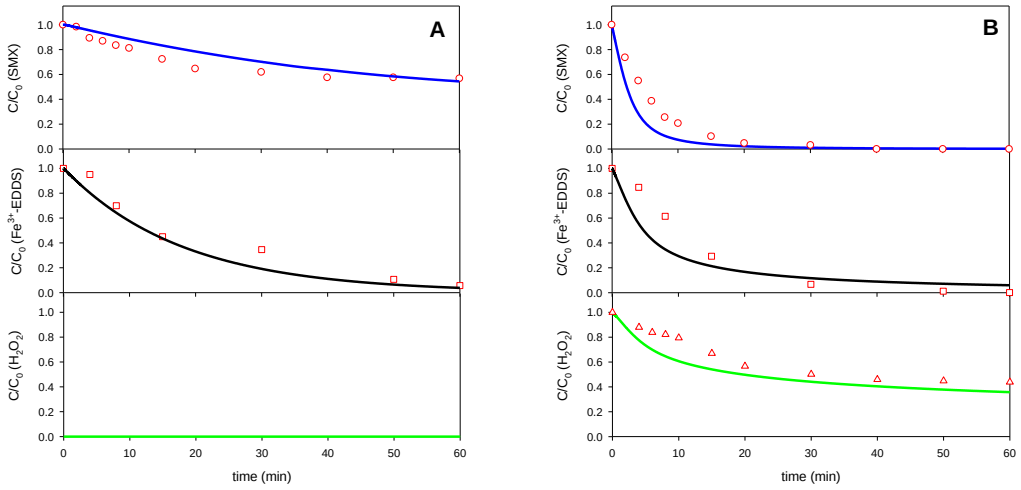

Figure 5-4 Experimental data (symbols) and profiles predicted by the proposed kinetic model (lines). Experimental conditions: [SMX] = 1.00±0.05 mg · L^{-1}; [$Fe^{3+}-$EDDS]=0.12±0.02 Mm; I=14 W · m^{-2} (25%); (A) $Fe^{3+}-$EDDS /UVA assay [H_2O_2]=0 mM and (B) photo-Fenton assay [H_2O_2]=1.5±0.01 mM

The goodness of fit (assays A1 and B1) is tabulated in Table 5-3.

Table 5-3 The goodness of fit (assays A1 and B1)

Assay ID	UV intensity	NRMSE			R^2		
	(W. m^{-2})	SMX	$Fe^{3+}-$EDDS	H_2O_2	SMX	$Fe^{3+}-$EDDS	H_2O_2
A1	14	0.070	0.089	NA	0.91	0.97	NA
B1	14	0.126	0.153	0.075	0.92	0.88	0.93

Despite their variability, the average values estimated for the model parameters (Table 5-2) allow producing practical model responses matching the experimental results. Figure 5-4 compares the experimental data and the SMX, $Fe^{3+}-$EDDS and H_2O_2 concentration profiles obtained using such averaged parameter values. Figure 5-4 compares two specific cases with (Assay B1) and without (Assay A1) H_2O_2 addition and shows the capability of the model to reproduce the measured behavior and explain the SMX, $Fe^{3+}-$EDDS and H_2O_2 concentration profiles in these two extreme situations. Additional simulations are carried out to check the consistency of the model and the capacity to estimate the behavior of the intermediate unobserved variables, Figure 5-5.

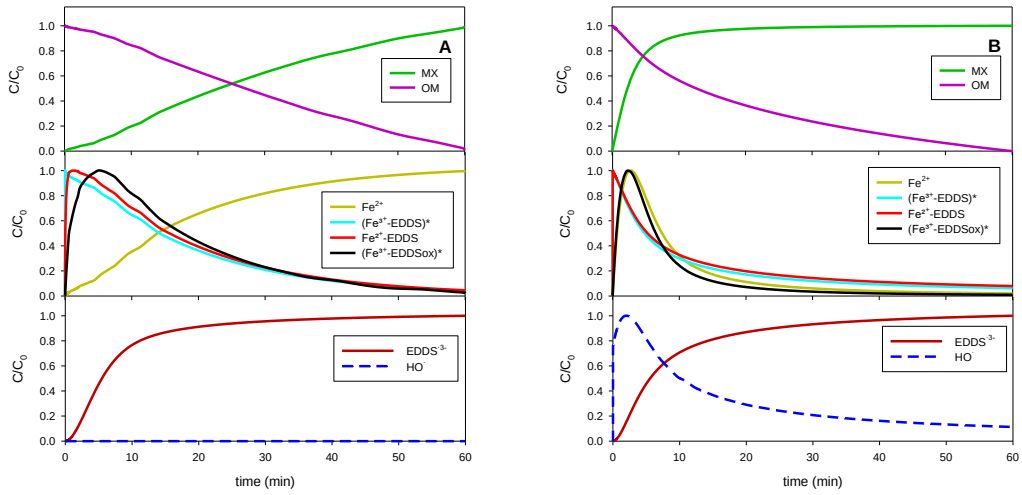

Figure 5-5 Profiles of the intermediates unobserved variables predicted by the proposed kinetic model. Experimental conditions: [SMX] = 1.00±0.05 mg · L^{-1}; [Fe^{3+} − EDDS]=0.12±0.02 Mm; I=14 W · m^{-2} (25%): (A) Fe^{3+} − EDDS /UVA assay [H_2O_2]=0 mM and (B) photo-Fenton assay [H_2O_2]=1.5±0.01 mM

Once the proposed model has revealed its practicality and capability to explain the process in a range of conditions beyond that addressed by the model by Molina et al. (2018), it should be further examined in regard of parameter uncertainty and the need for the different mechanisms proposed in the model, which may reveal the chances for the simplification of the model. This is next performed following the scheme reported by Nasr Esfahani et al. (2022).

5.3.3 Global sensitivity analysis

The complexity of the proposed model is next analyzed by means of Global Sensitivity Analysis (GSA). Model parameters are assumed independent, and a set of 500 samples for each model parameter is taken to apply the Latin Hypercube Sampling-Partial Ranking Correlation Coefficient (LHS-PRCC) analysis. The outputs considered for this analysis is the sum of the square error between measured and estimated values (SMX, Fe^{3+} − EDDS and H_2O_2), which focuses the analysis on the accuracy and fidelity of the model to the measured variables.

The analysis is performed at two complementary levels. On the one hand, a partial GSA is performed using assays B1 and B2 with hydrogen peroxide, Figure 5-6. On the other hand, is admitted that the presence of hydrogen peroxide may favor some reactions (R4, R6, R7 or R15), while masking some other (R5 and R11), which may

result in mistakenly concluding the scarce relative importance of the related kinetic constants (model parameters). Hence, the complementary analysis, Figure 5-7, is carried out using assays A1, A2 and A3, for which the absence of hydrogen peroxide will reveal the true significance of these mechanisms.

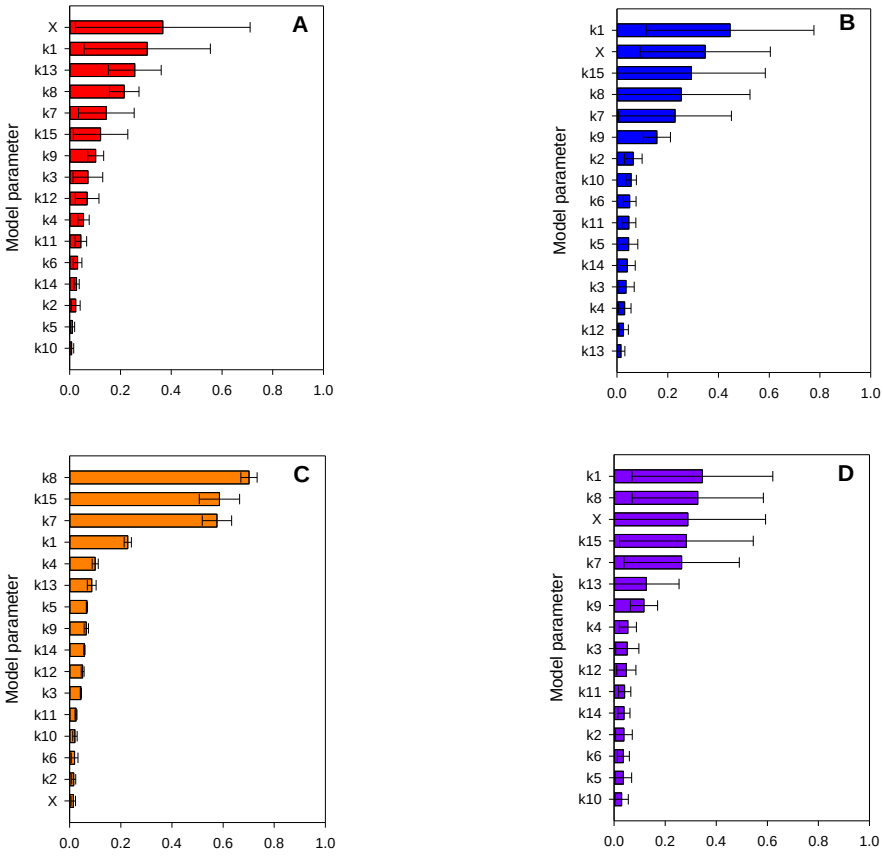

Figure 5-6 Sensitivity analysis and correlation coefficients R_{XY} for all the proposed model parameters (absolute value): (A) SMX, (B) $Fe^{3+}-EDDS$, (C) H_2O_2 and (D) Overall

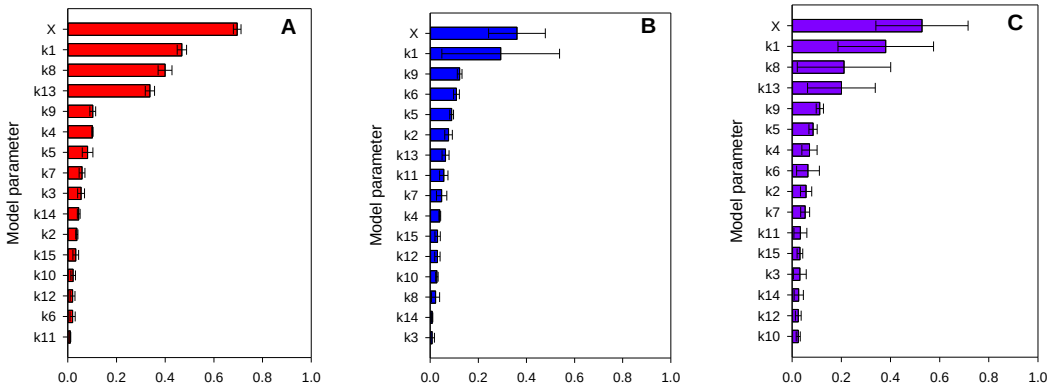

Figure 5-7 Sensitivity analysis and correlation coefficients R_{XY} for all parameters of the model without H_2O_2 ($Fe^{3+}-$ EDDS/UVA assays): (A) SMX, (B) $EDDS^{\bullet 3-}$ and (C) Overall

It is worth noting that Figure 5-7 shows non-zero values for the correlation coefficients of the parameters involved in the reactions that cannot occur in the absence of hydrogen peroxide (k_4, k_6, k_7, k_{15}). The values are very low, and they can be neglected, but the fact that the values are not strictly zero reveals the limitations of the LHS. While practical in terms of computational cost, LHS produces random samples for which the covariance between a set of random outputs and a set of non-correlated inputs cannot be expected to be strictly zero. A particular one-at-a-time sampling for k_{15} confirmed the absolutely null influence of this parameter in the fitting of assays B1 and B2, for which there is no hydrogen peroxide.

Figure 5-6 and Figure 5-7 show the absolute value of the averaged correlation coefficients found for all model parameters. The values are displayed in order of its importance for the fitting of the estimated values to the measured data available for SMX, $Fe^{3+} - EDDS$ and H_2O_2. Particularly, Figure 5-6 reveals that correlation coefficients for k_{10}, k_5 , and k_6 are below the threshold $|R_{XY}| \geq 0.05$ for all three outputs SMX, $Fe^{3+} - EDDS$ and H_2O_2, which indicates their scarce relevance to the capability of the model to fit the experimental data. In addition, Figure 5-7 reveals that correlation coefficients for k_{10}, k_{12} , and k_{14} are below the threshold $|R_{XY}| \geq 0.05$ for all outputs SMX and $Fe^{3+} - EDDS$, which indicates their scarce relevance to the capability of the model to fit the experimental data.

The negligible effect of k_{10} in both scenarios suggests that the reverse reaction 10 is negligible for the global process. Consequently, reaction 10 is eliminated, assuming that once the initial $Fe^{3+} - EDDS$ complex is oxidized to $Fe^{3+} - EDDS_{ox}$, its photo-activation to $(Fe^{3+} - EDDS_{ox})^*$ is not reversible. Certainly, this analysis and this assumption are acceptable only in the presence of light.

The resulting simplified model was fit again to each of the experimental data sets as previously reported using as initial guesses the obtained values during the previous model calibration. The new average values obtained are reported in Table 5-4, along with the corresponding standard deviation.

Table 5-4 Estimation of the kinetic parameters for the reduced model

Kinetic constants	Initial value	Fitted value (average)	SD
k_1 (min^{-1})	$5.30 \cdot 10^{-2}$	$8.49 \cdot 10^{-2}$	$1.15 \cdot 10^{-1}$
k_2 (min^{-1})	3.11	3.12	$1.58 \cdot 10^{-2}$
k_3 (min^{-1})	$8.97 \cdot 10^{+2}$	$7.61 \cdot 10^{+3}$	$4.93 \cdot 10^{+3}$
k_4 $(mM^{-1}.min^{-1})$	$1.10 \cdot 10^{+4}$	$1.23 \cdot 10^{+4}$	$1.71 \cdot 10^{+3}$
k_5 (min^{-1})	3.45	2.32	2.38
k_6 $(mM^{-1}.min^{-1})$	$2.98 \cdot 10^{+2}$	$2.53 \cdot 10^{+2}$	$2.81 \cdot 10^{+1}$
k_7 $(mM^{-1}.min^{-1})$	$1.44 \cdot 10^{-1}$	$1.41 \cdot 10^{-1}$	$6.91 \cdot 10^{-2}$
k_8 $(mM^{-1}.min^{-1})$	$4.10 \cdot 10^{+9}$	$5.11 \cdot 10^{+9}$	$1.11 \cdot 10^{+9}$
k_9 (min^{-1})	1.17	1.25	$3.09 \cdot 10^{-1}$
k_{10} (min^{-1})	$3.40 \cdot 10^{+2}$	$3.54 \cdot 10^{+2}$	$2.38 \cdot 10^{+1}$
k_{11} (min^{-1})	$8.41 \cdot 10^{+4}$	$8.43 \cdot 10^{+4}$	$7.55 \cdot 10^{+1}$
k_{12} $(mM^{-1}.min^{-1})$	$8.80 \cdot 10^{+9}$	$1.04 \cdot 10^{+10}$	$1.22 \cdot 10^{+9}$
k_{13} $(mM^{-1}.min^{-1})$	$5.10 \cdot 10^{+5}$	$4.20 \cdot 10^{+5}$	$2.26 \cdot 10^{+5}$
k_{14} $(mM^{-1}.min^{-1})$	$4.40 \cdot 10^{+8}$	$3.95 \cdot 10^{+8}$	$1.17 \cdot 10^{+8}$
k_{15} $(mM^{-1}.min^{-1})$	$1.15 \cdot 10^{-1}$	$1.09 \cdot 10^{-1}$	$2.02 \cdot 10^{-2}$
x	$5.30 \cdot 10^{-2}$	$8.49 \cdot 10^{-2}$	$1.15 \cdot 10^{-1}$

This interesting result shows that different model fittings could explain the same experimental data. This is clearly connected to the prior discussion on the multiple local optima that can be encountered by the optimization algorithm and reveals that while a model can be correctly adjusted for practical purposes, further mathematical research beyond the scope of this work is required to determine the best number of model parameters and their optimal value.

Simulations were performed to check and illustrate the fitting after the GSA, predicted profiles and experimental data are overlapped for each experimental condition (Figure 5-8). The simulations by the simplified model showed good fitting of the experimental data for both $Fe^{3+} - EDDS$/UVA process and $Fe^{3+} - EDDS$ mediated photo-Fenton process. Indeed, no decrease of the model prediction capability with respect to the non-simplified one was observed, which indicates the usefulness of the GSA in diminishing the computational cost in kinetic modeling.

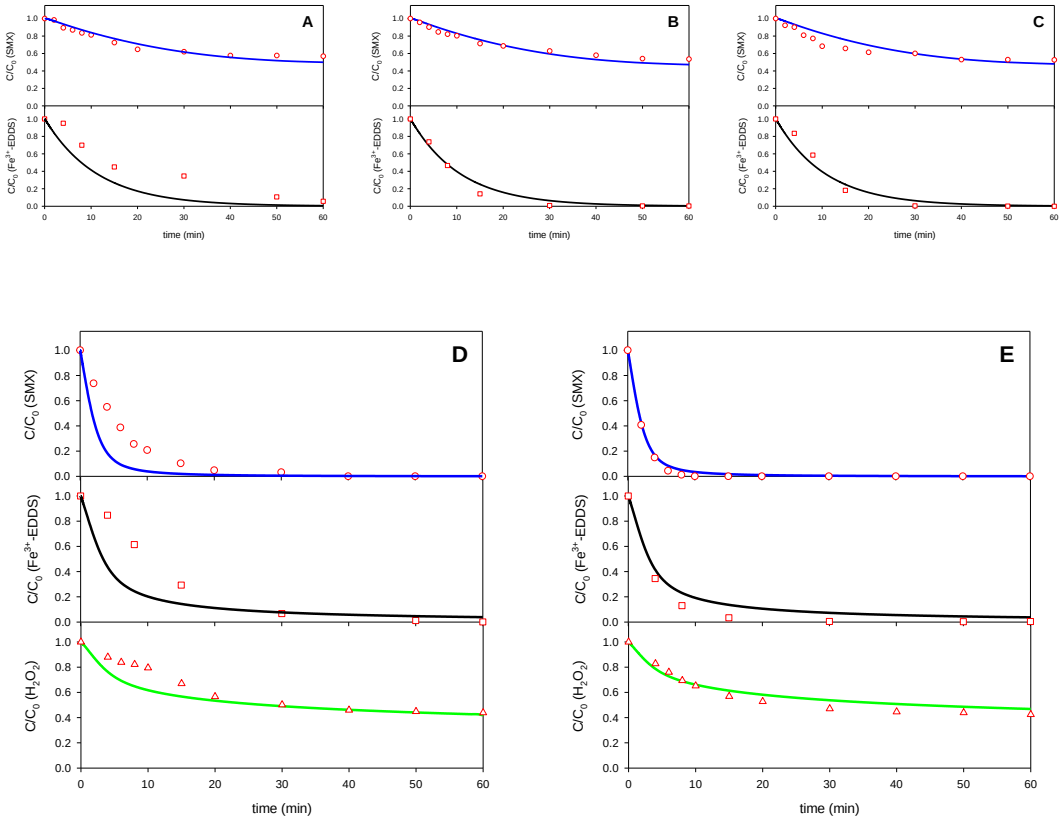

Figure 5-8 Experimental data (symbols) and profiles predicted by the reduced kinetic model (lines) after GSA. Experimental conditions: [SMX] = 1.00±0.05 mg · L^{-1}; [Fe^{3+} − EDDS]=0.12±0.02 Mm; Fe^{3+} − EDDS/UVA assays [H_2O_2]=0 mM at (A) 14 W · m^{-2}; (B) 42 W · m^{-2} and (C) 58 W · m^{-2}; photo-Fenton assays [H_2O_2]=1.5±0.01 mM at (D) 14 W · m^{-2} and (E) 58 W · m^{-2}

Once the kinetic model proposed has been fit to the training data sets (A1, A2, A3, B1, and B2) and the model parameters have been estimated, the calibrated model is next tested using the unseen data sets (V1 and V2). The model has been calibrated using assays including and excluding the use of hydrogen peroxide, and the validation is performed on assays covering these cases and a different intermediate light intensity (28 W · m^{-2}, corresponding to 50% of the UV LEDs maximum intensity –Table 5-1 Experimental series). The calibrated model produces concentration profiles for the measured variables (SMX, Fe^{3+} − EDDS and H_2O_2 –Figure 5-9) that, practically match the experimental data obtained for assays V1 and V2. When hydrogen peroxide is used, the process is mostly controlled by the photo-Fenton reactions (V2, Figure 5-9C). When there is no supply of hydrogen peroxide, the process becomes mostly dependent on Fe^{3+} − EDDS lysis (V1, Figure 5-9A), which is the part not contemplated in the model by Soriano-Molina et al. (2018).

The quantitative analysis of the fit of the calibrated model to the data sets V1 and V2 indicates an NRMSE value lower than 0.15 for the normalized data in both cases and for all measured variables (SMX, $Fe^{3+}-$EDDS and H_2O_2), which is reasonable, according to the precision of the measurements. Therefore, the validation confirms both a sensible goodness of fit and an extended generality of the model developed in this work. Model fitting also led to the adjustment of the reduction x factor, which allows concluding that the oxidation capacity of the $EDDS^{\bullet 3-}$ radicals can be estimated to be approximately 11% that of the hydroxyl radicals.

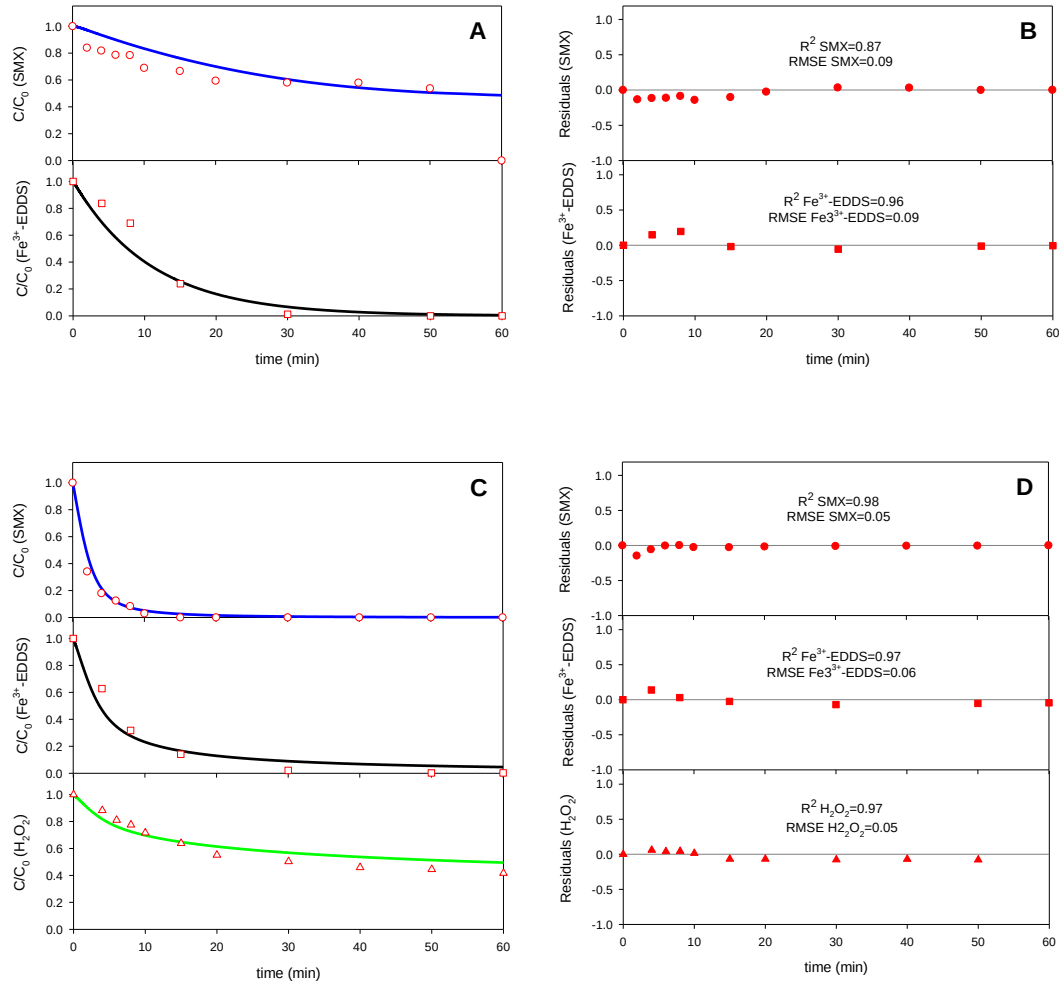

Figure 5-9 Experimental data (symbols) and profiles predicted by the reduced kinetic model (lines) after GSA for the validation experiments. Experimental conditions: [SMX] = 1.00±0.05 mg · L^{-1}; [$Fe^{3+}-$EDDS]=0.12±0.02 Mm; I=28 W · m^{-2} (50%); (A) $Fe^{3+}-$EDDS/UVA assay [H_2O_2]=0 mM with (B) the corresponding residuals and (C) photo-Fenton assay [H_2O_2]=1.5±0.01 mM with (D) the corresponding residuals

5.4 CONCLUSIONS

This study revisited the kinetic modeling of the $Fe^{3+} - EDDS$ mediated photo-Fenton process by expanding its usefulness in the absence of H_2O_2, which yields $EDDS^{\bullet 3-}$ radicals also capable of oxidizing MCs. A new, simple and low computational cost semi-empirical approach consisting of lumping $EDDS^{\bullet 3-}$ radicals and HO• radicals was adopted. Model calibration demonstrated the feasibility of this semi-empirical strategy for successfully predicting the system behavior. Afterwards, the GSA revealed the low importance of reaction 10, suggesting that once the initial $Fe^{3+} - EDDS$ complex is oxidized to $Fe^{3+} - EDDSox$, its photo-activation to $(Fe^{3+} - EDDSox)^*$ is not actually reversible despite possible. Finally, the reduced kinetic model was validated. Experimental data could be predicted properly, with NRMSE (Root Mean Square Errors) for normalized data<0.08 and 0.15 for SMX and $Fe^{3+} - EDDS$, respectively.

Thus, the new kinetic model presented in this work demonstrated sensible goodness of fit and extended applicability of the previous proposed models without increasing their complexity. In addition, the model can be easily adapted to work with other pollutants or mixtures of pollutants and the semi-empirical approach could be considered for other AOPs.

Chapter 6: Modeling of Ozone Decay in Secondary Wastewater Effluent with Initial Ozone Demand

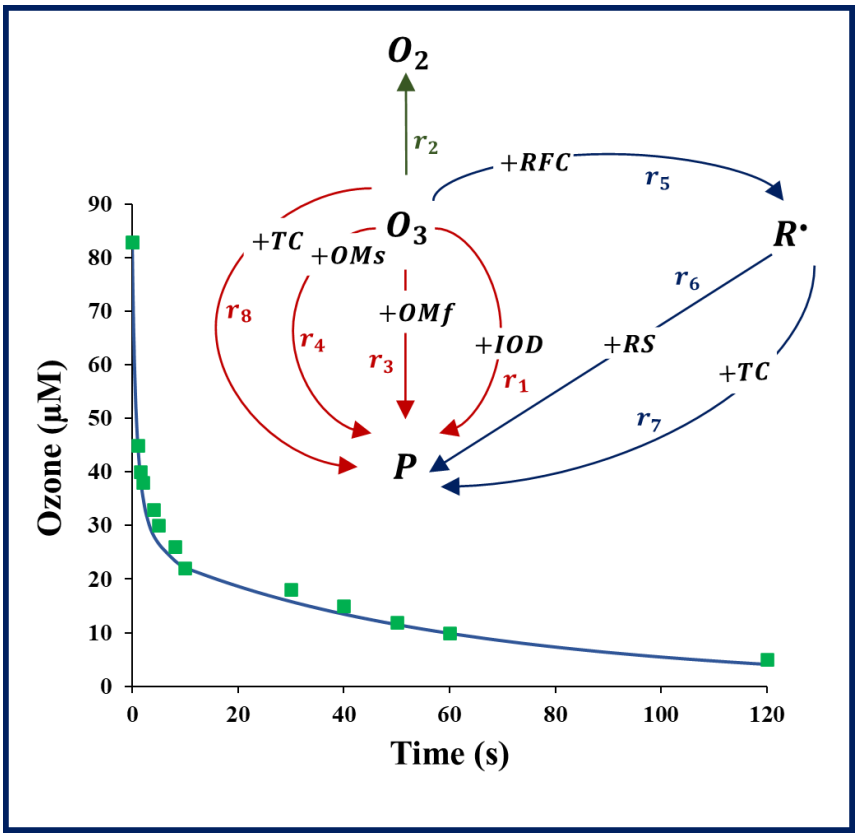

Redrafted from:

Nasr Esfahani, K., Santoro, D., Pérez-Moya, M., Graells, M (n.d.). Mechanistic Modeling of Ozone Decomposition Processes in Secondary Wastewater Effluent with Initial Ozone Demand. (Under review for submission).

Advanced Oxidation Processes (AOPs) employing ozone have complex kinetics. Ozone presents high instability and its decomposition during the treatment of complex matrices such as secondary wastewater effluents is not yet fully understood. Existing models for ozonation design and process control fall short in capturing the interaction between ozone and water quality, imposing intensive piloting studies. Attempts to simplify complex models risk introducing inaccuracies, and more advanced models incorporating detailed reactions have shown limited practical interest for the engineering community. Hence, this chapter introduces a new mathematical model designed for the ozonation of wastewater treatment, presenting a novel semi-empirical approach based on lumped variables including initial ozone demand, organic matter, radical forming compounds, radical scavengers, and target contaminants. The proposed model structure is able to mechanistically predict both the rapid initial ozone demand occurring at very short timescales (<10 s) and the slower ozone decomposition processes occurring at longer timescales (>30 s). The model utilizes a reduced number of state variables to describe initial ozone demand, two fractions of (fast and slow reacting) effluent organic matter, radical forming compounds, radical scavengers, and the target contaminant. The proposed model is implemented in MATLAB Simulink® using a set of ordinary differential equations representing eight kinetics and six initial states. The model is calibrated and verified using different initial ozone concentrations obtained by dilution of two secondary settled effluents from real municipal wastewater treatment plants. Results indicated that the model possesses an appropriate mathematical structure, demonstrated by a low error calibration and validation errors (RMSE$\leq 7 \cdot 10^{-6}$ mM), to capture both the rapid and the slow decomposition processes occurring during ozonation of secondary settled wastewater. A global sensitivity analysis employing partial rank correlation methods and Latin hypercube sampling is also conducted, leading to further model simplification with the rejection of three reactions connected to the generation and consumption of radicals from the proposed model (threshold $|R_{XY}| \geq 0.05$). Finally, the simplified model is fitted to the experimental data, underscoring its reliability and applicability in mechanistically modelling with reduced set of state variables, rapid and slow ozone decomposition processes in secondary wastewater effluent with initial ozone demand.

6.1 INTRODUCTION

In response to a growing need of an efficient use of water for sustainable growth, advanced wastewater treatment processes and technologies for water reuse have gained renewed attention, including advanced oxidation processes (AOPs) and photodegradation (Askari et al., 2020; Ledakowicz et al., 2001), electrocoagulation and membrane-based systems electrocoagulation and membrane-based systems (Shehata et al., 2023; Sheikh et al., 2023b, 2023a), and biological treatment (Narayanan and Narayan, 2019), either independently or in integrated configurations (Esfahani et al., 2021; Nidheesh et al., 2021; Oller et al., 2011b). Ozonation is a process employed for water and wastewater treatment both for disinfection (Y. Zhang et al., 2023) and micropollutant control (Mousset et al., 2021). Notably, ozonation has numerous applications also for industrial wastewater treatment (Krishnan et al., 2017) as well as for the removal or degradation of organic matter (OM) (Lim et al., 2022; Yargeau et al., 2023). In the context of municipal wastewater treatment, ozonation has been investigated experimentally in several studies as a tertiary treatment step for the secondary effluent (Fallah et al., 2023). Furthermore, ecotoxicological studies associated with the formation of potentially unsafe by-products have also been conducted, leading to several strategies for optimization of ozone dosage (Ashauer, 2016; Cunha et al., 2022; Morales et al., 2024).

Understanding ozone decomposition processes has been an area of focus for several decades (Audenaert et al., 2023, 2013; Buffle et al., 2006; Li et al., 2020). It has been reported that ozone reacts very rapidly with both organic matter and reduced inorganic compounds (Lim et al., 2022). In general, initial drop of ozone concentration in wastewater is followed by relatively a fast regime then stay on a slow regime until a certain steady state is reached (Zimmermann et al., 2011). Hence, considering the kinetics of ozone decomposition processes both in the fast and slow decomposition regimes provides is essential for being able to predict both the direct oxidation caused by the ozone molecule and the indirect oxidation mechanisms mediated by hydroxyl radicals and other radical species produced during treatment.

Early efforts on elucidating ozone reaction mechanisms and understanding its demand and decomposition processes led to simplified models to describe its evolution in complex matrices (Kinman and Rempel, 1975). Over time, with advancements in analytical techniques and computational capabilities, ozone decomposition models

with increased degree of complexity begun to emerge. Indeed, in the 1980s and 1990s, researchers began incorporating kinetic models to predict ozone decomposition and elucidate complex patterns in ozone decay profiles, mostly based on the use of pseudo-first or pseudo-second order kinetics (Farooq and Ahmed, 1989; von Gunten and Hoigne, 1994). With an increased understanding of radical reactions and the formation of by-products produced during ozonation, further model refinements occurred (Mizuno et al., 2007; Wert et al., 2007). In recent years, the integration of computational tools, coupled with experimental validation, has enhanced the accuracy of models, allowing for a more comprehensive exploration of ozonation processes in diverse water and wastewater treatment matrices. These more advanced modelling frameworks embraced detailed kinetics with a shift towards more complex models, incorporating initiation, propagation, and termination reactions, elucidating the complex radical pathways involved in ozone decomposition. Additionally, contemporary models began addressing interactions with organic matter, striving to simulate the intricate reactions between ozone and diverse organic compounds present in wastewater (Audenaert et al., 2023, 2013; Chys et al., 2018).

When employed for ozonation design and process control, existing models may not be adequate to address interaction between ozonation and the water quality without requiring intensive piloting studies. Moreover, complex models are not suitable for initial design stages where several design scenarios must be analysed in parallel. Hence, attempt to simplify complex models has shown the likelihood to introduce inaccuracy leading to unacceptable over- or under-prediction (Zimmermann et al., 2011), while more advanced ozonation model obtained by adding detailed reactions between ozone and water quality species have resulted in no practical interest for the engineering community (Audenaert et al., 2013). Furthermore, the literature portrays a wide range of kinetic values for the degradation kinetics during ozonation, reflecting the diverse nature of species and contaminants present in wastewater (Lim et al., 2022). In addition, a model structure able to mechanistically predict both the rapid initial ozone demand occurring at very short timescales (<10 s) and the slower ozone decomposition processes occurring at longer timescales (>30 s) has not yet been introduced and verified. Such a model would be instrumental in both design and control of ozonation processes, also contributing towards a deeper understanding on reaction mechanisms controlling the complex interplay between the ozone molecule

and the various water quality constituents. Consequently, new approaches to mechanistically model with a simplified network of reactions ozone decomposition processes are of great interest for the engineering community (Chys et al., 2018, 2017).

This paper aims to develop and verify a mechanistic yet simplified model against both literature-derived data and experimental data for ozonation decomposition processes in secondary wastewater effluents. The effluent samples are characterized with distinct qualities as separation step having two very different processes, namely a secondary clarifier and a membrane filter. An additional goal of this study involves the estimation of model parameters governing the fast and slow regimes of ozone initial demand and decay for effluents with different level of total suspended solids.

6.2 MATERIAL AND METHODS

The proposed approach involves developing the model for the ozonation considering lumped variables for the key species acting in the process. It includes conducting parameter estimation using experimental data, sensitivity analyses, and ultimately discussing the results for practical applications. The flow diagram depicting the sequential steps of this methodology is presented in Figure 6-1.

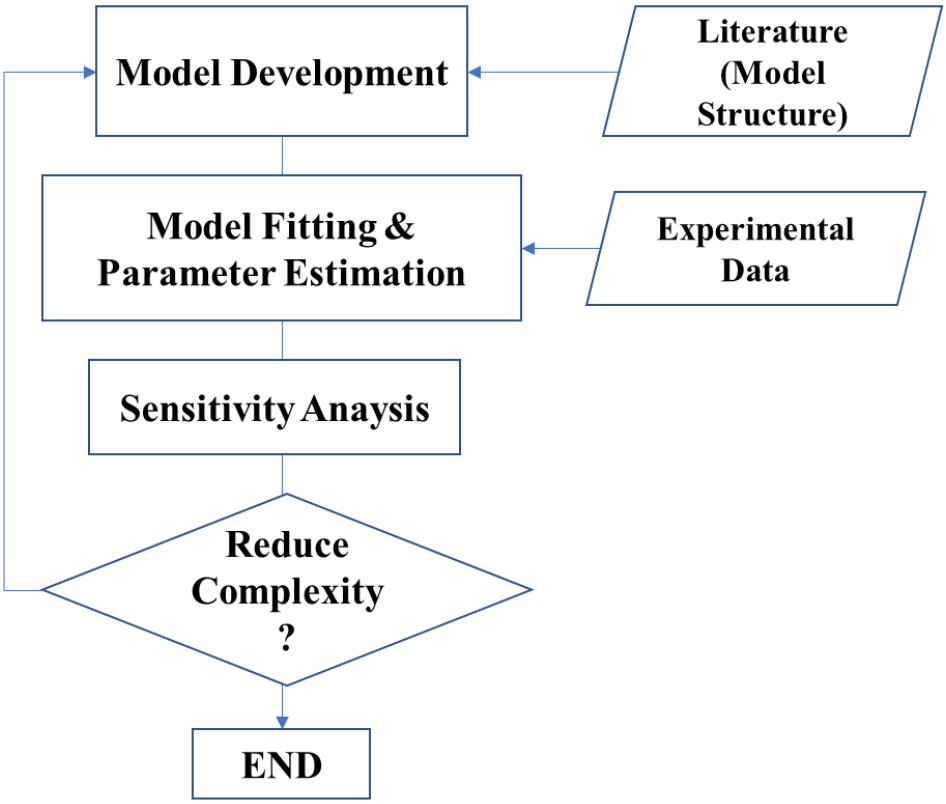

Figure 6-1 Methodological framework

6.2.1 Wastewater treatment plant samples

Samples of the effluents of conventional biological treatments are obtained from two municipal wastewater treatment plants (WWTPs) in Oxford and Adelaide (Canada). Oxford WWTP has been upgraded by a Membrane Bioreactor (MBR), operating with enhanced biological nutrient removal, while Adelaide WWTP relies on traditional activated sludge processes.

The main difference between the effluent of Adelaide WWTP (ADE) as an activated sludge treatment plant and Oxford WWTP (OXF) as an integrated system incorporating activated sludge with a MBR lies in the treatment processes and the quality of the treated water. In a conventional activated sludge treatment plant, wastewater undergoes biological treatment through the activation of microorganisms. The activated sludge, containing a diverse microbial community, treats the organic pollutants present in the water. However, the effluent from such a system may still contain suspended solids and may not meet stringent standards for nutrient removal or pathogen reduction.

In contrast, Oxford WWTP incorporating activated sludge with an MBR introduces a membrane filtration step. The MBR consists of a membrane unit that physically separates treated water from sludge, resulting in a higher quality effluent. The membrane acts as a barrier to suspended solids, bacteria, and other contaminants, producing a clearer and more polished effluent. This integrated approach enhances the removal of solids and pathogens, resulting in effluent that often meets stricter discharge standards. Therefore, in the second case providing an extra level of filtration, leading to a higher quality effluent with improved clarity and reduced levels of contaminants.

Hence, samples are collected from both facilities to investigate and compare the efficiency of these different treatment approaches in terms of water quality parameters and their compositions. Table 6-1 lists the characterization of the samples, detailing the essential parameters necessary for ozonation analysis.

Table 6-1 The characterization of the effluent samples taken from OXF and ADE WWTPs

Parameter	ADE	OXF	Unit
NO_2	0.13	0.19	(± 0.05) mg/L NO_2-N
NO_3	1.20	18.20	(± 0.05) mg/L NO_3-N
COD	15.30	9.25	(± 0.50) mg/L
NH_3	29.90	10.20	(± 0.10) mg/L NH_3-N
pH	7.10	6.90	(± 0.10) -
Alkalinity	273.74	57.75	(± 5.0) mg $CaCO_3$/L
EC	810.50	815.00	(± 50.0) µs/cm
TOC	9.45	9.42	(± 0.10) mg/L

6.2.2 Experimental procedure

In order to model the ozonation decomposition processes in secondary wastewater effluents, the effluent samples, characterized by distinct qualities as filtered and unfiltered, are targeted to initial ozone concentration by 3,5, and 7 mgO_3/L.

Table 6-2 shows the experimental series of the effluent samples taken from OXF and ADE WWTPs for the ozone decay test over time. The stock solution of ozone is prepared with saturated concentration between 10 to 12 mg/L (≈11 mg/L) using 1 L of ultra-pure water, adjusted the sample pH to 3. The sample is taken as a blank from this beaker and measure the ozone concentration. The beaker is placed into an ice bath in the fume hood with a thermometer in order to increase ozone solubility. Then to create an ozone stock solution, ozone is dispersed through a diffuser in the collection bottle using the ozone generator of 40 g/h (TG-40 Ozone Solutions Inc. USA). The concentration of ozone is measured several times recording the concentration until ozone concentration being stable. The ozone stock solution is spiked (blended) with the effluent samples to obtain ozone concentration of 3, 5, and 7 mgO_3/L, resulting subsamples with pH of 6.5, 5, and 3.5, respectively. The addition of ozone stock solution in such a batch set-up comprises some dilution of the sample effluent. Hence, the O_3 fraction is defined as the volume of O_3 stock solution per the total volume of effluent sample plus O_3. In order to ensure the quality and accuracy of the analysis, all experiments are repeated twice and the average values are reported correspondingly.

Table 6-2 Experimental runs

Assay ID	Dilution factor ($V_{total}/V_{eff.}$)	O_3 fraction ($V_{Spiked\ O_3}/V_{total}$)	$[O_3]_{in}$ (mg.L^{-1})	pH	Sample type
Sample 1: ADE.3	1.34	0.25	3	6.5	(Secondary clarifier)
Sample 2: ADE.5	2.16	0.42	5	5	(Secondary clarifier)
Sample 3: ADE.7	2.43	0.59	7	3.5	(Secondary clarifier)
Sample 4: OXF.3	1.34	0.25	3	6.5	(Tertiary membrane)
Sample 5: OXF.5	2.16	0.42	5	5	(Tertiary membrane)
Sample 6: OXF.7	2.43	0.59	7	3.5	(Tertiary membrane)

6.2.3 Analytical determinations and reagents

The water quality parameters, including pH, electrical conductivity (EC), and alkalinity, are measured using the multiparameter meter (HI98194 Multiparameter Meter Hanna Instruments), following standard calibration procedures with buffer solutions. The concentrations of nitrite (NO_2) and nitrate (NO_3), chemical oxygen demand (COD), and ammonia (NH_3) are spectrophotometrically analyzed using the spectrophotometer (Hach DR3900 Lab VIS), employing specific methods recommended by the manufacturer. Total organic carbon (TOC) levels are determined using the analyzer (TOC-L Series Shimadzu), utilizing high-temperature combustion and Non-Dispersive Infrared (NDIR) detection. Calibration for each instrument is conducted with certified standards, and routine quality control measures, including blank samples and duplicate analyses, are implemented to ensure the accuracy and precision of the obtained analytical results. For ozone determination, the ozone testing kit (Vacu-vials Instrumental Kit) is employed for all measurements of ozone levels in the experimental samples. The photometer is set to the wavelength of 515 nm. The Ozone Vacu-vials® test kit employs the DPD (N, N-diethyl-p-phenylenediamine) chemistry. The sample is treated with an excess of potassium iodide. Ozone oxidizes the iodide to iodine. The iodine then oxidizes DPD to form a pink-coloured species in direct proportion to the ozone concentration.

6.2.4 Kinetic modeling

In this work, the ozonation process is represented by six main groups of states: initial ozone demand compounds (IOD); two fractions of effluent organic matter (slow and fast ozone decomposing), namely OMf (fast) and OMs (slow); radical forming Compounds (RFC); radical scavengers (RS); and target contaminant (TC) as the final

mineralization which complete the contaminant treatment. The kinetic model scheme is given in Figure 6-2.

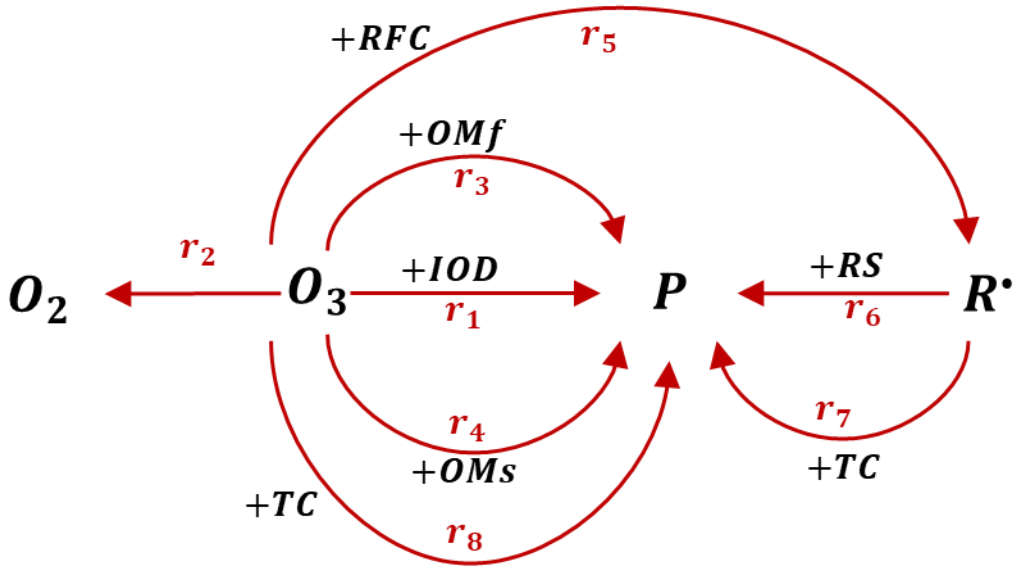

Figure 6-2 Model scheme

IOD describes the ozone demand at the initial stage of ozonation, where this oxidant is instantaneously consumed by the reactive components of the water matrix. Thus, this parameter represents the dose of ozone for which the transition between primary (very fast) and consequent ozonation stages takes place, equivalent to the value observed during the initial 15-20 seconds (approx.) in a batch mode experiment (Cruz-Alcalde et al., 2019; Hasegawa et al., 2008). This specific ozone consumption in the initial stage of ozonation, preceding the appearance of dissolved ozone, is termed as IOD in the context of this model research (r_1). Next, direct ozone decomposition is modelled assuming that ozone follows a first order decay (r_2). as the pH is elevated, spontaneous decomposition of ozone occurs in water through a variety of steps to ultimately produce many very reactive species.

Ozonation becomes more straightforward in experimental solutions devoid of OM. However, the complexity arises in controlling ozonation conditions, including ozone exposure, $HO^{\bullet}$exposure due to intricate interactions between $O_3/HO^{\bullet}$ and OM. To simulate the inherent consequences of OM and adjusting the ozone and $HO^{\bullet}$ exposures, the ozone-relevant properties of OM are assumed by fast and slow decomposition rates (r_3 and r_4), already reported to the same extent of methanol and acetate as promoter and inhibitor, respectively (Gulde et al., 2021).

Ozone reacts with radical-forming compounds as its powerful oxidizing agent, leading to the generation of additional radicals in a complex chain reaction. The decomposition of ozone involves the very reactive and catalytic intermediates such as $HO^{\bullet}$, O_2^-, O_3^-, HO_2 , HO_2^- and H_2O_2 (Gordon, 1995). This process is significant in various environmental and chemical contexts, contributing to the degradation of pollutants and the formation of secondary reactive species. The reaction mechanism involves the interaction of ozone with precursor molecules, resulting in the formation of radical intermediates (r_5). These radicals, in turn, can initiate subsequent reactions, creating a cascade effect that influences the overall oxidative capacity of the system. Likewise, radical scavengers, such as carbonates, is accounted for modelling the processes (r_6).

Finally, the subsequent removal of the target contaminants is modelled through exposure of O_3 and radicals ($R^{\bullet}$) (r_7 and r_8). The proposed model and the reaction expressions for the ozonation process assuming the most relevant components is presented in Table 6-3.

Table 6-3 The proposed model for the ozonation

Reaction rate		**Reaction expressions**
$r_1 = k_1[O_3][IOD_C]$	6-1	O_3 + Initial Ozone Demand Compounds(IOD) → Products
$r_2 = k_2[O_3]$	6-2	$O_3 \rightarrow O_2$
$r_3 = k_3[O_3][OMf]$	6-3	O_3 + Organic Matter * Fast Decompose (OMf) → Products
$r_4 = k_4[O_3][OMs]$	6-4	O_3 + Organic Matter Slow Decompose (OMs) → Products
$r_5 = k_5[O_3][RFC]$	6-5	O_3 + Radical Forming Compounds (RFC) → $R^{\bullet}$
$r_6 = k_6[R^{\bullet}][RS]$	6-6	$R^{\bullet}$ + Radical Scavengers (RS) → Products
$r_7 = k_7[R^{\bullet}][TC]$	6-7	$R^{\bullet}$ + Target Contaminant (TC) → Products
$r_8 = k_8[O_3][TC]$	6-8	O_3 + Target Contaminant (TC) → Products

The mass balance equations are shown as follows (Eq.6-9Eq.6-15):

$$\frac{d[O_3]}{dt} = -r_1 - r_2 - r_3 - r_4 - r_5 - r_8 + k_L a(O_3^* - O_3) \quad \text{Eq.6-9}$$

$$\frac{d[IOD]}{dt} = -r_1 \quad \text{Eq.6-10}$$

$$\frac{d[OM]}{dt} = -r_3 - r_4 \quad \text{Eq.6-11}$$

$$\frac{d[RFC]}{dt} = -r_5 \quad \text{Eq.6-12}$$

$$\frac{d[RS]}{dt} = -r_6 \quad \text{Eq.6-13}$$

$$\frac{d[R^{\bullet}]}{dt} = r_5 - r_6 - r_7 \quad \text{Eq.6-14}$$

$$\frac{d[TC]}{dt} = -r_7 - r_8 \quad \text{Eq.6-15}$$

Where $O_3{}^*$ is saturated liquid phase of ozone and $k_L a$ represents the overall mass transfer coefficient in a gas-liquid system, with k_L is the liquid-phase mass transfer coefficient and a is the interfacial area per unit volume. In this study $k_L a$ is less relevant and not applicable and it is set to zero that implies no mass transfer between the gas and liquid phases as there is no direct introduction of gaseous ozone into the system for the model.

Some process variables not contemplated by the model could have an effect on the reaction rates. Particularly, ozone decomposition into O_2 (r_2) may present a significant dependence on pH and temperature. Thermal effects are out of the scope of this work and temperature is kept constant in all assays. However, effluent samples are obtained at different pH. Hence, the model is fit to all these data sets accepting that pH would not have any influence in the quantitative explanation of the results. This assumption is next revised by analyzing to which extent the decomposition rate of ozone into O_2 (r_2) is correlated to pH. Results are presented and discussed in regard to the future extension of the model.

6.2.5 Initial state and parameter estimation (model fitting)

The initial state and parameter estimation for ozonation in this study involves the resolution of a complex nonlinear multivariate optimization problem. Conventional techniques (e.g., gradient-based methods) fail to address this kind of problems because of the high dimensionality, nonlinearity, and multimodality, making convergence challenging. Therefore, new techniques, such as evolutionary algorithms or Bayesian optimization (Surrogate algorithm), have been explored, leveraging their ability to handle complex, non-convex search spaces and expensive objective functions (Bliek et al., 2023). The surrogate optimization algorithm, which is implemented in MATLAB/Simulink®, comprises two alternating phases. In the "Construct Surrogate" phase, a surrogate of the objective function is created by evaluating the objective function (typically computationally expensive) at a set of randomly generated points within predefined bounds. A radial basis function is then interpolated through these points to construct the surrogate. In the "Search for

Minimum" phase, the algorithm seeks the minimum of the objective function by sampling numerous random points within the bounds. A merit function, based on the surrogate values and distances between these points and locations where the objective function has been evaluated, is computed. The point with the optimal merit function is chosen as a candidate, and the objective function is evaluated at this point (adaptive point). The surrogate is updated using this new value, and the process repeats iteratively.

This method aims to refine the initial conditions and parameters of the ozone reaction model by minimizing the sum of squared differences between the predicted values generated by the model and the corresponding experimental data. In this method, the optimization algorithm iteratively adjusts the parameters to achieve the closest possible match between the model's predictions and the actual experimental results. This iterative refinement enhances the accuracy of the model, enabling a more precise representation of the ozonation process.

The method is implemented in MATLAB/Simulink® (R2023b) to simultaneously estimate the states and parameters of the ozonation model. The concentration profiles of ozone are used to estimate the model parameters (model calibration). 8 kinetic constants and the 6 initial states are adjusted to minimize the square error for the ozone concentration (Eq.6-16).

$$\min Z = \sum_{j=1}^{m} \left(\sum_{i=1}^{n} \left(\widehat{[O_3]}_{(i,j)} - [O_3]_{(i,j)} \right)^2 \right) \qquad \text{Eq.6-16}$$

where the circumflex stands for the experimental data, the subscript i for each sample at specific reaction times and the subscript j represents the different experiments.

The Root Mean Square Error (RMSE, Eq.6-17) is used to assess the model's reliability and the quality of fit. Additionally, the coefficient of determination R-squared (according to Eq.6-18) is provided for illustrative purposes, given its widespread use, despite the distinction that R-squared in nonlinear models does not equate to the sum of squares in linear regression, comprising both regression and residual components.

$$RMSE_k = \sqrt{\left(\sum_{i=1}^{N_k} (\hat{y}_{ik}\text{-}y_{ik})^2 \Big/ N_k \right)} \quad \text{Eq.6-17}$$

$$R_k{}^2 = 1 - \left(\sum_{i=1}^{N} (\hat{y}_i\text{-}y_i)^2 \Big/ \sum_{i=1}^{N} (\hat{y}_i\text{-}\bar{y})^2 \right) \quad \text{Eq.6-18}$$

where $\hat{y}_i$ and y_i correspond to the measured and simulated values at the given time, respectively, and $\bar{y}$ is the mean of the measured data.

6.2.6 Global sensitivity analysis (GSA)

Parameter sensitivity analysis is employed to assess a mathematical model's robustness and the relative importance of its incorporated mechanisms in the face of parameter uncertainty (Latunde and Bamigbola, 2018). Local Sensitivity Analysis (LSA, (Castillo et al., 2004)) is a computationally inexpensive approach based on derivatives, examining the impact of one parameter while keeping others constant. However, LSA is limited in exploring only a fraction of the solution space. Global Sensitivity Analysis (GSA, (Saltelli et al., 1999)), particularly implemented using Monte Carlo techniques, overcomes LSA limitations by using a globally representative set of samples, allowing simultaneous variation of multiple input factors to assess interactions. The study adopts GSA, considering its frequent implementation in models with multiple correlated outputs. Among various GSA techniques, the application of Latin hypercube sampling with partial rank correlation coefficient index (LHS-PRCC) is conducted as an efficient statistical method for GSA, providing substantial uncertainty and sensitivity information with a relatively small sample size. The combined LHS-PRCC method is utilized to analyze correlations between model parameters and output, considering general monotonic relationships while removing the effects of remaining parameters. As the formulation is reported elsewhere (Nasr Esfahani et al., 2023, 2022b), the partial rank correlation coefficients for each parameter (R_{X_kY}) are computed using the following Eq.6-19.

$$R_{X_kY} = \frac{cov(X_k, Y)}{\sqrt{Var\,(X_k) Var(Y)}} = \frac{\sum_{i=1}^{N} (x_{ik} - \bar{x})(y_i - \bar{y})}{\sqrt{\sum_{i=1}^{N} (x_{ik} - \bar{x})^2 (y_i - \bar{y})^2}} \quad \text{Eq.6-19}$$

where for a model characterized by P model parameters and an output y can be expressed as a function of the values of all model parameters, denoted as x_k ($k = 1, 2, \dots, P$), such that $y = f(x_1, x_2, \dots, x_P)$. Consequently, generating N samples ($i =$

$1, 2, \ldots, N$) for each model parameter results in a collection of P sample vectors X_k ($1 \times N$) and a corresponding vector Y ($1 \times N$) representing output values. Subsequently, the $R_{X_k Y}$ values span from -1 to 1, with their magnitude signifying the extent of parameter influence, while the sign denotes whether an increase in the parameter value corresponds to an increase or decrease in the output. (Helton et al., 2006b).

6.3 RESULT AND DISCUSSION

6.3.1 Fitting the model against the reported data: Model calibration and verification

An initial verification step is undertaken to confirm the capability of the model to predict both fast and slow zones of ozone decomposition against two sets of reported data from the literature (Buffle et al., 2006). Unlike a pseudo-first order model, which fails to accurately capture the decay patterns in various zones, the model provides a comprehensive representation of ozone decay in different scenarios, contributing to its reliability and versatility.

Data sets for the calibration of the kinetic model are first obtained from a previous study by Buffle et al. (2006) that investigates the comparison between continuous quench-flow system (CQFS) and batch measurements in wastewater effluent, specifically in Opfikon at pH 8 (Buffle et al., 2006). The experiments were performed with different techniques at different time scales. Data from 0.35 s to 10.82 s (Dataset 1: rapid decay) were obtained by CQFS (Continuous Quench-Flow System), while data for larger times up to 120 s (Dataset 2: slow decay) were obtained using a batch setup.

As illustrated in Figure 6-3, the profile predicted by the developed model is plotted by a solid line, while the pseudo-first order model fits to the dataset 1 and dataset 2 are depicted with a dot line and a dash-dot line, respectively. It is noteworthy to highlight that the pseudo-first order model fits, both for both datasets 1 and 2, fail to accurately predict the experimental data. This emphasizes the limitations of the pseudo-first order models in capturing the intricacies of ozone decomposition in the specific conditions of municipal wastewater effluent. The model demonstrates an acceptable goodness of fit when applied to the datasets 1 and 2. This outcome is indicative of the model ability to generalize and accurately predict ozone

decomposition dynamics covering both rapid decay and slow decay phases. The successful calibration with the experimental data strengthens the model reliability and its potential for broader applicability in real-world scenarios.

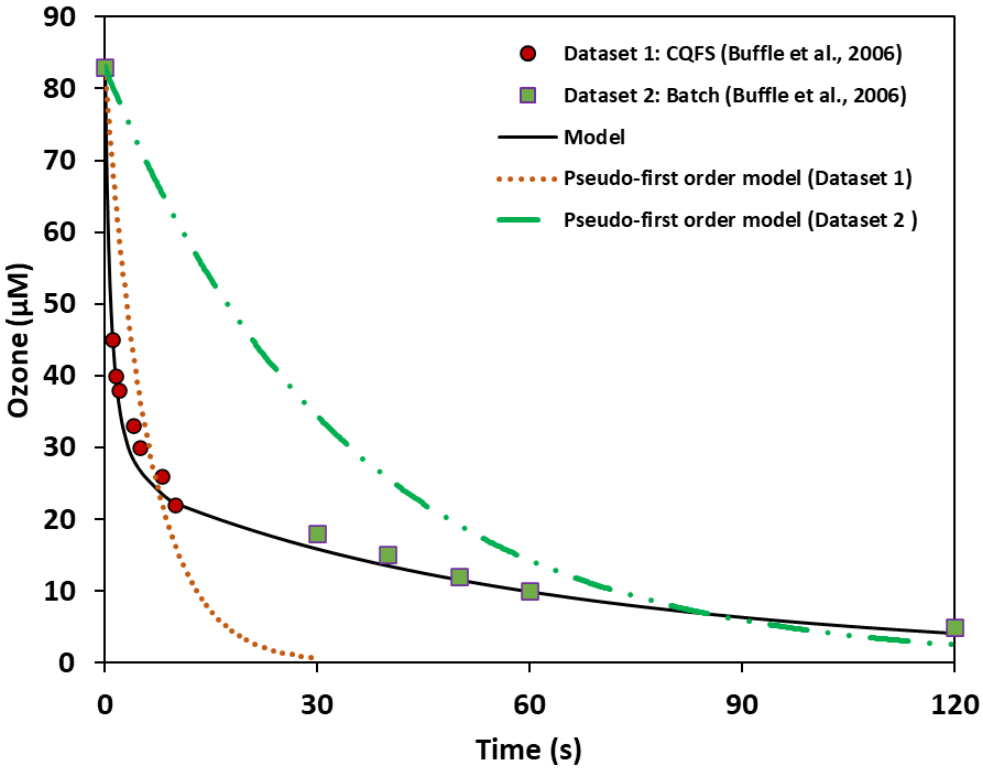

Figure 6-3 Comparison of the developed kinetic model for ozone decomposition profile (solid line) with pseudo-first order model fits to dataset 1 (●) (dot line) and dataset 2 (□) (dash-dot line), extracted from Buffle et al.'s (2006).

6.3.2 Model calibration: Initial state and parameter estimation

Following the successful fitting of the kinetic model to the training data sets, the experimental series of this study are employed with different initial ozone concentration in both samples (ADE and OXF) for the model fitting. The initial ozone concentrations are targeted to be 3, 5, and 7 mgO_3/L to identify the contribution of operational conditions (i.e., O_3 fraction) and effluent characterization (filtered and unfiltered effluent) to the decomposition of ozone over time. MATLAB/Simulink® solver is designed for seeking the global minimum of a real-valued objective function, particularly beneficial for functions requiring significant evaluation time. This algorithm depends on resource-intensive evaluations of the objective function, constructing and optimizing a surrogate function as a cost-effective substitute for the original function. This derivative-free approach is well-suited for addressing nonconvex problems. The parameter estimator application in MATLAB/Simulink®

R2023b Optimization Toolbox™ is employed to calibrate the model to experimental datasets aimed to simultaneously estimate the states and parameters of the ozonation model.

The model is rigorously adjusted to all experimental datasets resulted in good fit with RMSE values no more than $7 \cdot 10^{-6}$ mM. Table 6-4 displays the parameter values that are obtained for ADE and OXF samples.

Table 6-4 Estimation of the kinetic parameter values for the proposed model

Kinetic constants	**Fitted value (ADE)**	**Fitted value (OXF)**
k_1 $(mM^{-1}.s^{-1})$	$1.43 \cdot 10^{+3}$	$3.35 \cdot 10^{+3}$
k_2 (s^{-1})	$3.37 \cdot 10^{-5}$	$1.15 \cdot 10^{-3}$
$k_3(mM^{-1}.s^{-1})$	$9.82 \cdot 10^{-2}$	$3.72 \cdot 10^{-1}$
k_4 $(mM^{-1}.s^{-1})$	$1.05 \cdot 10^{-2}$	$1.04 \cdot 10^{-2}$
$k_5(mM^{-1}.s^{-1})$	$1.58 \cdot 10^{+3}$	$1.57 \cdot 10^{+3}$
k_6 $(mM^{-1}.s^{-1})$	$9.99 \cdot 10^{+4}$	$9.97 \cdot 10^{+4}$
k_7 $(mM^{-1}.s^{-1})$	$3.86 \cdot 10^{+5}$	$3.78 \cdot 10^{+5}$
k_8 $(mM^{-1}.s^{-1})$	$4.44 \cdot 10^{+2}$	$3.89 \cdot 10^{+2}$

Table 6-5 provides a detailed overview of the initial states obtained for all experimental assays, representing the estimated initial conditions of model variables. Dilution factors (DF=1.34, 2.16, and 2.43 for 3, 5, and 7 $mg.L^{-1}$, respectively) are considered for each initial state. These dilution factors are crucial for subsequent simulation purposes, ensuring that each profile run is simulated with its corresponding and appropriate initial states.

Table 6-5 Estimated initial concentration of the model variables

Initial state (IS)	**Fitted value ADE**	**ADE.3 (IS/1.34)**	**ADE.5 (IS/2.16)**	**ADE.7 (IS/2.43)**	**Fitted value OXF**	**OXF.3 (IS/1.34)**	**OXF.5 (IS/2.16)**	**OXF.7 (IS/2.43)**
OMf_{in} (mM)	$1.15 \cdot 10^{-3}$	$8.58 \cdot 10^{-4}$	$3.97 \cdot 10^{-4}$	$1.64 \cdot 10^{-4}$	$1.00 \cdot 10^{-3}$	$7.46 \cdot 10^{-4}$	$3.45 \cdot 10^{-4}$	$1.42 \cdot 10^{-4}$
OMs_{in} (mM)	$1.01 \cdot 10^{-3}$	$7.54 \cdot 10^{-4}$	$3.49 \cdot 10^{-4}$	$1.44 \cdot 10^{-4}$	$9.89 \cdot 10^{-4}$	$7.38 \cdot 10^{-4}$	$3.42 \cdot 10^{-4}$	$1.41 \cdot 10^{-4}$
R_{in} (mM)	0.0	0.0	0.0	0.0	0.0	0.0	0.0	0.0
TC_{in} (mM)	$6.30 \cdot 10^{-6}$	$4.70 \cdot 10^{-6}$	$2.18 \cdot 10^{-6}$	$8.96 \cdot 10^{-7}$	$2.05 \cdot 10^{-5}$	$1.53 \cdot 10^{-5}$	$7.08 \cdot 10^{-6}$	$2.91 \cdot 10^{-6}$
RFC_{in} (mM)	$9.47 \cdot 10^{-7}$	$7.07 \cdot 10^{-7}$	$3.27 \cdot 10^{-7}$	$1.35 \cdot 10^{-7}$	$1.78 \cdot 10^{-6}$	$1.33 \cdot 10^{-6}$	$6.15 \cdot 10^{-7}$	$2.53 \cdot 10^{-7}$
IOD_{in} (mM)	$1.30 \cdot 10^{-4}$	$9.70 \cdot 10^{-5}$	$4.49 \cdot 10^{-5}$	$1.85 \cdot 10^{-5}$	$5.28 \cdot 10^{-5}$	$3.94 \cdot 10^{-5}$	$1.82 \cdot 10^{-5}$	$7.51 \cdot 10^{-6}$
RS_{in} (mM)	$9.99 \cdot 10^{-8}$	$7.46 \cdot 10^{-8}$	$3.45 \cdot 10^{-8}$	$1.42 \cdot 10^{-8}$	$1.00 \cdot 10^{-7}$	$7.46 \cdot 10^{-8}$	$3.45 \cdot 10^{-8}$	$1.42 \cdot 10^{-8}$

6.3.3 Model simulations

Using the model parameter values and initial states fitted to the experimental data (Table 6-4 and Table 6-5), simulations are conducted to verify and demonstrate

the fitting. Figure 6-4 displays the experimental data alongside the predicted profiles for the corresponding experimental conditions at ozone concentrations of 3, 5, and 7 $mg.L^{-1}$. The initial phase of ozone decomposition involves a rapid reaction of ozone with easily degradable substances, followed by a medium phase with a moderate decay rate. The slow phase occurs when the remaining ozone reacts with more resistant pollutants, requiring a longer time to achieve complete degradation.

On the other hand, the difference of using filtered (OXF) and unfiltered (ADE) effluents with the same amount of initial ozone seems remarkable in cases of 5 and 7 $mg.L^{-1}$ of initial ozone while in case of 3 $mg.L^{-1}$ of ozone resulted in no residual ozone at the end of the experiments.

The rapid consumption of ozone occurs due to reactions with readily available organic and inorganic substances in the effluent. Ozone reacts quickly with substances like inorganic matter, metals, and other pollutants, leading to a fast decrease in ozone concentration.

As the initial reactivity decreases beyond 20 s, the decay rate slows down. Ozone continues to react with remaining pollutants, but at a moderate pace. Some of the slower-reacting contaminants are now targeted, contributing to a gradual decline in ozone concentration.

The remaining ozone is mainly consumed by persistent or harder-to-react substances. The decay rate becomes considerably slower as fewer reactive species are available. This phase may continue for an extended period until the ozone is nearly depleted, and further treatment may be required to address any remaining contaminants.

The high R-squared (≥ 0.99) and low RMSE values ($\leq 7 \cdot 10^{-6}$ mM), results in the good fit of the proposed model to the experimental data. As can be seen in Figure 6-4, the model is capable of predicting the ozone decay at different O_3 fractions as well as the unfiltered (Figure 6-4 (a)) and filtered effluents (Figure 6-4 (b)).

a)

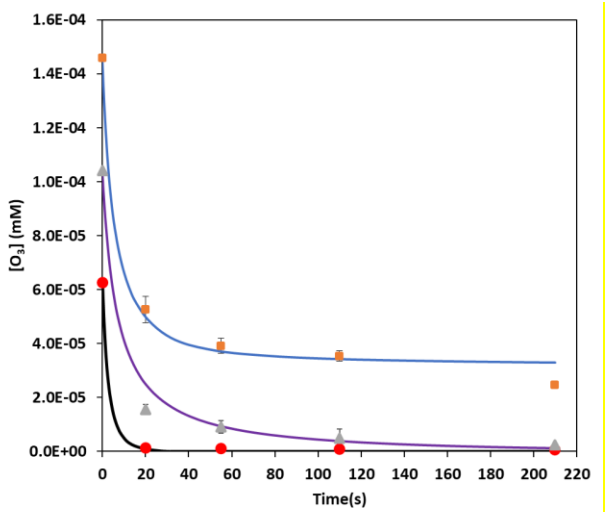

b)

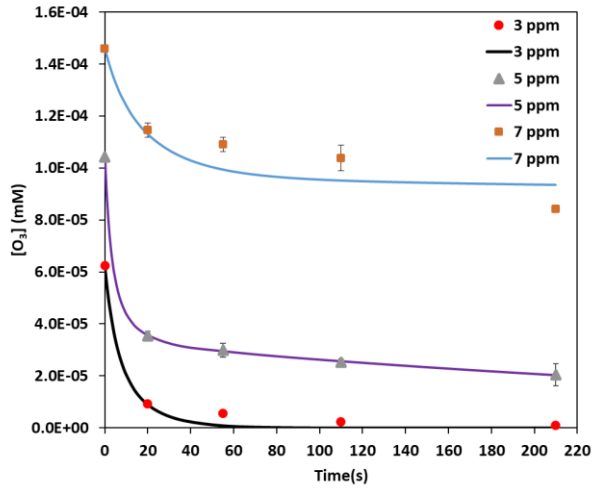

Figure 6-4 Experimental data (marker points) and profiles predicted by the proposed kinetic model (solid line) for $[O_3]$ =0.0000625 mM (3±0.1 mg.L^{-1}), $[O_3]$ =0.000104 mM (5±0.1 mg.L^{-1}), and $[O_3]$ =0.000147 mM (7±0.1 mg.L^{-1}), (a) Sample ADE, (b) Sample OXF

This graphical representation aims to elucidate the degree of closeness between the observed experimental data and the values predicted by the model, with a focus on evaluating patterns and potential discrepancies. The proximity of data points to the identity line indicates the model accuracy in replicating experimental outcomes.

Further simulations are conducted to verify the model consistency and its ability to estimate the behavior of intermediate unobserved variables. Figure 6-5 indicates

profiles of the model variables along with the derivatives. The plot provides insights into whether the exponential profile is a suitable representation for their dynamics. The assertion that the exponential profile can be applied to variables of the model, except for ozone decay, suggests that the behavior of most intermediate unobserved variables follows an exponential trend. However, the exception of ozone decay implies a deviation from this pattern, indicating that the decay process for ozone may be governed by a different set of dynamics or reactions, requiring a distinct representation.

a)

b)

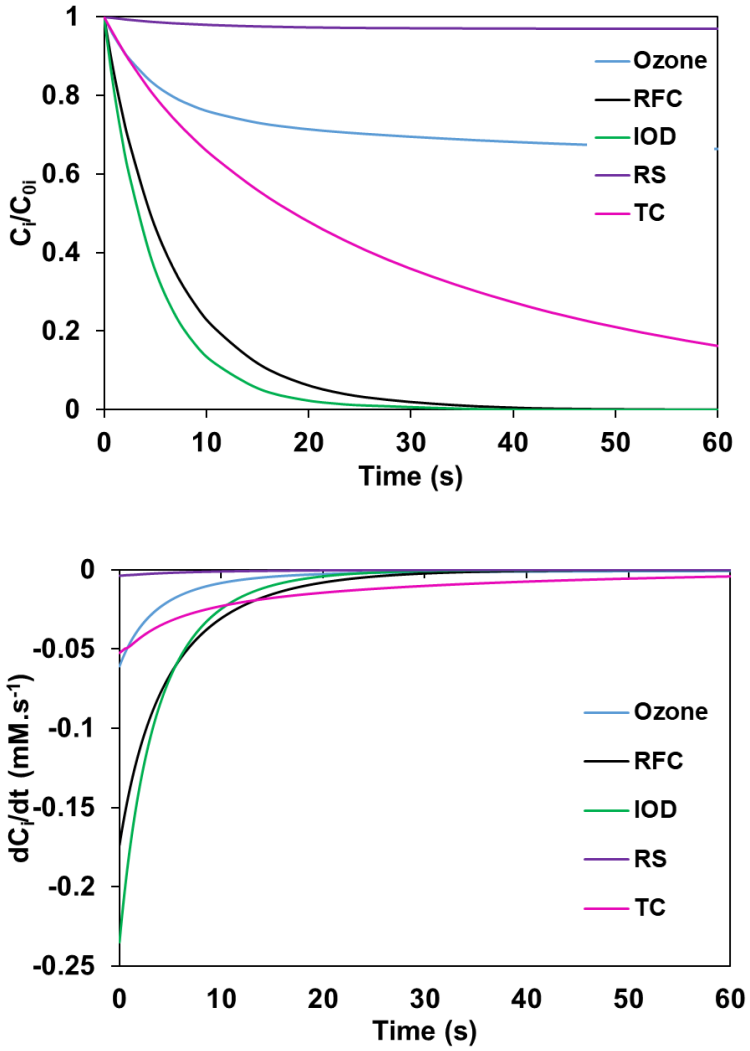

Figure 6-5 Simulation and concentration profiles using estimated model parameters at $[O_3]$ =0.000104 mM and initial conditions of OXF sample: $^{C_i}/_{C_{oi}}(a)$, $^{dC_i}/_{dt}$ (b)

Although the practicality of the proposed model is proved in explaining the process across various conditions, the investigation extends to evaluate parameter uncertainty and the necessity of the different mechanisms incorporated in the model.

This examination, aligning with the approach outlined elsewhere (Nasr Esfahani et al., 2023, 2022b), aims to identify opportunities for simplifying the model.

6.3.4 Global sensitivity analysis

A global sensitivity study is conducted on relevant parameters of the proposed model. Notably, the outputs considered for this analysis are the sum of the square error between measured values of ozone as well as the simulated values of the target contaminant (TC) and organic matter (OM) and estimated values in 200 sample runs for each model parameter. The decision to include simulated data for TC and OM in the GSA alongside the experimental data for ozone concentration serves a dual purpose. Firstly, it allows for a more comprehensive assessment of the model sensitivity to various parameters by incorporating multiple outputs. This inclusion enables a broader exploration of how changes in model parameters impact not only ozone concentration, which is experimentally measured, but also the simulated outputs for TC and OM. By analyzing the sensitivity of the model to a range of outputs, understanding of parameter influences on the overall system dynamics.

Secondly, the use of simulated data for TC and OM extends the analysis beyond the confines of experimental measurements, providing insights into the model behavior in scenarios where direct experimental observations might be limited. This approach enhances the robustness of the sensitivity analysis and ensures that the model performance is evaluated not only against observed data but also against the simulated behavior of additional relevant variables. In essence, employing simulated data for TC and OM in the GSA allows for a more thorough exploration of the model sensitivity and its ability to capture the broader dynamics of the system under consideration.

This analytical approach explores the influence of model parameters on the model output, allowing a comprehensive assessment of their individual contributions to the system dynamics. Following a meticulous GSA (Figure 6-6), the analysis reveals that three model parameters associated with radical ($R^{\bullet}$) reactions (r5, r6, and r7) can be safely removed (the threshold $|R_{XY}| \geq 0.05$ for all three outputs), as their impact on the fitting is found to be negligible. However, it is noteworthy that the self-decomposition of ozone, although exhibiting a low influential effect, is retained within the model. The rationale for preserving this aspect lies in its inherent role in capturing a comprehensive representation of the ozone degradation process. The self-

decomposition of ozone, despite its seemingly minor impact on the fitting, contributes to the holistic understanding of the intricate reaction kinetics involved in ozone decay. Consequently, its retention ensures a more nuanced and accurate portrayal of the ozone degradation dynamics within the proposed model.

This analysis suggests the potential removal of these parameters without significantly compromising the model ability to capture and represent the observed phenomena. Such insights contribute to a more streamlined and efficient model, emphasizing the importance of refining model complexity for improved interpretability and computational efficiency.

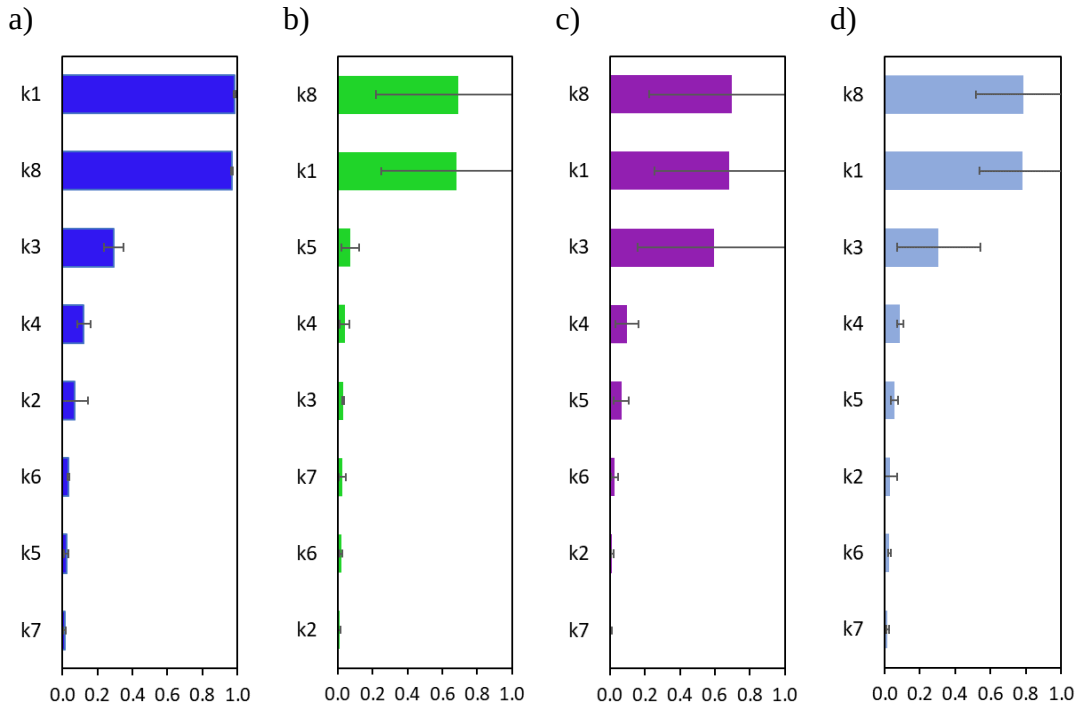

Figure 6-6 Sensitivity analysis and correlation coefficients R_{XY} for the all proposed model parameters (absolute value): a) ozone, b) TC, c) OM, and d) Overall.

Accordingly, reactions related to radical ($R^{\bullet}$) are removed from the model. This discernment is underpinned by the concept of concentration ratio (Rct), defined as the ratio of radical, specifically Hydroxyl radical exposure to ozone exposure (Kwon et al., 2017). The Rct concept provides a metric for evaluating the relative impact of radical reactions on the overall ozone degradation process. In instances where specific parameters related to radicals ($R^{\bullet}$) exhibit low sensitivity, their removal aligns with the notion that their contribution to the Rct ratio is minimal. Consequently, the GSA results, when interpreted through the Rct framework, not only facilitate model

simplification but also offer a mechanistic understanding of the interplay between radical exposures, supporting a nuanced refinement of the ozone degradation model.

Next, GSA is repeated after excluding the removed parameters (Figure 6-7), served as a complementary analysis to unveil the true significance of the retained parameters in the refined ozone degradation model. By eliminating the parameters identified as having low impact on fitting, the subsequent GSA focuses exclusively on the remaining set of parameters, allowing for a more concentrated examination of their individual contributions to the model's outputs. This complementary analysis is crucial for discerning the nuanced interactions and influences among the retained parameters, which may have been masked or overshadowed by the presence of less influential factors. It provides a clearer understanding of the retained parameters' relative importance in shaping the model's responses, aiding in the identification of key factors that significantly contribute to the system dynamics. Thus, the repetition of GSA, excluding the removed parameters, enhances the precision and accuracy of the sensitivity analysis, offering deeper insights into the essential elements driving the ozone degradation model.

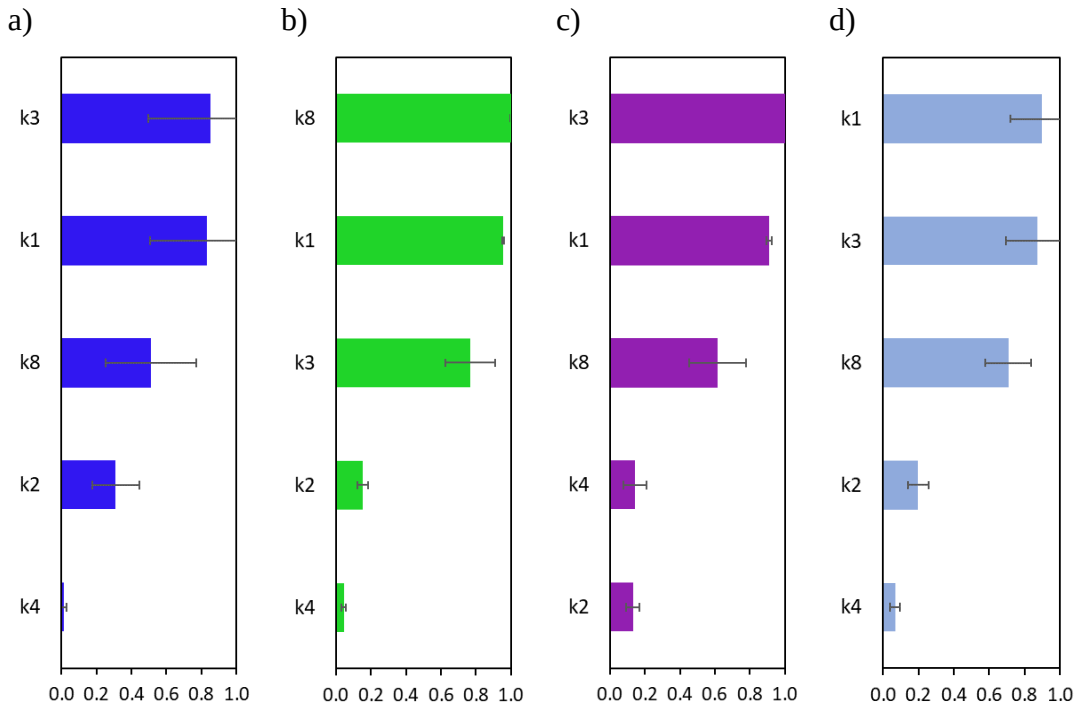

Figure 6-7 Sensitivity analysis and correlation coefficients R_{XY} for the reduced model (absolute value): a) ozone, b) TC, c) OM, and d) Overall.

A new estimation of kinetic parameter values (Table 6-6) is performed for the revised ozone model, derived after GSA and incorporating the influence of IOD, ozone

self-decomposition, and OMf and OMs decomposition rates, as well as the dynamics of TC. This reduced model not only accommodates the intricacies revealed through GSA but also captures the nuanced interactions among key components in the ozone degradation process. The inclusion of IOD, ozone self-decomposition, and different forms of OM oxidation acknowledges the multifaceted nature of the chemical reactions involved. As a result, the refined kinetic parameter values aim to represent the system's behavior under diverse conditions, ensuring a comprehensive and realistic portrayal of the complex interplay between these components in the context of ozone degradation. This iterative process enhances our understanding of the model behavior and guides decisions for refining its complexity based on the sensitivity of the parameters to the measured and simulated responses.

Table 6-6 New estimation of the kinetic parameter values for the reduced ozone model after GSA

Kinetic constants	**Fitted value (ADE)**	**Fitted value (OXF)**
k_1 $(mM^{-1}.s^{-1})$	$1.43 \cdot 10^{+3}$	$4.29 \cdot 10^{+2}$
k_2 (s^{-1})	$8.76 \cdot 10^{-4}$	$7.63 \cdot 10^{-12}$
$k_3(mM^{-1}.s^{-1})$	$6.22 \cdot 10^{-1}$	$2.96 \cdot 10^{-8}$
k_4 $(mM^{-1}.s^{-1})$	$1.20 \cdot 10^{-2}$	$3.34 \cdot 10^{-9}$
k_8 $(mM^{-1}.s^{-1})$	$9.04 \cdot 10^{+3}$	$1.60 \cdot 10^{-4}$

Figure 6-8 illustrates the reduced model fit to the same experimental data, serving as a crucial component in the context of earlier discussion on potential simplifications identified through the GSA. The reduction in complexity aims to streamline the model while maintaining its practical utility, demonstrating the balance between accuracy and simplicity.

The observed adjustments in the model are directly linked to the GSA insights, specifically highlighting the identified low importance of certain reactions (e.g., Reaction 5, 6, 7 related to $HO^{\bullet}$ radical interactions). By implementing these simplifications, the model is tailored for practical purposes, offering a more manageable and efficient representation of the ozone decomposition process. The visual representation of the model performance under the reduced complexity showcases how the model, with fewer parameters and simplified reactions, still aligns closely with the experimental data. This underscores the model's adaptability and its ability to be fine-tuned for practical applications, while maintaining accuracy in predicting ozone profiles within the context of wastewater treatment.

Additional mathematical exploration may uncover the optimal number of model parameters and their values. This implies that ongoing research and refinement are essential for enhancing the model's predictive capabilities and refining its precision.

a)

b)

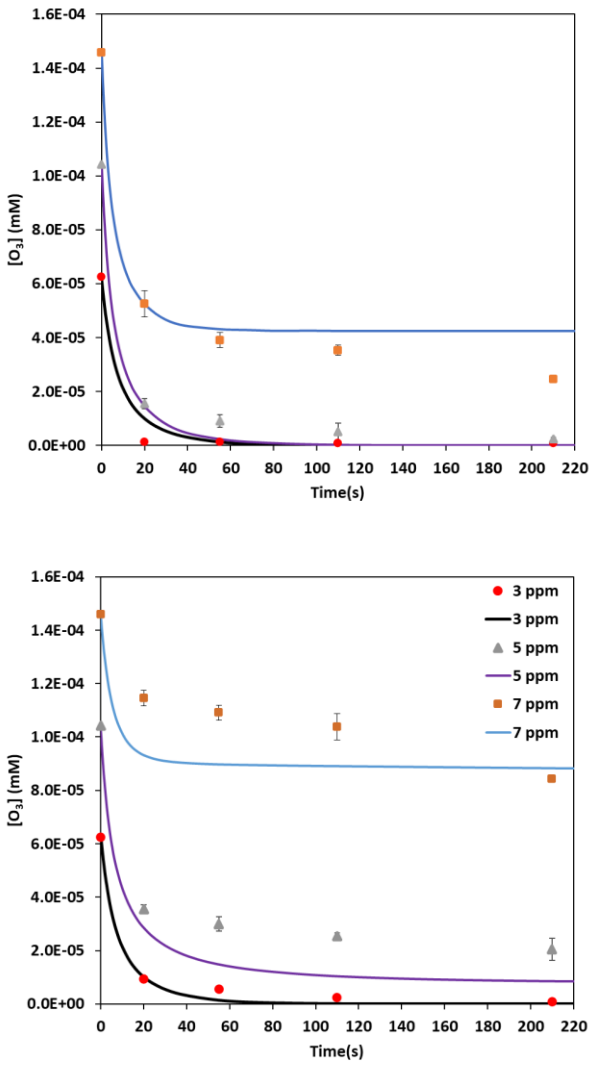

Figure 6-8 Experimental data (marker points) and profiles predicted by the reduced kinetic model (solid line) after GSA for $[O_3]$ =0.0000625 mM (3±0.1 mg.L^{-1}), $[O_3]$ =0.000104 mM (5±0.1 mg.L^{-1}), and $[O_3]$ =0.000147 mM (7±0.1 mg.L^{-1}), (a) Sample ADE, (b) Sample OXF

The good agreement of model estimations with experimental data under the reduced model provide confidence in the model's overall accuracy and practical applicability. However, a notable deviation is apparent at a high O_3 ratio of 0.6 (7 mg.L^{-1} of ozone), where the model appears to be less fit. This discrepancy can be

attributed to the higher dilution effect at elevated ozone concentrations, leading to a shift in the behavior of the system.

At high O_3 ratios, a substantial amount of ozone is introduced into the system, significantly exceeding the effluent sample volume. This increased ozone concentration, coupled with the higher dilution effect, creates a scenario where the self-decomposition of ozone becomes a key factor influencing the overall behavior of the system. The self-decomposition of ozone, a process where ozone spontaneously breaks down into oxygen molecules, plays a pivotal role in high-ozone environments. This behavior can result in deviations from the expected model fit, particularly when the system includes a much larger amount of ozone solution than the effluent sample. The interplay of self-decomposition dynamics and dilution effects at such elevated ozone ratios introduces complexities that may not be adequately captured by the reduced model.

This observed discrepancy at high O_3 ratios underscore the importance of considering system-specific conditions and the potential limitations of the model under certain scenarios. It prompts further exploration and refinement of the model to account for the unique dynamics associated with high ozone concentrations, emphasizing the need for a more comprehensive understanding of the complex interactions within the system.

6.3.5 Assessment of pH influence

The decomposition of ozone into oxygen (r_2) is next considered for assessing the extent to which pH is affecting the fitting of the model. The analysis is focused on reaction 2 due to its acknowledged dependence on pH (Bilińska et al., 2017; Yershov et al., 2009) and its net scavenging effect. pH may be expected to have reduced effect on fast reactions, such as initial ozone demand (r_2), and reactions involving organic matter (r_3 and r_4) are expected to be more influenced by the amount of organic matter and its nature and less by pH.

Given that, effluent samples were obtained at different pH for which the same model was fit with all eight reactions (presented in Table 6.3). Different values for k_2 were obtained taking into account Eq.6-16 for the objective function for each experiment independently. These values are plotted in Fig. 6-9 to reveal a clear direct

correlation of k_2 values and pH, while no significant difference can be attributed to the effluent (OXF, ADE).

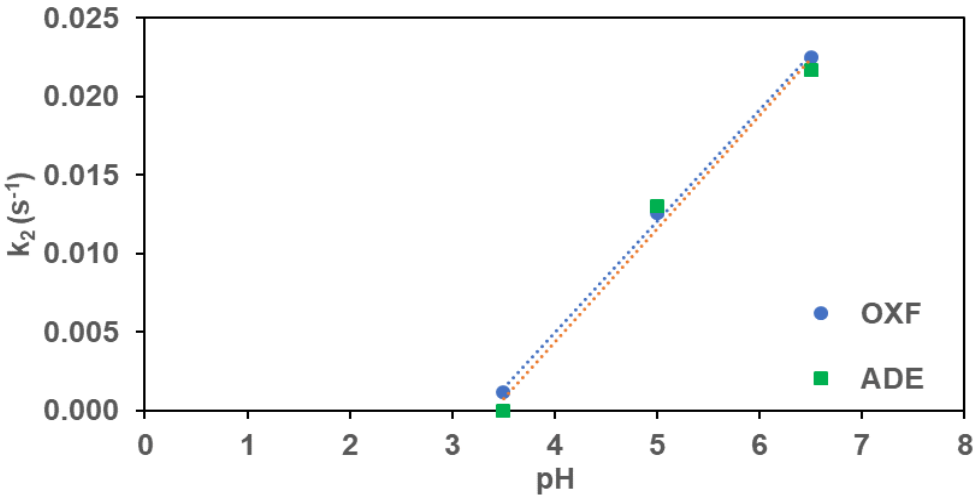

Figure 6-9 Ozone decomposition constant (k_2) as a function of pH from 3.5 to 6.5.

While the model developed has shown a practical capacity to describe the ozone evolution, this analysis shows that further work is required to extend and refine the model for applications spanning to larger pH ranges. A first attempt could be including this pH dependence of k_2 in the model as a linear relationship (k_2=b+a·pH), which will require one additional parameter to be adjusted.

However, this simple linear dependency may have a limited range of applications, for higher and lower pH values the effect of pH on k_2 will saturate and a sigmoidal behavior should be expected, as it is also supported by existing literature (Gardoni et al., 2012). However, incorporating a more complex behavior into the model would require the adjustment of more parameters.

6.4 CONCLUSIONS

This study delves into ozone decomposition in aqueous solutions, shedding light on a longstanding and complex phenomenon in ozonation processes. The development of a new mathematical model, based on a novel semi-empirical approach incorporating key surrogates such as IOD, OM, RF C, RS, and TC, represents a significant step forward for its simplicity yet demonstrates an acceptable goodness of fit, effectively predicting ozone behavior in wastewater treatment. This two-step methodology,

commencing with literature validation and advancing to under-study assays for calibration, indicated the robustness and validity of the proposed model in capturing the intricate dynamics of ozone decay kinetics.

The model's ability to capture varying degradation rates for organic matter adds a layer of precision, providing a more comprehensive representation of the intricate interactions within municipal effluent systems. The successful implementation of the model using Simulink® under realistic conditions underscores its practical applicability. Furthermore, the study not only contributes to theoretical advancements but also engages in experimental fitting and validation, revealing the model's efficacy in predicting ozone profiles.

The GSA performed in this study identifies opportunities for model simplification, emphasizing the importance of certain reactions related to $HO^{\bullet}$ radical interactions. This insight enables a refinement of the model, enhancing its efficiency without compromising accuracy. Through rigorous testing and validation, the model emerges as a reliable and valuable tool for wastewater treatment processes, offering the potential to improve the precision and efficiency of ozone-based strategies. While the reduced model demonstrates good agreement with experimental results in general, the deviation at high ozone ratio of 0.6 highlights the impact of factors such as dilution and self-decomposition on the system's behavior. This observation encourages continued research and refinement to enhance the model predictive capabilities, particularly in scenarios involving elevated ozone concentrations commonly encountered in wastewater treatment processes.

The developed mathematical model represents a promising step forward in advancing ozone-based wastewater treatment. This research contributes to ongoing efforts for more sustainable and effective solutions, addressing environmental challenges and enhancing the success of wastewater treatment processes.

Chapter 7: Integration of Advanced Oxidation Processes and biological treatments for wastewater decontamination

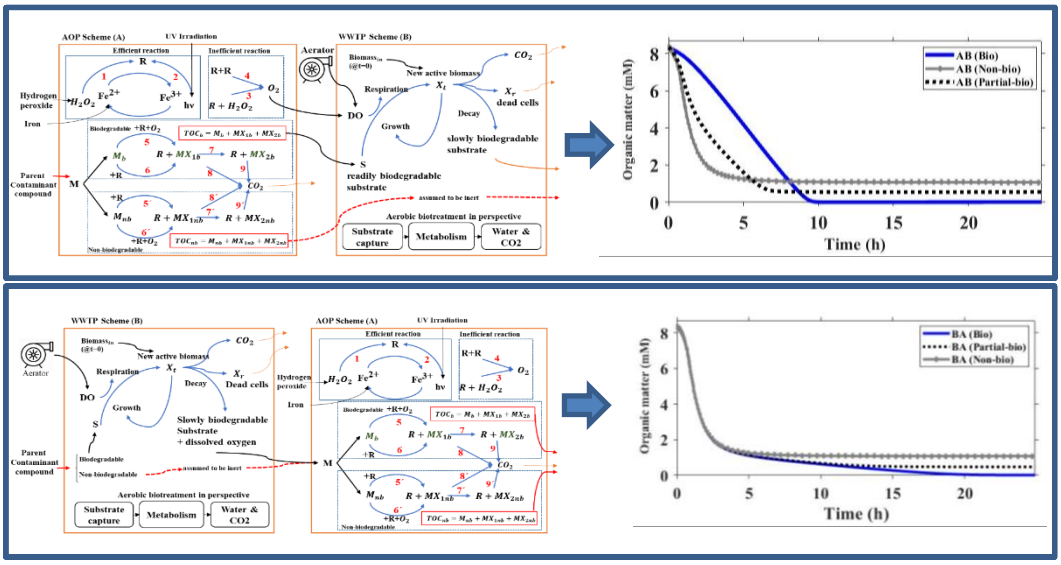

Redrafted from: (Esfahani et al., 2021)

Esfahani, K. N., Pérez-Moya, M., & Graells, M. (2021). A Hybrid Model Coupling Advanced Oxidation Processes (AOP) and Conventional Bio-processes for the Removal of Recalcitrant Contaminants in Wastewaters. In M. Türkay & R. Gani (Eds.), Computer Aided Chemical Engineering (Vol. 50, pp. 883–889). Elsevier. https://doi.org/https://doi.org/10.1016/B978-0-323-88506-5.50137-6

The combined use of Advanced Oxidation Processes (AOP) and conventional bio-processes has been suggested for the efficient treatment of wastewaters with a significant presence of recalcitrant contaminants. However, no models have been proposed to describe such combined processes, which prevents further design and operational optimization. Thus, by combining models previously reported, this work (Chapter 7) contributes a first model integrating AOPs and bio-processes. Mass balances were reformulated by consistently linking the variables used in each model. The model was implemented using Simulink® and it was tested and analyzed using several process configurations (photo-Fenton processes followed by a biological treatment as well as a biological treatment followed by a photo-Fenton process). The outlet concentrations of total organic carbon (TOC) and substrate (S) were monitored for various wastewater compositions, which allowed analysing the performance of the integrated system and suggesting suitable treatment arrangements. Different treatment options were discussed and the capability of the integrated bio/AOP and AOP/bio models was shown to allow a systematic approach to design, operation, and control of integrated wastewater treatment plants in the future. Further research will be oriented to improve the understanding of the potential key parameters as well as their inclusion in the model.

7.1 INTRODUCTION

Wastewaters contain an increasing number of persistent contaminants. Pollutants with high chemical stability and/or low biodegradability (e.g. emerging contaminants: pharmaceuticals, cosmetics, and personal care products) cannot be efficiently addressed by common wastewater treatment processes (WWTP). Conversely, AOPs, in particular, the photo-Fenton process, can oxidize a broad range of non-biodegradable from wastewaters by means of a catalytic reaction of ferrous iron and hydrogen peroxide (H_2O_2) in an acidic or circumneutral pH under UV–VIS radiation yields highly oxidant hydroxyl radicals. However, such chemical oxidation for complete mineralization is much more expensive, which limits large-scale applications.

Hence, combining AOPs with biological treatments has been reported as an opportunity to reduce design and operating costs (Huang et al., 2017; Oller et al., 2011a). Several configurations of hybrid AOPs as pretreatment or post-treatment with

bioremediation for wastewater treatment have been experimentally studied (Nidheesh et al., 2021).

However, the design and operation of such a hybrid process require suitable models. A great deal of mathematical models for WWTP have been developed and reported, while not many works have addressed the modeling of AOPs. Models combining AOPs and bio-processes have hardly been discussed. The modeling needs, and perspectives of AOPs and WWTP are different, as well as it is the nomenclature and the lumped parameters selected to characterize the system. This may explain the divergence of the research efforts of both areas, as well as the problems that converging them to a unique hybrid model entail. Therefore, a first and key step is consistently linking the variables used in both modeling approaches (biological and chemical) in a pilot coupled model.

Consequently, this study consisted on selecting kinetic models for WWTP and AOP, standardizing nomenclature, mapping lumped parameters, and finally extending the models to incorporate those essential aspects considered by only one model. This has been applied to the combination of photo-Fenton processes followed by a biological treatment as well as a biological treatment followed by a photo-Fenton process. Particularly, new equations for non-biodegradable contents in the WWTP needed to be introduced, as well as equations discriminating biodegradable and non-biodegradable matter in the AOP model. Hence, simulation examples are discussed in regard of the expected results, achievements, and limitations of the model.

7.2 METHODOLOGY

The main problem to be addressed is the identification of the significant parameters and reactions in each subsystem and appropriately linking kinetic expressions and material balances in a consistent model of the resulting hybrid system. The integration strategy consists on preparing two configurations: AOPs as a pre-treatment followed by biological treatment (plan AB), also in the opposite direction, considering the post-treatment of AOPs (plan BA). Three case studies will be used to test the model: wastewater with only non-biodegradable contaminants (W1), partially biodegradable wastewater (W2), and completely biodegradable wastewater (W3). The schematic diagram of the proposed approach is illustrated in Figure 7-1.

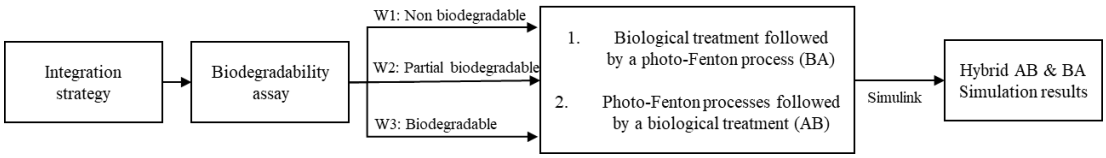

Figure 7-1 Schematic diagram of the proposed integrated modeling

The mathematical models already proposed for the photo-Fenton process and the activated sludge biodegradation (ASM1) were first selected and adapted, and later, the models were coupled by linking of the associated variables. The coupled ordinary differential equations (ODEs) were solved simultaneously concerning the conceptual consistency of the related parameters using Simulink®.

7.2.1 Biological treatment kinetic model

There is abundant literature developing reliable models for WWTPs with formulations fully elaborated and complicated. However, reduced versions are still required for quickly analyzing design trade-offs and layouts, which is the purpose at this stage. Furthermore, in the preliminary steps of developing a model, using simplified models may speed up the model evolution with consistent results and later, the model can be enriched with more complex concepts. Thus, the biological wastewater treatment model selected was the Activated Sludge Model No.1, ASM1, consisting of four non-linear differential equations (Vlad et al., 2011). The mass balance equations were adopted for modeling of the active sludge biomass (X) at the level of the aeration tank, the mass balance of the substrate (S), the mass balance of the oxygen in the water mass (DO), and the balance of the recycled biomass (X_r) at the level of the settling tank. The biomass growth rate (μ), was modeled by the Monod law.

7.2.2 Modeling of the AOP (photo-Fenton process)

Cabrera Reina et al. (2012) proposed and validated a photo-Fenton process model for batch operation and then the model was re-written by Audino et al. (2019) to describe the continuous operation. The model did not consider biodegradability, although it should be taken into account to apply integrated treatment processes including Fenton-based processes and biological treatment (Huang et al., 2017).

Thus, the model by Audino et al. (2019) was adapted by separating the biodegradable (subscripted by b) and non-biodegradable (subscripted by nb) parts of the organic matter to enable biodegradability footprint tracking in the combined model.

To do that, the equations and subsequently related mass balances were replicated for non-biodegradable contents. The proposed model includes the two ferric species, hydrogen peroxide, the radicals formed from peroxide (R), the dissolved oxygen, three states accounting for the biodegradable organic matter (two kinds of partially oxidized organics (MX_{1b} , MX_{2b}) plus the parent compound (M_b) present at the beginning of the reaction) which are responsible for the lumped parameter measured as TOC_b.

Three complementary states for the non-biodegradable organic matter were introduced to the model including two kinds of partially non-bio oxidized organics MX_{1nb} , MX_{2nb}) plus the parent non-bio compound (M_{nb}) present at the beginning of the reaction, aggregated as TOC_{nb} (i.e. $TOC = TOC_b + TOC_{nb}$). The values of the kinetic constants of the new reactions were also replicated at this stage.

7.3 DEVELOPMENT OF THE INTEGRATED MODELS

The two simulation schemes are next presented. The AOP pre-treatment followed by WWTP is designated as AB, while using AOP as a post-treatment is designated as BA.

7.3.1 Combined modeling: configuration AB

The biodegradability of wastewaters can be improved in a combined AOPs system, which is favorable to WWTPs, while WWTPs in the same combined system may stabilize the waste and reduce the use of chemical reagents (Huang et al., 2017). A partial oxidation treatment may produce intermediates even more recalcitrant, but chemically-oxidized intermediates are often less recalcitrant than the parent compound. Many studies have proved that prior chemical oxidation may cause the biodegradability changes of a waste stream (Mantzavinos and Psillakis, 2004). Therefore, the main role of the chemical pre-treatment may be explained as partial oxidation of the biologically persistent part to produce biodegradable reaction intermediates which remove the pointless expense of chemicals and energy (Oller et al., 2011a).

A conceptual challenge for developing a mathematical model for the AB is to find which variables in the AOP model require to be properly linked to which variables in the WWTP model. Moreover, the effect of the chemically-oxidized intermediates from the AOPs on the performance of the WWTP needs to be modeled. In this first

step, these intermediates are considered to have no adverse impact (toxicity or inhibitory effect). In this regard, for the integration of the processes using the set of reported reactions, the outlet biodegradable TOC and the oxygen concentration in the AOP were introduced equally as the inlet substrate content and the dissolved oxygen in the bio-treatment, respectively. The following linking conditions were associated to couple the photo-Fenton and the WWTP models as continuous stirred tanks reactor (CSTR):

• The outlet flowrate from the AOP reactor was directly entered to the WWTP;

• The biodegradable from the AOP was fed as the inlet substrate to the WWTP;

• The oxygen flow from the AOP was connected to dissolved oxygen in the bioreactor;

• The non-biodegradable compounds were assumed to be inert through the WWTP

Figure 7-2 illustrates the configuration of AB.

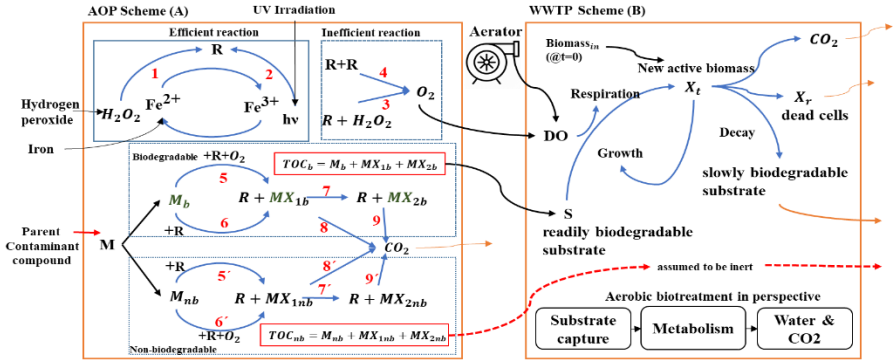

Figure 7-2 AB scheme presenting the photo-Fenton process (A) followed by the bio-treatment(B)

7.3.2 Combined modeling: configuration BA

The alternative post-treatment of AOPs is often suggested for WW containing the recalcitrant organic pollutants with low toxicity concentrations. The transformation products generated during biodegradation would be recalcitrant and even hazardous (Sánchez Peréz et al., 2014; Zimbron and Reardon, 2011). In this study, the combined model represents the biological treatment followed by the photo-Fenton reactor as CSTR using first-order kinetics and mass balances. The same conceptual integration process was applied correspondingly through linking the outlet substrate and the

dissolved oxygen in WWTP to inlet biodegradable TOC and the oxygen content in the AOP model as presented in Figure 7-3.

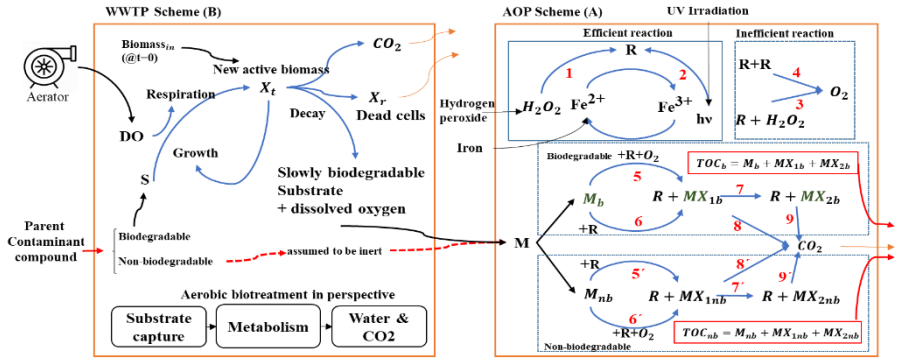

Figure 7-3 BA schematic presenting the bio-treatment(B) followed by the photo-Fenton process(A)

7.4 SIMULATION RESULTS

The preliminary simulations of the outlet organic matter concentration (TOC and/or substrate) in the single-reactor design (A or B) as well as the combined system for both AB and BA configurations were performed according to the data of the kinetic constants provided by Cabrera Reina et al. (2012) and Vlad et al. (2011). The simulation of the hybrid processes indicated promising results compared to each individual process. The integrated model was able to predict and track the biodegradability evolution, which is crucial for the WWTPs. Figure 7-4 shows the results obtained for the three case studies (non-biodegradable wastewater, W1; partially biodegradable wastewater, W2; and biodegradable wastewater, W3) and the four arrangements (A, B, AB, and BA). In general, the simulations produced the expected profiles as for the higher biodegradability, the lower outlet organic matter concentration was predicted. The outcomes of the integrated models produced similar trends and all of them confirm decreasing outlet organic matter concentrations as the inlet biodegradability increases (W1<W2<W3). This is not the case for a single AOP (Figure 7-4a), for which all profiles overlap according to the non-selective oxidizing capacity of the hydroxyl radicals. Figure 7-4(a) also shows a conversion limit given by an insufficient supply of hydrogen peroxide. Conversely, the single WWTP (Figure 7-4(b)) presents the most disparate outcomes: the total organic matter removal for a complete biodegradable input (W3) and no change at all for a totally non-biodegradable feed (W1).

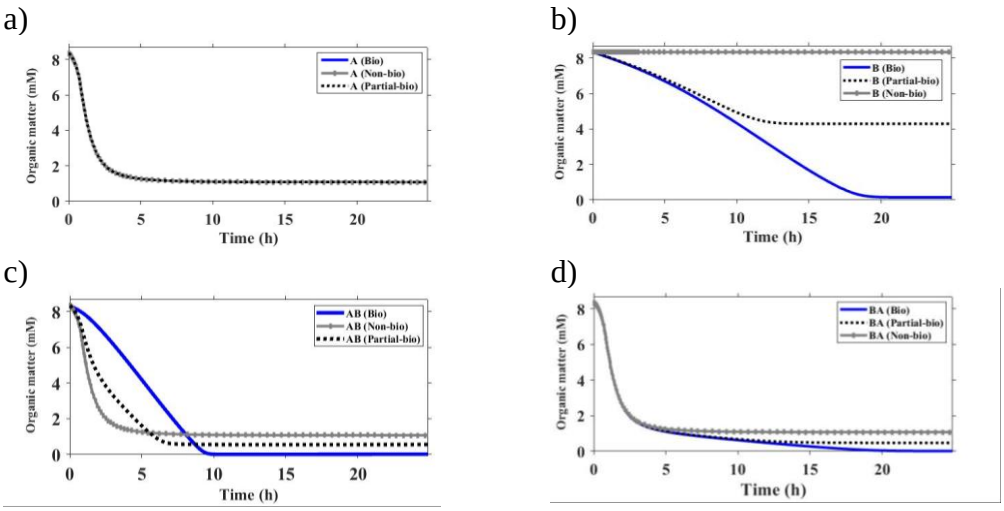

Figure 7-4 Simulated profiles of the single and integrated models for a) A, b) B, c) AB, and d) BA

On the other hand, the combined processes AB (Figure 7-4(c)) and BA (Figure 7-4(d)) resulted in different behavior in the transition period but, they showed the expected higher steady-state performance compared to the single processes A and B. Again, a total conversion for is not attained, this time only for the partially and non-biodegradable cases (W2 and W1) due to the lack of reagents (hydrogen peroxide), which hints at the need to adjust this variable. The different kinetics produce different transient periods in the combined models but show the same long-term behavior given by the biodegradability ratio.

These preliminary simulations of the combined model meet the expectations, but reveal the limitations and next steps, mainly the incorporation of new features allowing to discriminate the behavior of processes as a function of the biodegradability and the chemical nature of the contaminants, so that toxicity and inhibitory effects of recalcitrant species in the bio-treatment can be considered and the true system trade-offs could be addressed for decision-making support.

7.5 CONCLUSIONS

This contribution proposes a combined model coupling the photo-Fenton process and WWTP for the removal of recalcitrant contaminants in wastewaters. The lumped parameter TOC in the photo-Fenton process is considered equivalent to the substrate content in WWTP for the model integration of the processes. Additionally, dissolved oxygen is directly linked to the oxygen content in the photo-Fenton process. The simulations were consistent through all case studies designed including biodegradable, partial biodegradable, and non-biodegradable influent. The simulation

results from different configurations led to the variation curves of the outlet organic matter in the effluent that may be useful to design and control the integrated wastewater treatment systems. The analysis of the model arose some limitations to be addressed, such as the need, to include the inhibitory effect of recalcitrant species in the bio-treatment. Further research needs to be carried out through the proposed model to validate and improve the understanding of the potential key parameters as well as their inclusion in the model.

Chapter 8: Manufacturing and Application of 3D Printed Photo Fenton Reactors for Wastewater Treatment

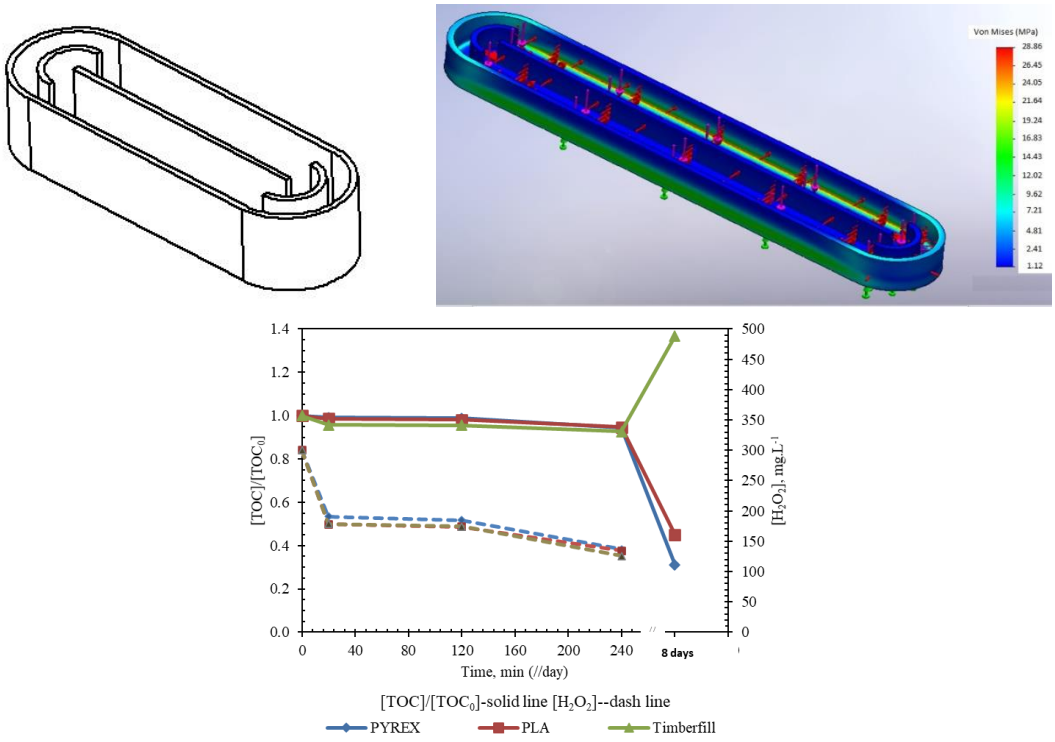

Redrafted from: (Nasr Esfahani et al., 2021)

Nasr Esfahani, K., Zandi, M. D., Travieso-Rodriguez, J. A., Graells, M., & Pérez-Moya, M. (2021). Manufacturing and Application of 3D Printed Photo Fenton Reactors for Wastewater Treatment. International Journal of Environmental Research and Public Health, 18(9), 4885. MDPI AG. Retrieved from http://dx.doi.org/10.3390/ijerph18094885

Additive manufacturing (AM) or 3D printing offers a new paradigm for designing and developing chemical reactors, in particular, prototypes. The use of 3D printers has been increasing, their performance has been improving and their price has been reducing. While the general trend is clear, particular applications need to be assessed for their practicality. This study (Chapter 8) develops and follows a systematic approach to the prototyping of Advanced Oxidation Processes (AOP) reactors. Specifically, this work evaluates and discusses different printable materials in terms of mechanical and chemical resistance to photo-Fenton reactants. Metallic and ceramic materials are shown impracticable due to their high printing cost. Polymeric and composite materials are sieved according to criteria such as biodegradability, chemical, thermal and mechanical resistance. Finally, 3D-printed prototypes are produced and tested in terms of leakage and resistance to the photo-Fenton reacting environment. Polylactic acid (PLA) and wood-PLA composite (Timberfill®) were selected and lab-scale raceway pond reactors (RPR) were printed accordingly. They were next exposed to H_2O_2/Fe(II) solutions at pH=3±0.2 and UV radiation. After 48 h reaction tests, results revealed that the Timberfill® reactor produced higher Total Organic Carbon (TOC) concentrations (9.6 mg.L^{-1}) than that obtained for the PLA reactor (5.5 mg.L^{-1}) and Pyrex® reactor (5.2 mg.L^{-1}), which suggests the interference of Timberfill® with the reaction. The work also considers and discusses further chemical and mechanical criteria that also favor PLA for 3D-printing Fenton and photo-Fenton reactors. Finally, the work also provides a detailed explanation of the printing parameters used and guidelines for preparing prototypes.

8.1 INTRODUCTION

Computer-aided design (CAD) and computer-aided manufacturing (CAM) technologies are today essential for designing and manufacturing functional objects. Additive manufacturing (AM) or 3D printing takes advantage of digitalization to enable crafting unique pieces at a cost and speed comparable to that given by mass production (Ngo et al., 2018). Although still in an early stage, the utilization of AM for producing chemical reactors is emerging as an opportunity to explore new geometries and integrated designs and speed up their validation. 3D printing is an enabling technology that is making increasingly cheaper and faster the shaping of complex reactor prototypes. Such rapid prototyping will shorten the development

process and the testing of inexpensive and more sustainable materials, which ultimately will lead to better processes.

Some works have reviewed the application of AM in chemistry and pharmaceutical, biological, and chemical engineering (Bettermann et al., 2019; Capel et al., 2018; Parra-Cabrera et al., 2018). Most of the recent works on this area report on approaches converging to process intensification via the miniaturization of the equipment and the adoption of continuous processing (continuous flow chemistry (Maier et al., 2018; Okafor et al., 2019), milli-, and micro-fluidics (Ahmadian Yazdi et al., 2016; Bhattacharjee et al., 2016)) and to modularity and on-demand reactionware (Hou et al., 2021; Kitson et al., 2012). 3D printing has also been explored for wastewater treatment processes; most developments reported aim again at process intensification through the design and production of high-surface-area biocarriers that enhance the performance of moving bed biofilm reactors (MBBR) (Elliott et al., 2017; Proano-Pena et al., 2020; Wan et al., 2020).

However, the application of 3D printing and computational modeling (CAD, CAM) for the design and fabrication of chemical reactors for AOPs, in particular photo-Fenton reactors, has been hardly addressed (Desipio et al., 2019; Mousset et al., 2017), and a systematic approach for material selection for 3D printing such reactors is also missing (Ngo et al., 2018).

Fenton-based processes are very successful options in terms of effective pollutant degradation that can be boosted by different ways such as solar light (Irene Carra et al., 2014) or electrochemical process (Nasr Esfahani et al., 2019). The photo-Fenton reaction can be summarized as a catalytic reaction of ferrous iron (Fe^{2+}) reagent with hydrogen peroxide in an acidic or circumneutral pH yielding hydroxyl radicals. The presence of UV–VIS radiation enhances the reaction rate, therefore this process is strongly dependent on iron concentration and irradiance which are important factors in reactor design and process operation (Obra et al., 2016). Iron nanoparticles present higher surface energy than iron salts and they have also been proposed and tested to substitute iron sulfate and reduce the sludge produced in the reactor (Falyouna et al., 2020; Keenan and Sedlak, 2008; Lee et al., 2008). In any case, photoreactor prototyping and subsequent testing are crucial for the modeling and application of the photo-Fenton processes.

Although the application of AM offers significant opportunities in controlling fluid dynamics and optimized reactor geometries, it poses new problems regarding the properties of the materials used for 3D printing, which are often only discussed in the context of mechanical characteristics, and rarely because of their chemical functionality (Parra-Cabrera et al., 2018). Indeed, materials selection for 3D printing needs to be considered according to chemical constraints such as solvent compatibility with the various reagents (Erokhin et al., 2019).

This paper addresses the selection of materials according to different criteria for reactor prototyping and subsequent testing of the chemical suitability of the reactor for carrying out advanced oxidation processes, in particular, photo-Fenton processes, and proposes a systematic approach to the selection procedure.

8.2 MATERIALS AND METHODS

The process proposed for determining a suitable material satisfying both chemical and mechanical requirements is illustrated in Figure 8-1. The diagram shows multiple criteria in several steps.

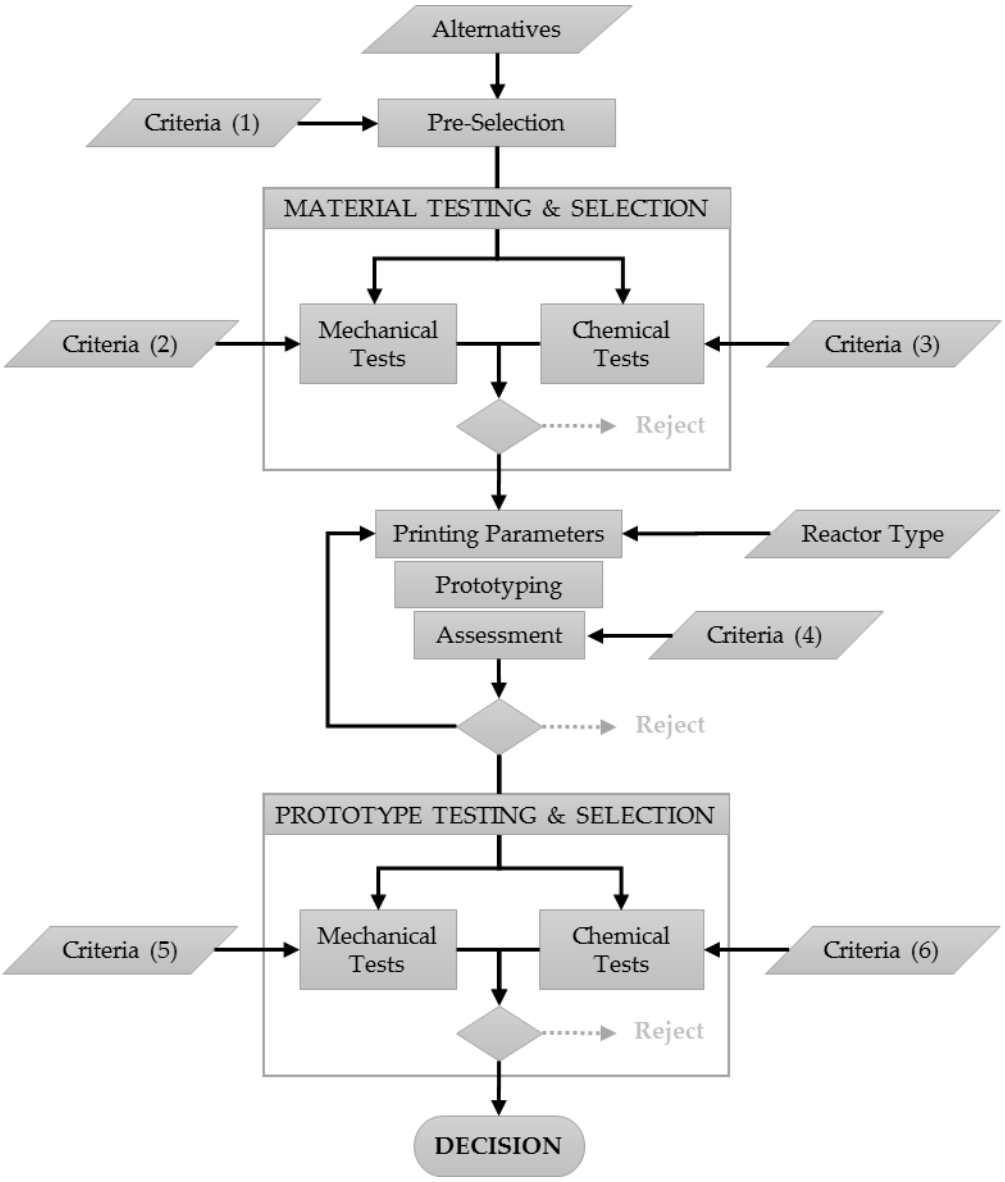

Figure 8-1 Proposed methodology: tests and criteria for preparing 3D-printed photo-Fenton reactors

8.2.1 Materials

The printing filaments used in the reactor manufacture were supplied by the Filamentum company (Czech Republic). Concerning the considerable effect of the material characterization including deformability, safety, printability, and stiffness or bending, the manufacture's material datasheets were considered, and also some tests were performed. Those tests will be described in the following subsections. The printed parts have been manufactured using a Sigma printer by the BCN3D company (Spain) and fused filament fabrication (FFF).

Hydrogen peroxide (H_2O_2) 33% w/v in analytical-grade was supplied from Panreac Química SLU (Barcelona, Spain). Iron sulfate heptahydrate ($FeSO_4\_7H_2O$)

by Sigma-Aldrich (St. Louis, MO, USA) was used as another Fenton reagent. Sulfuric acid H_2SO_4 (95–97%) for adjusting the initial pH and pure caffeine as the contaminant were purchased from Sigma-Aldrich (St. Louis, MO, USA). All solutions were prepared with deionized water having conductivity lower than 1.25 µs provided by Adesco S.A. (Barcelona, Spain). Actinic BL TL-DK 10 W/10 1SL lamp (UVA-UVB) (Barcelona LED, Barcelona, Spain) with the main emission at 254 nm was used as the UV light source.

8.2.2 Lab-scale experiments and analytical procedures

The design of experiments is summarized in three main parts:

I. A set of primary tests with different materials is carried out to determine the chemical behavior of the pieces of the material before and after the printing process. (Criteria #3, section 8.3.2.2 Chemical Tests)

II. Once the reactor prototypes are printed using each of the selected materials, their viability as a Fenton reactor is assessed. Thus, the same reactions are carried out without UV radiation in the reactor prototypes and, parallelly, in a Pyrex® flask used as a blank test. (Criteria #6, section 8.3.4.2 Chemical Tests)

III. Finally, the same assays are repeated for testing the reactor prototypes under the photo-Fenton environment. This time the assays are performed under UV irradiation and with caffeine as a contaminant. Caffeine is selected as a convenient substance for these new assays since, besides its easy availability and manageability, it is considered as an emerging contaminant (mostly due to its high water solubility and low degradability) that has been widely studied in the literature (Gómez et al., 2007; Rodriguez-Gil et al., 2010; Tokumura et al., 2008, 2006). (Criteria #6, section 8.3.4.2 Chemical Tests)

All reagents were added at the beginning of the assays. The temperature was not controlled. Samples were taken every 20.0 min and were refrigerated after extraction to slow down any further degradation of the organic matter.

8.2.3 Procedures and equipment

The concentration of total organic carbon was measured by Shimadzu TOC-VCSH/CSN analyzer, Japan. H_2O_2 concentration was determined through the spectrophotometric method developed by Nogueira and coworkers (Nogueira et al.,

2005). The absorption at 450 nm was detected via a Lambda 365 UV/Vis spectrophotometer (Perkin Elmer, United States).

The thermogravimetric analysis (TGA) of the samples was carried out by TGA Q50 PerkinElmer. For the tensile tests, the universal test machine Microtest has been used equipped with a 25 kN load cell, 50 mm extensometer, Spider and Microtest data acquisition system.

Important tests such as elasticity, tension, and elongation were performed following the ASTM D638-14 standard (ASTM D638-14, 2014).

8.3 RESULTS

8.3.1 Pre-selection of alternative printing materials

A wide range of 3D printing materials with different characteristics are available, whose properties and durability can be altered by the environment set by the photo-Fenton process (Parra-Cabrera et al., 2018).

The most common groups of materials used for 3D printing (Singh et al., 2017) are presented in Table 8-1.

Table 8-1 The most common sorts of materials used for additive manufacturing

Metallic	**Ceramic**	**Polymeric base**
Titanium	Alumina	Nylon
Aluminium	Zircon dioxide	Polycarbonate (PC)
Stainless Steel	Hydroxyapatite	Polyvinyl Alcohol (PVA)
Copper	Titanium oxide	Acrylonitrile Butadiene Styrene (ABS)
Inconel	Tri-calcium phosphate	Polylactic acid (PLA)
Gold/Platinum	Bio-glass	Composite PLA-Wood fibers (Timberfill®)

Ceramic materials have been studied and recommended for applications requiring high corrosion resistance (Gyak et al., 2019). Metals have well-known properties and high mechanical resistance. However, additive manufacturing is complex and expensive for both groups of materials. On the other hand, polymers and polymer-based composites, resist corrosion (to a lesser extent), their mechanical strength is acceptable (enough to tolerate the weight of the liquid inside the reactor), they are much lighter, and their manufacturing cost is much lower. They can be manufactured through both industrial and domestic additive manufacturing techniques, such as Fused Filament Fabrication (FFF). These considerations,

supported by some studies published in the bibliography (Singh et al., 2017), allow a first broad selection, which is shown in Table 8-2.

Table 8-2 Pre-selection of the type of 3D-printing material based on chemical, mechanical, and economic criteria (Criteria #1)

Criteria #1	**Criterion 1.1** **Chemical properties**	**Criterion 1.2** **Mechanical properties**	**Criterion 1.3** **Manufacturing Cost**	**Decision**
Metallic	Passed	Passed	Failed	Rejected
Ceramic	Passed	Passed	Failed	Rejected
Polymeric	Passed	Passed	Passed	Selected
Composite	Passed	Passed	Passed	Selected

Currently, there are many different polymeric and polymeric-based composite mate-rials available on the market that can be easily employed for FFF. Some of the most common are Nylon (Erokhin et al., 2019), Polycarbonate (PC) (Gross et al., 2014), Polyvinyl alcohol (PVA), Acrylonitrile Buta-diene Styrene (ABS), Polylactic acid (PLA), and a variety of composites such as Timber-fill®, a PLA-based material with wood fibers manufactured by Fillamentum Manufacturing Czech s.r.o (Bogdan and Michorczyk, 2020).

While these materials share important features as members of the same class, there are important differences regarding the specific application they are intended for. Hence, they can be preliminarily filtered using general criteria and easily available information (non-standardized data, commercial datasheets (Tang and Alavi, 2011), etc.), which allows avoiding more expensive testing.

Thus, Nylon is a non-biodegradable material, with a very high cost, compared to other filaments, and with low heat resistance. These are the reasons considered to reject it. PC is a thermoplastic polymer. Normally it is a strong and tough material that can be easily worked, molded, and thermoformed (Rohde et al., 2018). The cost is higher than other thermoplastics in the market, which is a serious drawback. PVA can be readily rejected due to its distinctive solubility in water, which is detrimental to its use in aqueous media. Incidentally, PVA is mainly used in FFF to build supporting structures upon which the true piece is printed; once finished PVA can be easily eliminated due to its water solubility (Tang and Alavi, 2011).

On the other hand, ABS, PLA, and Timberfill® can be preliminarily selected since they do not present any of these major drawbacks.

ABS is one of the most widely used thermoplastics. It could be used in many industrial applications such as automotive components. Among its valuable properties, tough-ness and good resistance to high temperatures are remarkable (Fries, 2018). In addition, the price is very competitive compared to most materials available in the market.

PLA is a biodegradable material, obtained from renewable sources such as corn-starch, etc. Thus, it is the most environmentally friendly material among many other 3D printing materials. Its advantages are small thermal contractility, very good mechanical resistance, and low price (Fries, 2018).

An alternate biodegradable material proposed is Timberfill®, which results from PLA combined with wood fibers. Although designed for a purely aesthetic purpose (imi-tating objects with a wood aspect) it is worth to be analyzed due to its reasonable price. Its inconvenient is that its mechanical strength is lower than that of PLA (Zandi et al., 2020b). All this is summarized in Table 8-3:

Table 8-3 Pre-selection of 3D-printing polymeric and composite materials based on economic and operational criteria (Criteria #1)

Criteria#1	**Criterion 1.4** **Cost**	**Criterion 1.5** **Heat resistance**	**Criterion 1.6** **Mechanical Strength**	**Criterion 1.7** **Sustainability**	**Criterion 1.8 Water solubility**	**Decision**
Nylon	Failed	Failed	Passed	Non-biodegradable	Passed	Rejected
PC	Failed	Passed	Passed	Biodegradable	Passed	Rejected
PVA	Failed	Passed	Passed	Biodegradable	Failed	Rejected
ABS	Passed	Passed	Failed	Non-biodegradable	Passed	Selected
PLA	Passed	Passed	Passed	Biodegradable	Passed	Selected
Timberfill®	Passed	Passed	Failed	Biodegradable	Passed	Selected

8.3.2 Material testing and selection

After the pre-selection (screening phase) of ABS, PLA, and Timberfill® as promising materials for 3D printing of Fenton and photo Fenton reactors, the performance of these materials needs to be further examined and compared based on chemical and mechanical criteria before attempting the printing process.

8.3.2.1 Mechanical Tests

The mechanical properties required could be determined using accepted standard measurement and assays, which define the material behavior with respect to its

resistance to load. Large strain plasticity, as observed in various materials, is one of the well-known phenomena requiring combined geometric and material nonlinear analysis of solids (Jiao and Fish, 2017; Xiao et al., 2006). Additionally, each one of these responses may be defined in relation to the loading mode: tension, compression, flexure, shear, or torsion (Ward and Sweeney, 2004), which depends on the way that the component carries out the loads. Regarding the practicability of 3D printing a reactor, static tests such as tensile and flexural tests have been executed on the mentioned materials.

In general, the materials selected for a 3D printing reactor require certain mechanical criteria to be verified. In particular, three mechanical criteria have been considered. In the following sections, the conditions that each evaluated material needs to meet with each of the three criteria considered will be explained.

Criterion 2.1: Printability

To manufacture the reactors, it is necessary to find a material easy to print. This means that the selected materials could be printed without presenting the most common problems that occur in an FFF process, such as Extruder plugging (Mackay et al., 2017), the first layer of material does not stick to the hot base (Prajapati et al., 2018), less or more material extruded during the pro-cess (Bellini et al., 2004), overheating (Peng et al., 2018), wrapping (very common in ABS) (Ajinjeru et al., 2018), uneven printing (Pigeonneau et al., 2020), etc.

Table 8-4 shows a preliminary evaluation according to printable conditions (criterion 2.1), for PLA, Timberfill®, and ABS. The characteristic properties required for this assessment can be extracted from the materials datasheets and do not require performing further assays. The material has been considered to meet this criterion if it does not present any of the problems mentioned in the previous paragraph or if they can be solved otherwise. Hence, not all materials meet this criterion in the same way, as shown in Table 8-4, although none of them can be discarded on this basis.

8.3.2.1.1 Criterion 2.2: Stiffness

Stiffness is another significant aspect to be considered. Stiffness is the extent to which an object resists deformation in response to an applied force (Baumgart, 2000).

Regardless of whether stiffness is closely related to the internal infill of the pieces, the properties of the selected material also have an important influence on it.

The datasheets by the material's manufacturers provide enough information to assess stiffness. To consider that a material meets this criterion, a limit of 53 MPa has been established, which allows discarding ABS on this basis (Table 8-4, Criterion #2.2).

8.3.2.1.2 Criterion 2.3: Heated Bed

The hotbed is the element that is responsible for heating the base of the 3D printer so that the parts remain adhered to during the manufacturing process. This avoids or reduces the effect of wrapping (pieces that detach and bend during the printing process). Not all materials require a hotbed printer to be printed (Prajapati et al., 2018).

Whether a hotbed is required or not can be also extracted from the manufacturer's datasheets, for the three pre-selected materials (Table 8-4, Criterion #2.3). If the hotbed is needed, the material is considered not to meet this criterion, which is the case of ABS.

Table 8-4 Mechanical comparison of PLA, Timberfill®, and ABS based on printability, stiffness, and required heated bed (Criteria #2)

Criteria#2	**Criterion 2.1 Printability**	**Criterion 2.2 Stiffness**	**Criterion 2.3 Heated Bed**	**Decision**
PLA	Passed	Passed	Not Required	Selected
Timberfill®	Passed	Passed	Not Required	Selected
ABS	Passed	Failed	Required	Rejected

Table 8-4 summarizes criteria #2 and the decisions made accordingly. Printability is better in PLA and ABS than Timberfill®. The last one is printed with greater difficulty than the previous ones, but by increasing the extruder diameter and decreasing the layer height (Zandi et al., 2020a), the problem is solved. The stiffness in the case of ABS decreased compared to PLA and Timberfill® (Travieso-Rodriguez et al., 2020). Print using a heated bed is only necessary in the case of ABS. So, the partial conclusion according to criteria #2 is that PLA and Timberfill® are more appropriate materials and ABS can be discarded.

8.3.2.2 Chemical Tests

A wide assortment of polymers resisting high temperatures and chemicals is currently available. Apart from printable metals (composites, powders, alloys) and ceramics, different types of inert polymers have been studied for 3D printing reactors: fluoropolymers (Kotz et al., 2019), Acrylonitrile Butadiene Styrene, ABS (Santos et al., 2010); Polycarbonate, PC; Nylon (Gross et al., 2014); Polypropylene, PP (Rao et al., 2017), Polystyrene, PS (Rossi et al., 2017); and Polylactic Acid, PLA (Neumaier et al., 2019). While the first polymers used in 3D printing had limited chemical and thermal stability, new materials have been introduced with increased performance (Sans, 2020).

Thus, materials commonly used for AM have been tested and ranked accordingly, for instance regarding the effect of prolonged exposure to an aggressive organic solvent such as methylene chloride (Erokhin et al., 2019).

General ideas for material selection and reactor design and development can be found in the literature (Parra-Cabrera et al., 2018). However, to the best knowledge of the authors, no studies address the specific issues of Fenton and photo-Fenton processes.

For the Fenton and photo-Fenton reactions, tests should be designed and performed to assess the chemical stress that the reacting media causes to the vessel holding it. Besides, the thermal stability of the material under heat stress and radiation should be considered.

Thus, three criteria can be envisaged according to the resistance to the Fenton reactants and intermediates (as the high oxidant hydroxyl radicals), the resistance to the irradiation itself causing the Photo-Fenton process, and the resistance to the temperature changes that the reactor may experience.

Since the chemical stress produced by the Photo-Fenton reaction is intrinsically linked to the stress produced by irradiation, both effects will be jointly tested after they are described (criteria 1, 2). Certainly, the irradiation stress could be tested separately from the Fenton reaction to discern the individual effects, but they are simultaneously addressed for the practical purposes of material selection.

8.3.2.2.1 Criterion 3.1: Reaction environment

The presence of the Fenton reactants, the need for acidic media, and the production of highly oxidant species are the conditions that should be specifically considered. Furthermore, since the purpose of Fenton and Photo-Fenton treatments is to remove organic contaminants from water, a reaction media attacking a polymeric reactor not only threatens the consistency of the reactor but also, and more significantly, the quality of the water and its measurement. The measurement of organic matter is commonly performed via a lumped parameter such as TOC (Pignatello et al., 2006), which also poses a detection limit and a practical threshold for the amount of polymeric material that could be detected in a water sample.

According to the literature (Rozas et al., 2010; Yamal-Turbay et al., 2012), a wide range of Fenton reactants ratios (H_2O_2:Fe(II) from 5:1 to 100:1) has been applied for treating different contaminants in wastewaters. Hence, a test has been designed by establishing 300±10 mg·L^{-1} H_2O_2 and 10±0.1 mg·L^{-1} Fe(II), which sets Fenton reagent mass ratio to 30:1. The ratio selected is within the threshold previously commented, the iron concentration is the maximum value allowed in wastewaters in Spain (Audino et al., 2019; DOGC, 2003), and the hydrogen peroxide concentration doubles that used in recent works (Romero et al., 2015). The media, a volume of 500 mL, is also set at the usual reaction pH, 3 ± 0.2.

A sample of each material to be tested is prepared in pieces of 80×10×4 mm (approximately, which corresponds to about 3 gr mass). The selected materials are dipped in the synthetic water prepared for 48 hours, which is considered long enough for a first material screening. The same procedure is carried out for a control sample, which is dipped in distilled water. The initial TOC concentration is measured for all the assays (test and control).

To pass criterion 3.1, TOC concentration after 48 hours should not increase the initial TOC concentration beyond an acceptable measurement limit to discard the hypothesis of a migration of the building material to the reaction environment. This limit is set to 0.23 mg·L^{-1}, according to the precision of the TOC analyzer (Audino et al., 2019). In addition, the aspect of the material should not present any modification at sight.

8.3.2.2.2 Criteria 3.2: UV Resistance

Common synthetic polymers can be attacked by sunlight and the Photo-Fenton process requires the presence of UV-vis light (Pignatello et al., 2006). The literature reports that the presence of UV-vis light (λ≤580nm) allows reducing Fe(III) again into Fe (II), which in turn produces further $HO^{\bullet}$ radicals and results in a cycle continuously supplying $HO^{\bullet}$ until H_2O_2 is depleted. Shorter wavelengths (λ≤310nm) cause hydrogen peroxide photolysis and the direct production of extra $HO^{\bullet}$. Therefore, the oxidation rate of photo-Fenton results much higher than that of the Fenton process.

Thus, materials should be tested under such irradiating conditions. UV light (artificial and solar light) was used and the conditions to pass criterion 2.2 are the same set for criterion 2.1 after 48 hours.

ABS is reported to significantly downgrade (Afshar and Mihut, 2020; Santos et al., 2010) when exposed to UV radiation in an oxygen-rich environment. While this reinforces the rejection of ABS as inappropriate for the Photo-Fenton reaction, it also suggests that the suitability for the Fenton reaction should be further investigated if required. Hence, tests were produced for Timberfill® and PLA and no significant changes in TOC and pH were measured after 48h. The results are summarized in Table 8-5.

8.3.2.2.3 Criterion 3.3: Thermal stability

Thermal degradation is another aspect to be considered (Zhang, 2018). When temperature exceeds the glass transition temperature of the polymer, the materials, as well as their products would become easy to distort, wrinkle or tear, and the mechanical properties would fall sharply (Wu et al., 2016). The exothermic photo-Fenton process under irradiation experiences an increase in temperature; this may cause additional stress.

Positively, higher temperatures could lead to more efficient use of H_2O_2 (amount of TOC removed per amount of H_2O_2 used) since temperature may increase the generation of $HO^{\bullet}$ radicals at low Fe^{2+}concentration. However, increasing the operating temperature as a way of improving the Fenton process has been scarcely investigated because the idea of thermal decomposition of H_2O_2 into O_2 and H_2O, seems to be widely accepted as a serious drawback (Zazo et al., 2011). Therefore, the

common temperature range in Fenton and photo Fenton processes may include between ambient temperature and 45-50 °C (Giwa et al., 2020).

Thermogravimetric analysis (TGA) has proved to be a suitable technique to study the thermal stability of polymeric materials, and it is proposed to assess the thermal stability of candidate materials. The weight of a sample is measured as the temperature changes and the measured changes are associated with decomposition and oxidation reactions as well as physical processes such as sublimation, vaporization, and desorption which provide valuable information on materials selection (Ng et al., 2018).

ABS, discarded by previous criteria, is reported to have low thermal stability (Wojtyła et al., 2017), which supports the decision. For PLA and Timberfill®, assays were made to measure their thermal stability. A criterion is set so that the material should present a maximum thermal decomposition rate at temperatures beyond 300ºC. Results in Figure 8-2 show a maximum thermal decomposition rate for PLA at 421 °C and a couple of peaks for Timberfill®, both beyond 300ºC. The two peaks can be explained by the fact that Timberfill® is a mixture (wood and PLA).

(a)

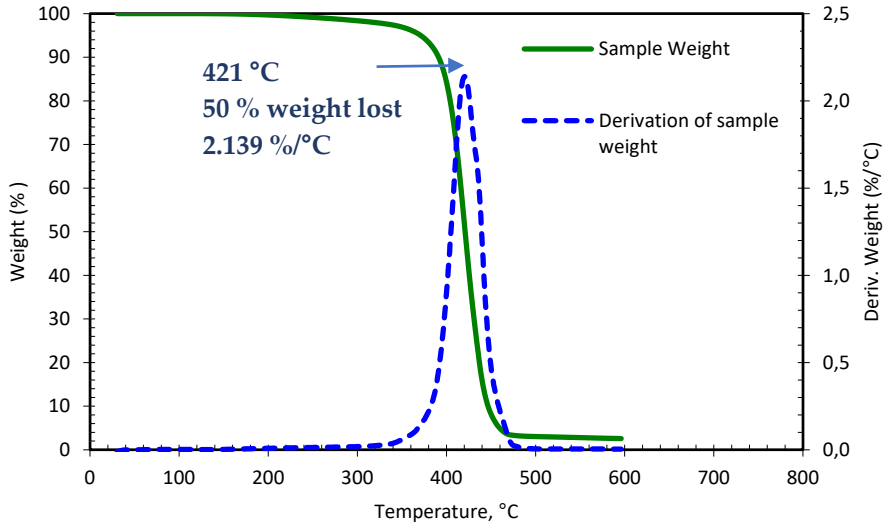

(b)

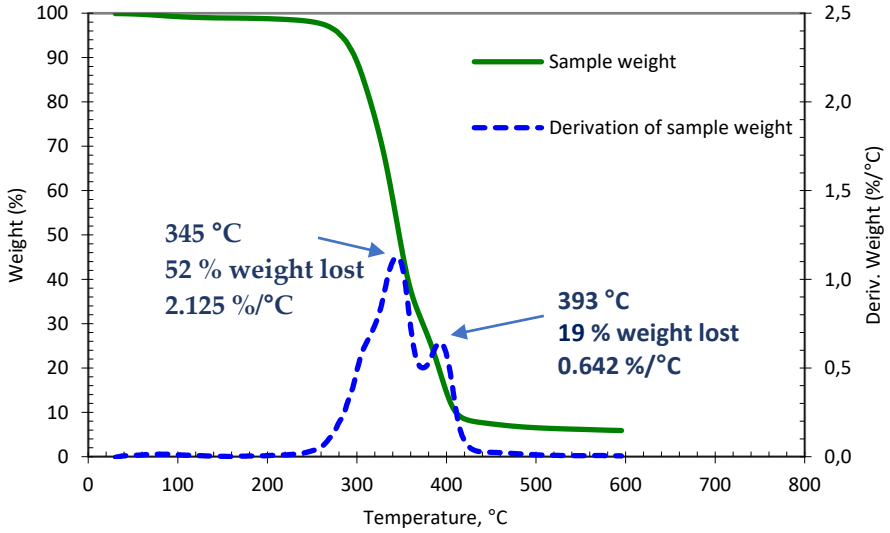

Figure 8-2 Thermogravimetric analysis (TGA) of PLA (a) and Timberfill® (b)

Table 8-5 summarizes the criteria and the decisions derived from them corresponding to the comparison investigation carried out in this section, according to the thermal stability too.

Table 8-5 Chemical comparison of PLA, Timberfill®, and ABS based on chemical and thermal stability (Criteria #2)

Criteria#3	**Criterion 3.1 & 3.2** **Reaction environment & light resistance**	**Criterion 3.3** **Thermal stability**	**Decision**
PLA	Passed	Passed	Selected
Timberfill®	Passed	Passed	Selected
ABS	Failed	---	Rejected

8.3.3 Reactor type, Prototyping, Printing parameters

Selecting the reactor type (geometry, optimization, etc.) is a process out of the scope of this work. Despite general guidelines, deciding on a reactor for Fenton and photo-Fenton processes required a manifold analysis. This work limits solar radiation to present an illustrative, non-exhaustive, comparison of three types of solar reactors Compound Parabolic Collectors (CPCs), Flat Collector Reactors (FPs), and Raceway Pond Reactors (RPR) referred to in the literature. According to Cabrera-Reina and co-workers (Cabrera-Reina et al., 2019), tubular photo reactors designed for efficient photon capture, as CPCs, have been used to treat high-polluted wastewater. Other reactors such as FP and RPR have also been tested and compared in terms of efficiency and cost to treat industrial wastewater by solar photo-Fenton. The re-ported properties and features are summarized in Table 8-6, and RPR is adopted for the next steps as the cost is prioritized as the main issue at this prototyping stage.

Table 8-6 Comparison between different types of reactors (RPR, CPC, and FP) based on cost, efficiency, treatment capacity, and accumulated energy (Criteria #3)

	Cost	**Efficiency (common polluted wastewater)**	**Efficiency (high polluted wastewater)**	**Treatment capacity**	**Accumulated energy**	**Decision**
RPR	Passed	Passed	Passed	Passed	Passed	Selected
CPC	Failed	Passed	Passed	Passed	Passed	Rejected
FP	Failed	Passed	Passed	Passed	Passed	Rejected

8.3.3.1 Prototyping

Hence, the selected materials, PLA and Timberfill®, were used to 3D print lab-scale raceway ponds. According to the literature (Afrose et al., 2016; Cabrera-Reina et al., 2019; Morales-Planas et al., 2018; Zandi et al., 2020a), the capacity of the prototype reactor was fixed at 0.5 L. A height of 51.0 mm was adopted assuming 50 mm for the optical path. The ratio length/width was set to 3, according to previous studies (Morales-Planas et al., 2018; Zandi et al., 2020a) recommending a value in the range 3-6. This led to a length of 250.0 mm and a width of 80.0 mm. Figure 8-3 gives the corresponding scheme.

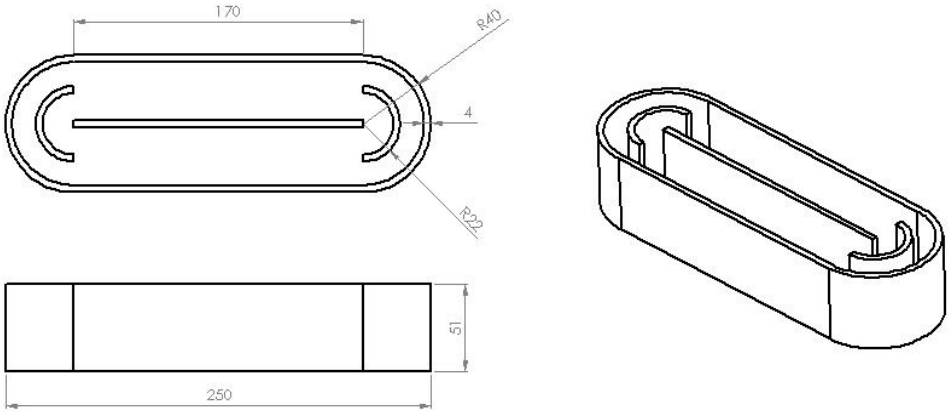

Figure 8-3 Scheme and dimensions (mm) of the Lab-scale RPR

Given the geometry of the reactor (RPR), materials need to be next assessed regarding the load they will bear while operating. This will be assessed by the minimum material thickness tolerating the maximum stress attained at any point of the reactor (Criterion 4.1). Certainly, sophisticated designs with variable thickness can be envisaged, but constant thickness is accepted as a reasonable condition to continue with the process of material selection. Hence, a Flexural test is proposed to evaluate the maximum stress resisted by the (pieces) materials, while the von Mises stress obtained using Finite Element Method (FEM) analysis is proposed to estimate the maximum stress in the reactor. The Flexural test was performed following the ASTM D6272 (ASTM D6272, 2002) standard. Five rectangular samples of each material (PLA and Timberfill®) were printed (Figure 8-4) using a Sigma printer by BCN3D (Barcelona, Spain).

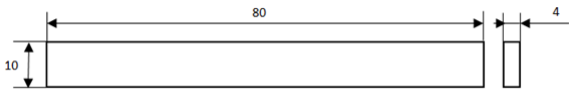

Figure 8-4 Shape and dimensions (mm) of the pieces used in the Flexural test (ASTM D6272)

The universal test machine Microtest has been used equipped with a 25-kN load cell, a 50-mm extensometer, a Spider and a Microtest data acquisition system. The procedure used to measure and analyze the data is the same followed by Zandi et al. (2020a). Hence, the maximum stress determined for Timberfill® is 47.26 ± 0.86 MPa, which is much lower than that determined for PLA (109.50 ± 4.70 MPa).

SolidWorks has been used to run the Finite Element Method (FEM) analysis. Figure 8-5 illustrates a simulation of the von Mises stress under the load given by 0.5L

of water, while the results of the analysis for different thicknesses are given in Table 8-7. Table 8-7 also gives the maximum design stress assuming a 1.5 safety factor applied to the FEM estimated values.

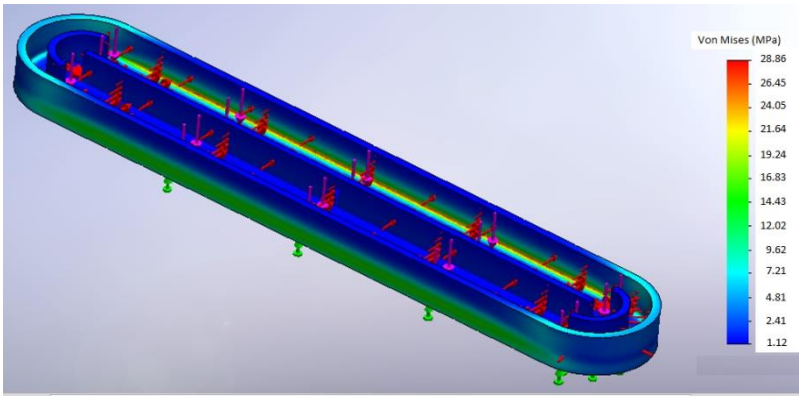

Figure 8-5 von Mises stress obtained from a Finite Element Method (FEM) simulation under a load given by 0.5L of water

Table 8-7 Results of the Finite Element Method (FEM) analysis for different thicknesses (40-50 mm) of PLA and Timberfill®

Thickness (mm)	**σ von-Mises (MPa)**	**Maximum design stress (safety factor 1.5 - MPa)**	**Timberfill® Maximum Stress(MPa)**	**PLA Maximum Stress(MPa)**
40	38.4	57.5		
45	28.9	43.3	47.26 ± 0.86	109.50 ± 4.70
50	22.1	33.1		

Results in Table 8-7 reveal that PLA can bear the prototype maximum stress with any of the studied thicknesses (and probably with much lower values), while Timberfill® requires a minimum thickness (45 mm according to the discrete values studied). Concerning Criterion 4.1, PLA is a better option. However, both materials are selected with a common thickness of 45 mm to continue with the comparative analysis. This is summarized in Table 8-8.

Table 8-8 Comparison between PLA and Timberfill® using maximum stress as a mechanical indicator (Criterion #4)

Criteria #4	**Criterion 4.1 Maximum Stress**	**Decision**
Timberfill®	Passed	Worst option
PLA	Passed	Best option

8.3.3.2 Printing parameters

FFF creates porosities in the printed pieces placed at the interface between the layers, so preventing liquid leakage in FFF printed products is a challenge (Morales-Planas et al., 2018). Usually, tuning these parameters is based on personal experience and know-how, but there is not enough comprehensive information to determine suitable manufacturing parameters (Afrose et al., 2016; Ciurana et al., 2013). Thus, printing parameters were selected from previous experiences of the research group (Travieso-Rodriguez et al., 2019; Zandi et al., 2020a), corresponding with the best mechanical properties. The printed parameters used are shown in Table 8-9.

Table 8-9 Parameters used for 3D-printing the PLA and Timberfill® reactors

Printing parameters			
Parameter	**Value**	**Parameter**	**Value**
Contour width	1.2 mm	Brim	5 mm
Solid upper layers width	1.2 mm	Overlap / contour intersection	15%
Solid lower layers width	1.2 mm	Support material	No
Extra contour	Required	Space between filaments	1.5 mm
Combine filling every	2 layers	Raft (base layer)	No
Flow ratios	1	Speed trips in vacuum	130 mm/s
Extruder parameters			
Retraction length	2 mm	Extra length when reprinting	0 mm
Raise in Z	0 mm	Minimum distance for shrinkage	2 mm
Speed retraction	40 mm/s	Infill Pattern	Honeycomb
Layer height (mm)	0.2	Density (%)	75
Nozzle diameter (mm)	0.6 for PLA, 0.7 for Timberfill®		
Printing velocity (mm/s)	40 for PLA, 30 for Timberfill®		

Finally, the two RPRs produced according to the printing specifications given in Table 8-9 are presented in Figure 8-6.

(a) (b)

Figure 8-6 Image of the 3D-printed Race Pond Reactors (RPRs): PLA (a) and Timberfill® (b)

8.3.4 Prototype testing and selection

8.3.4.1 Mechanical test

Once printed, the raceway ponds reactors, Figure 8-6, need to be finally tested as a vessel aimed at containing a liquid solution. Hence, water tightness is paramount. It is well known that FFF creates porosities in the printed pieces placed at the interface between the layers, so preventing liquid leakage in FFF printed products is a challenge (Morales-Planas et al., 2018). Increasing the nozzle diameter and the layer height are the usual printing strategies to achieve it. This was considered in section 8.3.3.2. when the printing parameters were tuned. Next, the complete structure is put to test.

Thus, the reactors were filled with water. The criterion at this final stage (5.1) is not observing any leakage after 10 days. This lapse of time is deemed convenient as regular use during the following months confirmed the vessel to be tightly sealed.

No leakage was detected during the given time in both printed reactors, which indicates that the selected design and the implementation (printing) parameters suffice to guarantee a reactor with robust cohesion between layers. This result is given in Table 8-10.

Table 8-10 summarizes the comparative assays carried out in this section. According to criteria 5, PLA and timberland resulted in good alternatives under the mechanical assessment section.

Table 8-10 Testing and selection of PLA and Timberfill® concerning leakage (Criterion #5)

Criteria #5	**Criterion 5.1** **Leakage**	**Decision**
Timberfill®	Passed	Selected
PLA	Passed	Selected

8.3.4.2 Chemical test

After assessing the performance as a container, the specific suitability of the different materials to be used as Fenton and Photo-Fenton reactors is next tested and evaluated. While this may be to some extent redundant, the options are definitively confirmed in this final pilot test and compared to a reference reactor. Such suitability was assessed in regard of two criteria:

Criterion 6.1: Reaction viability; the capacity of the reactor to handle both Fenton and photo-Fenton reactions.

Criterion 6.2: Material interference; the capability of the different reactors to significantly interfere with these reactions.

Accordingly, the performance of the 3D printed reactors is examined under conditions comparable to the Fenton and photo Fenton treatment of an organic load. An aqueous caffeine solution (500 mL, 30 ±0.5 mg·L-1) is used, and the following conditions are set: acidic pH (3 ± 0.2), 300 ±10 mg·L-1 H_2O_2, 10 ±0.1 mg·L-1 Fe (II). Experiments are conducted without light (Fenton process) and under UV light (photo-Fenton). The evolution of TOC and H_2O_2 concentrations are monitored along the reaction time.

The same treatment is performed in 500 mL regular Pyrex® Flask, which is intended as a control. Despite the different geometry, the Pyrex® high resistance to chemical attack is assumed to be very informative as a reference.

The results of the different assays with synthetic water (Figure 8-7) readily confirmed that organic matter from the Timberfill® reactor was contaminating the test solution in the long term, from which the interference of the material in the reaction is inferred.

Contrarywise, the same results indicated the promising capability of PLA to be used as a photo-Fenton reactor. The results from the PLA raceway pond were consistent with those obtained from the reference Pyrex® reactor.

(a)

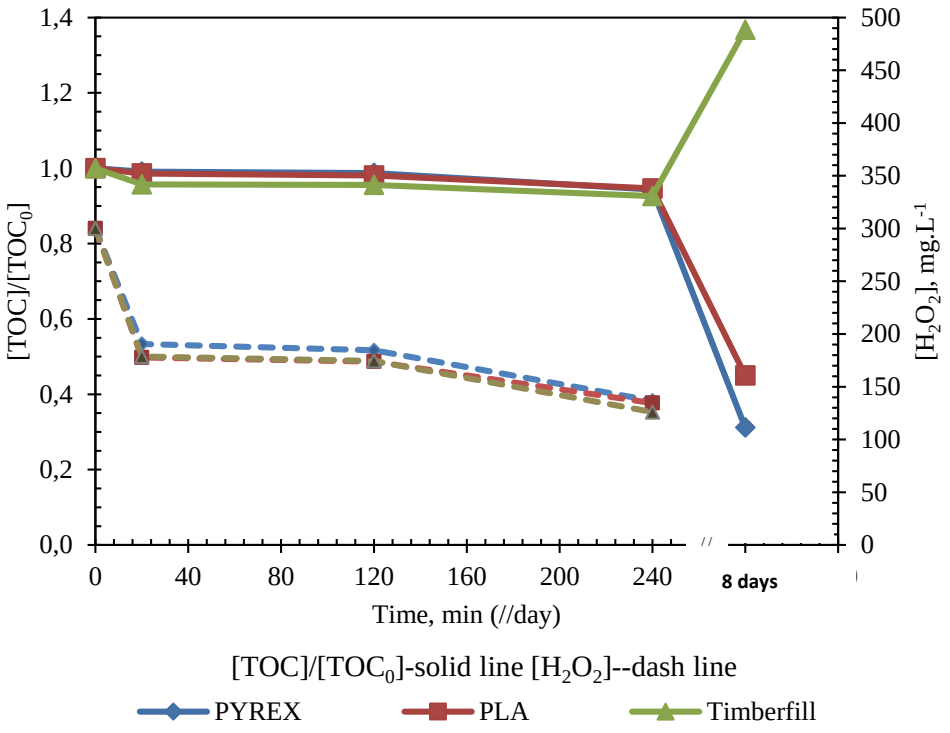

(b)

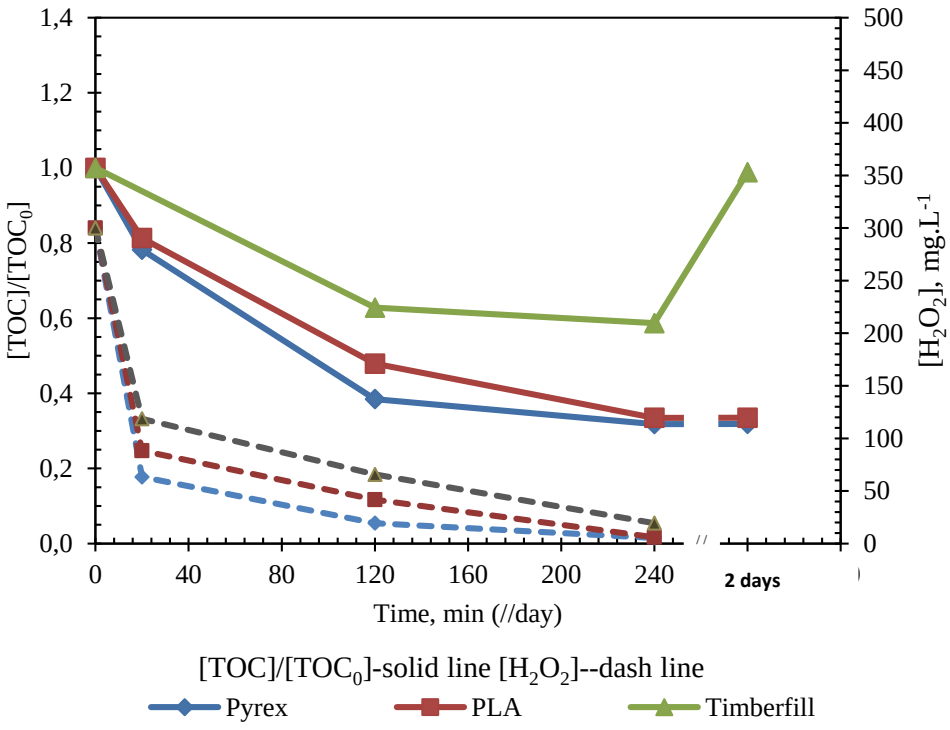

Figure 8-7 Evolution of TOC and H_2O_2 concentration a) without UV b) with UV irradiation: 30 ±0.5 $mg.L^{-1}$ caffeine solutions, TOC_0= 17.2 ± 1 $mg.L^{-1}$ in PLA, Timberfill®, and Pyrex® reactors. Experimental conditions: pH=3 ± 0.2, H_2O_2 =300 ±10 $mg.L^{-1}$.

The experiments were repeated without light and under UV irradiation. These repetitions are consistent and show the parallel response of Fenton and photo-Fenton processes, although the presence of UV light speeds up the oxidation of the organic matter, as expected. In the short term (i.e., 240 min), PLA and Timberfill® perform very similarly without light, although under UV light Timberfill® performs less efficiently than PLA. Thus, both can handle Fenton and photo-Fenton reactions (criterion 6.1), but the lower efficiency of Timberfill® indicates the interference of the material in the reaction and suggests the migration of organic matter from the material to the solution (criterion 6.2). The PLA profile running quite parallel to the Pyrex® profile also supports this idea, which is confirmed in the long term. After 8 days for the Fenton reaction and after only 2 days for the photo-Fenton reaction (faster, as expected) Timberfill® is revealed as completely unsuitable in both cases due to the evident interaction of the material with the processes.

The results for the chemical tests performed with PLA and Timberfill® and the conclusions drawn are provided in Table 8-10Table 8-11, which also shows the final assessment and decision.

Table 8-11 Final material assessment and selection between PLA and Timberfill® (Criteria #6)

Criteria #6	**Criterion 6.1** **Reaction viability**	**Criterion 6.2** **Material interference**	**Decision**
PLA	Passed	Not observed	Selected
Timberfill®	Passed	Observed	Rejected

8.4 CONCLUSIONS

3D printing is an enabling technology that allows producing low-cost reactor prototypes and improve process design and validation in a reduced time. This study focused on 3D printing for the prototyping of Fenton and photo-Fenton reactors and systematically addressed the selection and testing of printing materials, as well as the design parameters to be considered in the printing process. In addition to the methodological approach, this work also contributes specific results regarding the problems detected in the preparation of 3D-printed reactors and their use for photo-Fenton processes.

Although metallic and ceramic materials were included in the analysis they were readily discarded as these options are currently unaffordable. Polymeric and composite materials are presently the only accessible choice. They were assessed and selected applying systematically a set of criteria including biodegradability, and chemical, thermal and mechanical resistance. In the first stage of the procedure, Acrylonitrile Butadiene Styrene (ABS), Polylactic acid (PLA), and Timberfill® were identified as promising materials for prototyping photo-Fenton reactors.

3D printing criteria were next analyzed by preparing reactor prototypes. Race Pond Reactors (RPR) were selected and printed PLA and Timberfill® lab-scale RPRs were tested for their capacity for holding the photo-Fenton reaction. Measurements of Total Organic Carbon (TOC) were produced and compared with those obtained for a standard Pyrex® reactor under similar conditions (artificial UVA light, Fenton reagents, and contaminant).

The results of different assays confirm that no organic matter migrates from the container to the reaction solution when using the PLA reactor. Instead, the Timberfill® container presents such migration, which was shown by TOC levels higher than should be expected. Thus, results confirm the promising capability of PLA to be used as a photo-Fenton reactor.

In addition to the systematic approach to material selection, the work also contributes to the identification of specific problems as leakage. The work addressed the issue accordingly by tuning the printing parameters and reporting the values that produce stronger cohesion between printed layers and ensures the reactor is watertight.

Chapter 9: Final Conclusions and perspectives

This chapter encapsulates the key findings of the thesis and offers an examination of potential enhancements and avenues for further research that may stem from the outcomes of this study.

9.1 CONCLUSIONS

This thesis has successfully addressed its primary objective: enhancing the comprehension of AOPs via the utilization of mathematical modeling. The specific objectives were directed towards overcoming limitations in photo-Fenton processes and understanding the dynamics of ozonation processes. Notably, mathematical models were developed, adapted or reformulated, and validated for the AOPs addressed, particularly Fenton-based systems, like the photo-Fenton process, and ozonation processes. Finally, integrating AOP models, specifically Photo-Fenton, with conventional biological treatments was addressed and the developments discussed. The conclusions drawn from each objective are as follows:

1. Flexible hydrogen peroxide dosage in photo-Fenton processes:

A kinetic model for flexible hydrogen peroxide dosage has been developed, fitted to reported experimental data for the removal of MCs, and successfully validated. Results showed that the variable profiles of the concentrations of TOC, H_2O_2, and O_2, following a flexible dosage scheme were explained and reproduced by the model, with the average errors such as RMSE<0.009 mM for TOC, RMSE<0.42 mM for H_2O_2, and RMSE<0.127 mM for O_2. Furthermore, the formulation and validation of the model for the photo-Fenton process, with a specific focus on accommodating flexible hydrogen peroxide dosages, showcased the potential for the process simulation through tailored dosage strategies.

2. Photo-Fenton processes with iron complexing agents:

$Fe^{3+} - EDDS$ mediated photo-Fenton process (aimed at operating at circumneutral pH) for the removal of sulfamethoxazole (SMX) from water samples

was addressed. For this case, the mechanism by Soriano-Molina et al. (2018), was extended to take into account the capability of $EDDS^{\bullet 3-}$ radicals for oxidizing MCs in the absence of H_2O_2, based on lumping radical species. The kinetic model for this mechanism was implemented, fitted and validated using experimental data obtained in this thesis work. Results showed good agreement with the experimental data that could be predicted properly, with NRMSE for normalized data <0.08 and 0.15 of SMX and $Fe^{3+} - EDDS$, respectively.

The lumped radical's approach and sensitivity analyses enriched the understanding of the complex pathways involved in the process.

3. Ozonation process of water containing organic matter:

A model describing ozone decay in the treatment of secondary effluents has been developed, fitted to experimental data obtained from the ozonation of secondary effluents, and finally validated by the reported data from the literature. The model provides a comprehensive understanding of the dynamics of ozone decay in the presence of organic matter, thanks to the consideration of fast and slow lumped reactions consuming ozone. This allows enhancing the practical monitoring of the ozonation processes and provides good prediction of the experimental data as resulted in well adjustment with low RMSE ≤0.000007 mM for O_3.

4. Integrated processes using AOPs and standard bioprocesses:

An integration strategy mapping variables of both AOPs and conventional bioprocesses has also been developed aimed at developing an integrated model and simulation of both processes. The lumped parameter TOC in the photo-Fenton process is considered equivalent to the substrate content in WWTP and dissolved oxygen is directly linked to the oxygen content in the photo-Fenton process for the model integration of the processes. The consistency of the integrated model has been verified, and alternative processing scenarios have been discussed. Results showed the consistent simulations through all case studies including biodegradable, partial biodegradable, and non-biodegradable influent. This marks a step toward bridging the gap between advanced oxidation and conventional biological treatments, presenting an integration approach to such wastewater treatment processes.

Overall, the conclusions drawn from the mathematical models, experimental validations, and feasibility assessments contribute to the body of knowledge in

wastewater treatment. The specified objectives were effectively addressed, and knowledge and practical strategies and model implementations have been produced. These tools are expected to be useful in further developing advancements in the efficiency and sustainability of wastewater treatment processes through advanced oxidation techniques. The proposed integrated approach in the final objective is a promising step toward developing more comprehensive and effective wastewater treatment strategies. The study also explored the manufacturing and application of 3D printed Photo Fenton reactors, offering insights into their design, fabrication, and performance in comparison to traditional reactor systems.

The research has made substantial contributions to advancing wastewater treatment technologies, overcoming inherent limitations including the photo Fenton reaction settings through the dosage of H_2O_2 and pH adjustment, accurate representation of the ozonation process and exploring innovative integrated approaches.

9.2 LIMITATIONS AND RECOMMENDATIONS FOR FUTURE RESEARCH

- Further exploration of advanced dosage strategies and optimization

Extend further dosage strategies for hydrogen peroxide in photo-Fenton processes, considering variations in concentration and timing. Additionally, explore optimization and control of the photo Fenton model for different wastewater treatment plant configurations. Further analysis when addressing the optimization of the dosage profile and considering the capacity of the model to accurately describe the objective function (e.g., a process economic output). Therefore, the model development is ready to address broaden attempts the model-based optimization of the dosage profile in subsequent investigations.

- Extension of Iron complexing agents in AOPs:

Extend the study of iron complexing agents beyond EDDS covered in this thesis to explore other chelating agents in the photo-Fenton process. Assess their effectiveness in facilitating AOPs at circumneutral pH and expanding the range of contaminants targeted for removal in diverse wastewater matrices. In addition, develop

model for AOPs that can be easily adapted to work with other pollutants or mixtures of pollutants and the semi-empirical approach could be considered for other AOPs.

- Refinement of ozone decay model:

Refine the ozone decay model by considering additional factors influencing the treatment of secondary effluents. Extend the impact of different water matrices and diverse organic matter compositions on the dynamics of ozone decay. Develop the model with extended experimental data considering multi objective function for the parameter estimation focusing on organic matter and target contaminants.

- Further exploration of integrated AOPs and bioprocesses:

Expand the investigation into integrated processes combining AOPs and standard biotreatment processes, exploring the applicability of the developed models to different wastewater influents and variations in biodegradability and toxicity. Validate and improve the understanding of the potential key parameters as well as their inclusion in the integrated model with the influence of operational parameters on the overall treatment efficiency.

- Scale-up studies for 3D printed reactors

Undertake comprehensive scale-up studies for 3D printed photo Fenton reactors to assess their viability in large-scale wastewater treatment operations. Investigate potential challenges and modifications required for practical implementation.

In summary, this thesis has made an effort in the mathematical modeling of AOPs, validated the models through experimental settings, explored the integration of biological and AOPs processes, and investigated the application of 3D printed reactors. Acknowledging the limitations and providing recommendations for future research ensures a pathway for continued advancements in the realm of advanced oxidation processes for wastewater treatment.

References

Afrose, M.F., Masood, S.H., Iovenitti, P., Nikzad, M., Sbarski, I., 2016. Effects of part build orientations on fatigue behaviour of FDM-processed PLA material. Progress in Additive Manufacturing 1, 21–28. https://doi.org/10.1007/s40964-015-0002-3

Afshar, A., Mihut, D., 2020. Enhancing durability of 3D printed polymer structures by metallization. J Mater Sci Technol 53, 185–191. https://doi.org/https://doi.org/10.1016/j.jmst.2020.01.072

Ahmadian Yazdi, A., Popma, A., Wong, W., Nguyen, T., Pan, Y., Xu, J., 2016. 3D printing: an emerging tool for novel microfluidics and lab-on-a-chip applications. Microfluid Nanofluidics 20. https://doi.org/10.1007/s10404-016-1715-4

Ajinjeru, C., Kishore, V., Liu, P., Lindahl, J., Hassen, A.A., Kunc, V., Post, B., Love, L., Duty, C., 2018. Determination of melt processing conditions for high performance amorphous thermoplastics for large format additive manufacturing. Addit Manuf 21, 125–132. https://doi.org/https://doi.org/10.1016/j.addma.2018.03.004

Al Aukidy, M., Verlicchi, P., Jelic, A., Petrovic, M., Barcelò, D., 2012. Monitoring release of pharmaceutical compounds: Occurrence and environmental risk assessment of two WWTP effluents and their receiving bodies in the Po Valley, Italy. Science of The Total Environment 438, 15–25. https://doi.org/https://doi.org/10.1016/j.scitotenv.2012.08.061

Amor, C., Marchão, L., Lucas, M.S., Peres, J.A., 2019. Application of Advanced Oxidation Processes for the Treatment of Recalcitrant Agro-Industrial Wastewater: A Review. Water (Basel) 11. https://doi.org/10.3390/w11020205

Ashauer, R., 2016. Post-ozonation in a municipal wastewater treatment plant improves water quality in the receiving stream. Environ Sci Eur 28, 1. https://doi.org/10.1186/s12302-015-0068-z

Askari, N., Beheshti, M., Mowla, D., Farhadian, M., 2020. Synthesis of CuWO4/Bi2S3 Z-scheme heterojunction with enhanced cephalexin photodegradation. J Photochem Photobiol A Chem 394, 112463. https://doi.org/https://doi.org/10.1016/j.jphotochem.2020.112463

ASTM D638-14, 2014. Standard Test Method for Tensile Properties of Plastics. West Conshohocken, PA. https://doi.org/10.1520/D0638-14

ASTM D6272, 2002. Standard test method for flexural properties of unreinforced and reinforced plastics and electrical insulating materials by four-point bending.

Audenaert, W., Vandevelde, M., Van Hulle, S., Nopens, I., 2023. Influence of Concentration on Parameter Sensitivity of a Mechanistic Ozone Decomposition Model.

Audenaert, W.T.M., Vandevelde, M., Van Hulle, S.W.H., Nopens, I., 2013. Impact of Dissolved Organic Matter (DOM) on Parameter Sensitivity of a Kinetic Ozone Decomposition Model. Ozone Sci Eng 35, 338–349. https://doi.org/10.1080/01919512.2013.797884

Audino, F., Campanyà, G., Pérez-Moya, M., Espuña, A., Graells, M., 2019. Systematic optimization approach for the efficient management of the photo-

Fenton treatment process. Science of The Total Environment 646, 902–913. https://doi.org/https://doi.org/10.1016/j.scitotenv.2018.07.057
Audino, F., Conte, L., Schenone, A., Pérez-Moya, M., Graells, M., Alfano, O.M., 2017. A Kinetic Study for the Fenton and Photo-Fenton Paracetamol Degradation in a Pilot Plant Reactor, in: Espuña, A., Graells, M., Puigjaner, L.B.T.-C.A.C.E. (Eds.), 27 European Symposium on Computer Aided Process Engineering. Elsevier, pp. 301–306. https://doi.org/https://doi.org/10.1016/B978-0-444-63965-3.50052-0
Ayoub, H., Roques-Carmes, T., Potier, O., Koubaissy, B., Pontvianne, S., Lenouvel, A., Guignard, C., Mousset, E., Poirot, H., Toufaily, J., Hamieh, T., 2019. Comparison of the removal of 21 micropollutants at actual concentration from river water using photocatalysis and photo-Fenton. SN Appl Sci 1, 836. https://doi.org/10.1007/s42452-019-0848-y
Bacardit, J., Oller, I., Maldonado, M.I., Chamarro, E., Malato, S., Esplugas, S., 2007. Simple Models for the Control of Photo-Fenton by Monitoring H_2O_2. Journal of Advanced Oxidation Technologies 10, 219–228. https://doi.org/doi:10.1515/jaots-2007-0201
Bacci, F., Campo, P., 2022. Emerging and Less Commonly Recognized Chemical Contaminants: Organic Micropollutants, in: Mehner, T., Tockner, K. (Eds.), Encyclopedia of Inland Waters (Second Edition). Elsevier, Oxford, pp. 247–259. https://doi.org/https://doi.org/10.1016/B978-0-12-819166-8.00038-4
Baumgart, E., 2000. Stiffness - An unknown world of mechanical science? Injury 31 Suppl 2, S-B14.
Behrouzeh, M., Mehdi Parivazh, M., Danesh, E., Javad Dianat, M., Abbasi, M., Osfouri, S., Rostami, A., Sillanpää, M., Dibaj, M., Akrami, M., 2022. Application of Photo-Fenton, Electro-Fenton, and Photo-Electro-Fenton processes for the treatment of DMSO and DMAC wastewaters. Arabian Journal of Chemistry 15, 104229. https://doi.org/https://doi.org/10.1016/j.arabjc.2022.104229
Bellini, A., Güçeri, S., Bertoldi, M., 2004. Liquefier Dynamics in Fused Deposition. Journal of Manufacturing Science and Engineering-transactions of The Asme - J MANUF SCI ENG 126. https://doi.org/10.1115/1.1688377
Beltrán, F., 2004. Ozone Reaction Kinetics for Water and Wastewater System. https://doi.org/10.1201/9780203509173
Beltrán, F.J., Checa, M., Rivas, J., García-Araya, J.F., 2020. Modeling the Mineralization Kinetics of Visible Led Graphene Oxide/Titania Photocatalytic Ozonation of an Urban Wastewater Containing Pharmaceutical Compounds. Catalysts 10. https://doi.org/10.3390/catal10111256
Bettermann, S., Kandelhard, F., Moritz, H.-U., Pauer, W., 2019. Digital and lean development method for 3D-printed reactors based on CAD modeling and CFD simulation. Chemical Engineering Research and Design 152, 71–84. https://doi.org/https://doi.org/10.1016/j.cherd.2019.09.024
Bhattacharjee, N., Urrios, A., Kang, S., Folch, A., 2016. The upcoming 3D-printing revolution in microfluidics. Lab Chip 16. https://doi.org/10.1039/C6LC00163G
Bilińska, L., Żyłła, R., Smółka, K., Gmurek, M., Ledakowicz, S., 2017. Modeling of Ozonation of Reactive Black 5 Through a Kinetic Approach. Fibres Text. East. Eur. 25, 54–60. https://doi.org/10.5604/01.3001.0010.4628
Bliek, L., Guijt, A., Karlsson, R., Verwer, S., de Weerdt, M., 2023. Benchmarking surrogate-based optimisation algorithms on expensive black-box functions.

Appl Soft Comput 147, 110744. https://doi.org/https://doi.org/10.1016/j.asoc.2023.110744
Bogdan, E., Michorczyk, P., 2020. 3D Printing in Heterogeneous Catalysis—The State of the Art. Materials 13. https://doi.org/10.3390/ma13204534
Brink, A., Sheridan, C., Harding, K., 2018. Combined biological and advance oxidation processes for paper and pulp effluent treatment. S Afr J Chem Eng 25, 116–122. https://doi.org/https://doi.org/10.1016/j.sajce.2018.04.002
Bueno, M.J.M., Gomez, M.J., Herrera, S., Hernando, M.D., Agüera, A., Fernández-Alba, A.R., 2012. Occurrence and persistence of organic emerging contaminants and priority pollutants in five sewage treatment plants of Spain: Two years pilot survey monitoring. Environmental Pollution 164, 267–273. https://doi.org/https://doi.org/10.1016/j.envpol.2012.01.038
Buffle, M.-O., Schumacher, J., Salhi, E., Jekel, M., von Gunten, U., 2006. Measurement of the initial phase of ozone decomposition in water and wastewater by means of a continuous quench-flow system: Application to disinfection and pharmaceutical oxidation. Water Res 40, 1884–1894. https://doi.org/https://doi.org/10.1016/j.watres.2006.02.026
Bustillo-Lecompte, C.F., Mehrvar, M., 2016. Treatment of an actual slaughterhouse wastewater by integration of biological and advanced oxidation processes: Modeling, optimization, and cost-effectiveness analysis. J Environ Manage 182, 651–666. https://doi.org/https://doi.org/10.1016/j.jenvman.2016.07.044
Cabrera Reina, A., Casas López, J.L., Maldonado Rubio, M.I., Santos-Juanes Jordá, L., García Sánchez, J.L., Sánchez Pérez, J.A., 2014. Effects of environmental variables on the photo-Fenton plant design. Chemical Engineering Journal 237, 469–477. https://doi.org/https://doi.org/10.1016/j.cej.2013.10.046
Cabrera Reina, A., Santos-Juanes Jordá, L., García Sánchez, J.L., Casas López, J.L., Sánchez Pérez, J.A., 2012. Modelling photo-Fenton process for organic matter mineralization, hydrogen peroxide consumption and dissolved oxygen evolution. Appl Catal B 119–120, 132–138. https://doi.org/https://doi.org/10.1016/j.apcatb.2012.02.021
Cabrera Reina, A., Santos-Juanes, L., García Sánchez, J.L., Casas López, J.L., Maldonado Rubio, M.I., Li Puma, G., Sánchez Pérez, J.A., 2015. Modelling the photo-Fenton oxidation of the pharmaceutical paracetamol in water including the effect of photon absorption (VRPA). Appl Catal B 166–167, 295–301. https://doi.org/https://doi.org/10.1016/j.apcatb.2014.11.023
Cabrera-Reina, A., Miralles-Cuevas, S., Rivas, G., Sánchez Pérez, J.A., 2019. Comparison of different detoxification pilot plants for the treatment of industrial wastewater by solar photo-Fenton: Are raceway pond reactors a feasible option? Science of The Total Environment 648, 601–608. https://doi.org/https://doi.org/10.1016/j.scitotenv.2018.08.143
Cabrera-Reina, A., Miralles-Cuevas, S., Sánchez Pérez, J.A., Salazar, R., 2021. Application of solar photo-Fenton in raceway pond reactors: A review. Science of The Total Environment 800, 149653. https://doi.org/https://doi.org/10.1016/j.scitotenv.2021.149653
Căilean, D., Ungureanu, F., Teodosiu, C., 2015. Homogeneous Sono-Fenton Process: Statistical Modeling and Global Sensitivity Analysis. International Journal of Nonlinear Sciences and Numerical Simulation 16, 11–21. https://doi.org/doi:10.1515/ijnsns-2014-0051

Campolongo, F., Cariboni, J., Saltelli, A., 2007. An effective screening design for sensitivity analysis of large models. Environmental Modelling & Software 22, 1509–1518. https://doi.org/https://doi.org/10.1016/j.envsoft.2006.10.004
Capel, A.J., Rimington, R.P., Lewis, M.P., Christie, S.D.R., 2018. 3D printing for chemical, pharmaceutical and biological applications. Nat Rev Chem 2, 422–436. https://doi.org/10.1038/s41570-018-0058-y
Carra, I, Malato, S., Jiménez, M., Maldonado, M.I., Sánchez Pérez, J.A., 2014. Microcontaminant removal by solar photo-Fenton at natural pH run with sequential and continuous iron additions. Chemical Engineering Journal 235, 132–140. https://doi.org/https://doi.org/10.1016/j.cej.2013.09.029
Carra, Irene, Santos-Juanes, L., Acien, G., Malato, S., Sánchez Pérez, J.A., 2014. New approach to solar photo-Fenton operation. Raceway ponds as tertiary treatment technology. J Hazard Mater 279, 322–329. https://doi.org/10.1016/j.jhazmat.2014.07.010
Castillo, E., Hadi, A.S., Conejo, A., Fernández-Canteli, A., 2004. A General Method for Local Sensitivity Analysis With Application to Regression Models and Other Optimization Problems. Technometrics 46, 430–444. https://doi.org/10.1198/004017004000000509
Cavalheri, P.S., Machado, B.S., da Silva, T.F., Rodrigues, J.P.B.G., Gozzi, F., Filho, F.J.C.M., Cavalcante, R.P., de Oliveira, S.C., Junior, A.M., 2023. Optimization of a combined system of vertical flow constructed wetland and solar photo-Fenton for ketoprofen removal in sewage and landfill leachate. Chemical Engineering Journal 475, 146282. https://doi.org/https://doi.org/10.1016/j.cej.2023.146282
Chavoshani, A., Hashemi, M., Mehdi Amin, M., Ameta, S.C., 2020. Chapter 1 - Introduction, in: Chavoshani, A., Hashemi, M., Mehdi Amin, M., Ameta, S.C.B.T.-M. and C. (Eds.), . Elsevier, pp. 1–33. https://doi.org/https://doi.org/10.1016/B978-0-12-818612-1.00001-5
Chen, Y., Duan, X., Zhou, X., Wang, R., Wang, S., Ren, N., Ho, S.-H., 2021. Advanced oxidation processes for water disinfection: Features, mechanisms and prospects. Chemical Engineering Journal 409, 128207. https://doi.org/https://doi.org/10.1016/j.cej.2020.128207
Cheng, M., Zeng, G., Huang, D., Lai, C., Xu, P., Zhang, C., Liu, Y., 2016. Hydroxyl radicals based advanced oxidation processes (AOPs) for remediation of soils contaminated with organic compounds: A review. Chemical Engineering Journal 284, 582–598. https://doi.org/https://doi.org/10.1016/j.cej.2015.09.001
Chys, M., Audenaert, W.T.M., Deniere, E., Mortier, S.T.F.C., Van Langenhove, H., Nopens, I., Demeestere, K., Van Hulle, S.W.H., 2017. Surrogate-Based Correlation Models in View of Real-Time Control of Ozonation of Secondary Treated Municipal Wastewater—Model Development and Dynamic Validation. Environ Sci Technol 51, 14233–14243. https://doi.org/10.1021/acs.est.7b04905
Chys, M., Audenaert, W.T.M., Vangrinsven, J., Bauwens, M., Mortier, S.T.F.C., Van Langenhove, H., Nopens, I., Demeestere, K., Van Hulle, S.W.H., 2018. Dynamic validation of online applied and surrogate-based models for tertiary ozonation on pilot-scale. Chemosphere 196, 494–501. https://doi.org/https://doi.org/10.1016/j.chemosphere.2017.12.168
Ciurana, J., Serenóa, L., Vallès, È., 2013. Selecting Process Parameters in RepRap Additive Manufacturing System for PLA Scaffolds Manufacture. Procedia CIRP 5, 152–157. https://doi.org/https://doi.org/10.1016/j.procir.2013.01.031

Çokay, E., Eker, S., 2022. Pesticide Industry Wastewater Treatment with Photo-Fenton Process. Environmental Sciences Proceedings 18. https://doi.org/10.3390/environsciproc2022018015
Cruz-Alcalde, A., Esplugas, S., Sans, C., 2019. Abatement of ozone-recalcitrant micropollutants during municipal wastewater ozonation: Kinetic modelling and surrogate-based control strategies. Chemical Engineering Journal 360, 1092–1100. https://doi.org/https://doi.org/10.1016/j.cej.2018.10.206
Cunha, D.L., da Silva, A.S.A., Coutinho, R., Marques, M., 2022. Optimization of Ozonation Process to Remove Psychoactive Drugs from Two Municipal Wastewater Treatment Plants. Water Air Soil Pollut 233, 67. https://doi.org/10.1007/s11270-022-05541-9
Dattner, I., 2015. A model-based initial guess for estimating parameters in systems of ordinary differential equations. Biometrics 71, 1176–1184. https://doi.org/10.1111/biom.12348
Dębowski, M., Kazimierowicz, J., Zieliński, M., 2022. Advanced Oxidation Processes to Reduce Odor Emissions from Municipal Wastewater—Comprehensive Studies and Technological Concepts. Atmosphere (Basel) 13. https://doi.org/10.3390/atmos13101724
Desipio, M.M., Van Bramer, S.E., Thorpe, R., Saha, D., 2019. Photocatalytic and photo-fenton activity of iron oxide-doped carbon nitride in 3D printed and LED driven photon concentrator. J Hazard Mater 376, 178–187. https://doi.org/https://doi.org/10.1016/j.jhazmat.2019.05.037
Dogan, E.C., Kilicoglu, O., Narci, A.O., Mert, B.K., Durna, E., Akbacak, U.A., Aydiner, C., 2021. Fenton and photo-Fenton processes integrated with submerged ultrafiltration for the treatment of pulp and paper industry wastewater. J Environ Chem Eng 9, 105878. https://doi.org/https://doi.org/10.1016/j.jece.2021.105878
DOGC, 2003. Reglament dels serveis públics de sanejament. Diari Oficial de la Generalitat de Catalunya 11143–11158.
Dong, W., Jin, Y., Zhou, K., Sun, S.-P., Li, Y., Chen, X.D., 2019. Efficient degradation of pharmaceutical micropollutants in water and wastewater by FeIII-NTA-catalyzed neutral photo-Fenton process. Science of The Total Environment 688, 513–520. https://doi.org/https://doi.org/10.1016/j.scitotenv.2019.06.315
Echevarría, C., Valderrama, C., Cortina, J.L., Martín, I., Arnaldos, M., Bernat, X., De la Cal, A., Boleda, M.R., Vega, A., Teuler, A., Castellví, E., 2020. Hybrid sorption and pressure-driven membrane technologies for organic micropollutants removal in advanced water reclamation: A techno-economic assessment. J Clean Prod 273, 123108. https://doi.org/https://doi.org/10.1016/j.jclepro.2020.123108
Echevarría, C., Valderrama, C., Cortina, J.L., Martín, I., Arnaldos, M., Bernat, X., De la Cal, A., Boleda, M.R., Vega, A., Teuler, A., Castellví, E., 2019. Techno-economic evaluation and comparison of PAC-MBR and ozonation-UV revamping for organic micro-pollutants removal from urban reclaimed wastewater. Science of The Total Environment 671, 288–298. https://doi.org/https://doi.org/10.1016/j.scitotenv.2019.03.365
Elliott, O., Gray, S., McClay, M., Nassief, B., Nunnelley, A., Vogt, E., Ekong, J., Kardel, K., Khoshkhoo, A., Proaño, G., Blersch, D.M., Carrano, A.L., 2017. Design and Manufacturing of High Surface Area 3D-Printed Media for Moving

Bed Bioreactors for Wastewater Treatment. J Contemp Water Res Educ 160, 144–156. https://doi.org/https://doi.org/10.1111/j.1936-704X.2017.03246.x
Erokhin, K.S., Gordeev, E.G., Ananikov, V.P., 2019. Revealing interactions of layered polymeric materials at solid-liquid interface for building solvent compatibility charts for 3D printing applications. Sci Rep 9, 20177. https://doi.org/10.1038/s41598-019-56350-w
Esfahani, K.N., Pérez-Moya, M., Graells, M., 2021. A Hybrid Model Coupling Advanced Oxidation Processes (AOP) and Conventional Bio-processes for the Removal of Recalcitrant Contaminants in Wastewaters, in: Türkay, M., Gani, R. (Eds.), Computer Aided Chemical Engineering. Elsevier, pp. 883–889. https://doi.org/https://doi.org/10.1016/B978-0-323-88506-5.50137-6
Esfahani, K.N., Pérez-Moya, M., Graells, M., Miralles-Cuevas, S., Cabrera-Reina, A., 2023. Mechanistic modelling of Fe^{3+}-EDDS mediated photo-Fenton revisited: lumped radicals and sensitivity analysis. Chemical Engineering Journal 142559. https://doi.org/https://doi.org/10.1016/j.cej.2023.142559
Fallah, N., Bloise, E., Santoro, D., Mele, G., 2023. State of Art and Perspectives in Catalytic Ozonation for Removal of Organic Pollutants in Water: Influence of Process and Operational Parameters. Catalysts. https://doi.org/10.3390/catal13020324
Falyouna, O., Maamoun, I., Bensaida, K., Sugihara, Y., Eljamal, O., 2020. Removal of Ciprofloxacin from Aqueous Solutions by Nanoscale Zerovalent Iron-Based Materials: A Mini Review, in: Proceedings of International Exchange and Innovation Conference on Engineering & Sciences (IEICES). https://doi.org/10.5109/4102485
Farias, J., Albizzati, E.D., Alfano, O.M., 2009. Kinetic study of the photo-Fenton degradation of formic acid: Combined effects of temperature and iron concentration. Catal Today 144, 117–123. https://doi.org/https://doi.org/10.1016/j.cattod.2008.12.027
Farooq, S., Ahmed, M., 1989. Modeling of an ozone-wastewater system's kinetics. Water Res 23, 809–815. https://doi.org/https://doi.org/10.1016/0043-1354(89)90003-1
Fernández-López, C., González García, M., Sánchez-Lozano, J.M., 2021. Analysis of WWTPs technologies based on the removal efficiency of Pharmaceutical Activated Compounds for water reuse purposes. A Fuzzy Multi-Criteria Decision Making approach. Journal of Water Process Engineering 42, 102098. https://doi.org/https://doi.org/10.1016/j.jwpe.2021.102098
Fries, J., 2018. RECYCLING OF USED FILAMENT FROM 3D PRINTING. https://doi.org/10.5593/sgem2018/4.2/S18.020
Gamarra-Güere, C.D., Dionisio, D., Santos, G.O.S., Vasconcelos Lanza, M.R., de Jesus Motheo, A., 2022. Application of Fenton, photo-Fenton and electro-Fenton processes for the methylparaben degradation: A comparative study. J Environ Chem Eng 10, 106992. https://doi.org/https://doi.org/10.1016/j.jece.2021.106992
Ganiyu, S.O., Nidheesh, P.V., Oturan, M.A., 2022. Chapter 23 - Synthesis and application of nanostructured iron oxides heterogeneous catalysts for environmental applications, in: Giannakoudakis, D., Meili, L., Anastopoulos, I. (Eds.), Advanced Materials for Sustainable Environmental Remediation. Elsevier, pp. 583–608. https://doi.org/https://doi.org/10.1016/B978-0-323-90485-8.00014-X

Gardoni, D., Vailati, A., Canziani, R., 2012. Decay of Ozone in Water: A Review. Ozone Sci. Eng. 34, 233–242. https://doi.org/10.1080/01919512.2012.686354
Gernaey, K. V, van Loosdrecht, M.C.M., Henze, M., Lind, M., Jørgensen, S.B., 2004. Activated sludge wastewater treatment plant modelling and simulation: state of the art. Environmental Modelling & Software 19, 763–783. https://doi.org/https://doi.org/10.1016/j.envsoft.2003.03.005
Giwa, A.-R.A., Bello, I.A., Olabintan, A.B., Bello, O.S., Saleh, T.A., 2020. Kinetic and thermodynamic studies of fenton oxidative decolorization of methylene blue. Heliyon 6, e04454. https://doi.org/https://doi.org/10.1016/j.heliyon.2020.e04454
Gómez, M.J., Martínez Bueno, M.J., Lacorte, S., Fernández-Alba, A.R., Agüera, A., 2007. Pilot survey monitoring pharmaceuticals and related compounds in a sewage treatment plant located on the Mediterranean coast. Chemosphere 66, 993–1002. https://doi.org/https://doi.org/10.1016/j.chemosphere.2006.07.051
Gomis, J., Carlos, L., Prevot, A.B., Teixeira, A.C.S.C., Mora, M., Amat, A.M., Vicente, R., Arques, A., 2015. Bio-based substances from urban waste as auxiliaries for solar photo-Fenton treatment under mild conditions: Optimization of operational variables. Catal Today 240, 39–45. https://doi.org/https://doi.org/10.1016/j.cattod.2014.03.034
Gordon, G., 1995. The chemistry and reactions of ozone in our environment. Progress in Nuclear Energy 29, 89–96. https://doi.org/https://doi.org/10.1016/0149-1970(95)00031-E
Gross, B.C., Erkal, J.L., Lockwood, S.Y., Chen, C., Spence, D.M., 2014. Evaluation of 3D Printing and Its Potential Impact on Biotechnology and the Chemical Sciences. Anal Chem 86, 3240–3253. https://doi.org/10.1021/ac403397r
Guadalupe Pinna-Hernández, M., Casas López, J.L., Esteban García, A.B., Zurano, A.S., Fernández Sevilla, J.M., 2023. Experimental study of wastewater micropollutant removal by solar photo-Fenton using a virtual lab. Computer Applications in Engineering Education n/a, e22699. https://doi.org/https://doi.org/10.1002/cae.22699
Gualda-Alonso, E., Rodríguez-García, D., Soriano-Molina, P., Guzmán, J.L., García Sánchez, J.L., Casas López, J.L., Sánchez Pérez, J.A., 2023. FentonSims®: A novel interactive simulation tool for computational kinetics of microcontaminant removal by the solar photo-Fenton process. Chemical Engineering Journal 468, 143791. https://doi.org/https://doi.org/10.1016/j.cej.2023.143791
Gualda-Alonso, E., Soriano-Molina, P., Casas López, J.L., García Sánchez, J.L., Plaza-Bolaños, P., Agüera, A., Sánchez Pérez, J.A., 2022a. Large-scale raceway pond reactor for CEC removal from municipal WWTP effluents by solar photo-Fenton. Appl Catal B 319, 121908. https://doi.org/https://doi.org/10.1016/j.apcatb.2022.121908
Gualda-Alonso, E., Soriano-Molina, P., García Sánchez, J.L., Casas López, J.L., Sánchez Pérez, J.A., 2022b. Mechanistic modeling of solar photo-Fenton with Fe^{3+}-NTA for microcontaminant removal. Appl Catal B 318, 121795. https://doi.org/https://doi.org/10.1016/j.apcatb.2022.121795
Guergachi, A., Patry, G., 2003. Identification, verification and validation of process models in wastewater engineering: A critical review. Journal of Hydroinformatics 5. https://doi.org/10.2166/hydro.2003.0014

Gulde, R., Rutsch, M., Clerc, B., Schollée, J.E., von Gunten, U., McArdell, C.S., 2021. Formation of transformation products during ozonation of secondary wastewater effluent and their fate in post-treatment: From laboratory- to full-scale. Water Res 200, 117200. https://doi.org/https://doi.org/10.1016/j.watres.2021.117200

Gulkaya, İ., Surucu, G.A., Dilek, F.B., 2006. Importance of H_2O_2/Fe^{2+} ratio in Fenton's treatment of a carpet dyeing wastewater. J Hazard Mater 136, 763–769. https://doi.org/https://doi.org/10.1016/j.jhazmat.2006.01.006

Gyak, K., Vishwakarma, N., Hwang, Y.-H., Kim, J., Yun, H., Kim, D., 2019. 3D-printed Monolithic SiCN Ceramic Microreactors from a Photocurable Preceramic Resin for High Temperature Ammonia Cracking Process. React Chem Eng 4. https://doi.org/10.1039/C9RE00201D

Hamad, D., Dhib, R., Mehrvar, M., 2016. Effects of hydrogen peroxide feeding strategies on the photochemical degradation of polyvinyl alcohol. Environ Technol 37, 2731–2742. https://doi.org/10.1080/09593330.2016.1160959

Hasegawa, E., Yamada, H., Tsuno, H., 2008. Effective Ozonation of Secondary Effluents with Initial Ozone Demand. Ozone Sci Eng 30, 376–386. https://doi.org/10.1080/01919510802334157

He, R., Wu, X., Mu, H., Chen, L., Hu, H., Wang, J., Ren, H., Wu, B., 2023. Priority control sequence of 34 typical pollutants in effluents of Chinese wastewater treatment plants. Water Res 243, 120338. https://doi.org/https://doi.org/10.1016/j.watres.2023.120338

Helton, J.C., Johnson, J.D., Sallaberry, C.J., Storlie, C.B., 2006a. Survey of sampling-based methods for uncertainty and sensitivity analysis. Reliab Eng Syst Saf 91, 1175–1209. https://doi.org/https://doi.org/10.1016/j.ress.2005.11.017

Helton, J.C., Johnson, J.D., Sallaberry, C.J., Storlie, C.B., 2006b. Survey of sampling-based methods for uncertainty and sensitivity analysis. Reliab Eng Syst Saf 91, 1175–1209. https://doi.org/https://doi.org/10.1016/j.ress.2005.11.017

Hosseini, S.S., Denayer, J.F.M., 2022. Biogas upgrading by adsorption processes: Mathematical modeling, simulation and optimization approach – A review. J Environ Chem Eng 10, 107483. https://doi.org/https://doi.org/10.1016/j.jece.2022.107483

Hou, W., Bubliauskas, A., Kitson, P.J., Francoia, J.-P., Powell-Davies, H., Gutierrez, J.M.P., Frei, P., Manzano, J.S., Cronin, L., 2021. Automatic Generation of 3D-Printed Reactionware for Chemical Synthesis Digitization using ChemSCAD. ACS Cent Sci 7, 212–218. https://doi.org/10.1021/acscentsci.0c01354

Huang, D., Hu, C., Zeng, G., Cheng, M., Xu, P., Gong, X., Wang, R., Xue, W., 2017. Combination of Fenton processes and biotreatment for wastewater treatment and soil remediation. Science of The Total Environment 574, 1599–1610. https://doi.org/https://doi.org/10.1016/j.scitotenv.2016.08.199

Huang, W., Brigante, M., Wu, F., Mousty, C., Hanna, K., Mailhot, G., 2013. Assessment of the Fe(III)–EDDS Complex in Fenton-Like Processes: From the Radical Formation to the Degradation of Bisphenol A. Environ Sci Technol 47, 1952–1959. https://doi.org/10.1021/es304502y

Huber, M.M., GÖbel, A., Joss, A., Hermann, N., LÖffler, D., McArdell, C.S., Ried, A., Siegrist, H., Ternes, T.A., von Gunten, U., 2005. Oxidation of Pharmaceuticals during Ozonation of Municipal Wastewater Effluents: A Pilot Study. Environ Sci Technol 39, 4290–4299. https://doi.org/10.1021/es048396s

Javier Benitez, F., Acero, J.L., Gonzalez, T., Garcia, J., 2002. THE USE OF OZONE, OZONE PLUS UV RADIATION, AND AEROBIC MICROORGANISMS IN THE PURIFICATION OF SOME AGRO-INDUSTRIAL WASTEWATERS. Journal of Environmental Science and Health, Part A 37, 1307–1325. https://doi.org/10.1081/ESE-120005988
Jeppsson, U., 2012. Modelling Aspects of Wastewater Treatment Processes.
Jiao, Y., Fish, J., 2017. Is an additive decomposition of a rate of deformation and objective stress rates passé? Comput Methods Appl Mech Eng 327, 196–225. https://doi.org/https://doi.org/10.1016/j.cma.2017.07.021
Kebir, M., Benramdhan, I. kahina, Noureddine, N., Tahraoui, H., Nadia, B., Houssine, B., Rachid, A., Zhang, J., ASSADI, A.A., Mouni, L., Amrane, A., 2023. Sunlight Degradation and Mineralization of Food Dye Photoinduced by Homogenous Photo Fenton Fe(III) and Fe(II) /Complex: Surface Response Modeling. https://doi.org/10.20944/PREPRINTS202305.1573.V1
Keenan, C.R., Sedlak, D.L., 2008. Ligand-Enhanced Reactive Oxidant Generation by Nanoparticulate Zero-Valent Iron and Oxygen. Environ Sci Technol 42, 6936–6941. https://doi.org/10.1021/es801438f
Kim, S., Chu, K.H., Al-Hamadani, Y.A.J., Park, C.M., Jang, M., Kim, D.-H., Yu, M., Heo, J., Yoon, Y., 2018. Removal of contaminants of emerging concern by membranes in water and wastewater: A review. Chemical Engineering Journal 335, 896–914. https://doi.org/https://doi.org/10.1016/j.cej.2017.11.044
Kinman, R.N., Rempel, G., 1975. Water and wastewater disinfection with ozone: A critical review. C R C Critical Reviews in Environmental Control 5, 141–152. https://doi.org/10.1080/10643387509381625
Kitson, P., Rosnes, M., Sans, V., Dragone, V., Cronin, L., 2012. Configurable 3D-Printed millifluidic and microfluidic “lab on a chip” reactionware devices. Lab Chip 12, 3267–3271. https://doi.org/10.1039/c2lc40761b
Kotz, F., Risch, P., Helmer, D., Rapp, B.E., 2019. High-Performance Materials for 3D Printing in Chemical Synthesis Applications. Advanced Materials 31, 1805982. https://doi.org/10.1002/adma.201805982
Kowalska, K., Roccamante, M., Cabrera Reina, A., Plaza-Bolaños, P., Oller, I., Malato, S., 2021. Pilot-scale removal of microcontaminants by solar-driven photo-Fenton in treated municipal effluents: Selection of operating variables based on lab-scale experiments. J Environ Chem Eng 9, 104788. https://doi.org/https://doi.org/10.1016/j.jece.2020.104788
Krishnan, S., Rawindran, H., Sinnathambi, C.M., Lim, J.W., 2017. Comparison of various advanced oxidation processes used in remediation of industrial wastewater laden with recalcitrant pollutants. IOP Conf Ser Mater Sci Eng 206, 012089. https://doi.org/10.1088/1757-899X/206/1/012089
Kumar, R., Qureshi, M., Vishwakarma, D.K., Al-Ansari, N., Kuriqi, A., Elbeltagi, A., Saraswat, A., 2022. A review on emerging water contaminants and the application of sustainable removal technologies. Case Studies in Chemical and Environmental Engineering 6, 100219. https://doi.org/https://doi.org/10.1016/j.cscee.2022.100219
Kumar Shivappa Masalvad, S., Kumar Sakare, P., 2021. Application of photo Fenton process for treatment of textile Congo-red dye solution. Mater Today Proc 46, 5291–5297. https://doi.org/https://doi.org/10.1016/j.matpr.2020.08.650
Kusic, H., Koprivanac, N., Horvat, S., Bakija, S., Bozic, A.L., 2009. Modeling dye degradation kinetic using dark- and photo-Fenton type processes. Chemical

Engineering Journal 155, 144–154. https://doi.org/https://doi.org/10.1016/j.cej.2009.07.029
Kwon, M., Kye, H., Jung, Y., Yoon, Y., Kang, J.-W., 2017. Performance characterization and kinetic modeling of ozonation using a new method: ROH,O_3 concept. Water Res 122, 172–182. https://doi.org/https://doi.org/10.1016/j.watres.2017.05.062
Lafi, W.K., Al-Qodah, Z., 2006. Combined advanced oxidation and biological treatment processes for the removal of pesticides from aqueous solutions. J Hazard Mater 137, 489–497. https://doi.org/https://doi.org/10.1016/j.jhazmat.2006.02.027
Lal, B.S., 2019. Water for Life: Issues and Challenges. International Journal of Science and Research (IJSR) 8, 1949–1957. https://doi.org/10.21275/ART20199011
Latunde, T., Bamigbola, O.M., 2018. Parameter Estimation and Sensitivity Analysis of an Optimal Control Model for Capital Asset Management. Advances in Fuzzy Systems 2018, 4756520. https://doi.org/10.1155/2018/4756520
Ledakowicz, S., Solecka, M., Zylla, R., 2001. Biodegradation, decolourisation and detoxification of textile wastewater enhanced by advanced oxidation processes. J Biotechnol 89, 175–184. https://doi.org/https://doi.org/10.1016/S0168-1656(01)00296-6
Lee, C., Keenan, C.R., Sedlak, D.L., 2008. Polyoxometalate-Enhanced Oxidation of Organic Compounds by Nanoparticulate Zero-Valent Iron and Ferrous Ion in the Presence of Oxygen. Environ Sci Technol 42, 4921–4926. https://doi.org/10.1021/es800317j
Lee, Y., Gerrity, D., Lee, M., Bogeat, A.E., Salhi, E., Gamage, S., Trenholm, R.A., Wert, E.C., Snyder, S.A., von Gunten, U., 2013. Prediction of Micropollutant Elimination during Ozonation of Municipal Wastewater Effluents: Use of Kinetic and Water Specific Information. Environ Sci Technol 47, 5872–5881. https://doi.org/10.1021/es400781r
Lee, Y., Kovalova, L., McArdell, C.S., von Gunten, U., 2014. Prediction of micropollutant elimination during ozonation of a hospital wastewater effluent. Water Res 64, 134–148. https://doi.org/https://doi.org/10.1016/j.watres.2014.06.027
Lee, Y., von Gunten, U., 2016. Advances in predicting organic contaminant abatement during ozonation of municipal wastewater effluent: reaction kinetics, transformation products, and changes of biological effects. Environ Sci (Camb) 2, 421–442. https://doi.org/10.1039/C6EW00025H
Leyva-Díaz, J.C., López-López, C., Martín-Pascual, J., Muñío, M.M., Poyatos, J.M., 2015. Kinetic study of the combined processes of a membrane bioreactor and a hybrid moving bed biofilm reactor-membrane bioreactor with advanced oxidation processes as a post-treatment stage for wastewater treatment. Chemical Engineering and Processing: Process Intensification 91, 57–66. https://doi.org/https://doi.org/10.1016/j.cep.2015.03.017
Li, M., Chen, Z., Wang, Z., Wen, Q., 2019. Investigation on degradation behavior of dissolved effluent organic matter, organic micro-pollutants and bio-toxicity reduction from secondary effluent treated by ozonation. Chemosphere 217, 223–231. https://doi.org/https://doi.org/10.1016/j.chemosphere.2018.11.039
Li, X., Gan, X., 2022. Photo-Fenton degradation of multiple pharmaceuticals at low concentrations via Cu-doped-graphitic carbon nitride (g-C_3N_4) under simulated

solar irradiation at a wide pH range. J Environ Chem Eng 10, 108290. https://doi.org/https://doi.org/10.1016/j.jece.2022.108290
Li, X., Ma, J., He, H., 2020. Recent advances in catalytic decomposition of ozone. Journal of Environmental Sciences 94, 14–31. https://doi.org/https://doi.org/10.1016/j.jes.2020.03.058
Lim, S., Shi, J.L., von Gunten, U., McCurry, D.L., 2022. Ozonation of organic compounds in water and wastewater: A critical review. Water Res 213, 118053. https://doi.org/https://doi.org/10.1016/j.watres.2022.118053
Lin, W., Liu, X., Ding, A., Ngo, H.H., Zhang, R., Nan, J., Ma, J., Li, G., 2022. Advanced oxidation processes (AOPs)-based sludge conditioning for enhanced sludge dewatering and micropollutants removal: A critical review. Journal of Water Process Engineering 45, 102468. https://doi.org/https://doi.org/10.1016/j.jwpe.2021.102468
Lin, Y.-R., Hu, Y.-F., Huang, C.-Y., Huang, H.-T., Liao, Z.-H., Lee, A.-T., Wu, Y.-S., Nan, F.-H., 2022. Removing Malachite Green and Leucomalachite Green From Freshwater and Seawater With Four Water Treatment Agents. Front Environ Sci 10.
Liu, C., Xie, Y., Jiao, Y., Du, Y., Zheng, Q., Sun, Y., 2022. Visible-light-driven nanoscale zero-valent iron loaded rGO/g-C_3N_4 for fluoroquinolone antibiotics degradation in water. Front Environ Sci 10.
Lu, L.-A., Ma, Y.-S., Kumar, M., Lin, J.-G., 2011. Photochemical degradation of carbofuran and elucidation of removal mechanism. Chemical Engineering Journal 166, 150–156. https://doi.org/https://doi.org/10.1016/j.cej.2010.10.045
Lu, L.A., Wang, C., Kumar, M., Lin, J.-G., 2010. Influence of pH and H_2O_2 dosage on the decomposition of carbofuran by the photo-Fenton process. Sustainable Environment Research 20, 293–297.
Mackay, M., Swain, Z., Banbury, C., Phan, D., Edwards, D., 2017. The performance of the hot end in a plasticating 3D printer. J Rheol (N Y N Y) 61, 229–236. https://doi.org/10.1122/1.4973852
Mahbub, P., Duke, M., 2023. Scalability of advanced oxidation processes (AOPs) in industrial applications: A review. J Environ Manage 345, 118861. https://doi.org/https://doi.org/10.1016/j.jenvman.2023.118861
Mahmoudi, N., Farhadian, M., Solaimany Nazar, A.R., Eskandari, P., Esfahani, K.N., 2021. Investigation and optimization of the performance of sono-photo-electro-Fenton process for removal of Acid Black 172 and Disperse Blue 56 from polluted water: comparison of the degradation activity with electro-Fenton-based processes. International Journal of Environmental Science and Technology. https://doi.org/10.1007/s13762-021-03296-0
Maier, M., Lebl, R., Sulzer, P., Lechner, J., Mayr, T., Zadravec, M., Slama, E., Pfanner, S., Schmölzer, C., Pöchlauer, P., Kappe, C.O., Gruber-Woelfler, H., 2018. Development of customized 3D printed stainless steel reactors with inline oxygen sensors for aerobic oxidation of Grignard reagents in continuous flow. React Chem Eng 4. https://doi.org/10.1039/C8RE00278A
Manenti, D.R., Soares, P.A., Módenes, A.N., Espinoza-Quiñones, F.R., Boaventura, R.A.R., Bergamasco, R., Vilar, V.J.P., 2015. Insights into solar photo-Fenton process using iron(III)–organic ligand complexes applied to real textile wastewater treatment. Chemical Engineering Journal 266, 203–212. https://doi.org/https://doi.org/10.1016/j.cej.2014.12.077

Maniakova, G., Salmerón, I., Aliste, M., Inmaculada Polo-López, M., Oller, I., Malato, S., Rizzo, L., 2022. Solar photo-Fenton at circumneutral pH using Fe(III)-EDDS compared to ozonation for tertiary treatment of urban wastewater: Contaminants of emerging concern removal and toxicity assessment. Chemical Engineering Journal 431, 133474. https://doi.org/https://doi.org/10.1016/j.cej.2021.133474

Mantzavinos, D., Psillakis, E., 2004. Enhancement of biodegradability of industrial wastewaters by chemical oxidation pre-treatment. Journal of Chemical Technology & Biotechnology 79, 431–454. https://doi.org/10.1002/jctb.1020

Marino, S., Hogue, I.B., Ray, C.J., Kirschner, D.E., 2008a. A methodology for performing global uncertainty and sensitivity analysis in systems biology. J Theor Biol 254, 178–196. https://doi.org/https://doi.org/10.1016/j.jtbi.2008.04.011

Marino, S., Hogue, I.B., Ray, C.J., Kirschner, D.E., 2008b. A methodology for performing global uncertainty and sensitivity analysis in systems biology. J Theor Biol 254, 178–196. https://doi.org/https://doi.org/10.1016/j.jtbi.2008.04.011

Masood, A.S., Ali, Md.S., Manzar, M.S., Khan, N.A., Khan, A.H., 2023. 2 - Current situation of pharmaceutical wastewater around the globe, in: Khan, A.H., Khan, N.A., Naushad, Mu., Aziz, H.A. (Eds.), The Treatment of Pharmaceutical Wastewater. Elsevier, pp. 19–52. https://doi.org/https://doi.org/10.1016/B978-0-323-99160-5.00013-8

Mathon, B., Coquery, M., Liu, Z., Penru, Y., Guillon, A., Esperanza, M., Miège, C., Choubert, J.-M., 2021. Ozonation of 47 organic micropollutants in secondary treated municipal effluents: Direct and indirect kinetic reaction rates and modelling. Chemosphere 262, 127969. https://doi.org/https://doi.org/10.1016/j.chemosphere.2020.127969

Matos Rodrigues, M.H., Rodrigues de Sousa, P.A., Borges, K.C.M., Melo Coelho, L., Fátima Gonçalves, R., Teodoro, M.D., Vilella da Motta, F., Maribondo do Nascimento, R., Júnior, M.G., 2019. Enhanced degradation of the antibiotic sulfamethoxazole by heterogeneous photocatalysis using $Ce0,8Gd0,2O_2$-δ/TiO_2 particles. J Alloys Compd 808, 151711. https://doi.org/https://doi.org/10.1016/j.jallcom.2019.151711

Mecha, A.C., Onyango, M.S., Ochieng, A., Momba, M.N.B., 2017. Ultraviolet and solar photocatalytic ozonation of municipal wastewater: Catalyst reuse, energy requirements and toxicity assessment. Chemosphere 186, 669–676. https://doi.org/https://doi.org/10.1016/j.chemosphere.2017.08.041

Mihelcic, J.R., Naughton, C.C., Verbyla, M.E., Zhang, Q., Schweitzer, R.W., Oakley, S.M., Wells, E.C., Whiteford, L.M., 2016. The Grandest Challenge of All: The Role of Environmental Engineering to Achieve Sustainability in the World's Developing Regions. Environ Eng Sci 34, 16–41. https://doi.org/10.1089/ees.2015.0334

Mizuno, T., Tsuno, H., Yamada, H., 2007. Development of Ozone Self-Decomposition Model for Engineering Design. Ozone Sci Eng 29, 55–63. https://doi.org/10.1080/01919510601115849

Mohammed, A., Smith, D.W., 1992. Effects Of Ozone On Kraft Process Pulp Mill Effluent. Ozone Sci Eng 14, 461–484. https://doi.org/10.1080/01919512.1992.10555722

Moloantoa, K.M., Khetsha, Z.P., Kana, G.E.B., Maleke, M.M., Van Heerden, E., Castillo, J.C., Cason, E.D., 2023. Metagenomic assessment of nitrate-

contaminated mine wastewaters and optimization of complete denitrification by indigenous enriched bacteria. Front Environ Sci 11.
Morales, M., Rezayat, M., Mateo, A., 2024. Enhancing the corrosion resistance of 2205 duplex stainless steel in molten carbonate salts by laser-surface texturing. J Energy Storage 78, 110053. https://doi.org/https://doi.org/10.1016/j.est.2023.110053
Morales-Planas, S., Minguella-Canela, J., Lluma-Fuentes, J., Travieso-Rodriguez, J.A., García-Granada, A.-A., 2018. Multi Jet Fusion PA12 Manufacturing Parameters for Watertightness, Strength and Tolerances. Materials . https://doi.org/10.3390/ma11081472
Mousset, E., Frunzo, L., Esposito, G., Hullebusch, E.D. van, Oturan, N., Oturan, M.A., 2016. A complete phenol oxidation pathway obtained during electro-Fenton treatment and validated by a kinetic model study. Appl Catal B 180, 189–198. https://doi.org/10.1016/J.APCATB.2015.06.014
Mousset, E., Huang Weiqi, V., Foong Yang Kai, B., Koh, J.S., Tng, J.W., Wang, Z., Lefebvre, O., 2017. A new 3D-printed photoelectrocatalytic reactor combining the benefits of a transparent electrode and the Fenton reaction for advanced wastewater treatment. J Mater Chem A Mater 5, 24951–24964. https://doi.org/10.1039/C7TA08182K
Mousset, E., Loh, W.H., Lim, W.S., Jarry, L., Wang, Z., Lefebvre, O., 2021. Cost comparison of advanced oxidation processes for wastewater treatment using accumulated oxygen-equivalent criteria. Water Res 200, 117234. https://doi.org/https://doi.org/10.1016/j.watres.2021.117234
Narayanan, C.M., Narayan, V., 2019. Biological wastewater treatment and bioreactor design: a review. Sustainable Environment Research 29, 33. https://doi.org/10.1186/s42834-019-0036-1
Nasr Esfahani, K., Farhadian, M., Solaimany Nazar, A.R., 2019. Interaction effects of various reaction parameters on the treatment of sulfidic spent caustic through electro-photo-Fenton. International Journal of Environmental Science and Technology 16, 7165–7174. https://doi.org/10.1007/s13762-018-2126-8
Nasr Esfahani, K., Pérez-Moya, M., Graells, M., 2022a. Modelling and Parameter Fitting of the Dosage of Hydrogen Peroxide in a Photo-Fenton Process, in: Montastruc, L., Negny, S. (Eds.), Computer Aided Chemical Engineering. Elsevier, pp. 373–378. https://doi.org/https://doi.org/10.1016/B978-0-323-95879-0.50063-1
Nasr Esfahani, K., Pérez-Moya, M., Graells, M., 2022b. Modelling of the photo-Fenton process with flexible hydrogen peroxide dosage: Sensitivity analysis and experimental validation. Science of The Total Environment 839, 155941. https://doi.org/https://doi.org/10.1016/j.scitotenv.2022.155941
Nasr Esfahani, K., Pérez-Moya, M., Graells, M., Miralles-Cuevas, S., Cabrera-Reina, A., 2023. Mechanistic modelling of Fe^{3+}-EDDS mediated photo-Fenton revisited: Lumped radicals and sensitivity analysis. Chemical Engineering Journal 464, 142559. https://doi.org/https://doi.org/10.1016/j.cej.2023.142559
Nasr Esfahani, K., Zandi, M.D., Travieso-Rodriguez, J.A., Graells, M., Pérez-Moya, M., 2021. Manufacturing and Application of 3D Printed Photo Fenton Reactors for Wastewater Treatment. Int J Environ Res Public Health 18. https://doi.org/10.3390/ijerph18094885

Neumaier, J.M., Madani, A., Klein, T., Ziegler, T., 2019. Low-budget 3D-printed equipment for continuous flow reactions. Beilstein journal of organic chemistry 15, 558–566. https://doi.org/10.3762/bjoc.15.50

Ng, H.M., mohamad saidi, N., Omar, F.S., Kasi, R., T subramaniam, R., Baig, S., 2018. Thermogravimetric Analysis of Polymers 1–29. https://doi.org/10.1002/0471440264.pst667

Ngo, T.D., Kashani, A., Imbalzano, G., Nguyen, K.T.Q., Hui, D., 2018. Additive manufacturing (3D printing): A review of materials, methods, applications and challenges. Compos B Eng 143, 172–196. https://doi.org/https://doi.org/10.1016/j.compositesb.2018.02.012

Nidheesh, P.V., Couras, C., Ansaf, V.K., Nadais, H., 2021. A review of integrated advanced oxidation processes and biological processes for organic pollutant removal. Chem Eng Commun 209, 1–43. https://doi.org/10.1080/00986445.2020.1864626

Nogueira, R.F.P., Oliveira, M.C., Paterlini, W.C., 2005. Simple and fast spectrophotometric determination of H_2O_2 in photo-Fenton reactions using metavanadate. Talanta 66, 86–91. https://doi.org/https://doi.org/10.1016/j.talanta.2004.10.001

Obra, I., Ponce Robles, L., Miralles-Cuevas, S., Oller, I., Malato, S., Sánchez Pérez, J.A., 2016. Microcontaminant removal in secondary effluents by solar photo-Fenton at circumneutral pH in raceway pond reactors. Catal Today 287. https://doi.org/10.1016/j.cattod.2016.12.028

Oh, W.-D., Dong, Z., Lim, T.-T., 2016. Generation of sulfate radical through heterogeneous catalysis for organic contaminants removal: Current development, challenges and prospects. Appl Catal B 194, 169–201. https://doi.org/https://doi.org/10.1016/j.apcatb.2016.04.003

Okafor, O., Robertson, K., Goodridge, R., Sans, V., 2019. Continuous-flow crystallisation in 3D-printed compact devices. React Chem Eng 4, 1682–1688. https://doi.org/10.1039/C9RE00188C

Oller, I., Malato, S., 2021. Photo-Fenton applied to the removal of pharmaceutical and other pollutants of emerging concern. Curr Opin Green Sustain Chem 29, 100458. https://doi.org/https://doi.org/10.1016/j.cogsc.2021.100458

Oller, I., Malato, S., Sánchez-Pérez, J.A., 2011a. Combination of Advanced Oxidation Processes and biological treatments for wastewater decontamination—A review. Science of The Total Environment 409, 4141–4166. https://doi.org/https://doi.org/10.1016/j.scitotenv.2010.08.061

Oller, I., Malato, S., Sánchez-Pérez, J.A., 2011b. Combination of Advanced Oxidation Processes and biological treatments for wastewater decontamination—A review. Science of The Total Environment 409, 4141–4166. https://doi.org/https://doi.org/10.1016/j.scitotenv.2010.08.061

Ortega-Gómez, E., Moreno Úbeda, J.C., Álvarez Hervás, J.D., Casas López, J.L., Santos-Juanes Jordá, L., Sánchez Pérez, J.A., 2012. Automatic dosage of hydrogen peroxide in solar photo-Fenton plants: Development of a control strategy for efficiency enhancement. J Hazard Mater 237–238, 223–230. https://doi.org/https://doi.org/10.1016/j.jhazmat.2012.08.031

Ortega-Moreno, G.A., Ayala-Durán, S.C., Barbero, B.P., Narda, G.E., Bernini, M.C., Pupo Nogueira, R.F., 2022. Photo-Fenton degradation of sulfamethoxazole using MIL-53(Fe) under UVA LED irradiation and natural sunlight. J Environ Chem Eng 10, 107678. https://doi.org/https://doi.org/10.1016/j.jece.2022.107678

Otieno, B., Apollo, S., Naidoo, B., Ochieng, A., 2019. Modeling ozonation pretreatment parameters of distillery wastewater for improved biodegradability. Journal of Environmental Science and Health, Part A 54, 1066–1074. https://doi.org/10.1080/10934529.2019.1631089

Parra-Cabrera, C., Achille, C., Kuhn, S., Ameloot, R., 2018. 3D printing in chemical engineering and catalytic technology: structured catalysts, mixers and reactors. Chem Soc Rev 47, 209–230. https://doi.org/10.1039/C7CS00631D

Patrolecco, L., Rauseo, J., Ademollo, N., Grenni, P., Cardoni, M., Levantesi, C., Luprano, M.L., Caracciolo, A.B., 2018. Persistence of the antibiotic sulfamethoxazole in river water alone or in the co-presence of ciprofloxacin. Science of The Total Environment 640–641, 1438–1446. https://doi.org/https://doi.org/10.1016/j.scitotenv.2018.06.025

Peng, F., Vogt, B.D., Cakmak, M., 2018. Complex flow and temperature history during melt extrusion in material extrusion additive manufacturing. Addit Manuf 22, 197–206. https://doi.org/https://doi.org/10.1016/j.addma.2018.05.015

Peralta Muniz Moreira, R., Cabrera Reina, A., Soriano Molina, P., Sánchez Pérez, J.A., Li Puma, G., 2021. Computational fluid dynamics (CFD) modeling of removal of contaminants of emerging concern in solar photo-Fenton raceway pond reactors. Chemical Engineering Journal 413, 127392. https://doi.org/https://doi.org/10.1016/j.cej.2020.127392

Pigeonneau, F., Xu, D., Vincent, M., Agassant, J.-F., 2020. Heating and flow computations of an amorphous polymer in the liquefier of a material extrusion 3D printer. Addit Manuf 32, 101001. https://doi.org/https://doi.org/10.1016/j.addma.2019.101001

Pignatello, J., Oliveros, E., MacKay, A., 2006. Advanced Oxidation Processes for Organic Contaminant Destruction Based on Fenton Reaction and Related Chemistry. Critical Reviews in Environmental Science and Technology - CRIT REV ENVIRON SCI TECHNOL 36, 1–84. https://doi.org/10.1080/10643380500326564

Prajapati, H., Ravoori, D., Jain, A., 2018. Measurement and modeling of filament temperature distribution in the standoff gap between nozzle and bed in polymer-based additive manufacturing. Addit Manuf 24, 224–231. https://doi.org/https://doi.org/10.1016/j.addma.2018.09.030

Proano-Pena, G., Carrano, A.L., Blersch, D.M., 2020. Analysis of very-high surface area 3D-printed media in a moving bed biofilm reactor for wastewater treatment. PLoS One 15, e0238386.

Rao, Z.X., Patel, B., Monaco, A., Cao, Z.J., Barniol-Xicota, M., Pichon, E., Ladlow, M., Hilton, S.T., 2017. 3D-Printed Polypropylene Continuous-Flow Column Reactors: Exploration of Reactor Utility in SNAr Reactions and the Synthesis of Bicyclic and Tetracyclic Heterocycles. European J Org Chem 2017, 6499–6504. https://doi.org/10.1002/ejoc.201701111

Rezayat, M., Karamimoghadam, M., Moradi, M., Casalino, G., Roa Rovira, J.J., Mateo, A., 2023. Overview of Surface Modification Strategies for Improving the Properties of Metastable Austenitic Stainless Steels. Metals (Basel) 13. https://doi.org/10.3390/met13071268

Ribeiro, J.P., Nunes, M.I., 2021. Recent trends and developments in Fenton processes for industrial wastewater treatment – A critical review. Environ Res 197, 110957. https://doi.org/https://doi.org/10.1016/j.envres.2021.110957

Ried, A., Mielcke, J., Wieland, A., 2009. The Potential Use of Ozone in Municipal Wastewater. Ozone Sci Eng 31, 415–421. https://doi.org/10.1080/01919510903199111

Rivas, G., Carra, I., García Sánchez, J.L., Casas López, J.L., Malato, S., Sánchez Pérez, J.A., 2015. Modelling of the operation of raceway pond reactors for micropollutant removal by solar photo-Fenton as a function of photon absorption. Appl Catal B 178, 210–217. https://doi.org/https://doi.org/10.1016/j.apcatb.2014.09.015

Rizzo, L., Gernjak, W., Krzeminski, P., Malato, S., McArdell, C.S., Perez, J.A.S., Schaar, H., Fatta-Kassinos, D., 2020. Best available technologies and treatment trains to address current challenges in urban wastewater reuse for irrigation of crops in EU countries. Science of The Total Environment 710, 136312. https://doi.org/https://doi.org/10.1016/j.scitotenv.2019.136312

Rodriguez-Gil, J.L., Catalá, M., Gonzalez Alonso, S., Maroto, R., Valcarcel, Y., Segura, Y., Molina, R., Melero, J., Martinez Castillejo, F., 2010. Heterogeneous photo-Fenton treatment for the reduction of pharmaceutical contamination in Madrid rivers and ecotoxicological evaluation by a miniaturized fern spores bioassay. Chemosphere 80, 381–388. https://doi.org/10.1016/j.chemosphere.2010.04.045

Rohde, S., Cantrell, J., Jerez, A., Kroese, C., Damiani, D., Gurnani, R., DiSandro, L., Anton, J., Young, A., Steinbach, D., Ifju, P., 2018. Experimental Characterization of the Shear Properties of 3D–Printed ABS and Polycarbonate Parts. Exp Mech 58, 871–884. https://doi.org/10.1007/s11340-017-0343-6

Romero, V., Acevedo, S., Pilar, M., Giménez, J., Esplugas, S., 2015. Enhancement of Fenton and photo-Fenton processes at initial circumneutral pH for the degradation of the β-blocker Metoprolol. Water Res 88, 449–457. https://doi.org/10.1016/j.watres.2015.10.035

Rossi, S., Porta, R., Brenna, D., Puglisi, A., Benaglia, M., 2017. Stereoselective Catalytic Synthesis of Active Pharmaceutical Ingredients in Homemade 3D-Printed Mesoreactors. Angewandte Chemie International Edition 56, 4290–4294. https://doi.org/10.1002/anie.201612192

Rozas, O., Contreras, D., Mondaca, M.A., Pérez-Moya, M., Mansilla, H.D., 2010. Experimental design of Fenton and photo-Fenton reactions for the treatment of ampicillin solutions. J Hazard Mater 177, 1025–1030. https://doi.org/https://doi.org/10.1016/j.jhazmat.2010.01.023

Salimi, M., Esrafili, A., Gholami, M., Jonidi Jafari, A., Rezaei Kalantary, R., Farzadkia, M., Kermani, M., Sobhi, H.R., 2017. Contaminants of emerging concern: a review of new approach in AOP technologies. Environ Monit Assess 189, 414. https://doi.org/10.1007/s10661-017-6097-x

Saltelli, A., Tarantola, S., Chan, K.P.-S., 1999. A Quantitative Model-Independent Method for Global Sensitivity Analysis of Model Output. Technometrics 41, 39–56. https://doi.org/10.1080/00401706.1999.10485594

Sánchez Peréz, J.A., Carra, I., Sirtori, C., Agüera, A., Esteban, B., 2014. Fate of thiabendazole through the treatment of a simulated agro-food industrial effluent by combined MBR/Fenton processes at μg/L scale. Water Res 51, 55–63. https://doi.org/https://doi.org/10.1016/j.watres.2013.07.039

Sans, V., 2020. Emerging trends in flow chemistry enabled by 3D printing: Robust reactors, biocatalysis and electrochemistry. Curr Opin Green Sustain Chem 25, 100367. https://doi.org/https://doi.org/10.1016/j.cogsc.2020.100367

Santiago, D.E., Murcia Mesa, J.J., Pulido Melián, E., Vaiano, V., 2023. Editorial: Wastewater treatment: removal of recalcitrant compounds. Front Environ Sci 11. https://doi.org/10.3389/fenvs.2023.1288480
Santos, R.M., Botelho, G.L., Machado, A. V, 2010. Artificial and natural weathering of ABS. J Appl Polym Sci 116, 2005–2014. https://doi.org/10.1002/app.31663
Santos-Juanes, L., Sánchez, J., Casas López, J., Oller, I., Malato, S., Sánchez Pérez, J.A., 2011. Dissolved Oxygen Concentration: A Key Parameter in Monitoring the Photo-Fenton Process. Appl Catal B 104, 316–323. https://doi.org/10.1016/j.apcatb.2011.03.013
Saravanan, A., Deivayanai, V.C., Kumar, P.S., Rangasamy, G., Hemavathy, R. V, Harshana, T., Gayathri, N., Alagumalai, K., 2022. A detailed review on advanced oxidation process in treatment of wastewater: Mechanism, challenges and future outlook. Chemosphere 308, 136524. https://doi.org/https://doi.org/10.1016/j.chemosphere.2022.136524
Sarı, B., Türkeş, S., Güney, H., Keskinkan, O., 2023. The Utilization and Modeling of Photo-Fenton Process as a Single Unit in Textile Wastewater Treatment. Clean (Weinh) 51, 2100328. https://doi.org/https://doi.org/10.1002/clen.202100328
Shehata, N., Egirani, D., Olabi, A.G., Inayat, A., Abdelkareem, M.A., Chae, K.-J., Sayed, E.T., 2023. Membrane-based water and wastewater treatment technologies: Issues, current trends, challenges, and role in achieving sustainable development goals, and circular economy. Chemosphere 320, 137993. https://doi.org/https://doi.org/10.1016/j.chemosphere.2023.137993
Sheikh, M., Harami, H.R., Rezakazemi, M., Valderrama, C., Cortina, J.L., Aminabhavi, T.M., 2023a. Efficient NH3-N recovery from municipal wastewaters via membrane hybrid systems: Nutrient-Energy-Water (NEW) nexus in circular economy. Chemical Engineering Journal 465, 142876. https://doi.org/https://doi.org/10.1016/j.cej.2023.142876
Sheikh, M., Lopez, J., Reig, M., Vecino, X., Rezakazemi, M., Valderrama, C.A., Cortina, J.L., 2023b. Ammonia recovery from municipal wastewater using hybrid NaOH closed-loop membrane contactor and ion exchange system. Chemical Engineering Journal 465, 142859. https://doi.org/https://doi.org/10.1016/j.cej.2023.142859
Shinozawa, Y., Heggo, D., Ookawara, S., Yoshikawa, S., 2020. Photo-Fenton Degradation of Carbofuran in Helical Tube Microreactor and Kinetic Modeling. Ind Eng Chem Res 59, 3811–3819. https://doi.org/10.1021/acs.iecr.9b04213
Simunovic, M., Kusic, H., Koprivanac, N., Bozic, A.L., 2011. Treatment of simulated industrial wastewater by photo-Fenton process: Part II. The development of mechanistic model. Chemical Engineering Journal 173, 280–289. https://doi.org/https://doi.org/10.1016/j.cej.2010.09.030
Singh, S., Ramakrishna, S., Singh, R., 2017. Material issues in additive manufacturing: A review. J Manuf Process 25, 185–200. https://doi.org/https://doi.org/10.1016/j.jmapro.2016.11.006
Sinnaraprasat, S., Fongsatitkul, P., 2011. Optimal Condition of Fenton's Reagent to Enhance the Alcohol Production from Palm Oil Mill Effluent (POME). EnvironmentAsia 4, 9–16. https://doi.org/10.14456/ea.2011.12
Soriano-Molina, P., García Sánchez, J.L., Alfano, O.M., Conte, L.O., Malato, S., Sánchez Pérez, J.A., 2018. Mechanistic modeling of solar photo-Fenton process

with Fe^{3+}-EDDS at neutral pH. Appl Catal B 233, 234–242. https://doi.org/https://doi.org/10.1016/j.apcatb.2018.04.005
Soriano-Molina, P., Plaza-Bolaños, P., Lorenzo, A., Agüera, A., García Sánchez, J.L., Malato, S., Sánchez Pérez, J.A., 2019. Assessment of solar raceway pond reactors for removal of contaminants of emerging concern by photo-Fenton at circumneutral pH from very different municipal wastewater effluents. Chemical Engineering Journal 366, 141–149. https://doi.org/https://doi.org/10.1016/j.cej.2019.02.074
Spiess, A.-N., Neumeyer, N., 2010. An evaluation of R2 as an inadequate measure for nonlinear models in pharmacological and biochemical research: A Monte Carlo approach. BMC Pharmacol 10, 6. https://doi.org/10.1186/1471-2210-10-6
Tang, X., Alavi, S., 2011. Recent advances in starch, polyvinyl alcohol based polymer blends, nanocomposites and their biodegradability. Carbohydr Polym 85, 7–16. https://doi.org/https://doi.org/10.1016/j.carbpol.2011.01.030
Thiebault, T., 2020. Sulfamethoxazole/Trimethoprim ratio as a new marker in raw wastewaters: A critical review. Science of The Total Environment 715, 136916. https://doi.org/https://doi.org/10.1016/j.scitotenv.2020.136916
Ting, S., Xiaoning, W., Xinan, C., Yan, C., Zhenkai, W., Zhangxiong, W., Duo, W.W., Sheng-Peng, S., 2022. Fe^{3+}-NTA-Catalyzed Homogenous Fenton-Like Degradation of Trichloroethylene in Groundwater at Natural pH (~8.0): Efficacy, By-Products, and H_2O_2 Utilization. Journal of Environmental Engineering 148, 04021072. https://doi.org/10.1061/(ASCE)EE.1943-7870.0001951
Tokumura, M., Ohta, A., Znad, H.T., Kawase, Y., 2006. UV light assisted decolorization of dark brown colored coffee effluent by photo-Fenton reaction. Water Res 40, 3775–3784. https://doi.org/https://doi.org/10.1016/j.watres.2006.08.012
Tokumura, M., Znad, H.T., Kawase, Y., 2008. Decolorization of dark brown colored coffee effluent by solar photo-Fenton reaction: Effect of solar light dose on decolorization kinetics. Water Res 42, 4665–4673. https://doi.org/https://doi.org/10.1016/j.watres.2008.08.007
Traid, H.D., Vera, M.L., Escalada, G., López, I.E., Dwojak, A.N., Litter, M.I., 2022. Application of a Fenton process after a biological nitrification treatment: A successful case for leachate treatment. Case Studies in Chemical and Environmental Engineering 5, 100208. https://doi.org/https://doi.org/10.1016/j.cscee.2022.100208
Travieso-Rodriguez, J.A., Jerez-Mesa, R., Llumà, J., Gómez-Gras, G., Casadesús-Farràs, O., 2020. Comparative study of the flexural properties of ABS, PLA and a PLA-wood composite manufactured through fused filament fabrication. Rapid Prototyp J 27. https://doi.org/10.1108/RPJ-01-2020-0022
Travieso-Rodriguez, J.A., Jerez-Mesa, R., Llumà, J., Traver-Ramos, O., Gomez-Gras, G., Roa Rovira, J.J., 2019. Mechanical Properties of 3D-Printing Polylactic Acid Parts subjected to Bending Stress and Fatigue Testing. Materials . https://doi.org/10.3390/ma12233859
Trovó, A.G., Nogueira, R.F.P., Agüera, A., Fernandez-Alba, A.R., Sirtori, C., Malato, S., 2009. Degradation of sulfamethoxazole in water by solar photo-Fenton. Chemical and toxicological evaluation. Water Res 43, 3922–3931. https://doi.org/https://doi.org/10.1016/j.watres.2009.04.006
Tufail, A., Price, W., Hai, F., 2020. A critical review on advanced oxidation processes for the removal of trace organic contaminants: A voyage from

individual to integrated processes. Chemosphere 260, 127460. https://doi.org/10.1016/j.chemosphere.2020.127460
Van der Helm, A.W.C., Smeets, P.W.M.H., Baars, E.T., Rietveld, L.C., van Dijk, J.C., 2007. Modeling of Ozonation for Dissolved Ozone Dosing. Ozone Sci Eng 29, 379–389. https://doi.org/10.1080/01919510701573400
Van Gijn, K., Zhao, Y., Balasubramaniam, A., de Wilt, H.A., Carlucci, L., Langenhoff, A.A.M., Rijnaarts, H.H.M., 2022. The effect of organic matter fractions on micropollutant ozonation in wastewater effluents. Water Res 222, 118933. https://doi.org/https://doi.org/10.1016/j.watres.2022.118933
Venier, C.M., Conte, L.O., Pérez-Moya, M., Graells, M., Nigro, N.M., Alfano, O.M., 2021. A CFD study of an annular pilot plant reactor for Paracetamol photo-Fenton degradation. Chemical Engineering Journal 410, 128246. https://doi.org/https://doi.org/10.1016/j.cej.2020.128246
Villegas- Guzman, P., Giannakis, S., Rtimi, S., Grandjean, D., Bensimon, M., de Alencastro, L.F., Torres-Palma, R., Pulgarin, C., 2017. A green solar photo-Fenton process for the elimination of bacteria and micropollutants in municipal wastewater treatment using mineral iron and natural organic acids. Appl Catal B 219, 538–549. https://doi.org/https://doi.org/10.1016/j.apcatb.2017.07.066
Vlad, G., Robescu, D.N., Mocanu, C.R., 2011. Mathematical modelling of a biological wastewater treatment process. Case study: The wastewater treatment station of românofir S.A. trading co.-Tălmaciu 73, 299–310.
von Gunten, Urs., Hoigne, Juerg., 1994. Bromate Formation during Ozonization of Bromide-Containing Waters: Interaction of Ozone and Hydroxyl Radical Reactions. Environ Sci Technol 28, 1234–1242. https://doi.org/10.1021/es00056a009
Wan, A., Wu, Y., Xie, Y., Zhao, B., Qi, X., 2020. Experimental study and numerical simulation of moving bed biofilm reactor using 3D printed filler. Chemical Engineering and Processing - Process Intensification 157, 108146. https://doi.org/https://doi.org/10.1016/j.cep.2020.108146
Wang, F., Smith, D.W., El-Din, M.G., 2003. Application of advanced oxidation methods for landfill leachate treatment – A review. Journal of Environmental Engineering and Science 2, 413–427. https://doi.org/10.1139/s03-058
Wang, F.-X., Wang, C.-C., Du, X., Li, Y., Wang, F., Wang, P., 2022. Efficient removal of emerging organic contaminants via photo-Fenton process over micron-sized Fe-MOF sheet. Chemical Engineering Journal 429, 132495. https://doi.org/https://doi.org/10.1016/j.cej.2021.132495
Wang, K., Jiang, J., Ma, L., Zheng, L., Zhang, G., Wu, D., 2022. Study on Advanced Nitrogen Removal and Microbial Community Structure of Traditional Chinese Medicine Wastewater by a Novel System Coupling Anaerobic Sequencing Batch Reactor and Modified Sequencing Batch Biofilm Reactor. Front Environ Sci 10.
Ward, I.M., Sweeney, J., 2004. An Introduction to the Mechanical Properties of Solid Polymers.
Wardenier, N., Liu, Z., Nikiforov, A., Van Hulle, S.W.H., Leys, C., 2019. Micropollutant elimination by O_3, UV and plasma-based AOPs: An evaluation of treatment and energy costs. Chemosphere 234, 715–724. https://doi.org/https://doi.org/10.1016/j.chemosphere.2019.06.033

Wert, E.C., Rosario-Ortiz, F.L., Drury, D.D., Snyder, S.A., 2007. Formation of oxidation byproducts from ozonation of wastewater. Water Res 41, 1481–1490. https://doi.org/https://doi.org/10.1016/j.watres.2007.01.020

Wojtyła, S., Klama, P., Baran, T., 2017. Is 3D printing safe? Analysis of the thermal treatment of thermoplastics: ABS, PLA, PET, and nylon. J Occup Environ Hyg 14, 0. https://doi.org/10.1080/15459624.2017.1285489

Wu, G., Liu, S., Jia, H., Dai, J., 2016. Preparation and properties of heat resistant polylactic acid (PLA)/Nano-SiO_2 composite filament. Journal of Wuhan University of Technology-Mater. Sci. Ed. 31, 164–171. https://doi.org/10.1007/s11595-016-1347-2

Wu, X., Wang, Y., Xu, J., Wang, H., 2022. Cu/Fe Bimetallic Treatment Performance on Organophosphorus Pesticides. Front Environ Sci 10.

Xiao, H., Bruhns, O.T., Meyers, A., 2006. Elastoplasticity beyond small deformations. Acta Mech 182, 31–111. https://doi.org/10.1007/s00707-005-0282-7

Yamal-Turbay, E., Graells, M., Pérez-Moya, M., 2012. Systematic Assessment of the Influence of Hydrogen Peroxide Dosage on Caffeine Degradation by the Photo-Fenton Process. Ind Eng Chem Res 51, 4770–4778. https://doi.org/10.1021/ie202256k

Yamal-Turbay, E., Pérez González, L., Graells, M., Pérez-Moya, M., 2014. Degradation of sulphamethazine by means of an improved photo-Fenton process involving a hydrogen peroxide systematic dosage. Environ Technol 35, 1695–1701. https://doi.org/10.1080/09593330.2014.880516

Yang, X., Rosario-Ortiz, F.L., Lei, Y., Pan, Y., Lei, X., Westerhoff, P., 2022. Multiple Roles of Dissolved Organic Matter in Advanced Oxidation Processes. Environ Sci Technol 56, 11111–11131. https://doi.org/10.1021/acs.est.2c01017

Yargeau, V., Schlageter, B., Alungulesa, S., Gillis, P.L., Doran, M., Hayward, E.E., Metcalfe, C.D., 2023. Integrated ozonation as a strategy for enhancing treatment of municipal wastewater in facultative sewage lagoons. J Environ Chem Eng 11, 109406. https://doi.org/https://doi.org/10.1016/j.jece.2023.109406

Yershov, B., Morozov, P., Gordeev, A., Seliverstov, A., 2009. Kinetic regularities of ozone decomposition in water. J. Water Chem. Technol. 31, 381–388. https://doi.org/10.3103/S1063455X0906006X

Yu, X., Somoza-Tornos, A., Graells, M., Pérez-Moya, M., 2020. An experimental approach to the optimization of the dosage of hydrogen peroxide for Fenton and photo-Fenton processes. Science of The Total Environment 743, 140402. https://doi.org/https://doi.org/10.1016/j.scitotenv.2020.140402

Zandi, M.D., Jerez-Mesa, R., Llumà, J., Roa, J., Travieso-Rodriguez, J.A., 2020a. Experimental analysis of manufacturing parameters' effect on the flexural properties of wood-PLA composite parts built through FFF. The International Journal of Advanced Manufacturing Technology 106. https://doi.org/10.1007/s00170-019-04907-4

Zandi, M.D., Jerez-Mesa, R., Lluma-Fuentes, J., Jorba-Peiro, J., Travieso-Rodriguez, J.A., 2020b. Study of the manufacturing process effects of fused filament fabrication and injection molding on tensile properties of composite PLA-wood parts. The International Journal of Advanced Manufacturing Technology 108, 1725–1735. https://doi.org/10.1007/s00170-020-05522-4

Zazo, J.A., Pliego, G., Blasco, S., Casas, J.A., Rodriguez, J.J., 2011. Intensification of the Fenton Process by Increasing the Temperature. Ind Eng Chem Res 50, 866–870. https://doi.org/10.1021/ie101963k

Zhang, M., Li, S., Sun, Jian, Sun, Jianping, Wang, L., Zhao, R., 2023. Effect and degradation pathway of sulfamethoxazole removal in MBR by PVDF/DA modified membrane. Front Environ Sci 11.

Zhang, S.-U., 2018. Degradation Classification of 3D Printing Thermoplastics Using Fourier Transform Infrared Spectroscopy and Artificial Neural Networks. Applied Sciences . https://doi.org/10.3390/app8081224

Zhang, Y., Klamerth, N., Messele, S.A., Chelme-Ayala, P., Gamal El-Din, M., 2016. Kinetics study on the degradation of a model naphthenic acid by ethylenediamine-N,N'-disuccinic acid-modified Fenton process. J Hazard Mater 318, 371–378. https://doi.org/https://doi.org/10.1016/j.jhazmat.2016.06.063

Zhang, Y., Wang, Y., Li, Y., Xu, Z., Li, H., Jin, W., 2023. Reactivity of dissolved effluent organic matter (EfOM) with hydroxyl radical as a function of its isolated fractions during ozonation of municipal secondary effluent. Water Res 242, 120248. https://doi.org/https://doi.org/10.1016/j.watres.2023.120248

Zhou, X., Lin, H., Lin, H., 2008. Global Sensitivity Analysis BT - Encyclopedia of GIS, in: Shekhar, S., Xiong, H. (Eds.), . Springer US, Boston, MA, pp. 408–409. https://doi.org/10.1007/978-0-387-35973-1_538

Zimbron, J., Reardon, K., 2011. Continuous combined Fenton's oxidation and biodegradation for the treatment of pentachlorophenol-contaminated water. Water Res 45, 5705–5714. https://doi.org/10.1016/j.watres.2011.08.038

Zimmermann, S.G., Wittenwiler, M., Hollender, J., Krauss, M., Ort, C., Siegrist, H., von Gunten, U., 2011. Kinetic assessment and modeling of an ozonation step for full-scale municipal wastewater treatment: Micropollutant oxidation, by-product formation and disinfection. Water Res 45, 605–617. https://doi.org/https://doi.org/10.1016/j.watres.2010.07.080

Appendices

Appendix A

List of Articles, Conferences, Contributions, Presentations, and Projects:

1. Nasr Esfahani, K., Zandi, M. D., Travieso-Rodriguez, J. A., Graells, M., & Pérez-Moya, M. (2021). Manufacturing and Application of 3D Printed Photo Fenton Reactors for Wastewater Treatment. International Journal of Environmental Research and Public Health, 18(9), 4885. MDPI AG. Retrieved from http://dx.doi.org/10.3390/ijerph18094885
2. Nasr Esfahani, K., Pérez-Moya, M., & Graells, M. (2022). Modeling of the photo-Fenton process with flexible hydrogen peroxide dosage: Sensitivity analysis and experimental validation. Science of The Total Environment, 839, 155941. https://doi.org/https://doi.org/10.1016/j.scitotenv.2022.155941
3. Nasr Esfahani, K., Pérez-Moya, M., Graells, M., Miralles-Cuevas, S., & Cabrera-Reina, A. (2023). Mechanistic modeling of Fe^{3+}-EDDS mediated photo-Fenton revisited: lumped radicals and sensitivity analysis. Chemical Engineering Journal, 142559.
4. Nasr Esfahani, K., Pérez-Moya, M., Graells, M., 2022. Modeling and Parameter Fitting of the Dosage of Hydrogen Peroxide in a Photo-Fenton Process, in: Montastruc, L., Negny, S. (Eds.), Computer Aided Chemical Engineering. Elsevier, 373–378, Toulouse, France. https://doi.org/10.1016/B978-0-323-95879-0.50063-1
5. Nasr Esfahani, K., Cabrera Reina, A., Miralles-Cuevas, S., Pérez-Moya, M., Graells, M., 2022. Mathematical Modeling of Microcontaminants Removal by Fe^{3+}-EDDS Complex Photo-Activation, 5th Iberoamerican Conference on Advanced Oxidation Technologies, 500-501, Cusco, Peru.
6. Nasr Esfahani, K., Pérez-Moya, M., Graells, M., 2021. A Hybrid Model Coupling Advanced Oxidation Processes (AOP) and Conventional Bio-processes for the Removal of Recalcitrant Contaminants in Wastewaters, in: Türkay, M., Gani, R. (Eds.), Computer Aided Chemical Engineering. Elsevier, 883–889, Istanbul, Turkey. https://doi.org/10.1016/B978-0-323-88506-5.50137-6

7. Nasr Esfahani, K., Pérez-Moya, M., Graells, M., 2020. Integrated Mathematical Modeling of Advanced Oxidation Processes and Conventional Bio-Processes for Wastewater Treatment, 14th Mediterranean Congress of Chemical Engineering (MeCCE), Barcelona, Spain. https://doi.org/10.48158/MeCCE-14.DG.06.07
8. Nasr Esfahani, K., Zandi, M.D., Travieso-Rodriguez, J.A., Pérez-Moya, M., Graells, M., 2019. 3D Printed Lab-Scale Raceway Ponds Reactors Applied to Photo-Fenton Processes, 16th International Conference on Environmental Science and Technology, Rhodes, Greece. http://hdl.handle.net/2117/173322
9. Nasr Esfahani, K., Zandi, M.D., Travieso-Rodriguez, J.A., Pérez-Moya, M., Graells, M., 2019. Manufacturing And Application of Raceway Ponds For Wastewater Treatment, 6th European Conference on Environmental Applications of Advanced Oxidation Processes (EAAOP-6), Portorož-Portorose, Slovenia. http://hdl.handle.net/2117/1733237
10. Pérez-Moya, M., Nasr Esfahani, K., Graells, M., Roselló, E., 2022. Modeling The Photo-Fenton Process in the Presence of Sulphate or Chloride Ions with Experimental Validation, European Meeting on Solar Chemistry and Photocatalysis: Environmental Applications, Turin, Italy.
11. Nasr Esfahani, K., Graells, M., Pérez-Moya, M., Espuña, A., 2023. Deodorization and Disinfection of Garbage Containers and Leachates with the Multi Oxidants Solution, 15th Mediterranean Congress of Chemical Engineering, Barcelona, Spain

Participations in research projects:

- Advanced Integration Methods for the Efficient Symbiosis of Process Networks (AIMS), 2017-2021, DPI2017-87435-R, *http://hdl.handle.net/2117/347815*
- Soft sensors: Artificial intelligence systems for the early detection and management of pollution episodes in WWTPs (DiGEC), 2022-2023, ACE057/22/000024, *https://futur.upc.edu/35700726*
- Implementation of the Circular Economy in the Process Industry (CEPI): Methods and tools for the circular integration of systems, 2021-2024, PID2020-116051RB-I00, *https://futur.upc.edu/32040773*

Research stays and collaborative experiences:

- Mechanistic Modeling of Fe^{3+} – EDDS Mediated Photo-Fenton Revisited: Lumped Radicals and Sensitivity Analysis, 2022 (March to May), Supervised by Dr. Alejandro Cabrera-Reina, Universidad Tecnológica Metropolitana (UTM), Santiago, Chile.
- Modeling of Ozone Decay in Secondary Effluent Containing Organic Matter, 2023 (September to November), Supervised by Dr. Domenico Santoro, Western University (UWO), London ON, Canada.